A STUDY OF GAS-SOLIDS FLOWS AT VERY HIGH SPEEDS.

A Thesis submitted to the University of Leeds

for the Degree of Doctor of Philosophy by

H.M.Bowers B.Sc.(Hons), G.I.Mech.E.

Department of Mechanical Engineering

The University of Leeds.

December 1966.

BEST COPY

AVAILABLE

Variable print quality

ABSTRACT.

An investigation of the flow of suspensions of solids particles in gases at high flow velocities has been carried out. A literature survey into gas-solids flow at both low and high speeds has revealed that most of the existing work on high speed flows is of a theoretical nature and has been stimulated as a result of the presence of solids particles in the exhaust gases of solid-fuelled rocket engines.

In this project theoretical approaches are presented for both idealised flows where the solids and gas are in equilibrium or maintaining constant fractional lag and also for the more realistic case of variable gas-solids velocity and temperature ratios where solutions require numerical integration by a digital computer. The experimental approach has been limited to the flow of polystyrene solids particles in air through a long 1 in. nominal bore pipe at flows ranging from almost incompressible to choked flows. Measurements of air and solids mass flow rates, air velocity profiles and solids velocities have been obtained.

The indications are that provided an estimation of the frictional drag due to the gas skin friction and the solids particle to particle and particle to duct wall interaction can be obtained, the numerical solution gives good results. The constant fractional lag theory gives indications of providing a Mach number expression capable of predicting the choked flow of gas-solids suspensions.

ACKNOWLEDGEMENT.

I should like to thank all the academic staff and fellow research students of the Mechanical Engineering Department of Leeds University, who have assisted me over the past three years. I am especially indebted to Mr. F.R. Mobbs and Professor B.N. Cole, my supervisors, whose help and encouragement throughout this project has been invaluable.

I am also particularly grateful to Mr. A.V. Whitaker for his expert guidance in the preparation of computer programmes. My thanks are also due to all the technicians who have assisted in the preparation of the experimental rigs for this project, and especially to Mr. J. Mosedale.

For their financial assistance in providing a considerable amount of the experimental equipment, my thanks are due to The Central Electricity Research Laboratories, Leatherhead. I should also like to thank The Scientific Research Council for providing the Research Studentship which has enabled me to carry out this project.

Finally, I should like to thank my wife for her patience, understanding and not inconsiderable help throughout the last three years.

Errata

Page 47, line 19, delete - and the variable y - replace by - For $V_s \to 0$:-

Line 20, replace equation by

$$n = \frac{\gamma + xj\beta}{(\gamma + xj\beta) - (\gamma - 1)(1 + xk^2)/(1 + xk)}$$

Page 51 delete - where $y = y_o \left(\frac{Tg_o}{Tg}\right)^{\frac{-1}{n-1}}$

after the last line add - and $y = y_o \left(\frac{Tg_o}{Tg}\right)^{\frac{-1}{n-1}}$

Page 200 replace - therefore $\frac{p}{\rho_g{}^n}$ = a constant - by

therefore $\frac{dp}{d\rho_g} = N \frac{p}{\rho_g}$ .....(10)

after equation (11) insert - for $y \to 0$ $\frac{p}{\rho_g{}^n}$ = a constant

where $n = \frac{\gamma + xj\beta}{(\gamma + xj\beta) - (\gamma - 1)(1 + xk^2)/(1 + xk)}$

Page 209 delete equation (39), insert -

From equation (6) $\frac{\rho_g{}^*}{\rho_g} = \frac{y^*}{y}$ .....(39)

Page 210 equation (40) should read -

$$\left(\frac{A}{A^*}\right)^2 = \left(\frac{y^*}{y}\right)^2 \frac{(1 + y)^2 + \left(\frac{n}{(n-1)N} + (1 + y)\right)\frac{2}{NM_m{}^2}}{(1 + y^*)^2 + \left(\frac{n}{(n-1)N^*} + (1 + y^*)\right)\frac{2}{N^*}} \quad ..(40)$$

Page 213 equation (51) should read $\frac{p_o}{p_o{}^*} = \frac{1}{M_m}\left(\frac{Tg^*}{Tg}\right)^{\frac{n+1}{2(n-1)}}$

next line, replace - and for $V_g >> V_s$ - by - or -

CONTENTS LIST.

Chapter.		Page.
1.	Introduction.	1
2.	Literature Review.	7
2.1.	Incompressible Flow.	8
2.1.1.	Pressure Drop Measurement.	8
2.1.2.	Solids Velocity Measurement.	14
2.1.3.	Gas Velocity Measurement.	18
2.2.	Compressible Flow.	22
2.2.1.	Sonic Velocity.	26
2.2.2.	Flows through Nozzles and Normal Shock Waves.	30
2.2.3.	Gas-Solids Drag, Heat Transfer and Skin Friction.	32
2.2.4.	Experimental Work.	36
3.	Theoretical Analysis.	39
3.1.	Equilibrium Flow.	42
3.2.	Constant Fractional Lag Flow.	46
3.3.	Finite Difference Solution of the Equations.	53
3.3.1.	Solids Particle Drag Coefficient.	55
3.3.2.	Solids Particle Nusselt Number.	57
3.3.3.	Solids Particle Mean Diameter.	58
3.3.4.	Gas-Solids Friction Factor.	60
3.3.5.	Hand Solution.	62
3.3.6.	Computer Solution.	63
3.4.	Method of Solution for the Inclusion of Solids Particle Size Distribution.	67
3.5.	Suggested Computer Solution for the Duct Flow Rig.	69
4.	Description of Rig.	73
4.1.	Pipe Flow Rig.	73
4.1.1.	Solids Entrainment.	74
4.1.2.	Experimental Section.	77
4.1.3.	Solids Separation.	79
4.1.4.	Solids Re-loading.	82
4.2.	Rectangular Duct Flow Rig.	84
4.2.1.	Experimental Section.	84
5.	Description and Development of Instrumentation.	89
5.1.	Instrumentation for the Pipe Flow Rig.	89
5.1.1.	Pressure Drop Measurement.	89
5.1.2.	Solids Flow Rate Measurement.	94
5.1.3.	Air Flow Rate Measurement.	97

Chapter.		Page.
	5.1.4. Air Velocity Measurement.	100
	5.1.5. Solids Velocity Measurement.	106
5.2.	Instrumentation for the Duct Flow Rig.	110
	5.2.1. Pressure Drop Measurement.	110
	5.2.2. Air Velocity Measurement.	111
	5.2.3. Solids Velocity Measurement.	112
6.	Rig Development.	113
6.1.	The Solids Entrainment System.	113
6.2.	Damping of Pressure Fluctuations.	118
6.3.	Glass U-Tube to Nylon Pipe Connections.	120
6.4.	Pressure Testing the Pipe Flow Rig.	123
6.5.	Sealing the Duct Flow Rig.	124
7.	Experimental Procedure.	127
7.1.	Solids Material and Particle Size Analysis.	128
7.2.	Pressure Drop Measurement.	130
7.3.	Solids Flow Rate Measurement.	134
7.4.	Air Flow Rate Measurement.	137
7.5.	Air Velocity Profile Measurement.	138
7.6.	Solids Velocity Measurement.	141
8.	Experimental and Derived Results.	147
8.1.	Solids Particle Size Analysis.	147
8.2.	Pressure Drop Measurements.	150
	8.2.1. Pipe Line Pressure Drop.	150
	8.2.2. Cyclone Pressure Drop.	154
8.3.	Air Velocity Profile Measurements.	155
8.4.	Solids Velocity Measurement.	160
8.5.	Electrostatic Measurements.	161
8.6.	Computer Solutions for Pipe Flow.	163
9.	Discussion.	172
9.1.	Pipe Line Pressure Drop.	172
9.2.	Efficiency of Solids Conveyance.	175
9.3.	Comparison of Friction Factors with those of other Workers.	175
9.4.	Cyclone Pressure Drop.	176
9.5.	Air Velocity Profiles.	177
9.6.	Solids Velocity.	182
9.7.	Computer Solution of the Basic Equations.	184
9.8.	Pipe Exit Mach Number for Air Flow.	188
9.9.	Electrostatic Measurements.	190
10.	Conclusions.	192
Appendices.		
1.	A Theory for the Compressible, Equilibrium and Constant Fractional Lag Flow of Gas-Solids Mixtures.	198

Appendices. Page.

2. Aerodynamic Mean Effective Diameter. 219

3. Cyclone Design. 222

4. Air Flow Measurement Nozzle Design. 225

5. Rectangular Duct Flow Rig Design. 228

6. Methods of Estimating Manometer Response Times. 238

List of Symbols. 242

References. 245

CHAPTER 1.

INTRODUCTION.

Flows in which solid particles are suspended in a gas stream - "gas-solids flows" - arise in practice in a variety of ways. Some of these are listed below.

(a) Pneumatic conveying of granular solids. This method of conveying is widely used in chemical plants, flour mills, pulverised fuel fired electric power stations etc.

(b) Solids - contaminated gas streams, smokes etc.

(c) Abrasive or erosive jets, e.g. shot blasting.

(d) Pulverised fuel burners for boilers or gas turbines.

(e) The use of suspended solids in gas streams to increase the apparent specific heat for heat transfer cycles.

(f) The exhaust gases from solid fuelled rocket motors.

(g) The seeding of gas streams used in magneto-hydrodynamic power generators.

A considerable amount of work of both a theoretical and experimental nature has been done on the properties of gas-solids flows at low velocities, and under conditions where compressibility effects are very small, but until very recently, little work had

been done on flows where compressibility effects are not small. Over the last six years, however, a large amount of work has been published in America on the flow of gas-solids mixtures, mainly with low solids to gas ratios, through nozzles and shock waves, and some of this is discussed in the Literature Review. This work has been mainly theoretical, and there still appears to have been very little experimental work published on this type of flow. The object of this project, therefore, is to investigate the mechanics of heavily loaded gas-solids flows at high speeds, extending into the supersonic range of velocities, in which compressibility effects are of major importance.

The theoretical approach to this project is based on that derived for the one-dimensional flow of compressible gases. The solids are assumed to be suspended in the gas stream by turbulent motion such that at any cross-section of the flow, the mixture is uniformly dense, and the flow can be considered to have uniform velocity, temperature and density profiles. The flow of the mixture is then considered to be expressed by equations of continuity of mass flow, conservation of momentum, and the energy equation for both constituents, and by the gas equation of state for the gas phase only. This approach can

then be divided into three sections depending on the assumptions made:

(a) Equilibrium flow - where the solids particles and neighbouring gas particles are assumed to be in velocity and thermal equilibrium throughout the flow.

(b) Constant fractional lag flow - where the velocity and thermal relationship between the solids particles and neighbouring gas particles is assumed to be such that the ratio of solids velocity to gas velocity, and solids temperature change from stagnation temperature to the gas temperature change from stagnation temperature, are constant throughout the flow.

(c) Flows in which the ratio of solids velocity to gas velocity, and solids temperature change from stagnation temperature to the gas temperature change from stagnation temperature, are allowed to vary throughout the flow.

With the above assumptions, special attention has been paid to the concept of "the velocity of sound" in a gas-solids mixture. With the resulting definition of Mach number, it has been possible to consider in some detail the prediction of the "choked" condition for pipe flow, and the possibility of achieving a Mach number of unity at the throat of a convergent-divergent nozzle. For cases (a) and (b) above, it is possible to express the variables in the gas-solids mixture in terms of the mixture compressible flow index $\bar{n}$ and Mach number,

such that equations similar to those for the one dimensional flow of compressible gases are evolved. For case (c), however, because the gas-solids velocity ratio and temperature ratio are now varibbles, it has been necessary to use a digital computer and also utilise some of the experimental readings in order to obtain solutions to the equations.

The experimental approach to the project has been mainly concentrated on establishing rigs from which measurements pertinent to gas-solids flow may be taken, and obtaining as many measurements as time has permitted. Because studies of gas-solids flows is a new field to the Department of Mechanical Engineering at this University, a considerable amount of development work has been necessary in establishing the experimental apparatus.

Two rigs have been constructed, together with the necessary solids entrainment and separation techniques. One of these rigs is a 150 ft. long 7/8th.in bore brass walled straight pipe, the length and bore size being such as to achieve "choked" flow. The very long length was chosen as it was suspected that air-solids mixtures require a long entry length, and also since it was hoped to obtain measurements over the full Mach number range from about 0.1 to 1. The second of these

rigs is a rectangular duct flow rig of about 5 to 1 aspect ratio in the test section. This rig has an 18 ft. test section, 12 ft. of which has transparent side walls. A convergent-divergent nozzle is located in this rig so that supersonic flows may be achieved. These rigs were selected so that one dimensional flow was approximated in the pipe flow rig, and two dimensional flow in the rectangular duct flow rig.

Instrumentation has been developed for these rigs enabling the following measurements to be made: pressure drop profile along the pipe or duct, air flow rate, solids flow rate, some measurements of air velocity profile across the pipe using a total head tube, solids velocity measurements, and some measurements of electrostatic effects from an electrically isolated length on the pipe flow rig. Although it has been possible to design, construct and develop both rigs during the course of the project, time has only permitted actual measurements to be taken from the pipe flow rig.

The experiments on the pipe flow rig have all been carried out using only one solids material - polystyrene - a polydisperse powder of plastic material, in which the individual particles are perfect spheres. The powder has a mean particle size of 0.012 in. (310 microns) diameter, and about 90% by weight

of the particles lie in the range 0.0094 to 0.017 in. (240 to 430 microns). Air has been used as the gas phase of the two-phase mixture, and the air flow rates have been varied so that the full range of conditions, from flows where compressibility effects are small to flows well above the onset of choked flow, have been achieved.

In the following chapters of this Thesis, a background to the project is given in the form of a Literature Review, followed by a chapter on the theoretical approach. The subsequent three chapters give details of the design, instrumentation and development work necessary to commission the rigs, and the following two chapters give details of the experimental procedure adopted, the experimental results obtained from the pipe flow rig, and the results from the computer programme. Finally, in the last two chapters, these results are discussed and some conclusions drawn.

CHAPTER 2.

LITERATURE REVIEW.

A survey of technical publications shows that up to about 6 years ago there was very little published work on the conveyance of solid particles in a gas stream, under conditions where compressiblity effects are important. Since then, however, a considerable amount of work has been published, mainly in America, on the flow of gas-solids mixtures through nozzles at very high speeds. This work, which was initiated through the use of metallic fuel constituents in modern rocket engines, tends to concentrate on the flow of very small particles (usually in the range 1 to 20 microns) suspended at low solids to gas concentrations (typically less than 0.7 by weight for a contemporary solid fuel rocket), in initially very high temperature gas flows. Because of the difficulty in making any experimental measurements on the flow inside a rocket engine, most of the papers published to date concentrate on the theoretical aspects of gas-solids flow through nozzles, and the theoretical deductions are not usually collaborated by experimental findings.

In comparison with the relatively recent interest in high speed gas-solids flow, work of both a theoretical and experimental nature has been proceeding for many years on the properties of low speed gas-solids flow, where compressibility effects are

small. This work has often tended towards the derivation of empirical or semi-empirical relations to express the pressure drop of a gas-solids flow along a pipe-line and also to relate the solids velocity to the gas velocity. Other work of a rather more fundamental nature in which particle wake effects, acceleration effects and the effects of fluid turbulence on the particle drag coefficient has also been undertaken for flows in which the gas pressures and velocities are low. In view of this obvious division into compressible and incompressible gas-solids flow, this review will consider separately pertinent aspects of recent contributions to the understanding of flow in these two regimes.

2.1. Incompressible Flow.

2.1.1. Pressure Drop Measurement.

The expressions suggested for pressure drop evaluation can be divided into those derived from experimental data which incorporates the initial solids acceleration length, and those which only consider fully accelerated gas-solids flows. In view of the added complexity of including acceleration effects, the main interest in this review is with fully accelerated flows.

In 1954 Mithin put forward the empirical expression

$$\frac{\Delta p_s}{\Delta p_g} \frac{u_s^x}{W_s^y} = K$$

where constants K, x and y are evaluated experimentally for different solids materials. The expression was subsequently modified by Richardson and McLeman (1960) to the form

$$\frac{\Delta p_s}{\Delta p_g} \cdot \frac{u_s^2}{W_s} = \frac{45\ 000}{u_{so}}$$

In these expressions Δp_g is the pressure drop for pure air flow, Δp_s the excess pressure drop due to the presence of the solids, u_s the solids velocity, W_s the solids feed rate and u_{so} the solids free falling velocity. Values of K, x and y were obtained from experimental readings over a 114 ft. long by 1 in. bore pipe. A number of other expressions, largely of an empirical nature, have also been suggested by other workers, but work of a more fundamental nature has also been carried out and this is now considered.

Hinkle in 1953 (and Mehta in 1955) suggested that the total pressure drop over a pneumatic conveying pipe-line might be expressed as

$$\Delta p = \frac{u_g^2 \rho_g}{2g} + \frac{W_s u_s}{Ag} + \frac{W_s \Delta L}{A\ u_s} + \frac{4Cf_g \rho_g u_g^2\ \Delta L}{2gD} + \frac{4Cf_s u_s u_g \rho_g W_s \Delta L}{2gD\ W_g}$$

where $4Cf_s = \frac{3\ C_D\ D}{2d_p \rho_p}\ \rho g\left(\frac{u_g - u_s}{u_s}\right)^2$

Where the total pressure drop is comprised of component parts consisting of that due to the fluid acceleration, the particle acceleration, the solids static head in a vertical tube, the fluid to pipe skin friction loss and the particle to fluid friction loss. Here the expression for the particle to fluid friction loss appears to be derived by considering that the solids pressure loss can be expressed as a "Fanning" type friction equation where the dynamic pressure is given by the dispersed solids density x (the solids velocity)$^{-2}$. The dispersed solids density is the mass of solids per unit volume of mixture. This equation due to Hinkle is often quoted in books on pneumatic conveying and would appear to be accepted as a reliable equation for design work.

In a paper by Uematsu which appeared in 1964, an attempt has been made to express a gas-solids friction coefficient for flow in a straight pipe in terms of the pure gas skin friction coefficient and the solids to gas loading ratio by weight W_s/W_g only. In this derivation he assumes, as other workers before him, that the total pressure drop is comprised of that due to gas flow only plus a pressure drop due to the presence of the solids, and that this solids pressure drop can be expressed in terms of a "Fanning" type equation. Whereas Hinkle used a dispersed solids density and solids velocity in his

equation for solids pressure drop, Uematsu considers that the solids pressure drop can be expressed in terms of the gas density and velocity.

i.e. $\Delta p = \Delta p_g + \Delta p_s$ and $\Delta p_s = 4Cf_s \frac{\Delta L}{D} \cdot \frac{\rho_g u_g^2}{2}$

By then making use of the friction velocity concept and assuming that all the frictional drag takes place close to the pipe wall

i.e. $\tau_o = \frac{\Delta p}{\Delta L} \cdot \frac{D}{4}$ and $v^* = \sqrt{\frac{\tau_o}{\rho_g}}$

he derives an expression giving the friction coefficients in terms of the gas velocity and friction velocity

$$4Cf_g + 4Cf_s = 8 \left(\frac{v^*}{u_g}\right)^2$$

From a large number of experimental results (though with a tendency to largish diameter solids particles) Uematsu proceeds to plot u_g/v^* against W_s/W_g and show this is a straight line with slope of -1.72, intercepting the u_g/v^* axis at a value of $\sqrt{8/4Cf_g}$, this corresponding to pure gas flow. The expression for the solids friction coefficient is then given by

$$4Cf_s = 8/\left(\sqrt{\frac{8}{4Cf_g}} - 1.72 \frac{W_s}{W_g}\right)^2 - 4Cf_g$$

This expression has the advantage over Hinkle's that no knowledge of the solids velocity is required in order to obtain a value for $4Cf_s$.

In a recent paper, (1965) Peskin and Dwyer have considered the flow of gas-solids mixtures in straight pipes a little more fundamentally. By considering a momentum balance inside a differential control volume in the pipe, which surrounds the air but not the solids particles so that the particles are continually moving in and out of the system, they arrive at the following expression for incompressible gas flow.

$$\Delta p = \frac{4Cf_g \rho_g u_g^2 \Delta L}{2D_H} + \frac{n \bar{C}_D \rho_g (u_g - u_s)^2}{2} \frac{A_s}{A}$$

where n is the number of solid particles inside the differential control volume; $\bar{C}_D$ the mean particle drag coefficient, A_s the projected area of a solids particle and D_H the duct equivalent diameter = 4 x Duct Area/Duct Perimeter. Their experiments were in fact performed in a 3 in. square glass-walled section. They then proceed to evaluate u_s and n experimentally for the flow of 80 micron diameter glass spheres and substitute these into the above equation to determine $\bar{C}_D$. The $\bar{C}_D$ value they obtain tends to be considerably greater than that given by the standard drag - Reynolds number curve for flow round a single

sphere. However, after explaining that due to turbulence effects the $u_g - u_s$ value is somewhat greater than that given by the mean velocity difference in the axial direction, as suggested by S.L. Soo (1956), and that the gas skin friction factor should be increased to allow for losses due to particle-particle and particle to wall collisions, Peskin and Dwyer arrive at the conclusion that the value of $\bar{C}_D$ is not significantly different from that given by the standard drag curve.

The expressions for solids pressure drop of Hinkle, and Peskin and Dwyer although in different form are in fact identical. If the expression of Hinkle for particle to fluid friction loss (from his total pressure drop equation) is equated to the number of particles in an elemental length x the drag force per particle, Hinkle's expression for $4\ Cf_s$ is obtained. Peskin and Dwyer appear to have preferred to evaluate the number of particles n experimentally, instead of considering n to be expressed by

$$n = \rho_s\ A\ \Delta L / \frac{\pi}{6}\ dp^3\ \rho_p$$

2.1.2. Solids Velocity Measurement.

Because many of the expressions derived to give the pressure drop for a gas-solids flow through a straight pipe incorporate a solids velocity term, numerous empirical relationships for solids velocity have been put forward and some of the more recent of these will be discussed.

In their paper on pneumatic conveying, Richardson and McLeman give the following expression for solids velocity which, they state, is applicable to materials not exhibiting electrostatic effects.

$$u_g - u_s = u_{so} / \left(0.468 + \sqrt{\frac{u_{so}}{\rho_p}}\right)$$

This expression, they state, is also only really applicable to spherical or rounded solids particles with a fairly narrow size distribution and travelling at fairly high velocities. The expression indicates that for the range of variables considered by Richardson and McLeman, the relative velocity between the gas and solids is constant and independent of both solids feed rate and air velocity. Other workers in this field, Hariu and Molstad, 1949, and Culgan have also stated that the equilibrium particle velocity is independent of the solids loading.

Richardson and McLeman's method of measuring solids velocity was to interrupt the solids flow for a fraction of a second, thereby introducing an air pulse into the system and then to time this pulse electronically over a length of pipe-line. Because a pulse introduced in this way is presumably a pressure pulse, there would appear to be some doubt as to whether it does in fact travel at the solids velocity down the pipe-line, though in their paper Richardson and McLeman make no comment on this.

Mitlin in his project on pneumatic conveying used a method of trapping the solids in an isolating section in order to measure their velocity. This method consists of closing shutters at either end of the isolating section simultaneously and hence from the mass of solids trapped in the section and knowing the solids feed rate, determining the mean solids velocity from the following expression. $u_s = W_s L/m$, where m is the mass of solids collected in length L. According to Richardson and McLeman this method suffers the disadvantage of not being possible when plant is running continuously. If, however, the shutters can be made to close exactly simultaneously, with no delay due to sticking and also if the flow upstream can be diverted to prevent large pressure rises, the method should give reliable results. Owing to these latter limitations

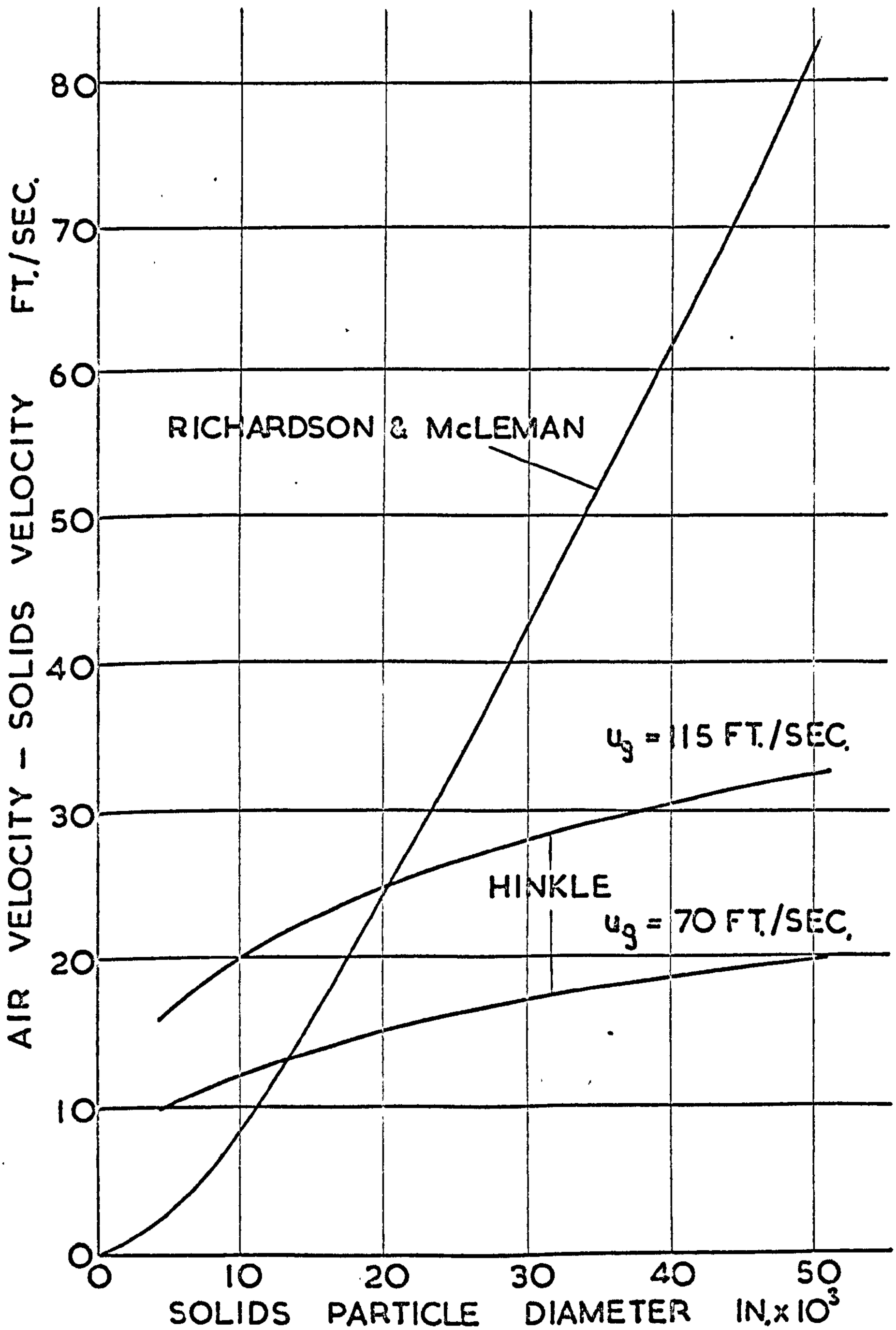

FIG I AIR-SOLIDS VELOCITY DIFFERENCE FROM RICHARDSON & McLEMAN'S AND HINKLE'S EXPRESSIONS

applicable below a particle diameter of 0.014 in.

In their recent paper, Peskin and Dwyer have developed a fibre-optic method for obtaining the solids velocity profile across a test section. Their method can be divided into two parts. The first part is the measurement of the local mass flux at any point in the flow by recording the passage of a single particle or group of particles past the probe, the probe being the fibre optic. Then from a knowledge of the total mass flow rate through the test section the variation in the local mass flow rate can be found, since the reading from the probe represents the relative number of particles passing the probe at a certain position. The second part consists of measuring the relative solid particle density distribution across the test section. The probe for this measurement, which was originally developed by Soo, basically consists of a small cylinder, which can traverse the test section and through which the gas-solid mixture is allowed to pass. On one side of this probe is a light source and on the other a glass rod inside a steel tube. When particles flow through the cylinder this causes attenuation of the light across the gap with the result that the signal output picked up from the glass rod

decreases. This attenuation of the light is then used to obtain the relative distribution of the solid particle density. These two measurements alone, however, are not sufficient and the absolute solid particle density must be obtained at some point. In order to obtain this, Peskin and Dwyer assumed that the solid particle velocities on the centre-line of their test section were the same as the air velocity. The relationship between local mass flow rate M_{SL}, solids particle density ρ_{SL}, and solids velocity u_{SL}, is $M_{SL} = \rho_{SL} . u_{SL}$. Then assuming u_{SL} equal to the air velocity on the centre-line (determined from a Pitot tube traverse), ρ_{SL} at this point is obtained and hence the variation in u_{SL} across the test section. The weakness in this method would appear to be in the assumption of $u_{SL} = u_g$ on the duct centre-line and also that a relatively large cross-sectional area is required for the probes not to cause any appreciable disturbance in the flow.

2.1.3. Gas Velocity Measurement.

Few measurements appear to have been taken of gas velocity profiles in gas-solids mixtures. Many authors, however, imply that they are similar to that of pure gas flow by assuming that the pressure drop due to the gas is given by the Fanning friction equation, with a skin friction coefficient corres-

ponding to the gas flow Reynolds number and the appropriate pipe roughness value.

Peskin and Dwyer claim to have taken total pressure readings, using a Pitot tube, for the flow of very small glass spheres (mean diameter 80 micron) and air in their 3 in. square test section, for solids to air loadings up to 3 to 1 by weight. They state that the presence of these solid particles did not, in fact, alter the shape of the air velocity profile from that for pure air flow; however, they do go on to state that under certain conditions the presence of solids may alter the profile. In this paper Peskin and Dwyer give a classification of gas-solids flows, based on experimental information, where the flows may be divided into four distinct regions.

Region 1 is the case of particles very close together, where the size of the solids particles is approximately the same size as the eddies in the turbulent part of the boundary layer. In this region the presence of solids particles can cause increased viscous damping in the boundary layer and this damping can result in the laminar sublayer extending further away from the pipe wall with a subsequent decrease in wall shear stress for a similar Reynolds number. They state that this

type of flow has been realised for some types of flocculated flows of small particles.

Region 2 is the case of small particles widely spaced (greater than 10 particle diameters) and is probably the region into which most pneumatic conveying applications can be classified. Because the solids particles are small, disturbances caused by them will be viscous in nature, and because of the relatively large spacing between particles there is no large scale damping as in region 1. The net result is that the mean velocity profile is not changed significantly and the shear stress at the wall remains the same.

Region 3 consists of large, heavy particles relatively widely spaced. Because of the particles size and weight, they can cause a change in the fluid motion by creating turbulence. In this region the laminar sublayer will tend to be reduced with a subsequent increase in the wall shear stress. Peakin and Dwyer compare this type of flow with that of gas flow in pipes with large roughness elements attached to the wall, which also cause inertial disturbances in the fluid motion, with a resulting decrease in the laminar sublayer. This reduction in the laminar sublayer may be beneficial for heat transfer.

Region 4 consists of large particles very close together, occupying a large percentage of the flow volume. Here the geometry of the flow is changed and is similar to that in packed beds.

The three major variables considered above, namely the pressure variation along a pipe and the gas and solids velocity variations, would appear to be the most important in any investigation into the nature of gas-solids flows. Other variables, however, have also been considered by some workers in this field. Soo, in a paper in 1962 in which he considered the flow of very lightly loaded gas-solid suspensions, states that the concentration of particles is not uniform over a horizontal pipe cross-section and is, in fact, greater towards the centre of the pipe. He also states that the velocity of the particles near the centre-line of the pipe will be close to that of the gas velocity, but that near the pipe wall the particle velocity will be greater than that of the gas. In a further paper in 1964, Soo et al designed an electrostatic solids mass flow meter. This worked on the principle that all particles of the same size become charged to the same magnitude and sign on repeated impact with the wall, thus a ball ended probe situated in the flow will pick up charge at a

rate proportional to the solids mass flow.

No review of incompressible gas-solids flow would be complete without mention of a paper published in six parts by Torobin and Gauvin over the period 1959 to 1961. This paper took the form of a review, up to 1960, of work on flows where the pressures and velocities were low. They first considered the motion of single solid particles in gas and liquid flows, taking into account particle wake effects, effects due to particles accelerating in the flow, the effects of particle rotation, roughness and shape, and the effects of fluid turbulence on the particle drag coefficient. They then proceeded to attempt to apply the knowledge of single particle flow to that of multi-particle flow in turbulent fluids. They state that added complications are caused by the generation of electrostatic effects, which probably in some cases obscure data by introducing force terms, which are not accounted for in the theoretical equations being tested. Their conclusion is that the difficulties are such that experimental observations will have to be relied upon for any useable information.

2.2. Compressible Flow.

As stated previously most work to date on the flow of

compressible gas-solids suspensions has been initiated because of the presence of solids particles in the exhaust gases of solid-fuelled rockets. This has meant that the work to date has mainly been concerned with the flow through convergent-divergent nozzles to achieve supersonic conditions, whilst the presence of shock waves in the flow has also been considered fairly extensively. Some authors have discussed the flow of compressible gas-solids mixtures through ducts, but for the most part very little analytical work and, it would appear, no experimental work is available on this aspect.

Most authors, in their analytical approach to this subject, formulate the basic fluid dynamic and thermodynamic equations relevant to this type of flow, and after some simplification proceed to solve these for specified data by programming for a digital computer. Because the concept of sonic velocity and Mach number lead to great simplification of the pure gas dynamic equations, attempts have been made to apply similar concepts to gas-solids flows. To date most of the published work has been on one dimensional flow and in this review only this type of flow is considered.

The following assumptions have usually been made by

workers when they formulate the basic equations.

(1) There are no mass or energy losses from the system.

(2) The solids particles do not interact and they are uniformly distributed over the duct cross-section.

(3) There is steady one-dimensional motion.

(4) Thermal (Brownian) motion of the particles does not contribute to the pressure of the system.

(5) The solids particles are sufficiently small and have a large thermal conductivity relative to that of the gas so that they may be assumed to be at uniform temperature.

(6) Energy exchange between the solids particles and the gas occurs only through convection.

(7) The gas may be considered a perfect gas of constant composition.

(8) The heat capacities of the gas and solids particles are constant.

(9) The gas is inviscid except for the drag it exerts on the solids particles and the duct walls, although most authors

neglect skin friction drag.

(10) The volume occupied by the solids particles is negligible.

(11) Drag forces are the only forces acting to accelerate the solids particles.

(12) The particles are uniform size solid spheres, or can be approximated by such. Some workers, however, take into account particle size distribution.

With these assumptions, the basic equations necessary to define the flow of a gas-solid suspension through a duct, not necessarily of uniform area, are as follows:-

(a) The gas continuity equation.

(b) The solids continuity equation.

(c) The gas equation of state.

(d) The conservation of momentum equation.

(e) The solids particle momentum equation.

(f) The overall energy equation, or conservation of energy

equation for adiabatic flow.

(g) The solids particle equation of heat transfer.

All these equations are set out in slightly varying forms in references Soo (Sept. 1961); Kliegel (1963) and Kriebel (1964), whilst Rudinger (Nov. 1964) in a paper on the analysis of non-steady two-phase flow also retains variations with time in the equations.

2.2.1. Sonic Velocity.

As stated previously, because the sonic velocity concept is so fundamental to the study of pure gas flows, attempts have been made to determine the characteristic sonic velocity expression for compressible gas-solids flows.

In his 1963 paper on gas-particle nozzle flows, Kliegel derives, by substitution from the basic equations, the following momentum equation:-

$$(M_g^2 - 1)\frac{du_g}{u_g} + \frac{1}{RT_g}\cdot\frac{W_s}{W_g}\left(\left(u_g - \frac{\gamma - 1}{\gamma} u_s\right) du_s - \frac{\gamma - 1}{\gamma} C_s dT_s\right) = \frac{d\Lambda}{\Lambda}$$

where M_g is the gas Mach number, i.e. the ratio of gas velocity to gas sonic velocity.

He then considers two cases, the first being that of high frequency sound propagation, when the time in which the disturbance occurs is much smaller than the relaxation time of the particles. The second case is that of low frequency sound propagation, in which the gas and solids particles remain essentially in equilibrium through the disturbance. For the first case the solids particle velocity and temperature will remain unchanged through a discontinuity, and since the flow area does not change across a discontinuity, the momentum equation across a small discontinuity becomes, since $du_s = 0$, $dT_s = 0$ and $dA = 0$

$$(M_g^2 - 1) \frac{du_g}{u_g} = 0$$

i.e. an infinitessimal discontinuity travels at the gas sonic speed. A further point of interest regarding the above momentum equation is that, because the second term in this equation is always positive in an accelerating flow, the gas Mach number must always be $<$ 1 at a throat and hence the $M_g = 1$ condition occurs downstream of the throat.

For the low frequency sound propagation case, where in the limit of complete gas-solid particle equilibrium $T_s = T_g$, $dT_s = dT_g$, $u_s = u_g$ and $du_s = du_g$, the momentum equation becomes

$$(Me^2 - 1)\frac{du_g}{u_g} = \frac{dA}{A}$$

and that across a small discontinuity

$$(Me^2 - 1)\frac{du_g}{u_g} = 0$$

where Me the equilibrium Mach number is given by

$$Me^2 = \frac{u_g^2}{RT_g} \cdot \frac{(1 + \frac{W_s}{W_g})(1 + \gamma \cdot \frac{W_s}{W_g} \cdot \frac{C_s}{C_p})}{\gamma(1 + \frac{W_s}{W_g} \cdot \frac{C_s}{C_p})}$$

i.e. the disturbance travels at the equilibrium speed of sound

$\sqrt{n\ R\ T_g/(1 + W_s/W_g)}$, where $n = \dfrac{\gamma\,(1 + \frac{W_s}{W_g}\ \frac{C_s}{C_p})}{1 + \gamma \cdot \frac{W_s}{W_g}\ \frac{C_s}{C_p}}$

since $n < \gamma$ the equilibrium speed of sound in a gas-solids mixture is less than the non-equilibrium (or frozen) speed of sound in the mixture.

In a mainly review paper in 1962, Hoglund compares the nozzle flow behaviour of a gas-solids mixture with that of a chemically reacting gas, where the reacting gas flow is characterised by two "sound velocities." The "frozen" sound velocity is associated with zero reaction rates and the "equilibrium"

sound velocity with reaction rates sufficiently high that local chemical equilibrium is approached everywhere. In non-reacting or "frozen" nozzle flow, the gas velocity at the nozzle throat is equal to the frozen sound speed; in equilibrium nozzle flow, the gas velocity at the nozzle throat is equal to the smaller equilibrium sound speed. Similarly, the gas-solids mixture can be characterised by a frozen sound velocity, associated with a disturbance propagating in the gas alone, and a mixture or equilibrium sound velocity associated with zero slip in the gas-solids mixture, as indicated in Kliegel's paper.

For the case of no lag, the mixture velocity at the throat of a nozzle is equal to the mixture sound velocity, whereas for complete lag, the gas velocity would be expected to be equal to the frozen sound velocity. Hoglund then states that the point where the gas velocity equals the frozen sound velocity is farthest downstream for the no-lag case, moving upstream as the lag increases. This rather implies that it should be possible to define a further sonic velocity, to take into account the velocity and temperature lags of the solids particles, such that the gas velocity would be equal to this sonic velocity at the throat of the nozzle. In fact Kliegel in his paper on "Gas Particle Nozzle Flows" does introduce such a concept.

2.2.2. Flows through Nozzles and Normal Shock Waves.

By making use of the equilibrium flow concept, a number of workers (e.g. Kliegel, Kriebel) have derived from the basic equations a set of relationships similar to the one-dimensional perfect gas flow relationships, except that the Mach number is now the equilibrium Mach number, and the ratio of the specific heats for a gas is replaced by that for a gas-solids mixture. Kliegel has also gone one step further in that he has derived a set of relationships, again similar to the one-dimensional perfect gas flow equations, but now the Mach number and ratio of specific heats are those corresponding to there being a constant fractional lag of solids velocity to gas velocity and of solids temperature to gas temperature.

In spite of the sonic velocity concepts, many workers tend to use the frozen flow or gas Mach number as the characteristic non-dimensional parameter for gas-solids flows. This is partly because of the inability of all but the smallest solids particles to respond to the passage of a small pressure discontinuity or sound wave even of low frequency, but also because in a real gas-solids flow the velocity and temperature lags are constantly changing, with the result that any definition of a compressible flow index n is no longer a constant.

Because the above theories only cover the cases of equilibrium and constant fractional lag gas-solids flow, most theoretical solutions to date of some of the simpler flow problems, such as flow through a convergent-divergent nozzle and through a normal shock wave, have been evaluated by computer solution of the basic equations. Kliegel, however, compares the numerically integrated solutions of the one-dimensional gas-solids flow equations with his constant fractional lag solutions and appears to obtain good agreement for nozzle flows. Any attempt to express terms in non-dimensional form has usually consisted of expressing them in terms of the initial conditions (e.g. Soo's paper of September, 1961).

Kriebel, in a rather idealised solution he offers for flow through a normal shock wave, adopts the following method. He assumes that the problem can be reduced to one of considering the flow between three stations. At station one, far upstream of the shock, the gas and solids particles are in velocity and temperature equilibrium, which is a condition difficult to imagine in practice for a supersonic flow. On entering the shock, he considers there is a sharp deceleration of the gas, so severe that the particles do not decelerate or transfer an appreciable amount of heat in the distance involved. This initial disturbance is, there-

fore, not appreciably influenced by the particles and all the gas properties immediately after this initial disturbance, station two, can be found from the usual one-dimensional normal shock relations for a clean gas and from conditions at station one. At a third station, far downstream of the shock, the particles and gas nearly return to velocity and temperature equilibrium. Then all the properties at this station can be found from the equilibrium flow relations for a gas-solids mixture using the initial conditions. Between stations 2 and 3 the solids particles are not in equilibrium with the gas, and a computer solution of the equations is necessary over this region. It may be noted that in this paper Kriebel does in fact make use of the equilibrium flow Mach number concept, but in expressing it he derives the equilibrium flow sonic velocity in terms of a modified gas constant rather than a modified specific heat ratio, taking into account the presence of solids in the gas.

2.2.3. Gas-Solids Drag, Heat Transfer and Skin Friction.

Before even a computer solution of the basic equations can be attempted, some assumptions must be made regarding attributing suitable values to the particle drag coefficient and Nusselt number and also, in flows where wall skin friction is significant,

to the skin friction coefficient.

The "standard drag curve" of sphere drag coefficient against particle Reynolds number appears to be used by almost all investigators to evaluate the force on a solids particle being accelerated by the surrounding fluid medium. This drag curve has been obtained by many workers from measurements of the drag force on a single sphere moving at constant velocity in still, isothermal, incompressible fluid of effectively infinite extent. When one compares this with conditions in gas-solids flows where the solids particle is present in a moving, often accelerating turbulent fluid stream, possibly of temperature different from that of the particle, and in the presence of many other particles and near to the containing duct walls, the above assumption appears quite sweeping. Because, however, there is very little other data available and also since, as shown by the review paper of Torobin and Gauvin, measurements of drag coefficient at any but the above conditions appear to produce conflicting results, the standard drag curve will continue to be used. A further reason appears to be that as far as can be gathered from the limited experimental data available, the use of the standard drag curve leads to fairly reasonable results. Earlier workers tended to use "Stokes Law", often when it was not

applicable, that is at particle Reynolds numbers greater than about 0.1, but with the adoption of computer solutions a more complicated expression for C_D presents no great difficulty.

Like the drag coefficient, the Nusselt number for a sphere has a theoretical solution only for the Stokes flow regime. In order, therefore, to determine the heat transfer between gas and solids particles, experimentally derived expressions for the Nusselt number, in the particle Reynolds number range encountered are usually employed. As with the drag coefficient, the Nusselt number may be influenced by other important effects, such as turbulence intensity, by the proximity of other particles and the containing duct walls. Besides these, another unknown could be radiative heat transfer for flows where the particles are very much hotter than the duct walls. The indications are, however, that thermal lag is normally less important than velocity lag.

Assigning numerical values to the skin friction drag coefficient is even more difficult for compressible gas-solids flows than it is for incompressible flows, due to possible variations with Mach number. Most measurements to date indicate that, for duct flow, the friction coefficient is considerably more influenced by the gas to wall drag than by the particle to particle and

particle to wall interaction, as long as the solids loading is not too great. It would be useful, therefore, to first consider the variation of skin friction coefficient with Mach number for pure gas flows. Kuethe (1956) indicated, from experimental results, that the skin friction coefficient for flow over flat plates decreases with increasing Mach number, for the same Reynolds number. However, the work of Mills and Cole (1956) with rough pipes, and Keenan and Naumann (1946) with smooth pipes suggest that up to a Mach number of unity the skin friction coefficient is reasonably constant, for flow in pipes at constant Reynolds number. Keenan and Naumann also indicate that for distances from the pipe inlet greater than 50 diameters, the skin friction coefficient remains approximately equal to that for incompressible flow up to Mach numbers considerably greater than unity, the Reynolds number again being kept constant.

Most workers to date have assumed a constant solids particle size in their solution of particular gas-solids flow problems. With the use of the digital computer, however, it is possible to arrange for the programme to take into account the particle size distribution, though this would considerably complicate the problem. Some workers, notably Klingel and Kriebel, are now devising programmes to take the solids particle size dis-

tribution into account.

Almost all workers have made the assumption that the solids density is so great in comparison with the gas density, that the solids volume may be neglected in the basic equations. Rudinger in a recent paper (1965) has looked into this assumption in rather more detail. He derives a relationship to show that the particle contribution to the pressure can be neglected even at extremes of density ratio and mass ratio, as long as the particle is larger than a few hundredths of a micron. His equation relating the solids particle volume fraction to the density ratio and loading ratio indicate that the particle volume fraction may become significant if the density ratio, or the loading ratio, or both become sufficiently large.

2.2.4. Experimental Work.

As stated previously, relatively few experimental measurements have been made on high speed gas-solids flows. Summaries of some of the those undertaken recently are given by Kliegel and Hoglund. In both of these papers the experiments of Brown, 1962, and Carlson, 1962, are reported. Brown used a high speed framing camera to measure the velocity of solids particles or groups of particles emerging from a rocket engine. Since no measurements

of the solids particle size is available, it is difficult to compare his results with any theoretical calculations. Kliegel, however, has made some comparison by calculating the velocities for three different particle sizes. His calculations are based on assuming that the Stoke's flow regime applies and that over the flow region considered there is constant fractional velocity lag between the gas and solids particles. By making these assumptions, the solids particle momentum equation is readily integrated to give

$$d_p^{\,2} = \frac{18\,\mu\,L}{\rho_p\,u_g} \cdot \frac{1-k}{k^2}$$

The agreement between experimental and calculated values of solids velocity is not particularly good, but considering the assumptions made the agreement obtained indicates that the method of calculation is on the right lines. Similarly, Carlson's measurements of thermal lag showed that the measured lags were in good agreement with those calculated.

In a recent paper (1965) Fulmer and Wirtz have made measurements of individual particle velocities in a simulated rocket exhaust. The technique adopted was to take two precisely timed photographic exposures of solids particles issuing from a nozzle. Knowing the time between exposures and the distance

between the streak-type images obtained on the film, they determined the velocity of the solids particles. They compared the ratio of solids velocity to gas velocity with theoretical values derived from one-dimensional gas-solids particle flow equations, assuming a constant particle to gas velocity ratio. They also appear to have made the assumption that the particle Reynolds number was such that the Stokes flow regime applied, in which case their equation relating the velocity fractional lag to the solids particle diameter would be similar to that given above by Kliegel. The trends of their experimental and theoretical curves are in good agreement, but the measured velocity lag was not as great as that predicted by the theory.

The above literature review indicates that there is still a large amount of work to be undertaken in the field of high speed gas-solids flow, in order that a fuller understanding of the mechanism of the flow may be obtained. The regimes in which little or no work seems to have been undertaken are those for flows in which wall friction and particle to particle interference effects cannot be ignored, and where the solids particle diameter and the solids to gas loading ratio are no longer small.

CHAPTER 3.

THEORETICAL ANALYSIS.

A theory is presented to cover the one dimensional flow of a compressible gas-solids mixture through constant area ducts with wall skin friction, and also through ducts where the area is no longer constant but where skin friction can be neglected. The expressions are restricted to adiabatic flow, i.e. the energy conveyed per second at any point in the flow is constant. The assumptions regarding this flow are the same as those made by other workers, and are listed in Section 2.2. The exception to this is that in certain parts of this analysis, solids volume will be included and only considered negligible in order to obtain the simpler solution.

The basic fluid dynamic and thermodynamic equations relevant to the one dimensional flow of a gas-solids mixture are listed in Section 2.2, but are here considered in more detail. The solids volume is assumed negligible in these equations.

Gas Continuity Equation: $W_g = A\rho_g u_g$

Dispersed Solids Continuity Equation: $W_s = A\rho_s u_s$

where ρ_s is the solids mass per unit volume of mixture.

Gas Equation of State: $p = \rho_g RT_g$

Overall Momentum Equation - Expressing the overall change in momentum along the duct: $\rho_g u_g A du_g + \rho_s u_s A du_s + A dp + F = 0$

where F is the frictional force taking into account the skin friction between gas and pipe wall, and also the loss in momentum due to collisions between particles and particles, and particles and duct wall.

This frictional force is considered as a shear force and will be expressed as though it comprised the pure gas flow to duct wall skin friction plus a factor to take into account the presence of the solids particles. It is expressed in terms of a Fanning type friction equation:

$$F = \tau_o . s . d\ell \quad = \quad Cf . \frac{1}{2} \rho_g u_g^2 . \pi D d\ell$$

where D is the pipe diameter or non-circular duct equivalent diameter.

Conservation of Energy Equation.

This is considered in the form of the total energy conveyed per second remaining constant and equal to that available at initial conditions when the flow velocity is so low that the

kinetic terms are negligible. For this condition the gas and solids temperature are assumed equal.

$$W_g \frac{u_g^2}{2} + W_s \frac{u_s^2}{2} + W_g C_p T_g + W_s C_s T_s = W_g C_p T_{go} + W_s C_s T_{go}$$

Solids Particle Momentum Equation.

This expresses the momentum exchange between a single solids particle and the surrounding gas.

Mass of Particle x rate of change of velocity = Particle-surrounding gas drag force

$$m_p \cdot u_s \frac{du_s}{d\ell} = C_D \cdot \frac{1}{2} \rho_g (u_g - u_s)^2 \times a_p$$

where the conventional fluid dynamics expression for drag force is used, i.e. Drag Force = Drag Coefficient x dynamic head x projected area;

and the value of C_D for a sphere is that given by the Standard Drag Curve.

Solids Particle Heat Transfer Equation.

This expresses the ratio of heat exchange between a single solids particle and the surrounding gas.

Mass of particle x specific heat x rate of change of temperature = Rate of heat transfer by convection.

$$m_p.C_s.u_s \frac{dT_s}{d\ell} = h.(T_s - T_g).a_s$$

where a_s is the surface area of a solids particle. Here the thermal conductivity of the solids material is assumed to be so much greater than that of the gas, and size of the particle sufficiently small for the temperature of the solids particle to be uniform.

The above seven equations, three of which are differential equations, contain the following eight variables:- p, ℓ, u_g, u_s, T_g, T_s, ρ_g and ρ_s, it being assumed that the heat transfer coefficient h can be expressed in terms of the other variables, and that the friction coefficient Cf is a known constant. A solution where the variables are expressed in terms of a selected variable, such as length ℓ is therefore theoretically possible, and solutions to the equations are now presented for the idealised cases of equilibrium flow and constant fractional lag flow, and also a numerical method requiring a digital computer to give a more realistic solution.

3.1. Equilibrium Flow.

As indicated in Section 2.2 for this idealised flow the solids particles are always assumed to be travelling at

the same velocity, and to have the same temperature as neighbouring gas particles. With this assumption, two of the above equations, the particle momentum equation and the particle heat transfer equation are no longer applicable. In Appendix 1 the solution to the remaining equations is given for equilibrium flow together with that for constant fractional lag flow, and in these solutions, the solids volume is not neglected. Only an outline of the technique adopted is given here.

As for the one dimensional flow of gases, the method of solving the equations is to express the variables, made non-dimensional by expressing them as ratios of some reference condition, such as for pipe flow the pipe exit condition, in terms of a Mach number. This then introduces a further equation to express the velocity of sound. The equation derived to express the velocity of sound in an equilibrium flow is:

$$a_e = (1 + y)\sqrt{\frac{nRT_g}{(1 + x)}}$$

where y is the ratio solids volume to gas volume

and x is the ratio of solids mass flow rate to gas mass flow rate.

For equilibrium flow, n is the ratio of the specific

heat of the mixture at constant pressure to that at constant volume and is given by

$$n = \frac{\gamma + x\beta}{1 + x\beta}$$

where β is the ratio of solids specific heat to constant volume gas specific heat. It can be seen for the condition $y = 0$ the above velocity of sound expression is similiar to that of Kliegel given in Section 2.2.1.

The concept of an equilibrium velocity of sound has in fact been considered previously in connection with the propagation of sound in a composite media. Urich and Ament in a paper published in 1949 suggested that the sonic mean velocity in a two phase flow is given by the expression

$$a_e^2 = \frac{E_m}{\rho m} = \frac{E_1 E_2}{(yE_2 + (1 - y)E_1)(y\rho_1 + (1 - y)\rho_2)}$$

where E_1, E_2, E_m and ρ_1, ρ_2, ρ_m are the elasticity Moduli and densities of the two constituents and the mixture, and y is the proportion of constituent 1 by volume. They obtain this by expressing $\rho_m = y\rho_1 + (1 - y)\rho_2$ and $\frac{1}{E_m} = \frac{y}{E_1} + \frac{1 - y}{E_2}$

Deriving an expression for $a_e^2 = E_m/\rho_m$ with symbols in line with those adopted in this project, as $E = \frac{\delta p}{\delta V/V}$, $\delta V_m = \delta V_s + \delta V_g$ and $\frac{1 + x}{\rho_m} = \frac{x}{\rho_p} + \frac{1}{\rho_g}$ then by substituting for

δV_m, δV_s and δV_g, and expressing the volumes in terms of the densities and ratio of masses x, the following expression is obtained

$$a_e^2 = \frac{(1 + y)^2 E_s E_g}{(1 + x)\rho_g (yE_g + E_s)}$$

then assuming that $E_s \gg E_g$ as is the case for gas-solids mixtures and that the relationship PV_g^n = a constant, applies to the gas-solids mixture (see Appendix 1)

$$\text{then } E_g = \frac{dp}{dV_g} \cdot V_g = np$$

and the above expression becomes:

$$a_e^2 = \frac{(1 + y)^2 np}{(1 + x)\rho_g}$$

It may be noted that if the solids are perfect insulators, then the isentropic expression PV_g^{γ} = a constant, applies, and the above equation becomes:

$$a_e^2 = \frac{(1 + y)^2 \gamma p}{(1 + x)\rho_g}$$

Urich and Ament state that the relationship has been found to hold for many typical suspensions and emulsions. While the concept may be thought to be sensibly true for particles extremely small compared with a wave-length, it will obviously fail to hold

eventually as the particles become larger. Bromoform-in-water and mercury-in-water emulsions they found have sufficiently high density difference between particles and fluid to give measurable difference between an experimentally obtained sonic velocity and that derived from the above equation for particle sizes in the micron range.

With this velocity of sound assumption, the remaining equations are quite easily manipulated into the required form. For the condition that the volume of the solids particles is negligible, the equations relating the flow variables to those at stagnation or total conditions, the adiabatic flow with friction in a constant area duct, the flow through a normal shock wave, and the Prandtl-Meyer expansion process are all similar to those for pure gas flow except that the Mach number is now the ratio of velocity to equilibrium sonic velocity, and the index n is that given above.

3.2. Constant Fractional Lag Flow.

The criteria for constant fractional lag flow are that the ratios of solids velocity to gas velocity, and solids temperature to gas temperature should remain constant throughout the flow. Though in this case the temperature referred to

is the differential temperature from stagnation conditions:

i.e. $u_s = ku_g$ and $Tg_o - T_s = j\ (Tg_o - T_g)$. Because of the number of variables involved it is not generally possible to obtain direct solutions to either the particle momentum equation or the particle heat transfer equation to predict the constant fractional lags. The result is that these two equations are not really applicable for this flow either.

The method of solving the equations and presenting the solutions appears in Appendix 1, but some of the more important aspects will be considered here. Unlike equilibrium flow, the velocity lag in this flow results in the mass ratio of solids to gas in unit volume of mixture being no longer equal to the ratio of solids to gas mass flow rates W_s/W_g. It is, in fact, equal to W_s/kW_g, with the result that the compressible flow index for the mixture now contains the constants k and j and the variable y.

$$n = \frac{\gamma + xj\beta}{(\gamma + xj\beta) - (1 + y)(\gamma - 1)(1 + xk^2)/(1 + xk) + (\gamma - 1)ly}$$

It can be seen for the condition $k = j = 1$ this expression is similar to that for equilibrium flow.

Although for equilibrium flow, the flow index n must lie between the values 1 and 1.4, the value 1 corresponding to x very large and hence isothermal flow and the value 1.4 to isentropic flow, these limitations do not apply to constant fractional lag flow. For this flow n has no limitation (except to be greater than 0). In fact it would appear that in an expansion process a value less than 1.4 would indicate that the energy transfer is from solids to gas, whilst a value greater than 1.4 indicates the energy transfer is from gas to solids. This is similar to the case of the expansion of a pure gas, which at the same time is made to take in heat and for this process the expansion index in the equation PV^n could be less than unity (Ref. Rogers and Mayhew).

The velocity of sound concept adopted for this flow is that constant fractional lag of velocity and temperature is maintained as a disturbance propagates through the mixture. The resulting velocity of sound expression is

$$a_m = (1 + y)\sqrt{\frac{\gamma R T_g}{(1 + xk)}}$$

It is interesting at this stage to consider some of the implications of this sonic velocity expression for the case

of negligible solids volume. If a flow is such that the fractional lags are equal and very large, so that there is practically no momentum or heat exchange between gas and solids, then as $k = j \rightarrow 0$, $n \rightarrow \gamma$, and the mixture sonic velocity is equal to the gas sonic velocity. At the other extreme, for a flow where $k = j = 1$ (i.e. equilibrium flow) the ratio of a_m/a_g now attains a minimum. Fig. 2 shows curves of a_m/a_g against k for various values of x and the extreme values of j. These curves were obtained for a powder with a specific heat of 0.32 C.H.U./lb.$^{\circ}$C. The curves would indicate for any pumping process, such as the flow of a gas solids mixture through a fan, that the critical condition of the gas velocity becoming equal to the sonic velocity might well occur at a much lower air velocity than if the fan were merely handling pure air. In the design of such a pumping device, therefore, this limitation might be of some importance.

In Appendix 1 it is shown that for the case of solids volume negligible it is possible to obtain compressible flow equations similar to those for pure gas flow. For constant fractional lag flow these are all obtained in terms of the compressible flow index n and the mixture Mach number, defined as u_g/a_m.

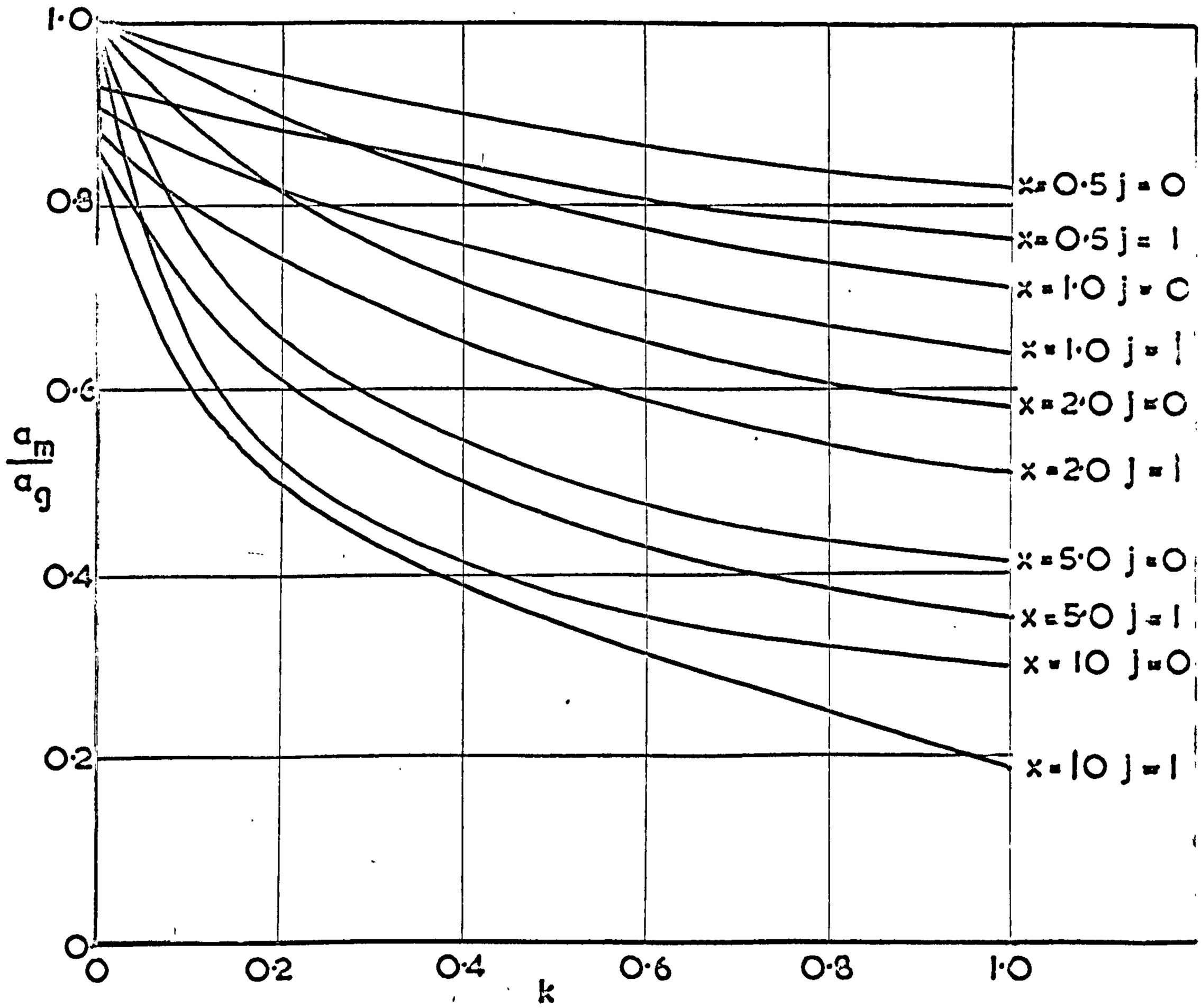

FIG 2 RATIO OF MIXTURE VELOCITY OF SOUND TO GAS VELOCITY OF SOUND FOR VARYING CONSTANT FRACTIONAL LAG PARAMETERS k AND j AND LOADING RATIO x

Equation 35 in Appendix 1 indicates that, as for pure gas flow, the expression obtained relating the Mach number and the gas velocity to the area, in a duct of varying area, if friction is neglected, is such as to predict a mixture Mach number of unity at a throat in the duct. Again, similarly to pure gas flow neglecting friction, for a mixture Mach number less than 1 a converging duct results in an accelerating flow and a diverging duct in a decelerating flow, whilst for $M_m > 1$, a converging duct gives a decelerating flow and a diverging duct an accelerating flow. This equation might be compared with the similar equations of Kliegel given in Section 2.2.1, expressed in terms of the gas Mach number and equilibrium flow Mach number. His equations showed that at a throat the gas Mach number was certainly not equal to unity, though an equilibrium Mach number could well be. The inclusion of solids volume in equation 35 appears to have the effect of reducing the friction term coefficient compared with this expression when solids volume is neglected. This reduction in the friction term on considering solids volume has the effect of decreasing the Mach number compared to flow with $y \rightarrow 0$, and results from the change in effective flow area due to the presence of the solids.

In Fig. 3 are shown curves of p_o/p and A/A^* against M_m for the flow of gas-solids mixtures with varying n values. In Fig. 4 the curves of p/p^* and $4C_f(\ell^* - \ell)/D(1 + xk)$ against M_m also with varying n values are given for the adiabatic flow with friction in a constant area duct for gas-solids mixtures. These curves are applicable to both constant fractional lag flow and to equilibrium flow.

At this stage, it is useful to try to gain some idea of the error involved in the constant fractional lag theory when the solids volume is neglected. In order to do this, the equations relating the temperature ratio for adiabatic flow are considered with numerical values substituted. For solids volume included:

$$M_m^2 = \frac{2}{N(1 + y)^2} \cdot \left(\frac{Tg_o}{Tg} - 1 \right) \left[\frac{n}{n - 1} + \frac{k(1 + xk)}{(1 + xk^2)} \left(\frac{Tg_o y_o - Tgy}{Tg_o - T_g} \right) \right]$$

$$\text{where } y = y_o \left(\frac{Tg_o}{Tg} \right)^{\frac{-1}{n-1}}$$

N is the index for solids volume included and n the index for solids volume neglected. If the case k = 1 is considered, N = n and there is no need to define values of j and x.

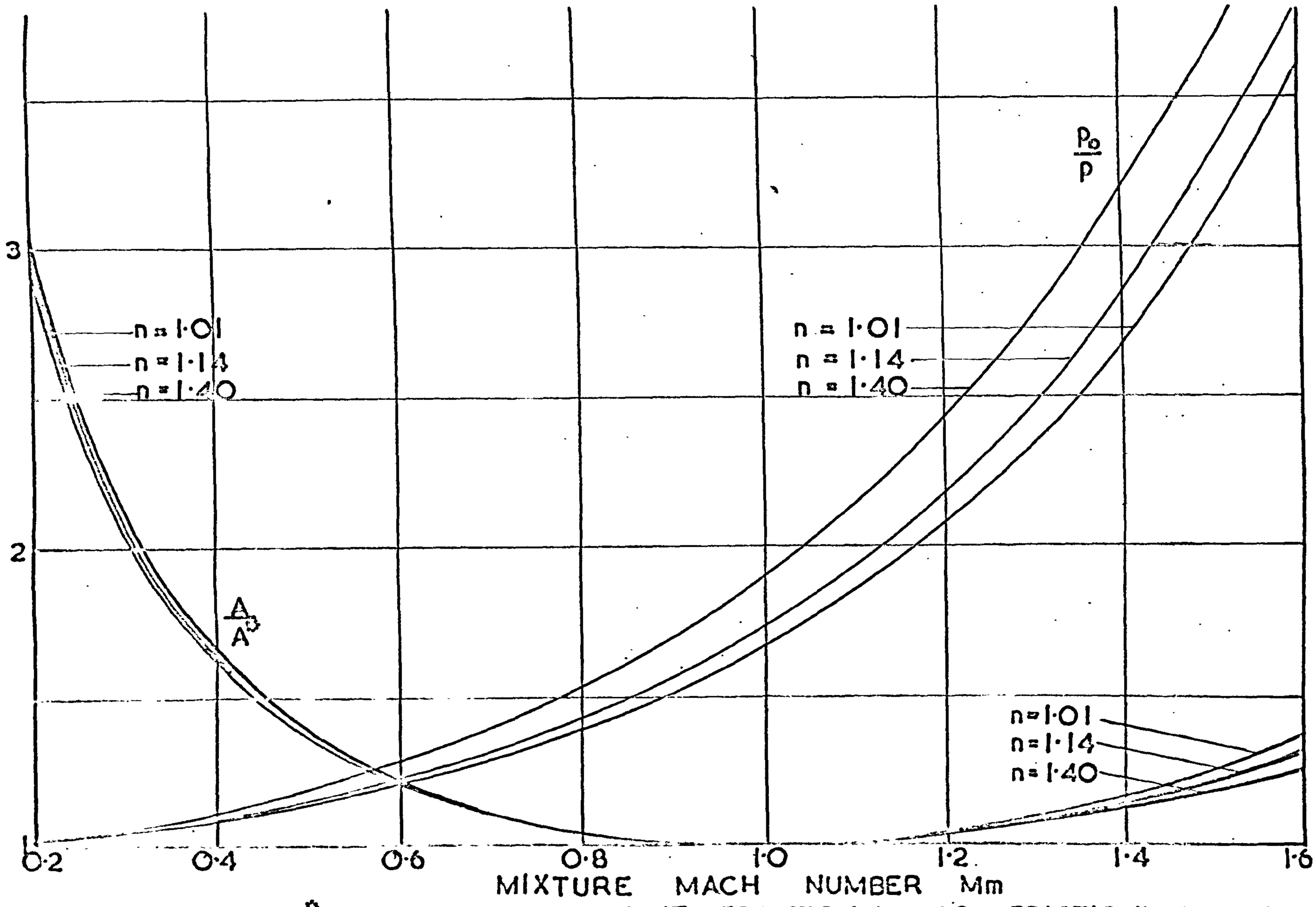

FIG 3 p_o/p AND A/A^* — Mm FOR CONSTANT FRACTIONAL LAG FRICTIONLESS ADIABATIC FLOW OF GAS-SOLIDS MIXTURES WITH VARYING n VALUES

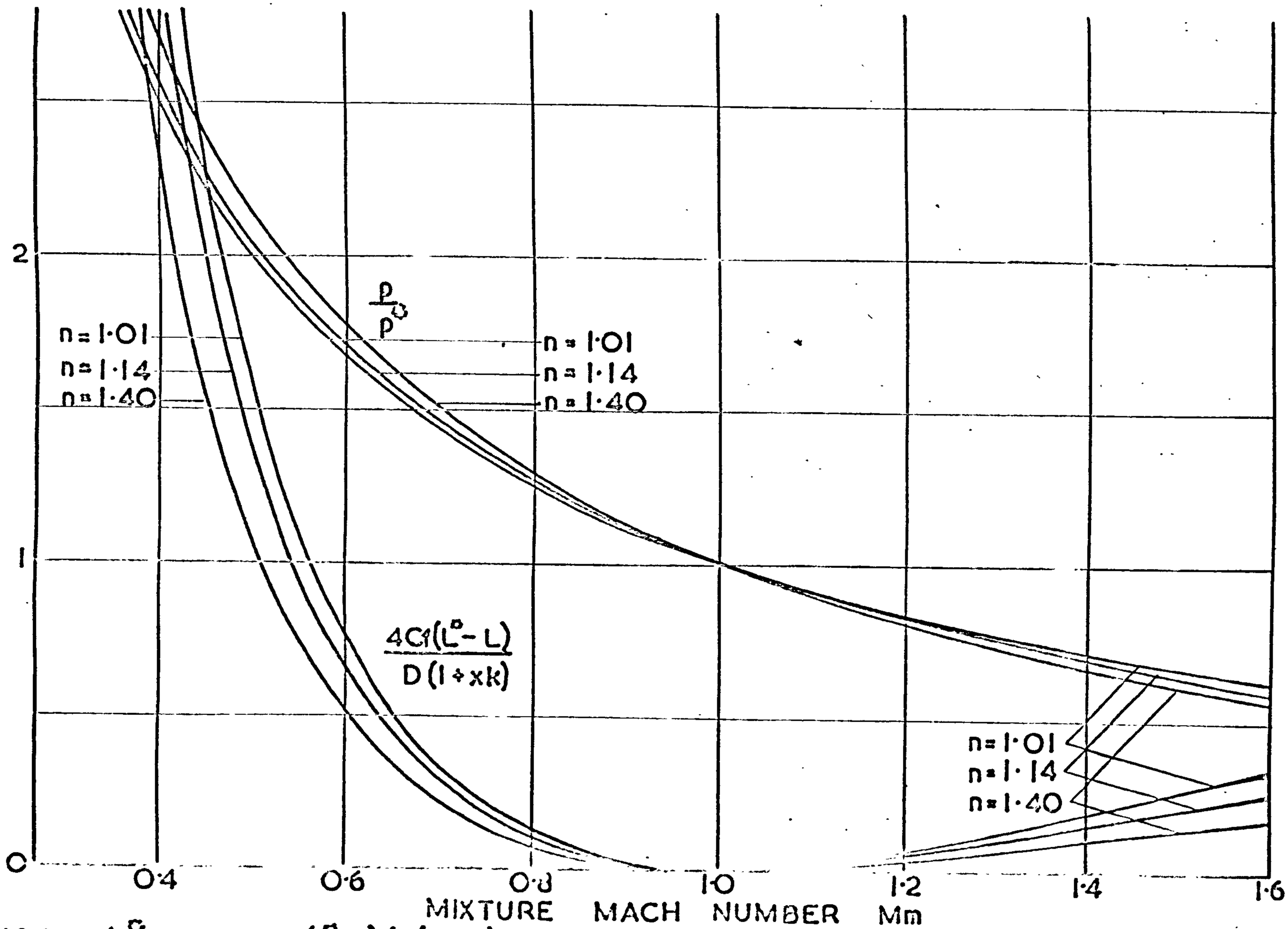

FIG 4 p/p° AND $4C_f(L^{\circ}-L)/D(1+xk)$ — Mm FOR CONSTANT FRACTIONAL LAG ADIABATIC FLOW OF GAS-SOLIDS MIXTURES WITH VARYING n VALUES

For the case $y \rightarrow 0$, i.e. solids volume negligible:

$$M_m^2 = \frac{2}{n-1}\left(\frac{Tg_o}{Tg} - 1\right)$$

Consider the case $y_o = 0.2$, $n = 1.14$ and $Tg_o/Tg = 1.6$ then for solids volume included $M_m = 2.995$ and for solids volume neglected and $M_m = 2.995$, $Tg_o/Tg = 1.63$, i.e. neglecting solids volume overestimates the temperature ratio by $< 2\%$.

For similar conditions but with $M_m = 1$, then neglecting solids volume overestimates the temperature ratio by $< 0.6\%$, whilst for $M_m < 1$ the error becomes even less, though now neglecting solids volume underestimates the temperature ratio. The n value of about 1.14 appears to give rise to the maximum error, as on increasing or decreasing n from this value, the errors tend to reduce.

Substituting the above values of Tg_o/Tg into the frictionless flow equation in order to determine values of the total pressure to static pressure ratio, gives the following:

$$\frac{p_o}{p} = \left(\frac{Tg_o}{Tg}\right)^{\frac{n}{n-1}}$$

for $M_m = 2.995$, $p_o/p = 45.9$ considering solids volume, and 53.5 when neglecting solids volume. There is, therefore, an overestimate in this case of 16.5%. For $M_m = 1$, neglecting solids

volume overestimates the pressure ratio by 4.1%. The reason for estimating the error in pressure ratio is because this gives the worst case as it contains the highest index value of all the relationships for a given n value.

For flows in a constant area duct, because the temperature ratio is now $T/T^* = T.T_o/T_o.T^*$ and the square root of this is also usually required, the error in neglecting solids volume is very much less than that for the previously considered case. From the practical aspect, a solids to gas volume ratio at initial conditions of $y_o = 0.2$ represents a W_s/W_g value of 13 at about 13 atmospheres pressure, for polystyrene powder of specific gravity 1.06.

The above shows that for the conditions considered, the worst errors incurred in applying constant fractional lag theory with neglected solids volume, as compared with considering the solids volume, are when the value of n is low, the value of M_m is high, and the equation PVg^n is considered to apply.

3.3. Finite Difference Solution of the Equations.

The equilibrium flow and constant fractional lag flow concepts of considering the gas solids flow problem, although they have the advantage of enabling the basic equations to be solved

(though for the constant fractional lag case they do not offer a means of solving the particle equations of momentum and heat transfer), suffer from the simplicity of the basic assumptions. For most flow problems there would appear to be good reasons for believing that the solids particles are neither in equilibrium with the gas nor maintaining constant fractional lag with the gas. In fact, for many compressible flow conditions, it would appear that the gas and particles may possibly be in equilibrium at the onset of the flow, but due to the accelerating nature of the flow, the lags continue to increase with increasing distance from the starting condition. This is almost certainly the case for flow through long constant area ducts and for convergent-divergent nozzle flow without shocks. A more realistic solution to the problem would, therefore, require that the velocity and temperature fractional lags should be considered as variables. With this specification, the basic equations are no longer readily solved, and it is necessary to resort to a finite difference technique.

For this condition, expressing in terms of a Mach number no longer leads to any appreciable simplification, so that an expression for sonic velocity is no longer vital. The mixture Mach number defined in 3.2 is not strictly applicable to flows

where k and j are varying. If their variation is small, however, no appreciable inaccuracy will be incurred in using this expression.

The difficulties in obtaining solutions would now appear to be in finding suitable expressions for the solids particle drag coefficient C_D, the solids particle Nusselt number, defining an effective solids particle diameter, and assuming that the frictional drag between gas and duct wall and the particle to wall and particle to particle interaction can all be expressed as a Fanning type equation, the method of evaluating this friction factor.

3.3.1. Solids Particle Drag Coefficient.

As has been stated in Section 2.2.3, most workers tend to use the "Standard Drag Curve" or an expression fitting this curve to assign values to C_D. The limitations of adopting this technique have previously been stated and will not be investigated here. It should be mentioned, however, that there appears to be a wide divergence of opinion as to what happens to the drag coefficient in a rapidly accelerating flow. Part 3 of Torobin and Gauvin's paper shows that some workers predict that the drag coefficient becomes greater than that given by the Standard Drag Curve, whilst others state it becomes less. There appears to be

a tendency, however, for the drag coefficient to approach that given by the Standard Drag Curve when the acceleration parameter $\dot{u}_p d_p / u_p^2$ is small, and this parameter would be expected to be small for small particle diameters and large particle velocities which is the case for maximum acceleration in pipe flow. It also appears from the limited experimental results available, that the use of the Standard Drag Curve does not lead to great inaccuracies.

For the Reynold's number range up to about 0.1, that is purely viscous flow, the drag between a solids sphere and the surrounding gas is theoretically given by the Stokes equation, which can be expressed as $C_D = 24/Re_p$. To cover the range up to $Re_p = 5$, Oseen put forward the theoretical expression $C_D = 24\ (1 + 0.188\ Re_p)/Re_p$ and this allows for inertial terms in the flow field away from the body. Above a Reynolds number of 5, there appears to be no theoretical expression for C_D available, so that any expression is really a "fit" to the experimental curve. Serafini (1954) has suggested that the expression $C_D = 24\ (1 + 0.158\ Re_p^{2/3})/Re_p$ gives reliable results for C_D over the range $0.5 < Re_p < 500$, and this expression has the advantage of reducing to the Stokes equation for small values of Re_p. In Fig. 5 is given the Standard Drag Curve together with the "fit" of Serafini's expression, and this has been extrapolated to $Re_p =$

800. It can be seen from the curve that above $Re_p = 800$, C_D can be considered reasonably constant with a value of about 0.44.

3.3.2. Solids Particle Nusselt Number.

As stated in Section 2.2.3, a similar difficulty applies in attributing values to the particle Nusselt number, as is the case for the particle drag coefficient. Like the drag coefficient, the Nusselt number has a theoretical solution over the Stokes flow regime, and that for particle Reynold's numbers greater than about 0.1 empirical expressions have to be relied upon. The theoretical solution for heat transfer from a sphere for the symmetrical Stokes flow field can be obtained by equating the rate of heat loss from the sphere by conduction to the rate of heat transfer by convection.

Heat loss by conduction, by integrating $Q = -k_g A dT/dr$

gives as $r \rightarrow \infty$, $Q = 4\pi k_g r(T_1 - T_2)$

By convection $Q = 4\pi h r^2 (T_1 - T_2)$

then the Nusselt number, $Nu = hd/kg = 2$.

In their book "Fluid Dynamics and Heat Transfer", Knudsen and Katz give an empirical expression derived from the experimental results of many workers, mainly on the flow of water droplets, but this expression is recommended by them for the prediction of

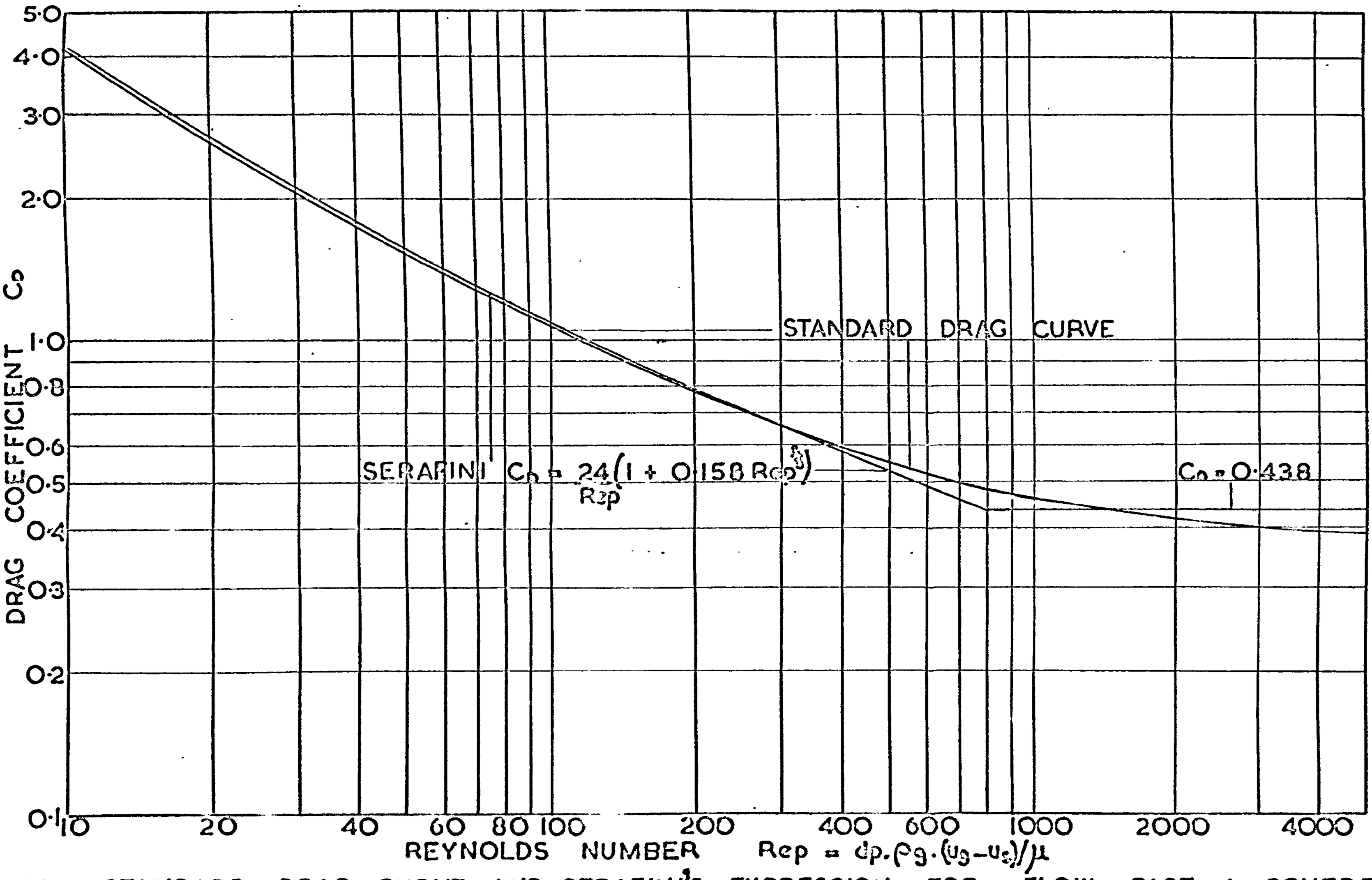

FIG 5 STANDARD DRAG CURVE AND SERAFINI'S EXPRESSION FOR FLOW PAST A SPHERE

average Nusselt numbers for the flow of fluids past spheres. The expression takes the form:-

$$Nu = 2 + 0.6(Pr)^{1/3}.(Re_p)^{1/2}$$

and is applicable for $1 < Re_p < 70{,}000$ and $0.6 <$ Prandtl number $Pr < 400$.

3.3.3. Solids Particle Mean Diameter.

For gas-solids flow in which the solids particles are present as a wide size distribution, (such a powder is usually referred to as polydisperse), some method of defining an effective particle diameter is required if a single set of basic equations is to be used. Allowing for a variation in solids diameter will be considered later, and it will then be seen that this added complexity makes solution considerably more difficult.

One method of assigning a diameter to a polydisperse powder is to obtain the arithmetic mean diameter from a size analysis of the actual powder (e.g. from a sieve analysis). This is very simple for a powder consisting of spherical particles, but where the particles are not spherical, it is necessary to assume a particle diameter by other means. The assumption of an equivalent-volume sphere or even an equivalent-surface area sphere are possibilities not requiring too much experimental work

for their application. They would probably only involve measuring the volumes or surface areas of a few of the particles, and assuming the bulk of the particles to be of similar shape.

The arithmetic mean diameter is given by:

$$\bar{d}_p = \sum n_p d_p / \sum n_p$$

where n_p, the number of particles of size d_p is given by

$$n_p = \sum m_p / \frac{\pi d_p^3}{6} \rho_p,$$

and m_p is the mass of particles of size d_p.

A further definition of effective solids diameter, possibly more applicable to gas-solids flow, is obtained from the equation for the fluid drag force on a body. If in this equation the drag coefficient and gas-solids velocity difference are assumed constant both for the polydisperse powder and uniform size powder representing it, the following is obtained:

$$(\sum n_p) . C_D . \frac{1}{2} \rho_g (u_g - u_s)^2 \bar{a}_p^2 = \sum (n_p C_D \frac{1}{2} \rho_g (u_g - u_s)^2 . a_p^2)$$

$$\text{then } \bar{a}_p^2 = \frac{\sum (n_p a_p^2)}{\sum n_p}$$

where a_p is the particle projected area.

If an equivalent-volume sphere is assumed, and this would be reasonable for rounded particles, the above expression

becomes

$$\bar{d}_p^{\,2} = \frac{\sum n_p d_p^{\,2}}{\sum n_p}$$

and a definition of $\bar{d}_p$ similar to this is often known as the Surface Mean Diameter (Reference J.M. Kay).

A further concept of effective diameter, which will be referred to as the aerodynamic effective diameter d_{ma}, is possible if the frequency of size distribution of the powder conforms to a Normal Distribution Curve. With this assumption, it will be shown in Appendix 1 that the relationship between aerodynamic effective diameter and arithmetic mean diameter is

$$d_{ma}^{\,2} = \sigma^2 + d_m^{\,2}$$

For none of the above effective diameters will the mass of the assembly of equivalent diameters be necessarily the same as that for the actual powder, though in all cases the number of particles is the same. This would appear reasonable for gas-solids flow as gravity effects are usually ignored in horizontal conveying.

3.3.4. Gas-Solids Friction Factor.

The method of assigning values to the friction factor $4C_f$ is not well defined. As shown in Section 2.1.1. some workers

in the incompressible flow region (e.g. Hinkle and Peskin & Dwyer) neglect the particle to particle and particle to wall interaction, and assume the gas-solids flow friction factor to be the same as the skin friction factor for pure gas flow at the same Reynold's number and pipe wall roughness. This would appear to be too great a simplification, and was probably responsible in Peskin & Dwyer's work for at least part of their lack of agreement between theoretical work and experimental. In this project, therefore, the value of $4C_f$ will be obtained from the experimental results.

With the above assumptions the basic equations can now be put in the form:

Gas Continuity Equation $W_g = A\rho_g u_g$

Dispersed Solids Continuity Equation $W_s = A\rho_s u_s$

Gas Equation of State $p = \rho_g R T_g$

Overall Momentum Equation - by substituting $u_s = ku_g$, $du_s = kdu_g$, $W_s = x W_g$ and for F in the previous equation

$$(1 + xk)\, \rho_g u_g du_g + dp + \frac{4C_f}{D} \cdot \frac{\rho_g u_g^2}{2}\, d\ell = 0$$

Overall Energy Equation - by substitutions similar to those above and isolating T_g.

$$T_g = T_{go} + x \frac{C_s}{C_p} \cdot T_{go} - x \frac{C_s}{C_p} \cdot T_s - (1 + xk^2) \frac{u_g^2}{2JC_p}$$

Solids Particle Momentum Equation

$$\frac{du_s}{d\ell} = \frac{3}{4} \cdot C_D \cdot \frac{\rho_g}{\rho_p} \cdot \frac{u_s}{d_p} \left(\frac{1}{k} - 1\right)^2$$

Solids Particle Heat Transfer Equation

$$\frac{dT_s}{d\ell} = \frac{6 \text{ Nu } k_g (T_s - T_g)}{d_p^{\,2} \rho_p C_s u_s}$$

The solution of the above equations for given initial conditions and by making use of the experimentally derived pressure drop curves for pipe flow is now considered, first by "hand" solution and then by computer solution.

3.3.5. Hand Solution.

The method adopted here is to solve the three differential equations by expressing them as the first two terms only of a Taylor expansion series, and hence, by also making use of the four ordinary equations, obtain solutions at small intervals of distance over the whole flow. It is realised that this is a very crude and time-consuming method, but as long as the variables are not changing too rapidly, such as in the case of pipe flow, it does give a possible solution.

The Taylor expansion may be expressed as:

$$y_{n+1} = y_n + h\, y_n' + \frac{h^2}{2} y_n'' + \text{higher powers}$$

applying the first two terms of this to, say, the solids particle momentum equation gives

$$u_{s2} = u_{s1} + h \left(\frac{du_s}{d\ell}\right)_1$$

where h is the incremental distance.

It is immediately apparent that in order to proceed with this method, initial values of u_s, T_g and T_s are required as well as values of $dp/d\ell$, to solve the overall momentum equation. The most reasonable assumption is to consider that for flow through a long pipe, far upstream the solids velocity and gas velocity, and solids temperature and gas temperature could be considered almost equal. The values of $dp/d\ell$ and the initial pressure far upstream are obtained from the experimental pressure drop curve.

3.3.6. Computer Solution.

As with the hand solution method, the three differential equations are solved numerically, though in this case the Runge-Kutta fourth order method of solving an ordinary first order differential equation is used, (Reference W.E. Milne). This method has the advantage over other numerical methods in that the derivatives are not required, and also that the step from y_n to y_{n+1} is made without the use of values of y preceeding y_n and so no special methods are required to start the computation. The

expression used for solving a differential equation has the form:

$$y_{n+1} = y_n + (k_1 + 2k_2 + 2k_3 + k_4)/6$$

where $k_1 = h.f(x_n, y_n)$, $k_2 = h.f(x_n + \frac{1}{2}h, y_n + \frac{1}{2}k_1)$

$$k_3 = h.f(x_n + \frac{1}{2}h, y_n + \frac{1}{2}k_2), \; k_4 = h.f(x_n + h, y_n + k_3)$$

The computer programme is written so that it first "fits" a polynomial equation to the pressure drop readings, such that values of p and $dp/d\ell$ may be readily obtained for any position in the flow. The three differential equations are then solved by using the values of p and $dp/d\ell$ from the polynomial equation, the four ordinary equations together with the specified expressions for C_D, Nu and $4C_f$. In solving the differential equations, the incremental distance h is varied from relatively long steps at the upstream end of the pipe to much shorter steps as the flow acceleration increases. A check on the accuracy of the results is obtained by constructing a finite difference table and ensuring that the fourth order difference terms are small, (Reference K.S. Kunz).

The sequence of computer operations is as follows:

(a) A polynomial equation is fitted to the experimental readings as stated above, with the pressure and distance expressed in non-dimensional form.

(b) The value of u_g at the start of the pipe line is determined from:

$$u_g = \frac{W}{A\rho_g} = \frac{WRTg}{Ap}$$

by substituting for ρ_g from the gas equation of state $p = \rho_g RTg$, putting $Tg = Tg_o$, the experimentally determined total temperature and obtaining p from the polynomial equation.

(c) The value to be attributed to the friction factor $4C_f$ is now determined from the equation

$$\frac{dp}{d\ell} = 4C_f.\frac{\rho_g u_g^2}{2D}$$

(d) The value of u_s is obtained by putting $u_s = 0.999u_g$.

(e) The gas temperature is now determined accurately from the overall energy equation

$$Tg = (x\frac{C_s}{C_p} + 1)Tg_o - x\frac{C_s}{C_p}.T_s - (1 + xk^2)\frac{u_g^2}{2JC_p}$$

To do this for the initial position it is necessary to assume a value for T_s, and the most reasonable assumption is $T_s = T_g$ at this point. Although the initial velocity in (b) is determined from Tg_o, no great inaccuracy is incurred, as at this position Tg will only differ slightly from Tg_o.

(f) The gas density is determined from the gas continuity

equation $\rho_g = \frac{W}{Au_g}$. All the variables at the start of the pipe line having been determined, the three differential equations can now be solved.

(g) The gas velocity at the end of the first incremental step is given by the overall momentum equation

$$\frac{du_g}{dL} = \left(\frac{-P}{\rho_g u_g} \cdot \frac{dp}{dL} - \frac{4C_f \lambda u_g}{2D} \right) \cdot \frac{1}{1 + xk}$$

using the $4C_f$ value from the above and values of p and $dp/d\ell$ from the polynomial equation, where P and λ are the reference pressure and length used for non-dimensionalising.

(h) The equivalent solids velocity is given by the solids momentum equation

$$\frac{du_s}{dL} = \frac{0.75\lambda}{d_p \rho_p} \cdot C_D u_s \rho_g \left(\frac{1 - k}{k} \right)^2$$

where $C_D = \frac{24}{Re_p} (1 + 0.158\ Re_p^{2/3})$ for $Re_p < 800$ & $C_D = 0.438$ for $Re_p > 800$ and $Re_p = \rho_g d_p (u_g - u_s)/\mu$.

(j) The solids temperature at the end of the step is given by the solids heat transfer equation

$$\frac{dT_s}{dL} = \frac{6kg}{C_s\ d_p^2} \frac{\lambda}{\rho_p} \cdot \frac{Nu}{u_s} (T_s - T_g)$$

where $Nu = 2 + 0.53\ Re_p^{1/2}$, by assuming $Pr = 0.68$ over the

expected temperature range.

After the determination of u_g, u_s & T_s at the end of the incremental step, the procedure from (e) is repeated for the new conditions, and this is continued until the end of the pipe line is reached. The output from the programme then consists of values of the variables u_g, u_s, T_g, T_s and ρ_g at all the incremental positions along the pipe line.

This programme was later revised to also determine the values of k, j, n, the mixture velocity of sound and mixture Mach number. The value of j is given by:

$$j = \frac{T_o - T_s}{T_o - T_g}$$

Then from this value of j, and from k ($= u_s/u_g$) the value of n is determined from $n = (\gamma + xj\beta)/(\gamma + xj\beta - \frac{(\gamma - 1)(1 + xk^2)}{(1 + xk)})$ for the case $y \rightarrow 0$. Using this value of n, the mixture velocity of sound is: $a_m = \sqrt{nRT_g/(1 + xk)}$ and the mixture Mach number $M_m = u_g/a_m$.

3.4. Method of Solution for the Inclusion of Solids Particle Size Distribution.

The size distribution of a powder can usually be obtained experimentally (such as by sieve analysis) in the form of proportions

by weight of known sizes (or more likely small size distributions which can be assumed to be represented by one size.) This can be readily put in the form of the number of particles at each size, if an equivalent-volume sphere is assumed. It is then possible to write the basic equations such that this size distribution is taken into account. Each particle size has at any position in the flow its associated Reynold's number, drag coefficient, k value and temperature. The overall momentum equation, overall energy equation, solids momentum equation and solids heat transfer equation can then be written for each particle size and expressed as follows:

$$(1 + x_1k_1 + x_2k_2 + \ldots\ldots)\rho_g u_g \frac{du_g}{d\ell} + \frac{dp}{d\ell} + \frac{4C_f}{D}\cdot\frac{\rho_g u_g^2}{2} = 0$$

$$Tg = Tg_o + \frac{C_s}{C_p} Tg_o(x_1 + x_2 + \ldots\ldots) - \frac{C_s}{C_p}(x_1T_{s1} + x_2T_{s2} + \ldots\ldots) -$$

$$- (1 + x_1k_1^2 + x_2k_2^2 + \ldots\ldots)\frac{u_g^2}{2JC_p}$$

$$\frac{du_{s1}}{d\ell} = \frac{0.75\ C_{D1}}{d_{p1}\rho_p} u_{s1}\rho_g\left(\frac{1 - k_1}{k_1}\right)^2, \quad \frac{du_{s2}}{d\ell} = \frac{0.75\ C_{D2}}{d_{p2}\rho_p}\cdot u_{s2}\rho_g\left(\frac{1 - k_2}{k_2}\right)^2, \text{ etc.}$$

$$\frac{dT_{s1}}{d\ell} = \frac{6k_g}{C_s\rho_p}\cdot\frac{Nu_1}{d_{p1}^2\, u_{s1}}(T_{s1} - T_g), \quad \frac{dT_{s2}}{d\ell} = \frac{6k_g}{C_s\rho_p}\cdot\frac{Nu_2}{d_{p2}^2 u_{s2}}(T_{s2} - T_g), \text{ etc.}$$

Then by initially assuming at the start of the pipe line that $u_{s1} = u_{s2} = 0.999\ u_g$(say), $T_{s1} = T_{s2} = T_g$, and a size distribution for the powder giving values to d_{p1}, d_{p2} .... and x_1, x_2, ... etc. it is possible to proceed with a computer programme similar to that described in Section 3.3.6. In this case, however, when the point is reached where the solids velocities and temperatures are evaluated, successive numerical integrations would be performed to determine u_{s1}, u_{s2}, ... and T_{s1}, T_{s2} ..... etc., before the procedure from (e) in Section 3.3.6 is repeated with the new conditions.

3.5. Suggested Computer Solution for the Duct Flow Rig.

In Section 3.1, 3.2 and Appendix 1 it is shown that for equilibrium flow and constant fractional lag flow, solutions for gas-solids flow through a convergent-divergent nozzle and through a normal shock wave can be obtained in terms of the equilibrium or mixture Mach number. When k and j are allowed to vary throughout the flow, the difficulties in obtaining solutions are similar to those experienced for the flow in pipes. In this Section, a method of obtaining numerical solutions from given initial conditions and the experimentally determined pressure drop profile is suggested. The basic equations are similar to those for pipe flow, except that through the nozzle, because the cross-sectional area is no longer

constant, this must be allowed for in the continuity and overall momentum equations. The flow through the duct flow rig can be broken down into three parts:

(a) The flow in the parallel-walled duct up to the convergent-divergent nozzle. This flow is similar to the pipe flow and the same equations and computer programme can be used if initial conditions and the pressure drop curve are given, except that in this case an equivalent duct diameter is required. From the computer solution for this flow, numerical values of u_g, u_s, T_g, T_s and ρ_g can be obtained at entry to the nozzle.

(b) The flow in the convergent-divergent nozzle. If it can be assumed that shock-free flow occurs through the nozzle, then the equations defining this flow are all of those for duct flow plus an additional equation expressing the nozzle cross-sectional area in terms of distance along the nozzle. In this case, however, the overall momentum equation might be simplified by neglecting friction, as the length of flow involved is small. If this is so, the overall momentum equation can be integrated to give:

$$(1 + xk)u_g + \frac{A.p}{W_g} = \text{a constant}$$

so that there are now only two first order differential

equations to be solved.

(c) The flow through the normal shock wave. It should be possible from the experimental pressure drop curve obtained to determine the position of a normal shock wave, such that conditions up to the onset of the shock can be obtained similarly to those in (a). The suggested method for solving the flow through the shock is similar to that put forward by Kriebel (1964). In the initial gas shock (i.e. the distance over which the gas decelerates sharply) the distance involved would be sufficiently small and the solids particle inertia so high that it could be assumed there is no change in solids velocity or temperature over this distance. Because of this inability of the solids to respond to rapid changes, it would seem reasonable to assume that the solids take no part in this initial shock, and that the gas conditions at the termination of the gas shock are given by the normal shock equations for gas flow. In Reference Houghton and Brock, tables are given such that values of gas temperature, gas velocity and gas density can be evaluated from the gas Mach number on the upstream side of the shock. Verification of this assumption might be obtained by comparing the experimental pressure drop profile with the pressure drop across the shock predicted from the normal shock gas flow

equation given in the above Reference. The experimental difficulties in measuring the pressure drop, however, are quite large, due to the difficulty in predicting the position of the shock.

At the termination of this gas shock, the numerical values of all the variables are now known. The flow in the relaxation region (following the initial gas shock) where the solids particles undergo momentum and heat transfer changes, such that their velocity and temperature approach that of the gas, can be obtained from a computer solution for the equations used for the flow in (a).

CHAPTER 4.

DESCRIPTION OF RIG.

4.1 Pipe Flow Rig

The rig was initially designed for pipe flow experiments, but the construction was such that at a later stage in the project modifications could be made to the experimental section to incorporate a rectangular duct with transparent walls. With this in mind, the entrainment and separation equipment for introducing the solids into and separating them out of the gas flow, were designed to suit pipe flow and duct flow experiments.

Due to the large amounts of gas required to achieve compressible flow conditions it is only possible to use air as the flow medium. The air supply is from two Ingersoll-Rand two stage reciprocating compressors with delivery ratings of 262.5 and 50 cu.ft. free air/min. Both deliver at a maximum pressure of 200 p.s.i. into an air receiver of capacity 250 cu.ft. Air for the rig is then led to a small air receiver, capacity approximately 1.5 cu.ft., fine and course air flow control being effected by valves, see Fig. 6. The small air receiver is available for taking air flow stagnation temperature and pressure measurements, with thermometer and Bourdon pressure gauge, prior to introducing the solids, but it is also of sufficient length to accept a heater

for the possible investigation of temperature effects if time had permitted. This receiver which was designed to B.S.3601 is capable of withstanding working pressures and temperatures of up to 300 p.s.i. and 500 °F. One of the end plates has a drain plug to facilitate the removal of any condensation.

4.1.1. Solids Entrainment

Downstream of the receiver is the solids feeder, which in its rotary form was estimated to have a maximum feeding capacity of 2 cu.ft. of bulk solids per minute, though, as is seen later, in the final feeder design this was rather exceeded. As is described in Chapter 6 on the rig development, some time was spent in developing the rotary feeder before it was finally decided to abandon it in favour of pressure assisted gravity flow feed, which although it did not have the metering qualities of the rotary feeder, was found to be much more reliable.

The feeding system finally adopted consists of a cylindrical solids hopper 18 ins. diameter by 4 ft 10 ins. long, with a solids capacity of about 6½ cu.ft. designed to B.S. 1500, to withstand internal pressures of 200 p.s.i.

with a rectangular slot 6 ins. long by 2¼ ins. wide in its base plate. Mounted immediately below the hopper is the solids flow control valve, which is of the "tutterfly" type, with a mild steel vane of sufficient strength to withstand maximum hopper to atmospheric pressure differential across it, and with nylon inserts on the end rubbing faces. The valve spindle bearings are of oil impregnated phosphor bronze, with so small a gas leakage path to atmosphere that no gas seal is required where the valve actuating handle emerges from the body. The internal dimensions of this valve are similar to those of the slot in the hopper base plate. On opening the solids flow valve, the solids flow into a cylindrical chamber (originally the rotary feeder casing) where entrainment with the air supply occurs, and the air-solids mixture is led from the feeding system through a 7/8 in. bore nylon pipe. Control of the solids flow rate is effected by the set of the solids flow valve and also by the rate at which air is allowed to bleed into the top of the hopper through a 1 in. bore diaphragm valve A Fig. 6. By this means it is possible to obtain a wide range of solids flow rates. When delivering polystyrene powder, flow rates in the range 0.03 to 1.1 lb/sec were obtained,

though this upper figure by no means represents the maximum.

The main advantage of the pressurised feeding system appears to be that due to the fairly high air velocity at the solids entrainment point (about 100 ft/sec) there is a substantial pressure drop across the solids in the hopper, as the air above the solids level is at stagnation pressure. This pressure drop is then sufficient to ensure that air is always percolating through the solids bed and this air helps to keep the particles "fluidised" as they flow down through the solids control valve, so that "bridging" or "sticking" at the outlet does not occur (Ref. Zenz & Othmer - Fluidisation and Fluid Particle Systems).

In order to reduce the amplitude of the pressure pulsations, which were always present in the rig pipe-line whilst feeding the polystyrene powder and which were especially severe when delivering at high solids-air ratios, a vertical damping chamber is located immediately down-stream of the feeding system. It was considered that to achieve the maximum effect the damping chamber should have as large a diameter as possible, consistent with conveying the solids particles with no tendency to settle.

As minimum conveying velocities are usually lower for vertical than for horizontal conveying (Ref. E.E.U.A. Handbook No.15) the damping chamber is mounted vertically. The chamber finally adopted is of 3 in. bore by 6 ft. long, the length being governed by the headroom available, and is designed to give a minimum mean air velocity of about 10 ft/sec at the anticipated air flow rates. Connection from the feeding system to the damping chamber and from the damping chamber to the experimental section is through 7/8 in. bore nylon tubing of 1/8 in. wall thickness. This tubing was adopted because it is readily bent into large radius bends of about 2 ft. diameter offering low pressure drops and also since its bore is almost identical with that of the experimental section brass pipe-line.

4.1.2. Experimental Section

A 7/8 in. bore pipe size was selected for the experimental section as being readily available in a smooth bore material and of a size consistent with the available air supply, such that compressible flow conditions might be readily achieved.

The experimental section of the pipe flow rig is made up of seven 18 ft., one 12 ft. and one 9 ft., lengths of 7/8 in. bore by 16 S.W.C. wall thickness brass

pipe to B.S. 885, 1963. The 18 ft. maximum length was selected as the pipe was readily available in these lengths and also not too long as to be difficult to handle in the rig assembly area. The pipe bore is hydraulically smooth to obviate the added complication of pipe wall roughness factors. At two points along the pipe-line glass walled observation sections 10 in. long are incorporated, as also is a 12 in. long tube housing a pitot-static system. The bores of these three sections are similar to that of the main piping, and their positions along the pipe-line can be varied. Special care was taken to make all pipe joints good spigot fits in order to ensure the least possible discontinuity in wall surface. Yorkshire Imperial Metals fittings, high duty type 1 in. number 10 P.E., which are in fact a high pressure fitting with "O" ring seal and silver soldered connection, were modified to take the 7/8 in. bore brass piping and give the spigot fitting, see Fig. 8 . In the case of the glass walled observation sections the fittings were modified to accept 0.867 in. bore by 0.08 in. nominal wall thickness Veridia precision bore tubing, the joint to the fittings and the copper tube strengthener being made using Twin-packed Araldite adhesive, see Fig.6. Veridia precision bore tubing is made by Chance Brothers Ltd., from a hard

resistance glass of low expansion coefficient. The tube housing the pitot-static section is of the pipe-line material with similar end fittings. By making two of the pipe joint couplings of polytetrafluorethylene, see Fig. 8 , the 9 ft. long pipe section was rendered an insulated section from which measurements of electrostatic effects, due to the solids in the air flow, are recorded. The pipe-line is attached by brass wall brackets, "Yorkshire" fittings type 108 to take 1" bore piping, to a 6 in. wide wooden boarding, which is in turn carried on wooden supports placed at 10 ft. intervals, the boarding being also used to carry static pressure measurement tubing to a manometer board. Apart from the insulated section, the pipe-line is earthed, with earthing straps, to avoid the build-up of large electrostatic voltages.

4.1.3. Solids Separation

The pipe-line is terminated with a diffuser increasing the pipe bore to 18 sq. in. (rectangular section), which is in turn connected to the inlet of a cyclone, designed to collect the majority of the solid particles. The diffuser, which is of 16 S.W.G. mild steel galvanised after fabrication, has a maximum angle of divergence of 10 degrees and a gradual change of section from 7/8 in.

circular to rectangular. At the upstream end it incorporates a spigot fitting to match that of the pipe-line, whilst a flanged joint with rubber gasket sealing is provided between diffuser and cyclone. The cyclone design was based on that recommended in The Chemical Engineers Handbook-editor J.H.Perry. It is constructed from 16 S.W.G. mild steel, galvanised after fabrication, and its 10 in. diameter by 35 in. overall length dimensions were arrived at taking into account the estimated smallest size particle capable of being collected, the allowable pressure drop, and limitations in length due to the head-room available. See Appendix 3 for cyclone design criterea.

The solids separated from the air stream by the cyclone are collected in a cylindrical drum bolted to the base of the cyclone. This drum is 2 ft. 3 in. diameter by 15 in. high of 16 S.W.G. mild steel with ¼in. thick base, galvanised after fabrication. It is estimated to have a capacity of about 5 cu.ft.. The drum is fitted with four castors to facilitate its removal back to the solids hopper on the completion of a "run". Space limitation and the estimated angles of repose of the solids to be collected governed the collector drum design. A rubber gasket provides the seal between drum and cyclone to ensure

no air leakage.

The air flow, with any uncollected solids, is led from the top of the cyclone through a 5 in. bore by 10 ft. long flexible smooth bore hose into a fabric bag filter located in a relatively large air receiver . The flexible hose, which is made by The Compoflex Co.Ltd., and has their code number 609, incorporates a 12 in. long perspex observation section to give some idea of the quantity of solids evading capture in the cyclone. Attachment of the flexible hose to the cyclone, to the filter housing end plate and also to the perspex section is by means of "Jubilee Clips".

The fabric filter which is 5 ft. long by 2 ft. diameter and bag shaped, is made of singed terylene and has the makers specification number A.M.T.8. The makers, Porritt, Brother and Austin Ltd., claim it is capable of an efficiency of 99.9% for particle size less than 1 micron at flow rates of between 10 and 12 cu.ft./minute/sq.ft. and at these flow rates the pressure drop across the filter will be 5 to 6 in. water gauge. The filter housing, 2 ft. 3 in. diameter by 11 ft. long, is mainly constructed of 18 S.W.G. mild steel galvanised after fabrication, and besides housing the filter it also provides a means of obtaining final stagnation temperature and pressure meausurements. Rubber gaskets provide seals between the filter housing and its end plates to ensure minimum air leakage. The

rig is terminated with a 13 ft. long 4 in. nominal bore mild steel exhaust pipe in which is housed an air flow measurement nozzle, located 2 ft. from the end, after which the air exhausts to atmosphere.

4.1.4. Solids Re-loading

The system for re-loading the hopper after a "run" is simply to unbolt the collector drum from the cyclone and wheel it with its contents to a position adjacent to the feeding hopper. From the top of the hopper a 1½ in. pipe leads to a rubber diaphragm valve, capable of withstanding full hopper pressure, on the other side of this valve a flexible tube leads to a "Spenstead" extractor fan, which is capable of a capacity of 200 c.f.m. against a 5 in. water gauge pressure drop, but in this application is probably working against a much greater pressure drop. Immediately below the top end plate of the hopper is a fabric filter, of the same material as used for the bag filter, backed by a metal supporting gauze. Suction from the fan is thus made to act across this filter. Then through another 1½ in. pipe entering the hopper immediately below the filter and, via diaphragm valve and flexible tubing, dipping into the solids in the collecting drum, the solids may be sucked into the hopper when the solids valve and air bleed valve are closed.

The flexible tubing is $1\frac{1}{2}$ in. bore "Flexi-lant" polyvinylchloride suction hose, and the end dipping into the solids in the collector drum has a special mouthpiece. If the plain end of thetube was put into the solids it would immediately block, as air flow is required to maintain conveyance. The mouthpiece adopted in this case was one consisting of two co-axial tubes, made of polythene from convenience, the inner tube of $1\frac{1}{4}$ in. and the outer of 2 in. bore, the tubes are attached to the flexible tubing by means of a "Jubilee Clip". As shown in Fig. 6 , the outer tube has 4 holes at a position about 6 in. from the end and its end extends $\frac{1}{2}$ in. beyond that of the inner tube. By this means a continual flow of air is maintained up the centre tube and the system may be left to suck up powder for considerable periods without attention. A counter-weight over a pulley is used to balance the weight of the flexible tube. To assist this feeding process, the solids are introduced into the hopper at an angle tangential to the hopper wall, to gain some cyclone separation effect. After a load of solids has entered the hopper, the diaphragm valves are closed to re-seal the hopper. The rig is then ready for an experimental run.

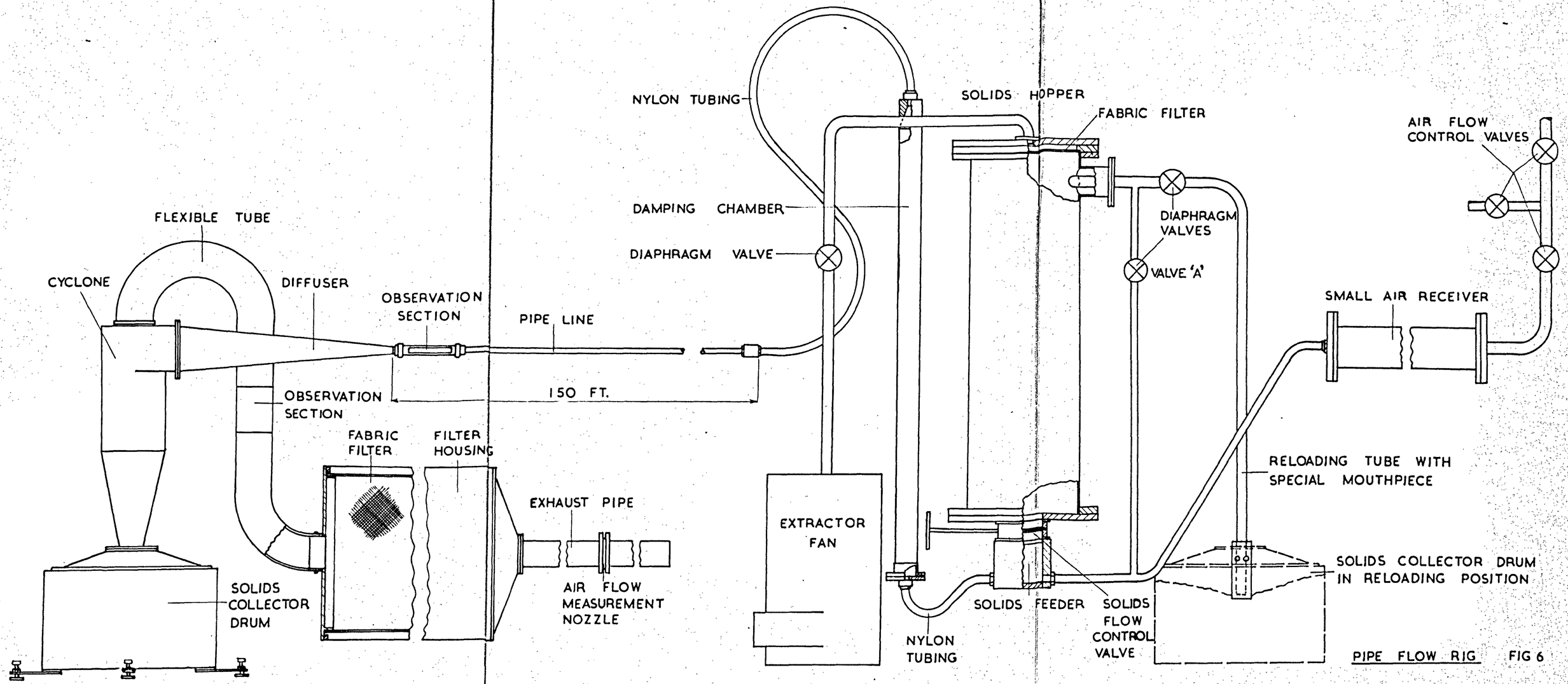

PIPE FLOW RIG FIG 6

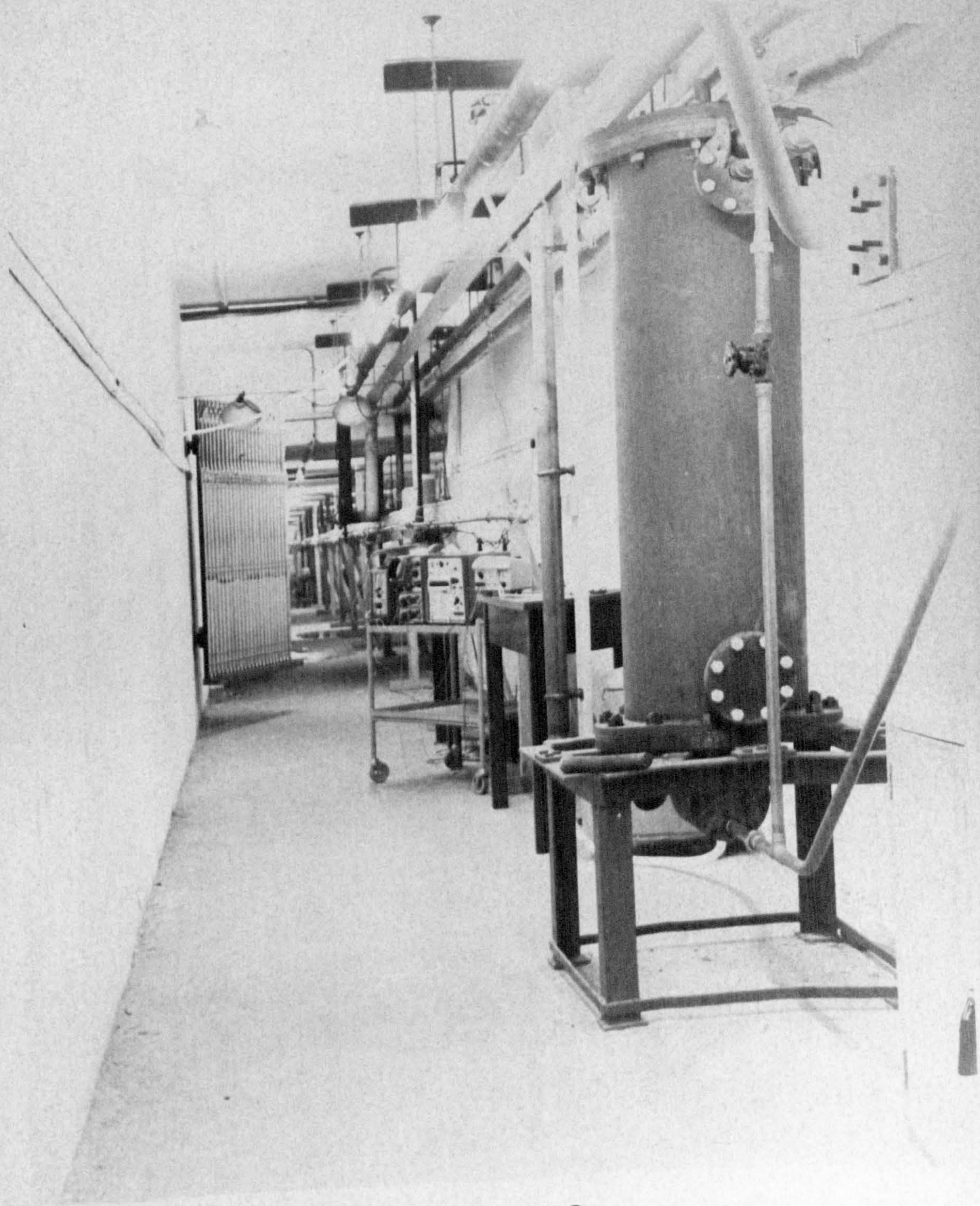

FIG 7 PIPE FLOW RIG

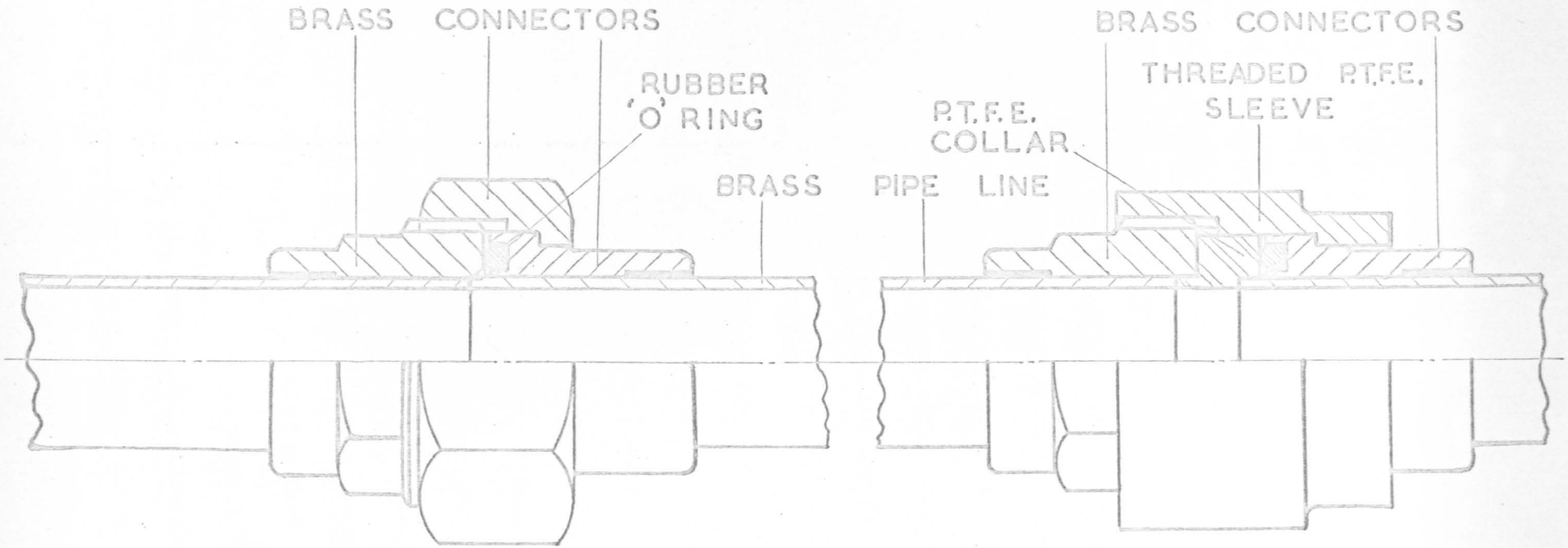

FIG 8 NORMAL PIPE JOINT INSULATED PIPE JOINT

4.2. Rectangular Duct Flow Rig

4.2.1. Experimental Section

The duct flow rig is designed such that it replaces a portion of the pipe flow rig and hence still utilises the solids entrainment and separation features. A labelled parts diagram of this rig is shown in Fig 9 . The rig is designed to obtain supersonic flows by expansion of the gas-solids mixture through a convergent - divergent nozzle. The basic design is similar to that applied to high speed air wind tunnels, in that because transparent-walled sections are required for flow visualisation and photographic purposes, all the nozzle divergence is made to occur along two walls. The nozzle in the rig was designed using the constant fractional lag gas-solids flow theory described in Section 3.2. and appendix 1, which may be applied to derive similar expressions to those obtained for the Prandth-Meyer expansion process for the supersonic flow of gas round a corner. The expressions obtained specifying the angle through which a supersonic stream must be turned to give a prescribed Mach number and the angle of the resulting Mach wave are similar to those for gas dynamics, except that a mixture Mach number and the compressible flow index n of the mixture are now the governing dimensionless parameters.

A full description of the Mach wavelet method of designing a two dimensional supersonic nozzle for gas flow is given in the book Elements of Compressible Flow by F.Cheers and the procedure adopted for gas-solids flow has been exactly the same. The assumptions made in the application of the constant fractional lag theory are as follows :-

1. The sonic plane at the nozzle throat is assumed to be perpendicular to the longitudinal axis of the nozzle, the sonic condition being that of the mixture Mach number equal to one.

2. In the application of the constant fractional lag theory it is necessary to make some assumption regarding the particle to gas velocity and temperature lags. In this initial design the value of the compressible flow index n was selected as $\eta = 1.075$. This corresponds to a solids-air ratio of about 3.36 to 1 with gas-solids particle velocity and temperature fractional lags of 0.5 & 0.4. The design is such, however, that the nozzle profiles can be readily replaced by others corresponding to different fractional lag assumptions.

3. The area ratio required to obtain a given Mach number increases with decreasing values of η. Use of this has therefore been made in that by selecting a rather low value of η there is a built-in allowance for boundary layer build-up in the diverging portion of the nozzle.

No attempt, however, has been made to estimate the magnitude of this boundary layer.

On the basis of the constant fractional lag theory, the nozzle is designed to accelerate an air-solids flow to a mixture Mach number of 1 at the throat and 2.1 at the nozzle exit, with a pressure ratio of approximately 9.1 inlet to exit. The aspect ratio of the nozzle exit is 5 to 1, which is similar to that of a high speed wind tunnel in this Department. The throat area of the nozzle was selected as 0.342 sq.in., this being of a sufficiently small area to produce a Mach number of unity for air flow at the pressures envisaged. It being argued that if constant fractional lag theory applies, the throat area required to produce a mixture Mach number of 1 can be larger than that required to produce Mach 1 for air flow. This being the case then for similar throat areas, a lower mass ~~throat~~ flow rate is required to produce a mixture Mach number of 1. If, therefore, the nozzle is capable of accelerating an air flow to the supersonic condition, it should, on this basis, be readily capable of producing supersonic flow in an air- solids mixture, though the supersonic flow produced may not necessarily be shock free even in the nozzle section. The nozzle profile upstream of the throat has a straight wall such that the nozzle can be reversed and this part used as the diverging

section, if it is suspected that a more gradual divergence gives a better flow, as is suggested by Hogland (1962) for large fractions of large diameter particles.

In order to be able to photograph the supersonic flow of the air-solids mixture, the side walls of the duct are of clear polished perspex. In order to keep the weight of the structure down and also because in the manufacture machining costs and not material costs were expected to be the predominant factor, the upper and lower walls and the side retaining plates are made from a high strength aluminium alloy (grade H.E. 30 s.w.p.). Design calculations for the duct are given in Appendix 5 but some of the criterea will be stated here. As a result of specifying the throat area of the nozzle, the area ratio to produce Mach 2.1 and the aspect ratio of the duct at nozzle exit, the width and height dimensions of the flow area at nozzle exit are 0.4 and 2.0 in. In order to obtain greater flexibility the nozzle upstream and downstream areas and aspect ratios were made the same. Two 6 ft. long transparent walled sections were decided upon with the nozzle housed at the upstream end of one of these. With the two sections it is possible to have either a 5 ft. or 11 ft. length of duct downstream

of the nozzle exit. If a 5 ft. length is selected the other section may be used to provide an observation section upstream of the nozzle. A further 6 ft. length of metal walled ducting is provided in order to give at least 108 equivalent diameters of duct upstream of the nozzle. The 6 ft. lengths of ducting were selected as being readily capable of manufacture on machinery available in a small workshop, such as was the case. At either ends of the three 6 ft. lengths ofduct are diffusers. The upstream diffuser is designed to connect with a section of the 7/8 in. bore brass pipe-line. This diffuser has a maximum included angle of 3.6 degrees and increases the flow area from 0.6 to 0.8 sq. in. The downstream diffuser leads the flow from the duct into the particle separation cyclone. This diffuser has a maximum included angle of 6.6 degrees and increases the flow area from 0.8 to 12.9 sq.in.

As is stated in Appendix 5 the transparent walled section of the duct is designed to withstand a safe working pressure of 150 p.s.i., whilst the metal duct and upstream diffuser are capable of withstanding 200 p.s.i. By making the transparent walled duct lengths of bolted construction as shown in Fig 9, the nozzle profile or even the duct aspect ratio may be altered if the replacement parts are available.

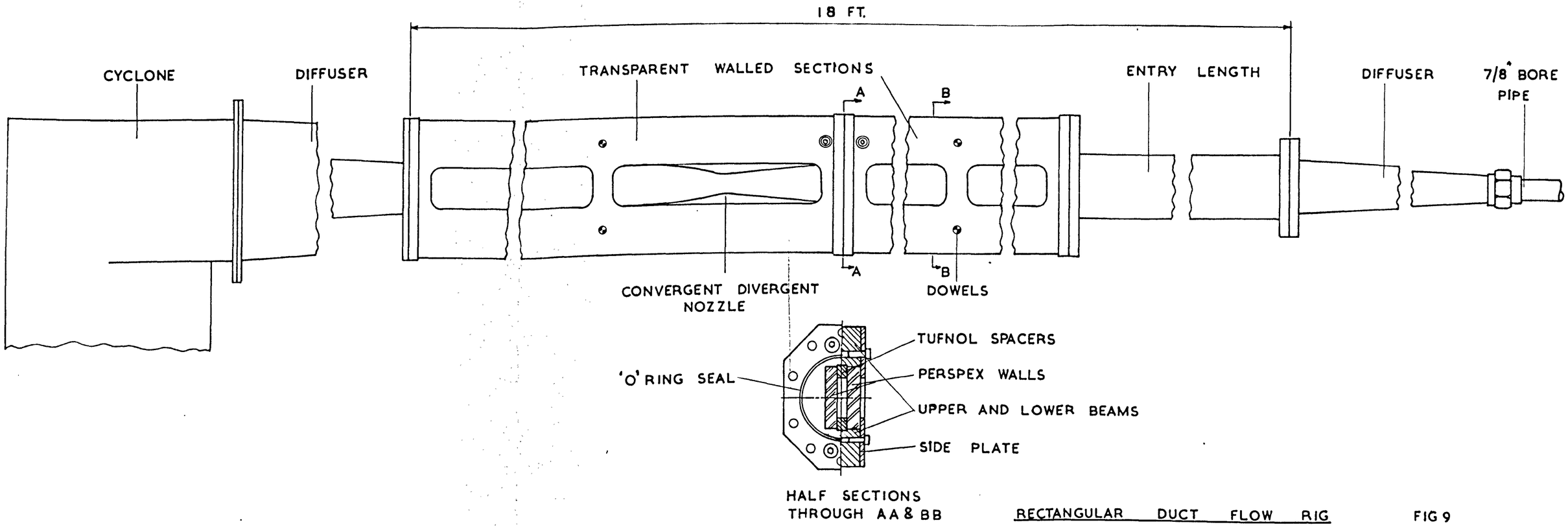

RECTANGULAR DUCT FLOW RIG

FIG 9

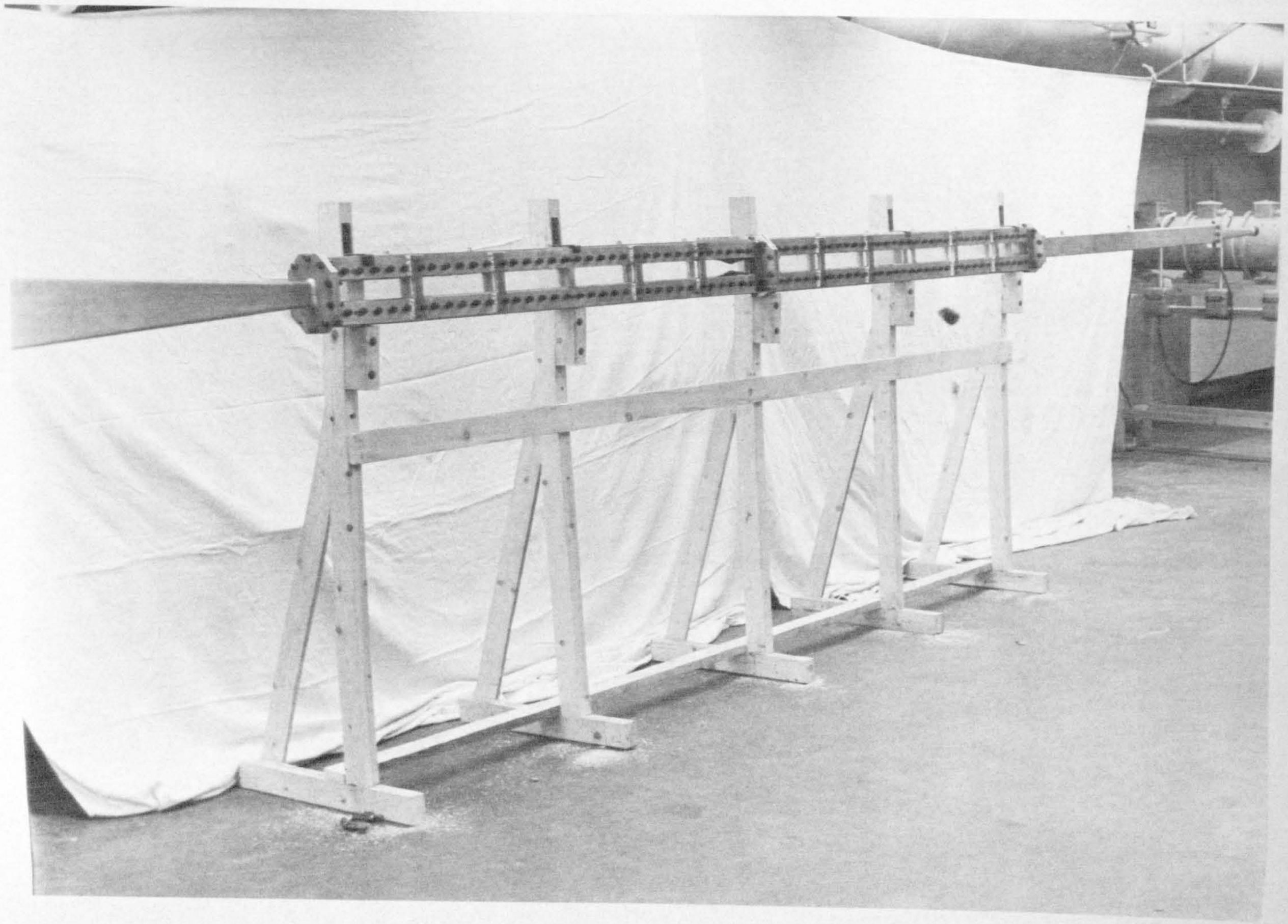

FIG 10 RECTANGULAR DUCT FLOW RIG

CHAPTER 5.

DESCRIPTION AND DEVELOPMENT OF INSTRUMENTATION.

In order to gain as full a picture as possible of the mechanism of gas-solids flow, at least measurements of air velocity profile, solids velocity profile, air and solids mass flow rates, as well as pressure drops should be obtained. Ideally, of course, measurements of solids density profiles, solids mass velocity profiles, air turbulence levels, and temperatures because the flow is compressible, together with measurements of electrostatic effects would help to complete the picture. In this project, however, as the velocity profiles, the flow rates and the pressure drops are assumed to be of major importance, the main concentration is centred on measuring these, whilst some measurements of electrostatic effects are also taken. The description of the instrumentation will, therefore, be given under headings of pressure drop, solids flow, air flow, air velocity profile and solids velocity profile, whilst the measurement of electrostatic effects, temperature and relative humidity will be considered in a final paragraph.

5.1. Instrumentation for the Pipe Flow Rig.

5.1.1. Pressure Drop Measurement.

Three methods of pressure drop measurement were considered:

Bourdon Tube dial gauges to measure gauge pressure, pressure transducers to measure absolute pressures, and a differential pressure U-tube manometer system to measure gauge pressures. In the case of Bourdon Tube dial gauges and the differential U-tube system, the readings would be photographed on some centrally placed board, requiring long lengths of small bore tubing to carry the pressure signal to the board, whilst if pressure transducers were used these may be mounted actually at the pressure tapping point and the electrical signal from them would be brought through sheathed cabling to a centrally placed recording system. Because a large number of pressure readings were to be taken in a "run", obtaining sufficient pressure transducers would have proved expensive. Bourdon Tube dial gauges are also expensive for the accuracy which would be required in these experiments. A differential pressure U-tube manometer system was, therefore, selected as being capable of giving sufficient accuracy, and could be built in such a way that it could be photographed throughout a run and the readings later recorded on projection of the films.

The number of static pressure tapping points along the pipe-line would normally be governed by an estimation of the maximum anticipated pressure drop. For air flow with choking conditions at the pipe exit, the pressure drop required over

the whole pipe length would be about 120 p.s.i. if a mean Mach number of unity were achieved at pipe exit and for 15 p.s.i. exit pressure. In order not to have any limit on flow conditions due to the manometer system not being able to record the full pressure drop being used, the differential U-tube manometer board should be capable of recording the total pressure drop which would ever be available over the rig experimental section. As stated in Chapter 4, the air compressors are capable of maintaing the large air receiver at 200 p.s.i.g. For the flow rate associated with choking conditions, the pressure drop between large air receiver and experimental section should never exceed 10 p.s.i. for pure air flow. The manometer board should, therefore, be capable of recording a pressure drop of about 190 p.s.i. Because for the pipe flow experiments the pressure drop will not be linear, ideally the static pressure tapping points should be closer together as the pipe exit is approached. As it was thought that there might be some need to move individual pipe lengths from one position to another, it was decided to maintain a constant pitch of pressure tapping position along the pipe line, except for the last 12 ft., which would have tappings closer together, though still at constant pitch. In order to record a maximum pressure drop of about 190 p.s.i., it was

decided that 21 U-tubes would be necessary to make up the board, and this would give ample margin for recording the non-linear pressure drop.

The criteria in the design of the U-tubes were that they should be capable of withstanding full rig pressure, and also that the bores of the tubes should be sufficiently large for the manometric liquid meniscus levels to be readable from a projected photograph. There is also an advantage in using larger bore tubes in that the U-tube response time to a change in pressure is inversely proportional to the square of the tube diameter. In this design, however, the response time of the long connecting leads from static tapping point to manometer board was much greater than that of the manometer. The U-tubes were made from 7.6. mm. bore precision bore glass tubing with limbs about 4 ft. long, the limb length being such that with 21 U-tubes mounted on the manometer board the picture just filled a 35 mm. film frame.

A certain amount of development work was involved in obtaining the connection between pressure tapping connecting leads and the glass U-tubes and this is considered in detail in Section 6.3. A compression fitting, comprising a brass "Enots" ½ in. tube to tube connector type Z36 together with

3 rubber "O" rings 7/16 in. i.d. x 5/8 in. o.d. to B.S.O.S.9, was eventually tried. This method of jointing proved capable of withstanding the full rig pressure of 200 p.s.i. and has caused no trouble since.

The selection of the tubing to connect the rig static-pressure tappings with the U-tubes in the manometer board was governed by what pressure response time was acceptable over the longer lengths. It is known from previous work (ref. T. Garrett's Ph.D. Thesis) that some experimenters have had to put lengths of hypodermic tubing in their pressure tapping leads to act as "pulsation dampers" and reduce the magnitude of pulsations reaching the manometers. With this in mind, it was thought that by selecting a tubing of fairly small bore, the necessity for "pulsation dampers" would be avoided. "Enots" 3/16 in. nylon tubing and fittings were selected, therefore, the tubing having a bore of 0.11 in. which was estimated to give a maximum pressure response time of 3.4 sec. using the methods of calculation put forward in Appendix ó . The "Enots" tubing and fittings are also of a convenient size for fitting into the rig, and will withstand pressures very much greater than 200 p.s.i.

5.1.2. Solids Flow Rate Measurement.

In the early days of the project when an atmospheric hopper of relatively light weight was being used as a solids supply vessel, this was cantilevered from the wall with strain gauges mounted on the cantilever arm, and hence a continuous recording of solids flow rate obtained. This method relied on the solids level in the hopper dropping evenly to give accurate results, and in fact this was found to be reasonably true.

When it became necessary to use a pressurised hopper as solids supply vessel, it was no longer sufficiently accurate to mount strain gauges on the stand of the hopper, as, due to the large dead weight of the hopper, the strains set up by the solids weight were too small to be measured very accurately, and hence a reading of solids flow rate would be inaccurate.

Due to the variation in solids flow rate through the supply hopper orifice and "butterfly" valve with decreasing solids bed depth (see ref. Zenz and Othmer), it is essential that at the time of reading the pressure levels on the manometer board (i.e. at the instant of photographing the board) the solids flow rate should be recorded. This means that any method of weighing the collected solids over a given time and obtaining

a mean solids flow rate would not be sufficiently accurate. Since the cyclone had been designed to capture all particles down to 0.0005 in. or 12.5 microns diameter (see Appendix 3) it would appear that if a load cell could be incorporated into the cyclone collector drum, and because the bulk of the solid particles are collected in this drum, if a signal from the load cell could be continuously recorded, this would represent, when plotted against time, the solids flow rate. The cyclone will not, of course, capture all the solids particles entering it; a certain amount will be carried over into the fabric filter, but if this filter is weighed periodically, then a correction factor can be applied to all previous solids flow rate readings. This correction factor will be based on the assumption that the cyclone efficiency remains the same at all solids to air ratios; however, due to the anticipated low magnitude of this correction factor, this should not be an unreasonable assumption. If for finer powders it was found that the carry over became appreciable, then steps could be taken to weigh the filter more often and ensure that the solids to air flow rate ratios for "runs" between weighings did not vary greatly.

The load cell for the collector drum consists of resistance strain gauges mounted on four equi-spaced short canti-

lever arms projecting from the base of the drum and taking the full weight of the drum, cyclone and diffuser when in position (see Fig. 6). The arms are of mild steel and the strains set up at the position of attachment are estimated to be in the range 2.8 - 6.5 x 10^{-4}, for solids powders of bulk density about 40 lb./cu.ft. The ends of the arms incorporate loading screws which are wound down onto metal pads resting on the floor, until the castors on the collector drum are all raised about 1/8 in. above floor level. By using ball ended loading screws and keeping the pads well greased, the friction force resisting movement of the screws is kept low. The strain gauges, which are attached to the cantilever arms by using 'Eastman 910' adhesive, are "Phillips PR 9813" type with matched resistances of 300 ohms. Two of the strain gauges are mounted to experience compressive strains and the other two tensile strains, the four of them being connected as a Wheatstone Bridge circuit. By mounting four strain gauges as described, any uneven collecting of solids in the drum should not result in an error in solids flow rate reading. This was, in fact, verified by placing a 50 lb. weight at various eccentric positions in the empty drum and noting the signal from the energised bridge circuit. This was never found to differ by more than 3% from the signal obtained for the weight placed centrally in the

drum. During the running of the rig, the solids were in fact never observed to have collected in an eccentric manner, when the collector drum was examined after removal from the cyclone. Two 4½ volt electric batteries connected in series are used to give a 9 volt dc. supply to the bridge circuit. The output signal from the load cell is conveyed via a 150 ft. length of twin-core screened cable to an "S.E.L." 24 channel ultra-violet galvanometer recorder type S.E.2000, where the signal is made to deflect an "S.E.L." type A35 galvanometer of 0.00074 m.a./cm. sensitivity. By this method, a continual record of solids loading with time is obtained in the form of a trace on sensitised paper. Owing to the difficulty in obtaining a constant calibration for the system, the collector drum was weighed after each run and the calibration coefficient, for converting the bridge out of balance signal into a solids flow rate, was evaluated from the weight of solids collected and the total change in magnitude of the signal.

5.1.3. Air Flow Rate Measurement.

The only methods of air flow rate measurement considered were those recommended in the British Standard on flow measurement B.S.1042. From this a nozzle was selected in preference to an orifice plate, a venturi being considered unnecessarily

expensive, on the basis that if at any time the bag filter developed a hole, the sharp edge on an orifice could become quickly erroded if an abrasive powder was being used at the time, with a resulting effect on flow measurement accuracy. The nozzle also offers better pressure recovery than the orifice, so that the build up of pressure in the thin walled sections of the rig (filter housing and collector drum) would be slightly less for a nozzle than for an orifice with the same area ratio and air flow rate.

In Appendix 4 is given the method of selection of the nozzle size. The value of "m" (the ratio of nozzle throat area to exhaust pipe area) was selected in order to give a reasonably measurable pressure drop, on an inclined manometer at low flow rates. Too high a value was avoided, as metering with large values of the area ratio "m" is much more sensitive to installation faults than with small values. Upstream of the nozzle there is a straight length of piping 33 diameters long before the sudden contraction from filter housing to exhaust pipe. B.S.1042 quotes 25 diameters as being the minimum that should be used. Although the cyclone will impart a helical motion to the air flow, which if present in air at the nozzle would effect the metering accuracy, it is considered

that this motion will be fully damped out in the large volume of the filter housing.

The pressure signal from the nozzle is relayed to the manometer board through 120 ft. long 3/16 in. o.d. "Enots" nylon tubing, similar to that for the static pressure tappings. This system has a maximum estimated pressure response time of 3.2 seconds, when connected to a 5/16 in. bore by about 4 ft. long U-tube containing liquid of 0.785 specific gravity, the calculation is outlined in Appendix 6 . For air flow rates up to about 0.15 lb/sec., however, in order to obtain sufficient accuracy, the pressure difference across the nozzle is measured on a Negretti and Zambra 0 - 1.5 in. of water inclined manometer, containing liquid of 0.785 specific gravity. For this system the maximum pressure response time is estimated at 29 seconds, and experiments confirmed that the instrument delay in reading a pressure drop of 0.1 in. water could be as high as 30 seconds for an instantaneous pressure change. Any air flow changes, however, will always be gradual so that the manometer lag should not be as great as it appears. It was also noticed that this response time seemed to be rather less for the pressure differential increasing and hence readings were always taken with the pressure slowly increasing.

One of the manometer board U-tubes containing water as manometric fluid is used to measure the pressure up-stream of the nozzle by means of a "tee" connection into the tapping lead. This reading together with the atmospheric pressure reading enables the correct nozzle calibration to be evaluated for each run.

5.1.4. Air Velocity Measurement.

The only method considered for air velocity measurement was the use of a pitot-static system to measure stagnation pressure variation across the pipe and static pressure at the pipe wall. It being realised, of course, that a proportion of solids velocity head might well be included in these readings.

The pitot-tube was "L"-shaped with the short leg $\frac{3}{4}$ in. long. There is a photograph of the traverse mechanism in Fig. 11 . The traverse is motorised so that the readings may be taken more quickly than would be the case with a manual traverse. A micrometer head provides the traverse mechanism and the drive to this is from an "Enicron" miniature gear box and skeleton shaded pole motor, giving a final drive of about 13 r.p.m. with max. torque 12 lb.in. A clutch mechanism, to disengage

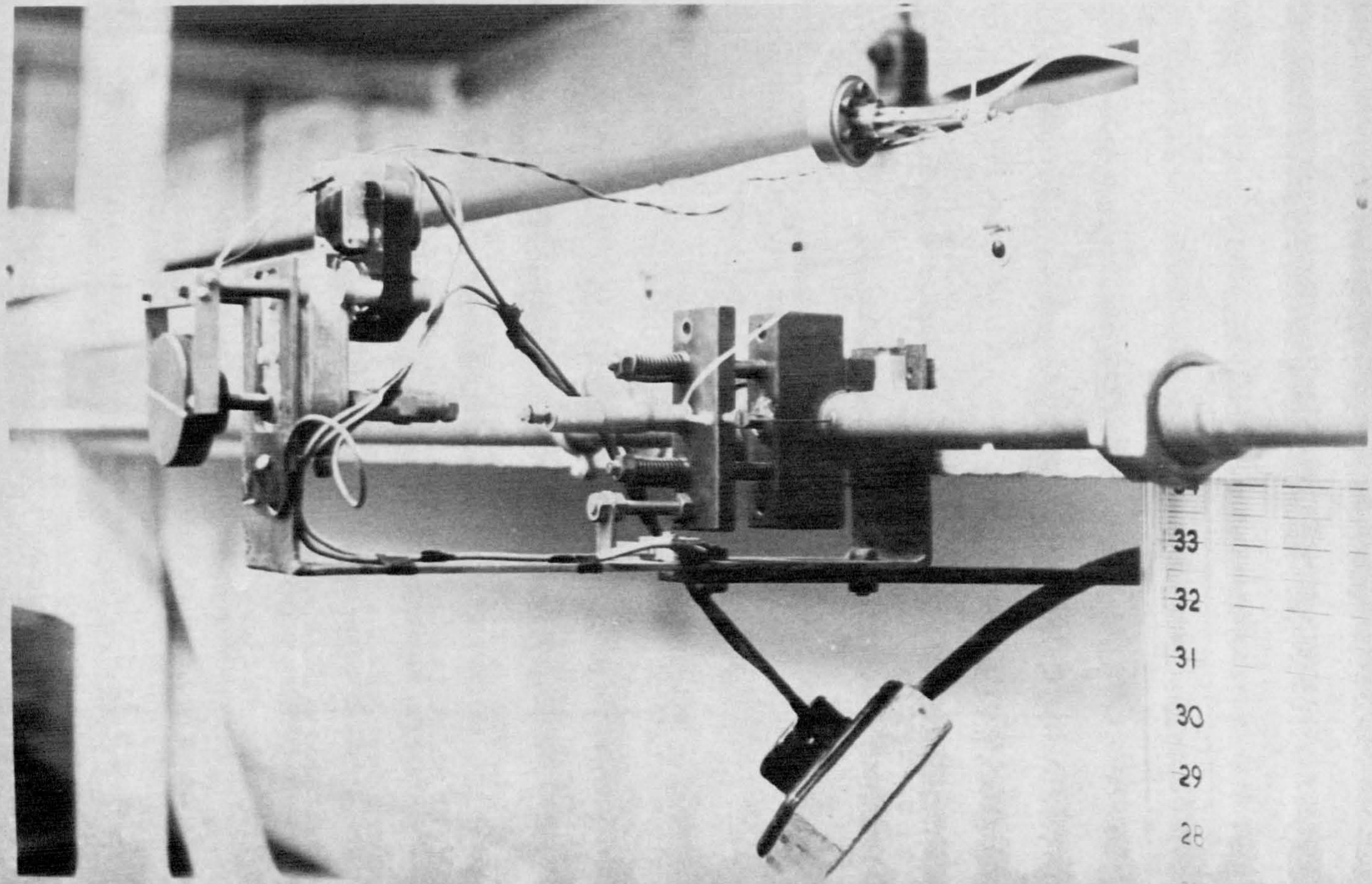

FIG 11 PITOT TUBE TRAVERSE MECHANISM

the micrometer drive at the end of a traverse, consists of a short length of "Enots" 3/16 in. o.d. nylon tubing and adaptors connecting to the $\frac{1}{4}$ in. o.d. drive shaft from the gear box. Besides a clutch, this also provides a flexible drive to accommodate any misalignment of drive shaft and micrometer head. On the other side of the gear box is attached a "make and break" device which, with the appropriate electrical circuit and recording set-up, provides a record representing the traverse across the pipe-line radius. By housing the pitot-static system in a 12 in. length of the pipe-line, traverses can be obtained at any of 9 different positions along the pipe-line.

The pressure signals from pitot-tube and static tapping are fed onto either side of a differential pressure transducer "Solartron" type NT4-313(s) 0-25 p.s.i. This range of pressure measurement was selected so that the transducer could also be used for supersonic velocity measurements in the duct flow rig, where for air flow at Mach 2 the ratio of pressures would be 5.65 and this might be measured with this transducer if the associated static pressure was sufficiently low. Connections from the tapping points to transducer are through 1 mm. bore plastic tubing. The power supply for the transducer is from a "Solartron" type AS 974

strain gauge power pack. This gives a 5 v.d.c. supply and also a means of balancing the transducer bridge circuit to reduce the output signal to zero when there is no pressure differential across the transducer diaphragm. The transducer signal and signal from "make and break" device are then conveyed via a 150 ft. length of 4 core screened cabling to the U-V galvanometer recorder. The transducer signal is amplified using a "Solartron" d.c. decade amplifier type AA 900, with a gain of about 500, if from a low velocity region, before being connected to one of the U-V galvanometers. Because of the noise pickup from the amplifier, however, whenever possible the signal was connected directly to a sensitive galvanometer. Calibration of the signal from the transducer was achieved by connecting a 1.4 mm. precision bore capillary U-tube in series with the pitot and static connections, and separate calibrations were made for the various amplifier gains and galvanometer combinations used. All calibrations were made with the 150 ft. long electrical connections from transducer to recorder to avoid any variation in lead resistance.

The "make and break" circuit is powered by a 1½ volt battery which, by means of a 1000 ohm rheostat, gives a signal of about .3v and 1.5 m.a. This signal is only recorded, by a

galvanometer on the U-V recorder, whenever the pitot traverse micrometer head rotates through half a revolution, which corresponds to a traverse of .0125 in. By this means, a pulsed signal is obtained alongside the differential pressure signal on the U-V recorder and by starting the traverse from the pipe wall, the necessary co-relation is obtained.

A considerable variety of pitot-tubes have been tried in an effort to obtain one which did not block too quickly, but only partial success has been obtained. The first pitot tube tried had a tip about ½ in. long, with bore of .0075 in. and .016 in.o.d. This was tried in the premise that having a mouth considerably smaller than the diameter of most of the particles, this might take a considerable time to block. This did not prove to be case, however, either because of the fines present in the powder or because of particle break-up on impingement with the pitot tube, and the tube blocked very quickly in a relatively dense solids-air flow. Similar pitot tubes of 25 S.W.G. (.010 in. bore x .020 in.o.d.), 20 S.W.G.(.022 in.bore x .035 in. o.d) 18 S.W.G, (.0315 in. bore x .049 in. o.d.) and .05 in. bore x .067 in. o.d. were also tried with slightly better success but even these blocked up before a full traverse could be

obtained, when the solids-air flow was dense. A tube with flattened end, to enable the traverse to be taken closer to the pipe wall, had the end broken by the impaction of the particles. To determine whether the 90 degree bend in these pitot tubes was the point of initial blockage, a straight tube was tried, which had a "spider" support at its downstream end. This, however, also blocked rapidly over its first $\frac{3}{4}$ in. length.

Because of the difficulties involved in taking conventional pitot-tube readings, a tube facing downstream of the flow was tried. Initially a traverse was made with a .05 in. o.d. straight tube set across a pipe diameter with a 0.024 in. diameter hole $\frac{1}{4}$ in. from the end and facing downstream. The readings from this bore no resemblance to those expected, probably due to the tube end effect disturbance and to the flow of air escaping between pitot tube and the hole in the pipe wall, which it was found impossible to seal and still be able to traverse. A second attempt was made with a reversed tube, this time a long length of .034 in. o.d. tubing was used with the upstream end soldered to the pipe wall 10 in. above the downstream open end. With this tube, although the pressure differential did increase as the tube was traversed from the wall, this increase from pipe wall to centre-line was

so slight that calibration of the tube to obtain accurate results was impossible. The reason why the variation in pressure differential across the pipe was so small, as indicated by this tube, is probably that the effect of the tube upstream of the open end causes the boundary layer to be disturbed, and a more uniform velocity profile generated in this region.

As a result of this development work, it was considered that the best results were obtained with either the 20 or 18 S.W.G. pitot tubes, but even these had severe limitations.

To determine whether readings obtained from the pitot tubes were reliable, an estimation of the tube limitations was made. In the book Modern Developments in Fluid Dynamics - S. Goldstein, a minimum pitot tube Reynold's number is quoted, above which a tube will indicate true total head readings. This Reynold's number is based on the pitot hole diameter, and if greater than 125, the tube should give reliable results. At the minimum air flow for this project (about .08 lb/sec.), a pitot Reynold's number of 125 corresponds to a hole diameter of .002 in., which indicates that all the above tubes are satisfactory in this respect. An estimate of the pitot tube response time as given by the expression in Appendix 6

indicates that for the .022 in. bore pitot the response time is of the order of .005 secs. This, when compared with the traverse rate of .006 in/sec., suggests that there is ample time for pressure response.

A third limitation to this method would appear to be how large a pitot tube can be tolerated before appreciable flow disturbance occurs. In their book, Chemical Engineering Volume 1, Coulson and Richardson indicate that for a ratio of pipe diameter to pitot-tube diameter greater than 50, disturbances to the flow can be ignored. For the .875 in. pipe bore, however, it is not possible to use small enough pitot-tubes to comply with this requirement.

5.1.5. Solids Velocity Measurement.

The only feasible methods of measuring solids particle velocity in this project appear to be either photographic or to make use of a radioactive labelling method, as any mechanical method, such as trapping the particles in an isolating section would be out of the question at the particle speed anticipated. The radioactive labelling technique appears to suffer from the following disadvantages:

1. Only the mean solids particle velocity could be measured

at any one section, and this method could give no indication of the solids velocity profile across the section.

2. The constituents of the solids particles to be used in this project would almost certainly not be activated sufficiently by any form of irradiation to provide a suitable gamma ray emitter. This would mean that the solids particles to be labelled would have to be loaded with a material of high neutron cross -section (usually the heavy metals), and almost certainly this would change their behaviour in the air-stream.

3. Other complications, such as the difficulty in recovering the treated particles and the expense involved in acquiring the necessary precise detecting equipment because of the high solids particle velocities envisaged, make this method inapplicable to this project.

The first photographic method considered was to illuminate a flow of the suspension by means of two synchronised flash discharge light sources. By this method, any single particle in the flow would be represented by two exposures on the same film negative. Then, because the time between exposures would be known and the distance travelled by a particle in this time could be measured from the film taken, the particle velocity would be obtained. Flash discharge units of this type are

available, but the limitations here would appear to be that the amount of light available from these flash discharges in the time small enough to "stop" a particle from a photographic standpoint, is not really sufficient for reflected light photography. Shadow or silhouette techniques, whilst probably feasible, would mean that the solids loading could only be low. The difficulty in identifying individual particles would also probably mean that only low solids loadings could be considered.

During the course of the project, a high speed cine-camera Fastax Type W.F.17, 0-8,000 pictures per second, was acquired by the Department of Mechanical Engineering at this University, and as a result, a method of using this camera to determine particle velocities was investigated. It was suggested by the suppliers of the camera that a technique used in ballistic photography might well be suitable if the size of the particles was not too small. This technique consists of obtaining a continuous photograph of the flowing particles on a very fast moving cine-film. Because the film is exposed in this manner and not frame by frame, the processed negative depicts a series of streaks stretching diagonally across the film, and each of these represents the path of a single or bunnh of particles moving along the length of the photographed section. Then, knowing the speed of the film for a particular

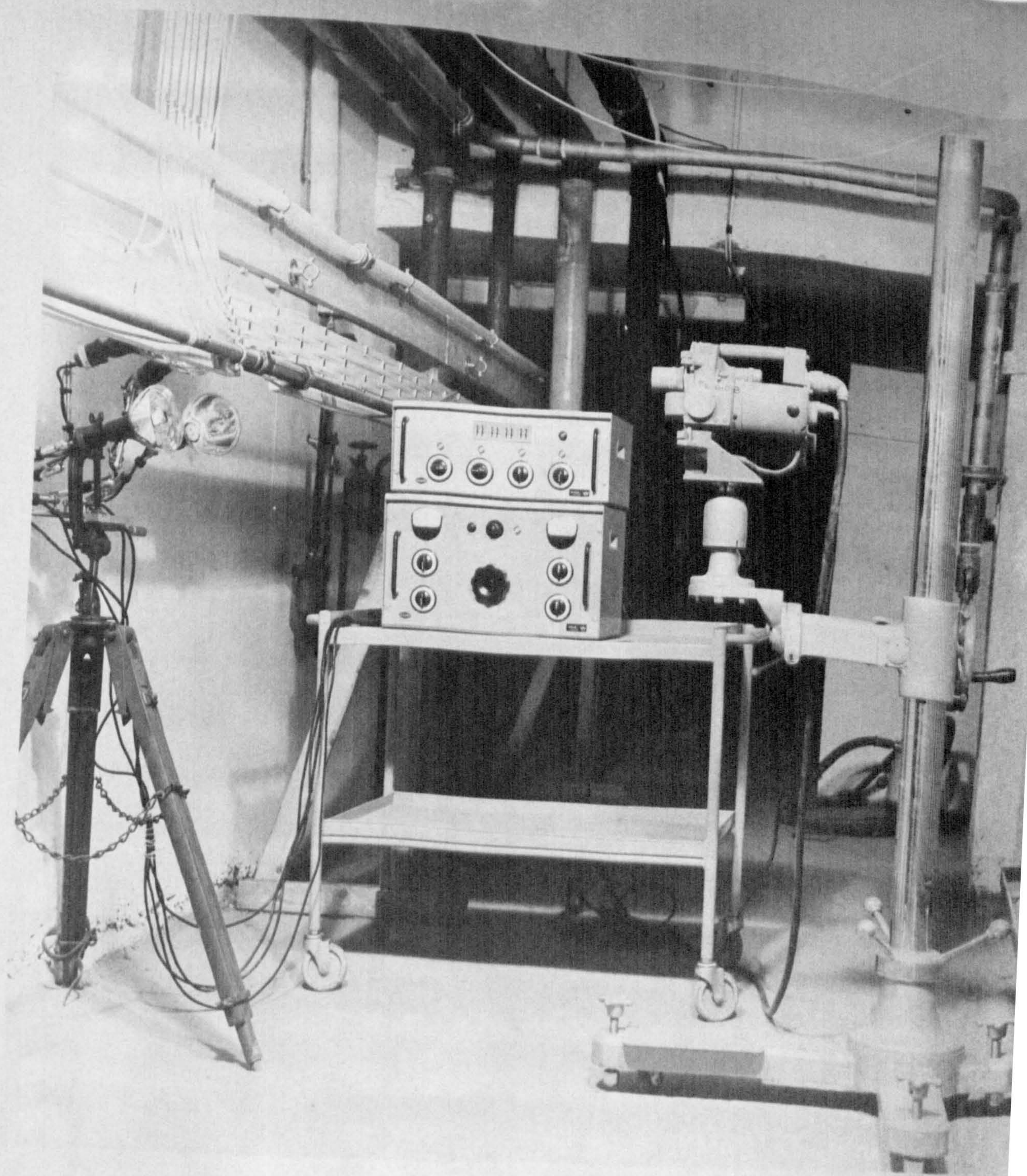

FIG 12 HIGH SPEED CAMERA

streak from timing marks on the film and the length of the field of view, the time to travel this length is represented by the length of film in which a streak moves across the film. For this method to give reliable results, the particles must, of course, be moving parallel with the axis of the tube. It is considered, however, that most of the particles will be either moving parallel with or at a slight angle to this axis, especially so at high air velocities, so that by taking sufficient streak length measurements, a reliable indication of solids particle velocity should be obtained.

With the Fastax camera, the film can be exposed in the necessary continuous way by using the camera oscilloscope channel. Various methods of lighting the flow were used, but it was found that the best results were obtained with back lighting, and the field of view was restricted to a strip 6 ins. long by $\frac{1}{4}$ in. wide. The observation glasses described in section 4.1.2 were found to be quite suitable if the field of view was mounted along the centre-line of the glass.

The instrumentation described so far is relied upon to obtain the major experimental readings; however, other instruments used to obtain readings which are taken occasionally or are ancillary to the above will be mentioned here. The

temperature of the air flowing through the rig is measured, using mercury in glass thermometers, at the small air receiver immediately upstream of the solids flow feeder and also in the filter housing, that is, just prior to the air flow measurement nozzle. These measurements are used to give some idea of how nearly the process is adiabatic; to provide the air temperature necessary for the air flow measurement nozzle calibration, and to provide the necessary flow stagnation temperature. The air humidity is measured with a sling wet and dry hygrometer which is held in the air stream as it exhausts from the rig, and the calibration for these readings is obtained from the 1965 Institute of Heating and Ventilating Engineers Guide psychometric chart. Electrostatic measurements are restricted to measurements of current to earth from the 9 ft. insulated pipe length, using a Pye Scalamp galvanometer and measurements of pipe-line voltage relative to earth using a Pye 40 kV Electrostatic Voltmeter. During a run, the atmospheric pressure is read from a Fortin barometer.

5.2. Instrumentation for the Duct Flow Rig.

5.2.1. Pressure Drop Measurement.

As explained in section 5.1.1., the pressure recording system was designed to be easily adapted to the duct flow rig.

Twenty-five static pressure tapping positions are provided in the duct flow test section. Over the transparent walled section these are spaced at 12 in. intervals with 10 recording pressure over the convergent-divergent nozzle length. The remaining 3 tappings are located in the metal-walled section serving as an entry length. The manometer board is only capable of taking readings from 21 tappings, but this should be sufficient to give all the detail required for a pressure drop profile. For constant fractional lag gas-solids flow, the pressure drop required to achieve a Mach number of 2.1 at nozzle exit is 9.1 from stagnation to exit condition with frictionless flow. So that even if the absolute pressure at the nozzle exit is as great as atmospheric, and the pressure drop is greater than that predicted by the constant fractional lag theory, there is still ample capacity on the manometer board for measuring this.

5.2.2. Air Velocity Measurement.

Because of the depth of the upper and lower beams of the test section of this rig, it would be very difficult to mount a pitot tube in the flow, such that it could be easily removed and cleaned. It should be possible, however, to mount the pitot tube in the entry length.

5.2.3. Solids Velocity Measurement.

The technique for solids velocity measurement should be almost identical to that for the pipe flow rig. In this case, however, due to the fairly high aspect ratio of the rig, such that an almost uniform velocity profile should be obtained in this plane, there should not be the same difficulty in deciding how far into the depth of field the streak photograph obtained relates. It should also be possible to obtain a fuller indication of the solids velocity profile by mounting a field of view, of similar size to that used in the pipe flow, at various heights along the duct wall.

For the remaining measurements on this rig such as solids and air flow rates, stagnation temperatures, and any humidity recordings, the technique is identical with that for the pipe flow rig.

CHAPTER 6.

RIG DEVELOPMENT.

6.1. The Solids Entrainment System.

The main item for development on the rig was expected to be the feeding system. As most pneumatic conveying systems seem to use a "star" feeder, it was decided that this form of feeding system would be tried first, but be designed in such a way that it could be readily modified if required.

In its original form, the feeding system consisted of a rotary feeder with driving motor slung beneath, suspended from the base of a conical shaped feed hopper, which was in turn cantilevered from the wall. In between the feeder and hopper was a rectangular "gate valve" of similar dimensions to that of the solids flow port into the feeder. (i.e. 6 in. x 2¼ in.) By using this technique and mounting strain gauges on the cantilever arm, a continuous recording of the solids feed rate could be obtained by feeding the signal from the strain gauge system into a ultra-violet galvanometer recorder. See Fig. 7.

This solids feeder had a cylindrical rotor with radially mounted vanes, sufficiently strong to withstand 200 p.s.i. air pressure, and with absolute minimum side clearance to reduce air leakage. The dimensions of the rotor were 6 in. diameter

with 11 x 1 inch deep pockets 6½ inches long. Initially the vanes were of medium carbon steel, spring loaded using small single leaf springs to maintain metal to metal contact with the rotor casing. The rotor casing, which was of centrifugally cast iron, had a raked inlet throat with "knife-edge" to minimize shearing of particles as the vanes passed the entry point and the pockets between the vanes filled with solids material. It was soon realised, however, that the solids particles were dropping between the vanes and the rotor causing jamming, which in some cases occurred with the vanes clear of the rotor casing, leaving a substantial air gap. Nylon vanes were then substituted for the steel ones, the nylon vanes being a "press fit" in the 1/8 in. wide slots in the rotor. The nylon was machined after fitting in order to give the minimum clearance between rotor casing and vanes, and also between vanes and phosphor bronze end plates, this clearance being of the order of 0.002 in. The flexibility of the nylon helped to ensure that jamming of the particles between vanes and casing did not occur, whilst its low friction coefficient helped to reduce the load on the driving motor.

It was also soon realised that in spite of taking great care in the feeder manufacture to ensure that the clearances between the vanes, the casing and the end plates were an absolute minimum, a large amount of air leakage occurred up through the

feeder, especially at high air supply pressures. The effect of this was to impede the gravity flow of solids to the feeder, with a subsequent falling off in solids flow rate as the air pressure was increased. This difficulty was overcome by replacing the previous hopper with the present pressurised hopper described in Chapter 4. This then explains why the hole in the hopper base plate was made rectangular instead of circular, as is usual for gravity feeding through an orifice.

The feeding system at this stage consisted of the pressurised hopper with air pipe supplying pressurised air to the hopper above the solids level, the modified rotary feeder slung from the hopper base plate with "butterfly" type solids control valve (described in Chapter 4) between it and the hopper, and the feeder driving motor slung beneath the feeder. The "gate valve" had also been replaced by this stage, as it was found to stick rather badly as a result of the small clearance between the "gate" and the body of the valve. Also, this type of valve would have been no use in a pressurised system due to its relatively large air leakage path. The driving motor was a $\frac{3}{4}$ h.p. 110 volt D.C. shunt wound electric motor geared down to 100 r.p.m. through an integral gear box. Drive to the feeder was through Fenner $\frac{1}{2}$ in. pitch single roller chain and number 41 type change sprockets incorporating Taper-lock bushes

for ease of fitting and removal. By this means, feeder rotor speeds in the range 50 to 110 r.p.m, could be obtained, whilst fine speed control was available through a 12 ohm variable resistance wired in series with the motor armature. For a time this system appeared to work satisfactorily for low solids feed rates, not exceeding about 0.15 lb/sec., however, above these the motor would stall and blow a 7 amp protecting fuse. At this stage, a d.c. ammeter was wired into the motor armature circuit to determine the power required to drive the feeder. When delivering the polystyrene solids at a feed rate of about 0.16 lb/sec. with an air flow rate of 0.08 lb/sec. and at a line pressure of about 30 p.s.i.g., it was discovered that the power to drive the feeder was of the order of 6 times that required when no solids were being delivered, but with the same air flow rate. To cope with this sort of power requirement would probably need a 2 h.p. motor (compared with the $\frac{3}{4}$ h.p. at present) and modifications to the rotor shaft and bearings of the feeder to ensure they would withstand the increased loading. In view of this, it was decided to experiment with gravity flow from the pressurised hopper into the pipe-line by removing the rotor from the feeder. Flow control would be obtained by the solids control valve and the diaphragm valve supplying air into the top of the hopper as described in Chapter 4.

It should be emphasised that although the "star" feeder as described above did not prove successful, there has recently been developed a rotary feeder rather similar to it. This feeder uses a rotor of cast nylon impregnated with molybdenum disulphide, manufactured by "Polypenco Engineering Industrial Plastics" and described in their December, 1965, newsletter. In the light of this, the Author considers that the "star" feeder as designed by him could be made to work successfully with a power unit supplying 2hp. In a paper on pneumatic conveying of granular plastics by J. Fisher (1962), unfortunately not seen by the Author until relatively recently, it is quoted that tests performed with plastic materials using a star feeder with 8 pockets and rotating at 40 r.p.m. showed that 0.05 - 0.25 hp/in. of star feeder vane length would be required to overcome the resistance of materials to shear. By comparison, this indicates that for the feeder used by the Author, power requirements might be up to 1.6 h.p., which is in fair agreement with the 2 h.p. figure quoted previously. The reason for not persevering with this development was that the pressure assisted gravity flow feed system experimented with after the star feeder troubles, proved to be quite suitable for delivering the polystyrene solids, although there appears to be a greater tendency for the flow rate to vary with run

time, i.e. with solids bed height.

An interesting observation at this stage was that the pressure fluctuations in the pipe-line when feeding the polystyrene solids were of about the same magnitude for both types of feeding systems. It was at one time thought that the "star" feeder was producing these pulsations; however, it is now thought that they are probably due to the intermittent nature of the gravity flow of solids in the hopper. Other experimenters appear to have experienced similar pressure fluctuations when delivering polystyrene solids, e.g. Mitlin stated that pneumatic conveying of polystyrene particles gave very high fluctuating pressure drops.

6.2. Damping of Pressure Fluctuations.

Because, as stated above, pressure fluctuations are produced during the feeding of solids into the air flow, and these cause the liquid levels in manometers to oscillate, a damping chamber was positioned downstream of the feeding system in order to reduce the amplitude of the pressure fluctuations. The first damping chamber to be tried was one of $1\frac{3}{4}$ inch bore by 6 ft. long. This was positioned vertically and connected to the feeding system through a 7 ft.

length of 7/8 in. bore nylon tubing, and to the pipe-line through an 11 ft. length of similar nylon tubing. The entry to the damping chamber was a sudden sharp-edged expansion to promote mixing of solids and air, whilst the exit from the chamber was via a 10 degree included angle conical section to give a low pressure drop. The effect of fitting this damping chamber was to slightly reduce the amplitude of fluctuations compared with no damping chamber.

It was still considered, however, that a greater effect could be gained by fitting an even larger bore vertical chamber. To this end a 3 inch bore by 6 ft. long chamber was constructed with sudden expansion inlet and tapering outlet as for the previous one, except that in this case, in order to ease the machining requirements, the tapering section was made with an included angle of about 20 degrees. This was found to significantly reduce the pressure fluctuation amplitude compared to that measured with the previous chamber for similar air and solids flow rates.

The reason for adopting a vertical damping chamber was that from experiments of other workers (Ref. E.E.U.A. Handbook No. 15) it has been shown that "settling out" of particles occurs at a considerably higher velocity for horizontal conveying

than it does for vertical conveying. This means that a much larger bore chamber could be used if mounted vertically before the particles of solids would begin to settle. The above reference quotes the following figures as the minimum allowable air velocity, before settling out occurs, for a powder similar to the 0.012 in. mean diameter particle size polystyrene powder used - 10 ft/sec. for vertical and 30 ft/sec. for horizontal conveying. As a result, the bore of the vertical tube was made 3 in. giving an estimated minimum air velocity of 10 ft/sec. To achieve a similar vessel capacity, a horizontal tube would have required a bore of 1¾ in. and a length of 18 ft. Although at the low air flow rates the damping chamber was found to have a beneficial effect in reducing the amplitude of pressure oscillations, on going to higher air flow rates, its beneficial effect was no longer apparent. It is felt that this was mainly because at the high air flow rates it was no longer possible to deliver at high mass flow ratios. Because it gave rise to a relatively high pressure drop, the damping chamber was, therefore, removed for the higher air flow rate experiments.

6.3. Glass U-Tube to Nylon Pipe Connections.

A certain amount of development work was also necessary

before the pipe-line static pressure measurement system was proved reliable. A detailed description of this system has been given in Section 5.11, and only the necessary development work is mentioned here. It was known that the most difficult joints to make leak tight in the system would be those between the 3/16 in. nylon tubing leads from the pipe-line tapping points, and the glass U-tubes recording differential pressures.

Initially it was decided to use a joint comprising, a connector machined from $\frac{3}{4}$ in. diameter perspex rod, as joints of this material had previously proved successful in the department. The connector was made 1 in. long with a $\frac{1}{4}$ in. deep recess at one end to take the end of the glass U-tube, whilst the other end was tapped 1/8 in. B.S.P. thread to take a 3/16 in. Enots adaptor. The jointing of the glass to perspex was made using "Araldite Twin-Pack" adhesive as suggested by the manufacturers Ciba (ARL) Ltd., Duxford. To test the design, a short length of the glass tubing had connectors put on both ends and was subjected to an hydraulic pressure test in a "dead weight tester". Pressure for this test was gradually increased from 0 - 400 p.s.i.g. in increments of 20 p.s.i. and the load of 400 p.s.i.g. was maintained for 30 minutes. During this time no leaks were observed, whilst the test pressure had

been maintained at more than double the pressure any part of the rig would ever be subjected to. As a result of this test, these fittings were assumed to be suitable, and all the U-tubes were fitted with similar connectors. After assembly of the U-tubes into the differential pressure manometer board and their connection to the rig via the 3/16 in. tubing, the whole system was pressurised to 170 p.s.i.g. and no leaks were apparent at any of the "Araldite" joints, when tested with a soap and water solution.

Subsequently, the rig was run numerous times without any leaks becoming apparent, until about six months after the above test, when it was noticed that about nine of the "Araldite" joints between glass and perspex connectors had developed slight leaks. These were resealed using the Twin-Pack Araldite, and appeared satisfactory when pressure tested. After further runs, however, it was observed that some of the joints were again leaking, including some of the ones that had been remade. In view of this, it was decided to replace all perspex connectors with a compression joint in which both a seal and the necessary strength to prevent the joint parting are achieved by the compression of a rubber "O" ring onto the glass tubing. Details of these connectors are given in Section 5.1.1. A possible explanation offered to account

for the development of leaks in the "Araldite" joints is that they are due to fatigue in the "Araldite" bond between glass and perspex. It is known that the elasticity modulus of glass is about 20 times that of perspex, so that on pressurising, the differential strains set up, could, after a number of loadings, be sufficient to crack the "Araldite" bond which appears to be rather brittle. All the cracks, however, did not appear to be in the "Araldite"; some were between glass and "Araldite", implying that the bond to perspex was better than that to the glass.

6.4. Pressure Testing the Pipe Flow Rig.

During this period of development work, the rig was pressure tested so that parts subjected to high pressures during the running of the rig could be established as safe. The method of leak testing adopted was to subject all parts of the rig upstream of the diffuser into the cyclone to a high pressure test, whilst the thin wall components were tested by inserting a blanking plate downstream of the nozzle and subjecting the whole rig to a low pressure test. A number of severe leaks and blow-outs came to light during these tests, but in the final pressure test, all parts of the rig upstream of the diffuser into the cyclone, were subjected

to a pressure of 165 p.s.i.g. for a period of 75 minutes with no appreciable leaks, whilst the integrity of parts downstream of the diffuser was established at a pressure of 40 in. water. Special care was taken to ensure that there were no leaks in the pressure tapping lines by testing with soap and water solution, as these could result in misleading pressure readings.

6.5. Sealing the Duct Flow Rig.

The major sealing difficulty on this rig was found to be between the transparant side wall sections and the upper and lower beams. The initial design of the rig was with glass side walls 5/8 in. thick, and these were clamped up against a "Tufnol" spacer on the upper and lower beams by means of metal side plates, with bolts located at 2 in. pitch along upper and lower edges, see Fig. 9 . The joint between glass and "Tufnol" was to be sealed with p.t.f.e. tape. The method of sealing the glass to the flanges at each test length end was to be by means of "Twin-Pack Araldite" with the surplus filed off the flange face to permit the "O" ring seal. Because the "Tufnol" spacer was not absolutely flat, the test sections were so long, and glass is particularly inflexible, it was found that the glass wall always cracked

before a seal could be obtained. Another aspect coming to light during this development work was that for this purpose p.t.f.e. tape, even the 1/8 in. circular cross-section type, was not particularly suitable as a sealing compound.

Because of the above difficulties, it was decided that the most likely means of obtaining a successful seal lay with a more flexible material than glass, and also to concentrate on obtaining the actual seal by smearing sealing compound over both glass to "Tufnol" and glass to metal faces. These modifications could have two effects:

(a) The adoption of a more flexible transparent material - perspex was selected - meant that its surface was not as hard as that of glass and therefore more likely to be marked by impinging solids particles. No reduction in the rig safety factor was incurred, however, as perspex has a higher working stress than glass.

(b) Because in the initial design the intention was to achieve a seal between glass and "Tufnol", it was only necessary to have three struts on each of the side plates connecting upper and lower metal beams via the dowel

pins. With the modified method of sealing, however, the rig internal pressure might act on the full width of upper and lower beams instead of an about one third of this width as initially intended. As a result, in order to provide the rig with sufficient strength for the test pressure, it was necessary to have a further four 1 in. wide struts welded onto each side plate and provide dowel pins so that when under pressure, the load tending to deflect the upper and lower beams was transferred to these struts.

Tests with various sealing compounds, including p.t.f.e. tape, Bostik 5 sealing strip, Epple-22 (a German product), and cold cure Silastomer types 9160 and 9161, showed that the Silastomer type 9161, a compound that sets like rubber and is made by Midland Silicones Ltd., gave the best results.

As a result of the above modifications it was possible to achieve a sufficiently good seal to subject all parts of this rig, upstream of the diffuser leading into the cyclone, to an hydraulic test pressure of 300 lb/sq. in. and this could be maintained with only slight leakage.

CHAPTER 7.

EXPERIMENTAL PROCEDURE.

The experimental procedure described in this Chapter is restricted to that applicable to the pipe flow rig, as time did not permit any experiments on the duct flow rig.

At the onset of the project it was decided that all experimental readings would be performed at conditions corresponding to four different air flow rates. These air flow rates were selected to cover the range from a flow which could be practically considered incompressible, through an intermediary flow to one at the onset of the choked condition, and then a further flow well above the initial choking. The flow rates selected to give these conditions are approximately 0.082, 0.15, 0.23 and 0.31 lb/sec.

At each of the selected air flow rates, the solids loading has been varied to cover the range of solids to air mass flow rates of from 0 - 5 as far as possible. This range was selected as it may be considered to be approximately that corresponding to the limits of conventional pneumatic conveying with which comparisons are made where applicable. A loading ratio of 5 was not achieved at the high air flows, because of limitations due to severe vibration of the nylon pipe-line and

the flow becoming intermittent, with the solids tending to travel as "slugs" rather than a truly suspended mixture. The solids flow control valve was never in fact fully opened, so that although the maximum solids flow rate achieved was 1.1 lb/sec., this does not represent the limit of this method of feeding.

Details of the experimental procedure are now considered under various headings corresponding to the measurements being made, and some of the limitations encountered and estimates of the accuracy obtained will be given.

7.1. Solids Material and Particle Size Analysis.

The experimental side of the project has been carried out using only one solids material. This was because it was considered of more value to cover the range of variables fairly completely with one material than to only partly cover the range with a number of different materials. Polystyrene powder was selected as the solids material for the following reasons:

(a) The powder is available with a reasonably narrow size band compared with that of many other commercially available powders.

(b) The particles are perfectly spherical with the resulting

simplification that the drag coefficient for a sphere is probably applicable, and particle diameters are easily determined.

(c) The particles are solid and homogeneous.

(d) The physical properties of polystyrene are well known.

(e) The powder is readily available commercially in large quantities, since it is used as a moulding plastic for electrical components, household wares etc.

(f) The powder is not particularly expensive. This was important as fairly large quantities of powder are required in order to obtain a reasonable "run time" when delivering the solids at high flow rates.

(g) The particles, although not hard, are fairly tough with the result that they do not break down so readily on impaction as would a hard brittle material such as glass.

As a result of the above properties, polystyrene is a good material to use for a gas-solids flow project, although it does have one disadvantage in that it tends to exhibit large electrostatic effects. Since some investigation of electrostatic effects was undertaken in this project, however, this

was not considered a disadvantage.

The size analysis adopted was that of the dry sieve method, and this was carried out in general accordance with B.S. 1796 : 1952. The following range of B.S. mesh number sieves were found to cover the size range for the polystyrene powder: 36, 44, 52, 60, 72, and 85. About 10 grammes of the solids powder was sieved on a nest of the above sieves using a mechanical sieve shaker for a period of about 20 minutes, which was sufficient time to ensure that sieving was complete.

7.2. Pressure Drop Measurement.

When solids are introduced into an air flow, the pressure drop is altered, and this results in a change in the air mass flow rate compared with that for pure air flow with the same control valve setting. As a result, it is extremely difficult to ensure that the pressure drop measurements taken for varying solids loading ratios are all made with the same value of air flow. Instead, therefore, of trying to ensure absolutely comparable air flows for every solids loading (which would have meant discharging a vast quantity of solids vefore the selected air flow rate was attained by manipulating the control valve) the air flow rate was allowed to vary and a normalising process applied to enable comparisons to be made. The normalising

process, for example, for flows of about 0.15 lb/sec. air flow consists of applying to each pressure reading a correction factor, being the ratio of the pressure for pure air flow of exactly 0.15 lb/sec. at that position, to the pressure for the air flow of that particular run. It should be stated, however, that because the pressure drop for pure air flow is almost constant after the choking condition is reached (the pressure drop is in fact reduced slightly with increasing air flow rate above the choked condition due to an increase in Reynold's number, and hence a slight decrease in smooth pipe skin friction factor) this normalising process only really applies to the 0.082 and 0.15 lb/sec. air flow rates.

As is stated in Section 5.1.1. at high solids flow rates the levels of manometric liquids, measuring static pressure drop along the pipe, tended to oscillate at a low frequency. Since the camera setting used for recording the pressure drop was quite capable of "stopping" this movement, an inaccuracy in pressure profile could be obtained as a result of a pressure wave travelling along the pipe and causing oscillation of the manometric liquid. To try to reduce this inaccuracy, photographs of the manometer board were only taken when the levels in the U-tubes were reasonably steady.

The method of recording the pressure drop readings was to take a film of the manometer board when conditions were steady. A 35 mm. camera was used, and the film found to give good results was Kodak Plus X with a film speed of 125 A.S.A. A camera setting of f 5.6 and a shutter speed of 1/50th of a second, with the manometer board illuminated by four 250 watt flood lights gave good exposures. The film was projected in a negative form for the pressure drop readings to be recorded. A typical film of the manometer board during a run is shown in Fig. 13.

It is conventional to express the pressure along a pipe conveying a compressible fluid in non-dimensional form as a ratio of the pipe exit pressure. This is because for one dimensional adiabatic flow with wall friction of a pure gas, this pressure ratio is readily expressed in terms of the gas Mach numbers at the position considered and the pipe exit, and the ratio of the specific heats. The flow of a pure gas in a pipe is such that for a large proportion of the length of the pipe, the gas acceleration is fairly low; however, as the pipe exit is approached, this acceleration becomes more rapid, with the result that the pressure gradient towards pipe exit is becoming progressively steeper. In a pipe exhausting

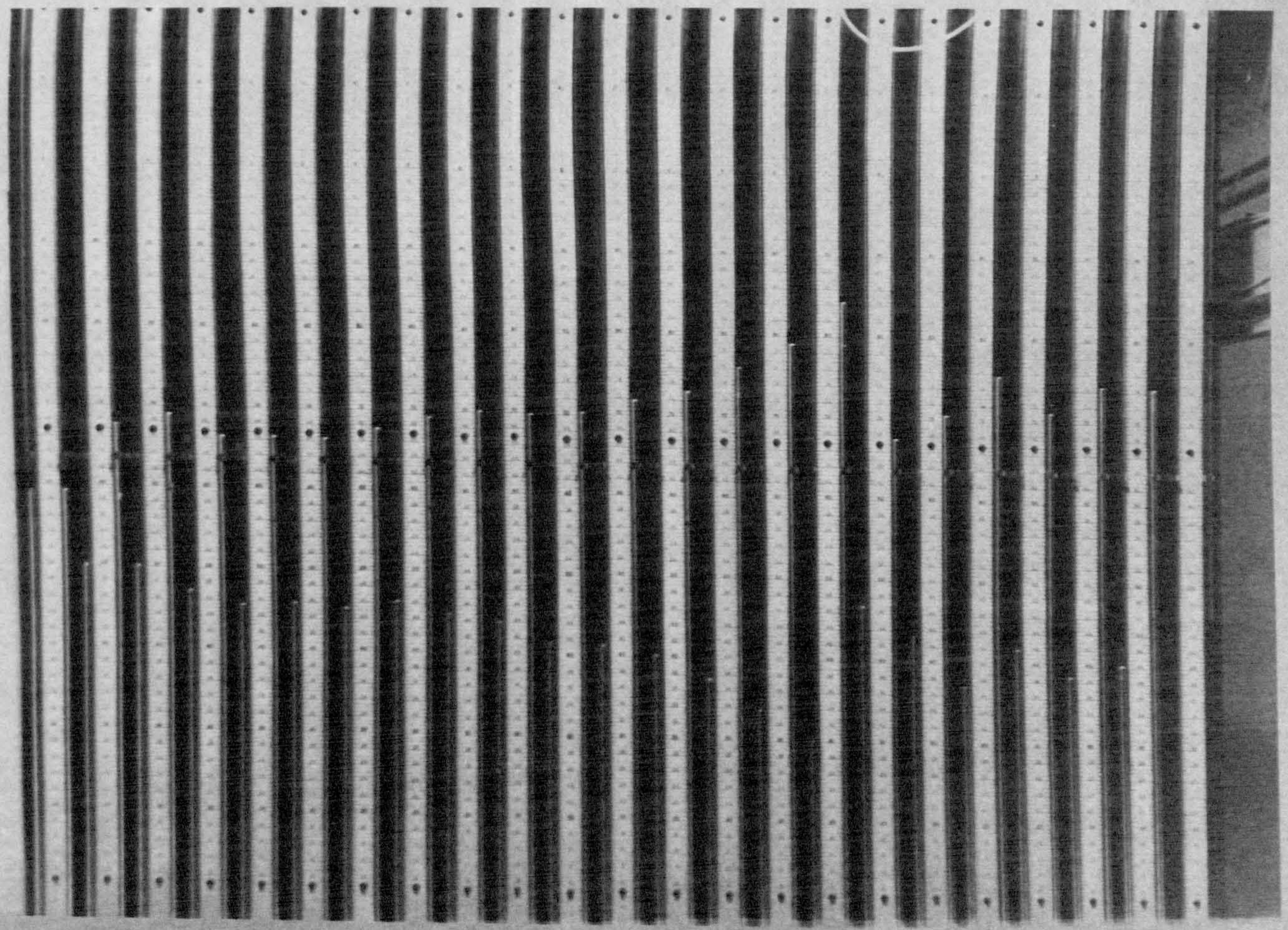

FIG 13 MANOMETER BOARD

to the atmosphere, the pipe exit is well defined. However, when the pipe connects to a shallow angled diffuser, as is the case in this rig, the pipe exit position is no longer immediately obvious, and can only be obtained by a static pressure measurement traverse of the region suspected as pipe exit, at the gas flow rates anticipated. Because the pressure gradient at pipe exit is so steep, any small error in estimating the exit position can result in a large error in measurement of pipe exit pressure, and this in turn would lead to incorrect evaluation of the pipe line non-dimensional pressure. Because part way through the experiments it was suspected that the pressure tapping representing pipe exit was, in fact, a little upsteam of this position, the method adopted for presenting the pressure readings was to non-dimensionalise with respect to this pressure measured close to exit and regard it as a reference pressure. At the end of the pipe line gas-solids flow experiments, it was found possible to mount a series of pressure tapping positions at $\frac{1}{4}$ in. pitch in the vicinity of the pipe exit, and hence from the pressure curve obtained, predict the position of pipe exit. However, because of the almost impossibility in exactly repeating a gas-solids flow experiment, due to difficulties in controlling the gas flow rate and solids flow rate, no correction to give the exact exit pressure was applied to the previous readings. This

did not apply to the pure air flow readings which could be retaken without great difficulty.

Because of the oscillation of the manometric liquid levels in the U-tubes measuring static pressure, it is difficult to assess the accuracy of this method of static pressure measurement. However, if this oscillation is ignored, it can be stated that from the photographs of the manometer board it was possible to read the liquid levels in the U-tube limbs to an accuracy of ± 1 mm. If it is assumed that these errors are distributed randomly over the 42 limbs of the U-tubes comprising the full manometer board when taking a pressure drop profile, the total expected error can be evaluated statistically. For a normal distribution of errors, statistical theory shows that there is one chance in 20 that the total error will exceed $2(n/3)^{\frac{1}{2}}e$, and only one chance in 370 that the error will exceed $3(n/3)^{\frac{1}{2}}e$, where e is the magnitude of individual errors and n the number involved. Applying this to the minimum pressure recorded of about 160 cm. mercury, shows there is a 1 in 370 chance of the total error exceeding 0.75%. (Reference B. Noble.)

7.3. Solids Flow Rate Measurement.

As described in Section 5.1.2. the solids flow rate

measurement is obtained from a trace on the U-V recorder representing the weight of the drum against time of running. In order to ensure that the solids flow rate is measured at the same time that the photograph of the manometer board is taken, an event marker on the recorder is depressed at the instant of taking the photograph. This means that the air flow rate, solids flow rate and pressure drop profile are all recorded at the same instant.

For a reliable calibration to be obtained from the weight of solids collected and the total change in magnitude of the signal recorded, the following factors were considered:

1. The battery voltage supply should not vary over the time of the run, as the signal to the U-V recorder is directly proportional to this. On checking this, it was found that over a period of 30 minutes, which represents the longest time for a run, the battery voltage could drop by 1%.

2. The frictional force between the ball-ended loading screws and support pads on the solids collector drum should be kept to a minimum, or the coefficient of friction should be kept constant. The bending moment producing strain at the position of the strain gauges is directly proportional

to the reaction force between loading screws and pads, as long as the coefficient of friction remains constant. Because this could not be ensured, the pads were kept well greased so that any frictional force was kept small, and hence the bending moment from this source and its variation as the solids load increased were also small.

3. The response time of the system should be good. It is felt that both the electrical response time via the 150 ft. long leads, and also the mechanical response representing the time taken for the load cell to react to the solids collection should both be extremely good.

The largest error in the measurement of solids flow rate undoubtedly results from inaccuracies in the measurement of the slope of the collector drum weight against time trace from the recorder. To reduce this inaccuracy, the most sensitive galvanometer available with the recorder was used, though amplification was avoided as this tended to produce a large amount of "noise" in the trace. In spite of this, it is estimated that at the lowest solids flow rates recorded (i.e. when the solids flow rate was of the order of 0.001 lb/sec.) the inaccuracy in measurement could be as much as 25%. At the high solids flow rates, however, this would be reduced

to the order of 4%.

The spring balance, used to weigh the collector drum after a run, was accurate to within ± .25% over the range of loads used, so that no great inaccuracy occurred here.

7.4. Air Flow Rate Measurement.

During commissioning of the rig, pressure tests were performed to establish the safety of parts which would be subjected to high pressures, and also to gain some idea of the magnitude of any leaks upstream of the airflow measurement nozzle, which could affect the air flow rate measurement. It was established from the drop in pressure during these tests, and from the size of the gap surrounding the pitot tube exit through the pipe wall, that the maximum leakage occurring never exceeded 1% of a possible air flow rate, and this could only occur at the maximum air flow rates used.

The air flow rate measurement nozzle was designed as recommended in B.S. 1042 : 1943, and the dimensions are within the tolerances quoted. Any appreciable error in obtaining the air flow rate would, therefore, result from inaccuracies in the measurement of pressure drop across the nozzle. As is stated in Section 5.1.3. the pressure response time of the

inclined manometer measuring this pressure for the low air flow rates should not be excessive, provided that the air flow rate is steady or slightly rising, but not falling. Precautions were, therefore, taken to ensure that this reading was taken with the air flow rate rising slightly as it was never found possible to keep the air flow rate absolutely steady.

Although measurements of atmospheric pressure and the temperature of the air in the filter housing were always recorded for each run, corrections to the calibration for standard temperature and pressure were only applied if they amounted to an error exceeding 2%. The manometer containing liquid of specific gravity 0.785 could be read to an accuracy of ± 1 mm. whilst the inclined manometer used for the low air flow rates could be read to about ± 0.005 in. of water, both these representing an accuracy of within 1% for air flow rate. The overall maximum error in reading air flow rate is, therefore, estimated to be about 3%.

7.5. Air Velocity Profile Measurement.

From the description in Section 5.1.4. it is apparent that great difficulty has been encountered in trying to obtain stagnation pressure traverses for air solids flows. The rapid

blocking of the pitot tube with solids particles has meant that very few traverses have been obtained at high solids to air loading ratios, and even those that were successful could only be obtained from the low velocity regions of the pipe line.

A further difficulty in taking stagnation pressure traverses either in pure air flow or in air-solids flow, has been the disturbance to the flow caused by the relatively large pitot tube. The size of tube adopted was found to be necessary, as smaller tubes tended to be deflected by the drag from the flow, and as is stated in Section 5.1.4. this size is considerably greater than that recommended for traversing a 0.875 in. bore pipe line. A further source of inaccuracy was the "noise" pick-up by the galvanometer in the U-V recorder, which tended to make the trace representing pitot tube to static pressure difference rather wide, especially when it was necessary to use the D.C. amplifier in the circuit.

In taking traverses in pure air flow, because there is no means of knowing how great the disturbance to flow is, and how great the inaccuracies occurring from the galvanometer trace and subsequent calibration, the criterion adopted for accepting a stagnation pressure traverse has been that the air

mass flow rate evaluated from the traverse readings should not differ by more than 4% from the air flow rate as indicated by the flow measurement nozzle. This rather arbitrary figure of 4% has been selected as it would appear to be in line with the accuracy of most other measurements in this project. Most of the readings have agreement which is much better than 4%, and in fact differ by only 1 or 2%.

For evaluating the air mass flow rate from the pitot traverse for air solids flow, the method adopted has been to consider that the solids particles do not influence the readings, that is, they do not contribute to the measured velocity head. Making this assumption, the Mach number profile across the pipe can be evaluated, assuming the relevant specific heat ratio and velocity of sound are those for the air only, as discussed in Section 8.3. The method of calculation is given in detail in Section 8.3. The agreement between the evaluated air mass flow rate and that indicated by the air flow measurement nozzle is not, however, nearly as good as that for pure air flow. For over half the evaluations agreement is within 5%, whilst all except one of the other values lie between 5 and 10%, with the odd value of 12%.

The method of obtaining static pressure during a pitot tube traverse has generally been to connect a bank of U-tubes from the manometer board to the static tapping, and read the levels during the pitot traverse. In a few cases, however, the static pressure has been obtained by inference from the pipe line pressure drop measurement profiles. It was also necessary to take a number of air flow readings during the traverse to obtain a mean, as the air flow rate fluctuated slightly.

7.6. Solids Velocity Measurement.

It was decided that solids velocity measurements need only be made at three positions along the pipe line rig, to give a full indication of the solids velocity variation along the pipe. The three positions selected correspond to:

(1) A position at the end of the pipe line air solids flow entry length. The entry length here is considered as the length of pipe line necessary for the solids particles to be accelerated to a velocity close to that of the gas velocity. This obviously varies with the solids loading, but for flows where compressibility effects can be neglected, that is the gas velocity is constant, this

length should not exceed 20 feet. The first position was, therefore, selected 20 ft. downstream of the pipe entrance.

(2) A position where the gas flow begins to accelerate rapidly. This position is not well defined, but for gas flow through a pipe it is found that the gas acceleration is not constant, but starts to increase rapidly at a relatively short distance from the pipe exit. A position 18½ ft. from the pipe exit was selected to comply with the available individual pipe lengths, and it may be considered that upstream of this position compressibility effects are not of major importance.

(3) The third position was chosen to be as close as possible to the pipe exit, in order to obtain measurements of the maximum velocity attained by the solids particles. The centre of the observation glass in this position was 7 in. from the pipe exit.

At each of these positions, solids velocity measurements were made at all of the four selected air flow rates, and for each air flow rate the solids flow rate was varied to correspond to the light, medium, and heavy solids to

air loading ratios by weight. Kodak Tri X Negative film was used for all the readings, this having a film speed of 320 A.S.A. By making use of the programming unit supplied with the camera, it was possible to obtain four velocity measurements from one 100 ft. length of film. As stated previously, back lighting was found to give the best results, and this was supplied by four 750 watt bulbs; the programming unit arranges that the lights only come on at a selected time when the film is running through the camera. Diffuse lighting was obtained by inserting a double sheet of drawing office tracing paper between the lights and the observation glass, whilst the 8 in. long by $\frac{3}{4}$ in. wide slot in the observation glass cover enabled the lighting to illuminate the full field of flow.

The technique adopted for analysing the processed films was to project portions of the film, such that the complete width of film including the sprocket holes was in view, and then to measure the slope of the streaks relative to one edge of the film, and also to measure the distance between timing marks. These measurements were made on a Hilger Universal Measuring Projector, which has a magnification of x10. This instrument has a rotatable viewing table, calibrated in degrees and minutes, and a micrometer screw enables the film

to be traversed through a distance of 1 in. After lining up the datum line on the viewing table with the line on the film corresponding to one of the edges of the field of view, the table was rotated until this same datum line was inclined at the same angle as the streaks on the film. To do this, the film was traversed to and fro using the 1 in. micrometer traverse, until the datum line was parallel with the mean slope of the streaks. There was a slight variation in streak slope, which corresponds to solids particles with different velocities, but this was surprisingly small, and no difficulty was encountered in obtaining the mean streak slope angle. This procedure was then repeated at nine other positions along the film length, and the mean of the resulting ten readings represented a mean solids velocity.

The major drawback to this method of solids velocity measurement would appear to be in estimating the depth of field into the flow over which the camera can record the path of a solids particle. The depth of field was, in fact, always governed by the opacity of the flow of the solids in the air stream, and not by any limitation in camera focusing. This depth of field would be expected to vary with the density of the solids flow, and in order to obtain some indication of this, a probe was mounted on the pipe line axis projecting about 1 in.

into the field of view. This probe was a 0.049 in. o.d. stainless steel rod, as this diameter was necessary to keep it rigid, and was obviously more capable of resolution by the camera lens than a 0.012 in. diameter solids particle. However, it was thought it might give some idea of the depth of field. Because the density of solids in terms of volume of solids per unit volume of air is always greatest at the entry to the pipe line, measurements with the probe present were only taken at the farthest upstream position selected. A check was always made prior to running the film to determine whether the probe was visible in the air solids flow selected. For all flow rates the probe was visible, though for some of the high loadings it was barely so. Also the presence of the probe could always be noticed as a light patch on the projected film. Because of the size of the probe relative to that of a particle, these observations only show that there was a significant depth of field, but give no real indication of the actual depth.

The technique necessary in taking the temperature measurements, electrostatic measurements and relative humidity need only be mentioned briefly. The measurement of air temperatures in the small air receiver and the filter housing were taken once during a run, where a run is considered to

be the period during which the solids flow rate is kept reasonably constant, i.e. it corresponds to one setting of the solids flow valve. Readings of current to earth from the insulated section were taken for the range of air flows and at various solids loadings, whilst a few readings of voltage on the nylon pipe line, just downstream of the solids feeding point, were obtained by wrapping a copper wire with turns at about 1 in. pitch round the pipe. The meqsurements of relative humidity were taken to cover the full rnage of air flow rates and solids loadings.

CHAPTER 8.

EXPERIMENTAL AND DERIVED RESULTS.

In this chapter the experimental results obtained during the course of the project are presented. Included also are derived results which are considered relevant at this stage together with the method of derivation where necessary, and also the results for the computer solution of the basic equations applicable to air-solids pipe flow. Discussion of the results, however, is left until Chapter 9. As adopted previously, the chapter is sub-divided with separate headings corresponding to the measurements obtained.

8.1. Solids Particle Size Analysis.

The sieve analysis described in Section 7.1 was carried out on three samples of the polystyrene powder. These samples were selected as follows:

(a) Sample A, of new, unused powder.

(b) Sample B, taken from the rig at a time when the experiments on the pipe flow rig were about half complete.

It should be realised that the same 150 lb. of polystyrene powder originally fed into the rig was retained throughout all the pipe flow experiments.

(c) Sample C, taken when the pipe flow experiments were nearing completion.

Fig. 14 shows curves of percentage ~~undersize~~ oversize (by weight) plotted against particle size, as indicated by the sieve analysis for samples A, B and C. This method of plotting on log-linear graph paper gives an indication of particle size dispersion. A steep slope on the almost linear part of the graph indicating that most of the particles are of almost uniform size.

In Fig. 15 the number of solids particles is plotted against particle diameter. For this plot, the particles collected on a sieve were assumed to have a diameter given by the mean of the nominal apertures on the collecting sieve and the sieve above. This is not the method adopted by other workers, (e.g. Mitlin considered the solids particle diameter to be given by the nominal aperture of the last sieve through which the particle had fallen), but for this work it is felt to be more reliable as an absolute and not a compartive diameter is required for the theoretical approach. Arithmetic mean diameters have been derived from the results of the above sieve analyses and these also are given in Fig. 15 for each sample. Surface mean diameters (see Section 3.33) were also

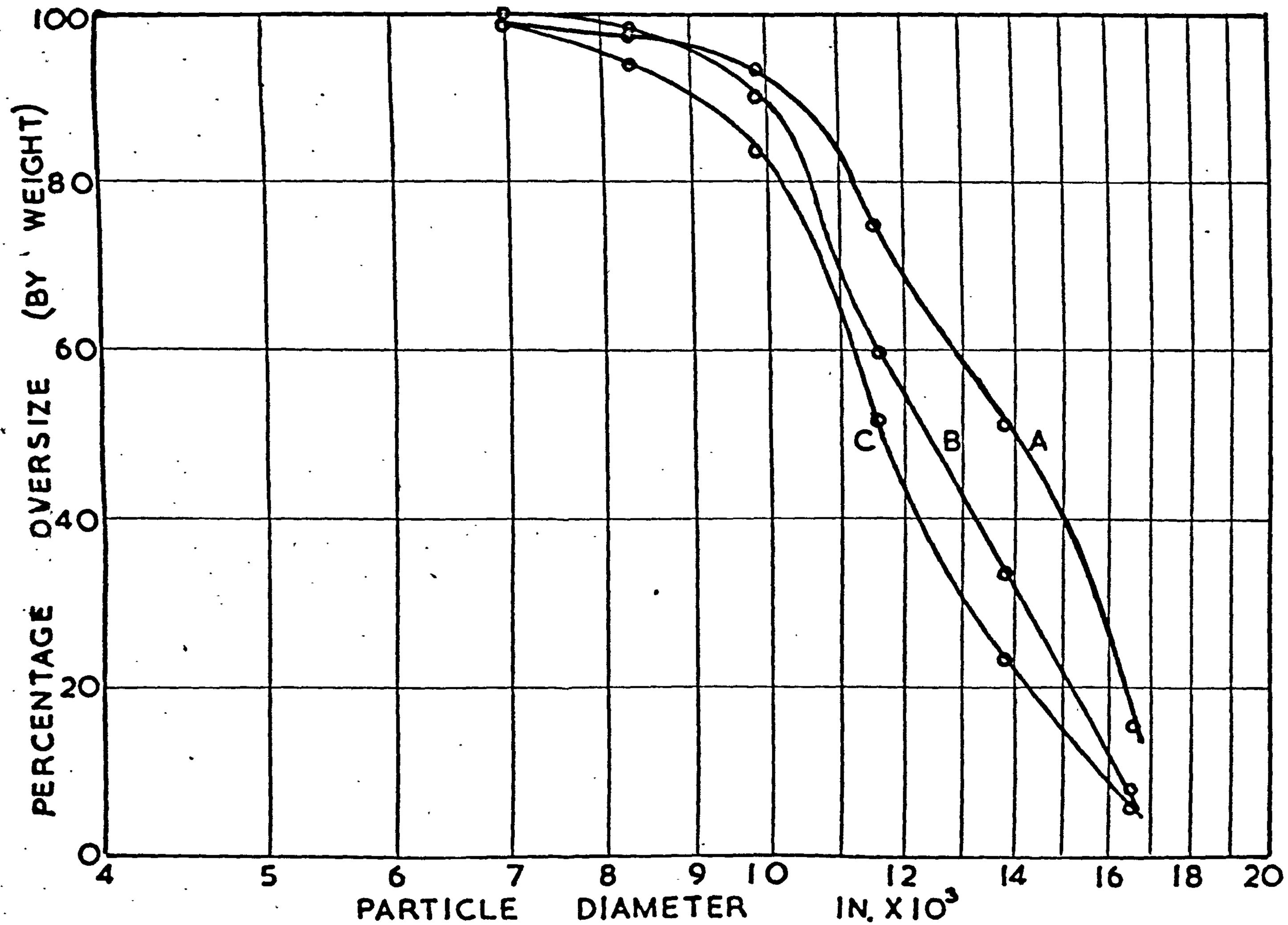

FIG 14 SOLIDS PARTICLE SIZE DISTRIBUTION FOR SAMPLES AB & C

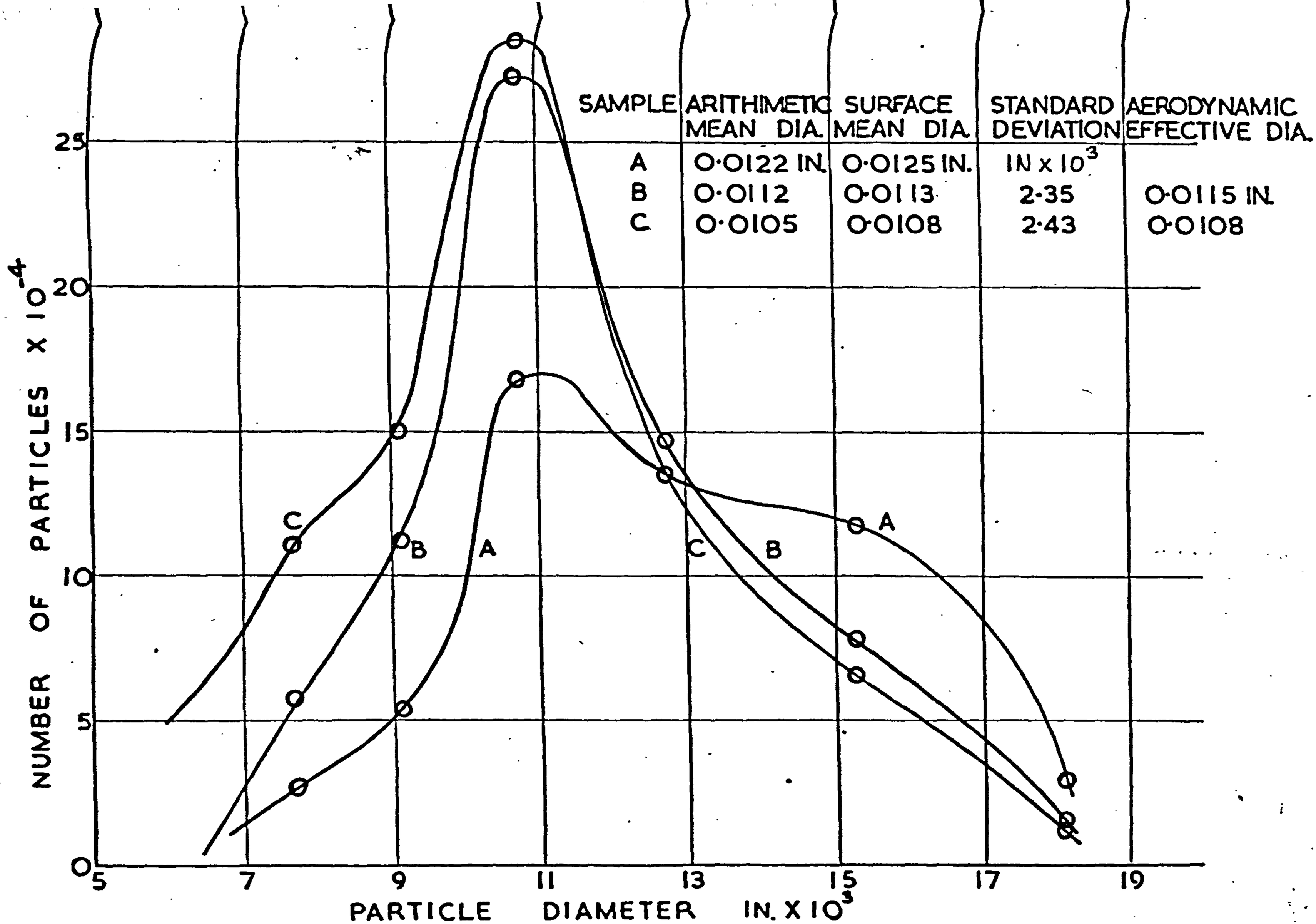

FIG 15 SOLIDS PARTICLE SIZE DISTRIBUTION

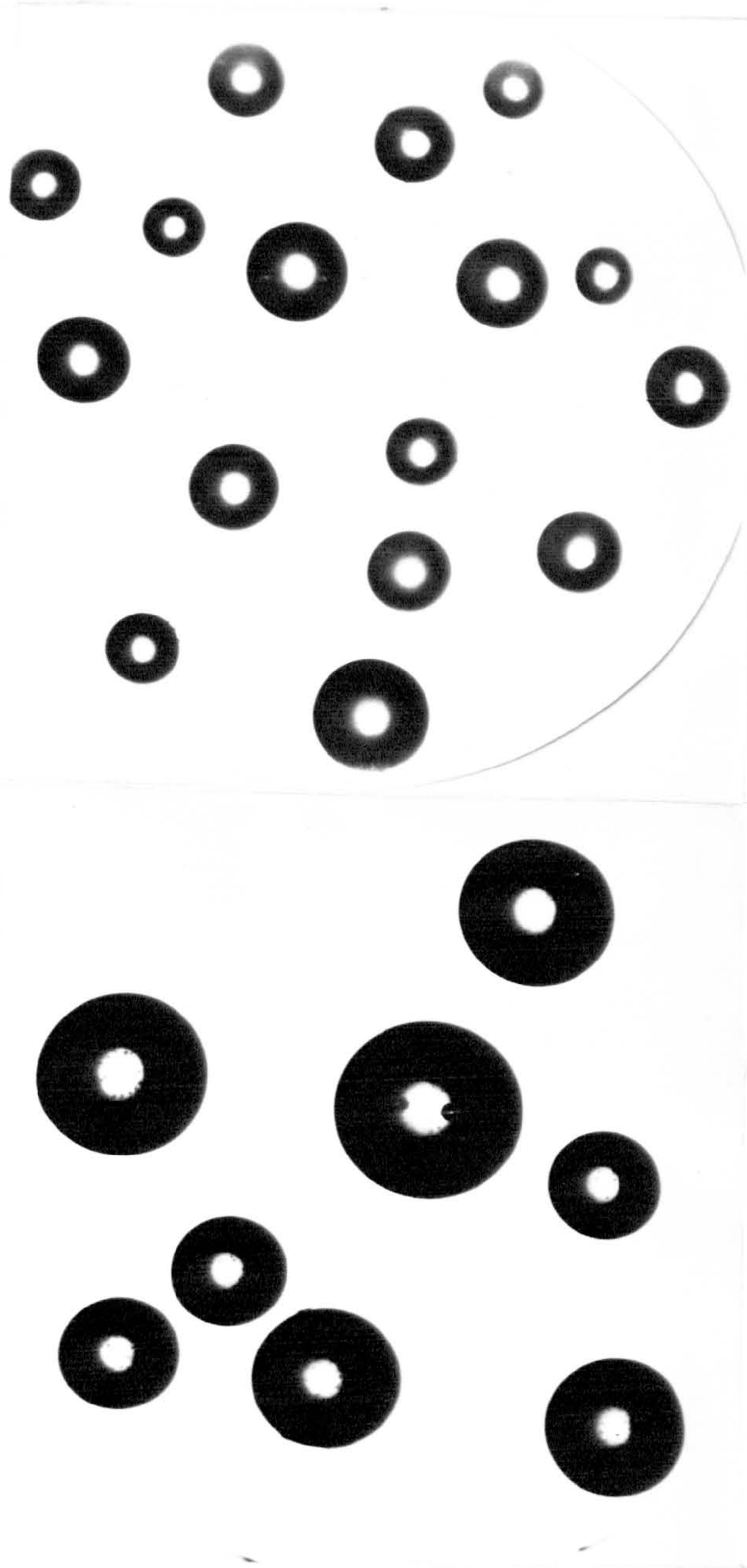

SAMPLE A

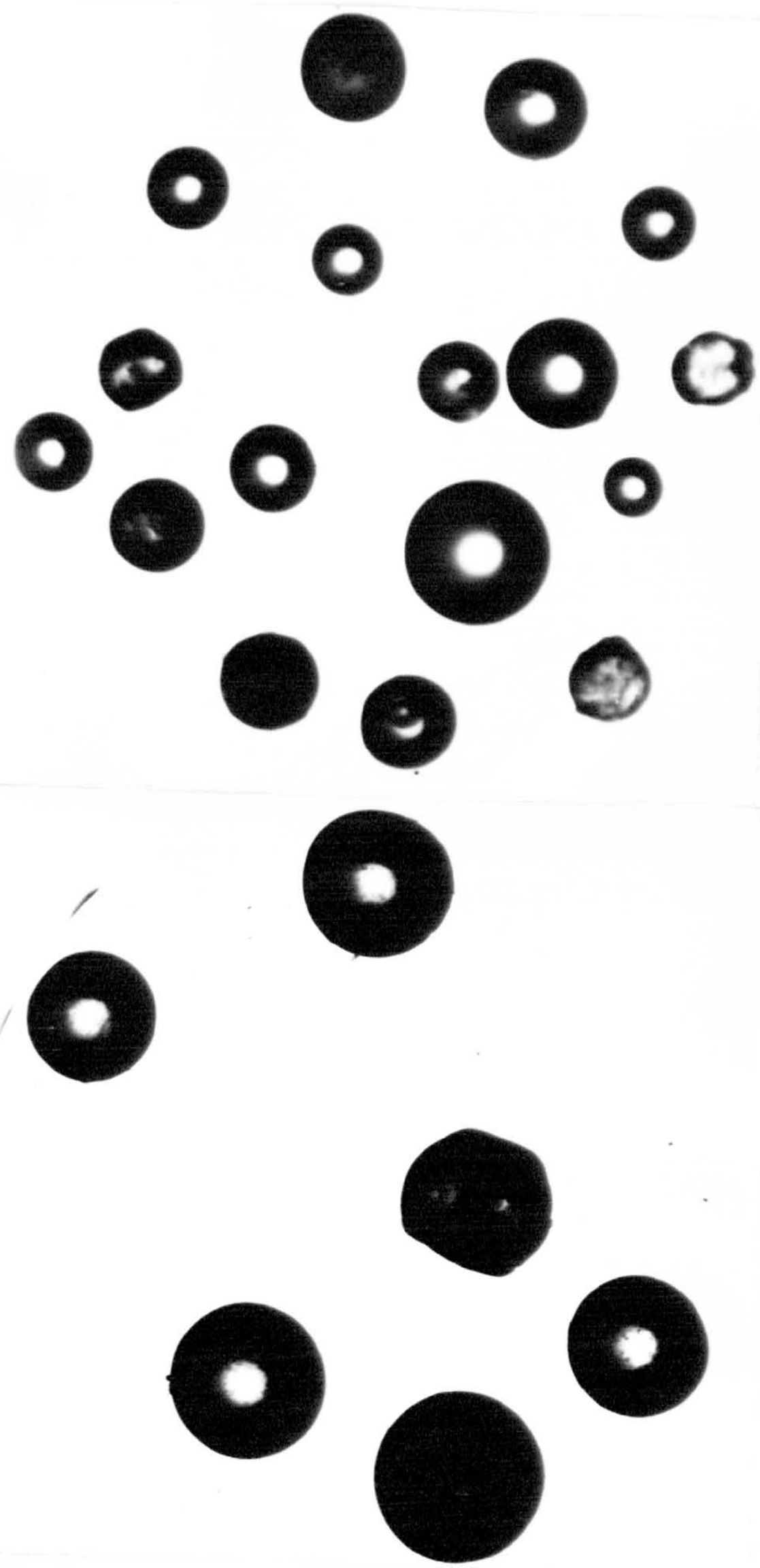

SAMPLE B

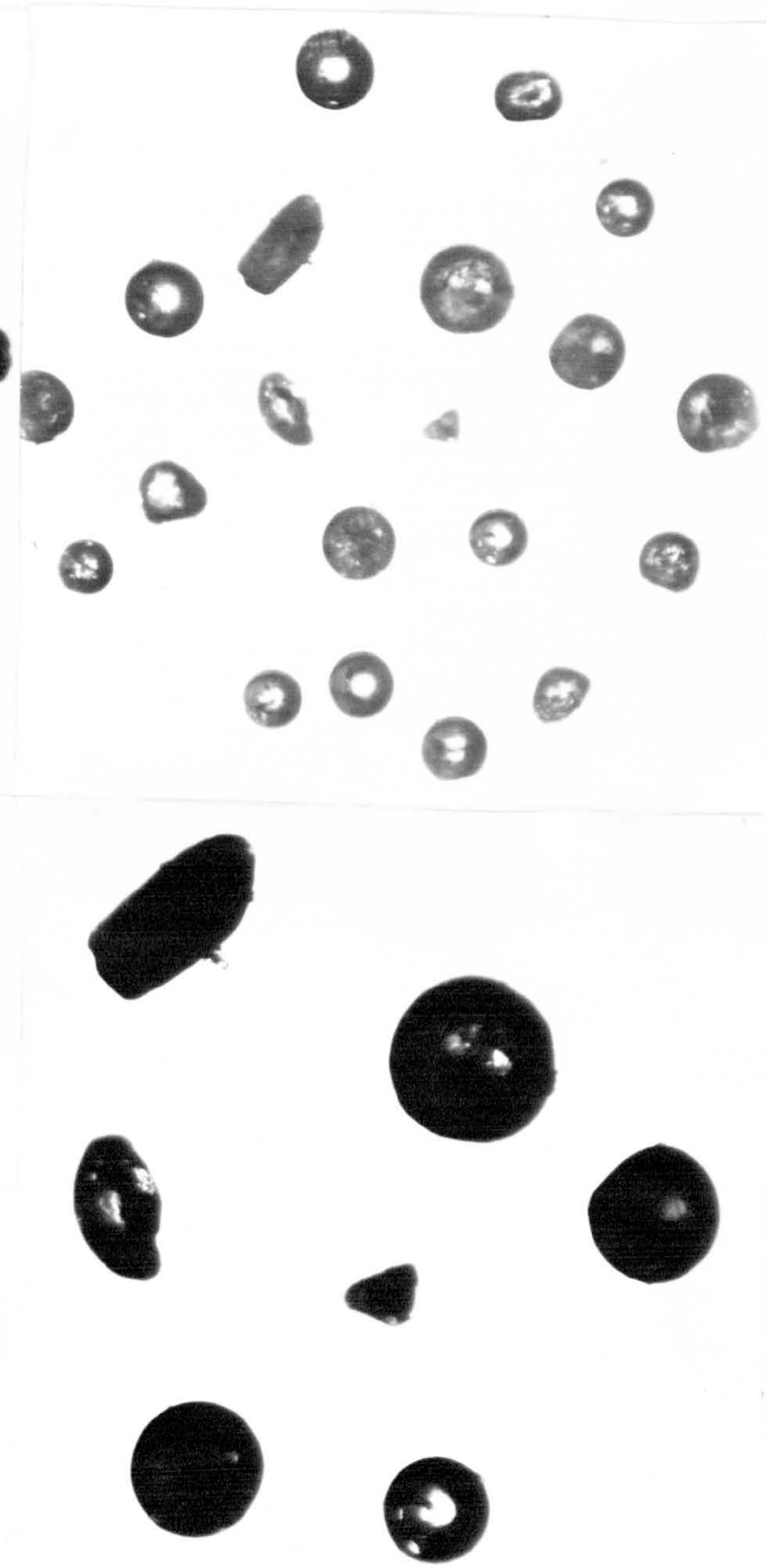

SAMPLE C

evaluated, but for all three samples the resulting diameter was almost exactly identical with the mean arithmetic diameter. As shown in Fig. 15, although Sample A has a markedly unsymmetrical distribution, the used particles samples B and C have fairly symmetrical distributions. The standard deviations have, therefore, been determined and are given in Fig. 15. Aerodynamic effective diameters (see Section 3.33 and Appendix 2) have been evaluated for the three samples and these have values within 3% of the arithmetic mean diameter.

The technique adopted for attributing mean sizes to the particles collected on the top sieve and the tray at the base of the nest of sieves needs some explanation. In the case of the top sieve, the particles collected were assumed to have a diameter given by the mean of the aperture of this sieve and the next largest sieve in the B.S. range. The diameter for those particles collected in the tray was defined as the mean of the sieve aperture through which the particles had last fallen and the next smallest sieve in the B.S. range. Although this method of determining the diameters is rather questionable, because the quantities of particles collected of these diameters was small, they have only a small influence on the arithmetic mean diameter.

In Fig. 16 are shown photographs of the polystyrene powder particles taken from samples A, B and C. These photographs were taken on a Vickers Projection Microscope, made by Cooke, Troughton and Simms, using Ilford photographic plates of 10 A.S.A. film speed, with magnifications as indicated. As can be seen from both the high and low magnifications, when new, the particles are perfectly spherical. The photographs of Samples B and C give an indication of how the particles break-up after continual use, and should not be considered to represent the number of particles breaking-up, as this was probably much less than the 50% or so indicated in Sample C. It can be seen that even after break-up the particles are of rounded shape and not at all angular.

8.2. Pressure Drop Measurements.

8.2.1. Pipe Line Pressure Drop.

Before presenting the air-solids flow pressure drop readings, the agreement of the pure air flow pressure drops with those predicted theoretically will be considered. As stated in Section 7.2, the pipe line pressure is usually non-dimensionalised by dividing it by the pipe exit pressure, and this has been done for the static pressure readings obtained. The plotted points in Figs. 17 and 18 show this pressure ratio

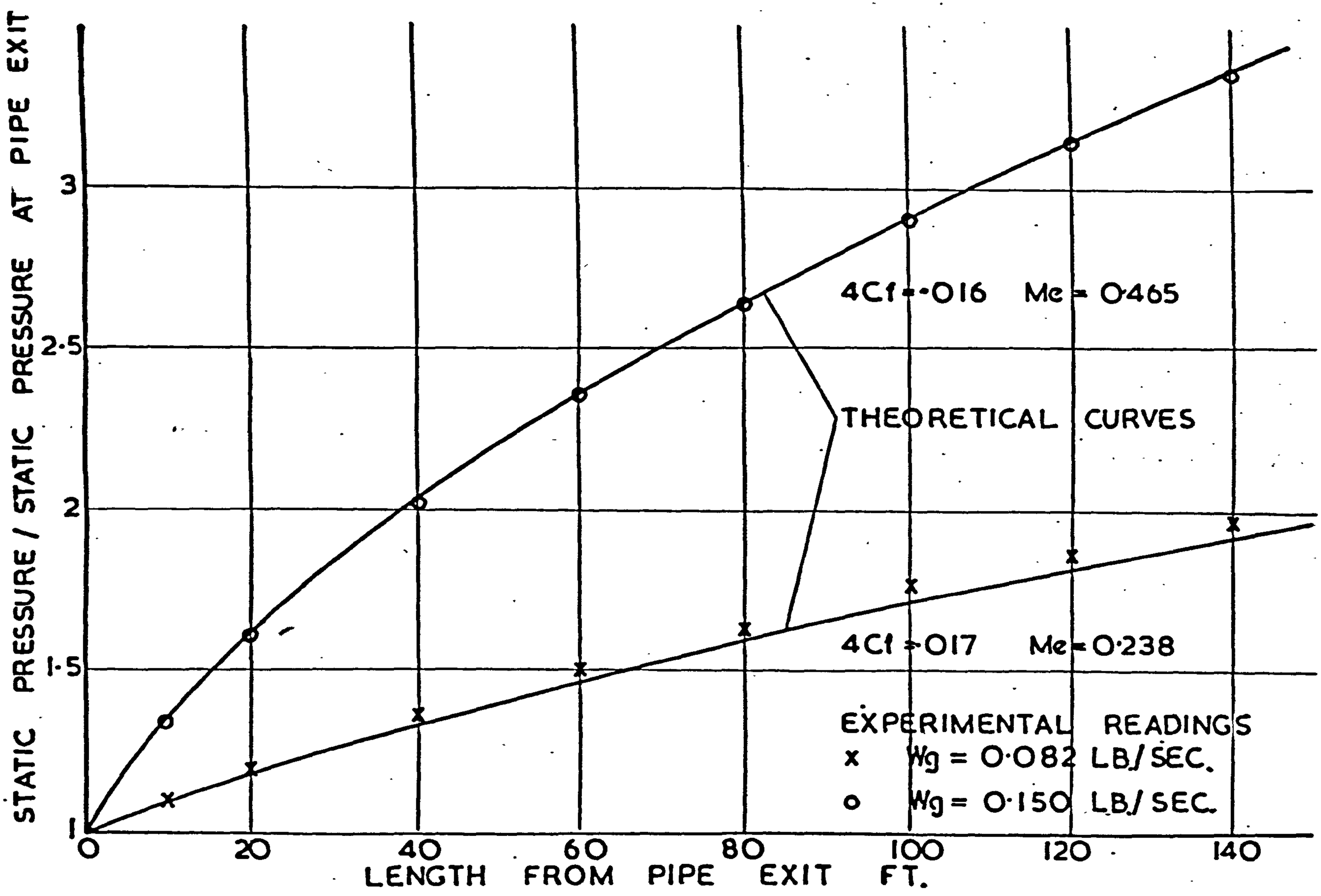

FIG17 PRESSURE DROP CURVES FOR Wg=0·082 & 0·150 LB/SEC — AIR FLOW

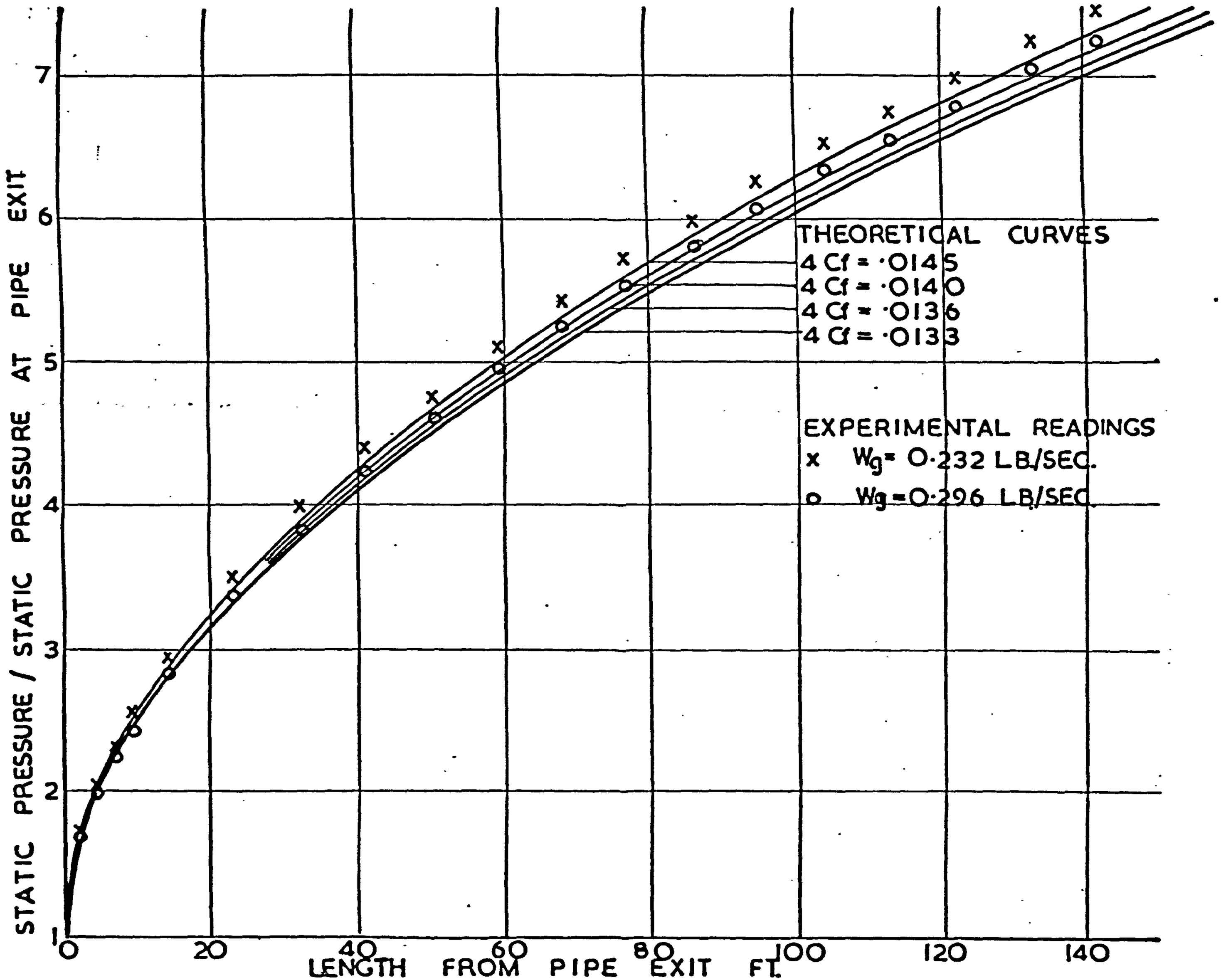

FIG 18 PRESSURE DROP CURVES FOR Wg = 0·232 & 0·296 LB/SEC. – AIR FLOW

plotted against pipe length from exit for the four different air flow rates. In order to make a comparison with a theoretically predicted curve, some assumption regarding a pipe wall skin friction factor is necessary. Normally, for reasonably dust free air flow in a smooth bore pipe such as this, the pipe flow friction factor would be taken from a friction factor against Reynolds number curve, available in most fluid mechanics text books, or the Blasius equation $4C_f = 0.316\ (Re)^{-.25}$ used if the Reynolds number lies in the range 3,000 to 100,000. However, after a few runs delivering solids the pipe wall becomes coated with fine particles, so that it was no longer thought reasonable to assume the wall smooth. The method adopted, therefore, for deriving the skin friction factor was to assume that over the first 10 ft. length of pipe the flow could be assumed incompressible. In which case the Fanning friction equation could be applied and the skin friction factor was derived knowing the pressure drop, mean air velocity, temperature and density over this length and also the mass flow rate. Further assumptions in applying this friction factor to the full pipe flow are that the Reynolds number is considered constant along the pipe, whereas it would in fact increase slightly as the air viscosity decreases with the decreasing air static temperature towards the pipe exit. No variation

of skin friction factor with Mach number is considered, which according to Keenan and Naumann (1946) also is reasonable. With the foregoing assumptions, theoretical curves of p/p_e - ($\ell_e - \ell$) are obtained by making use of tables available for the compressible flow of dry gases, such as those by Houghton and Brock. In the case of the air flow rates below the "choked" flow condition, the pipe exit Mach number must first be determined. This can be obtsined by substituting for the static temperature and the air density in the Mach number equation, making use of the continuity of mass flow, gas equation of state, adiabatic temperature and gas velocity of sound equations. The exit Mach number is then a function of mass flow rate, pipe diameter, exit static pressure, total temperature and ratio of specific heats, and these measurements are all available from the experiments i.e.

$$\frac{\gamma - 1}{2} Me^4 + Me^2 - \left(\frac{W_g}{A}\right)^2 \frac{R\,T_o}{\gamma . p^2} = 0$$

The pipe is then extrapolated to give a choked flow and the pressure ratios and pipe lengths considered relative to the pipe exit position. The full curves in Figs. 17 and 18 represent the theoretically derived pressure ratios for the four air flow rates used. In the cases of the high airflow rates curves have also been drawn using the skin friction factor given

by a $4C_f$ - Reynolds number curve for smooth pipes. For the curves corresponding to 0.082 and 0.15 lb/sec. air flow rates, the exit Mach number derived from the above equation is also given in Fig. 17.

The pressure drop curves for the air-solids flow are presented in a similar form to those for pure air flow. In this case, however, as previously explained in Section 7.2, the non-dimensionalising pressure is not the pipe exit pressure, but it is a pressure close to pipe exit and is regarded as a reference pressure. A static pressure traverse indicated it was 0.75 in. from the actual pipe exit for an air flow rate of 0.15 lb/sec. Figs. 19, 20, 21 and 22 corresponding to the four air flow rates selected, show the effect of increasing solids to air loading ratio on the pressure drop, and curves for pure air flow are also included for comparison. As stated in Section 7.2, because of the difficulty in maintaining a constant air flow for all the various solids flow rates, a normalising procedure was adopted for the air flow rates of 0.082 and 0.15 lb/sec. to ensure that of the pressure measured at any position, that proportion representing air flow pressure was the same for all the different solids loadings.

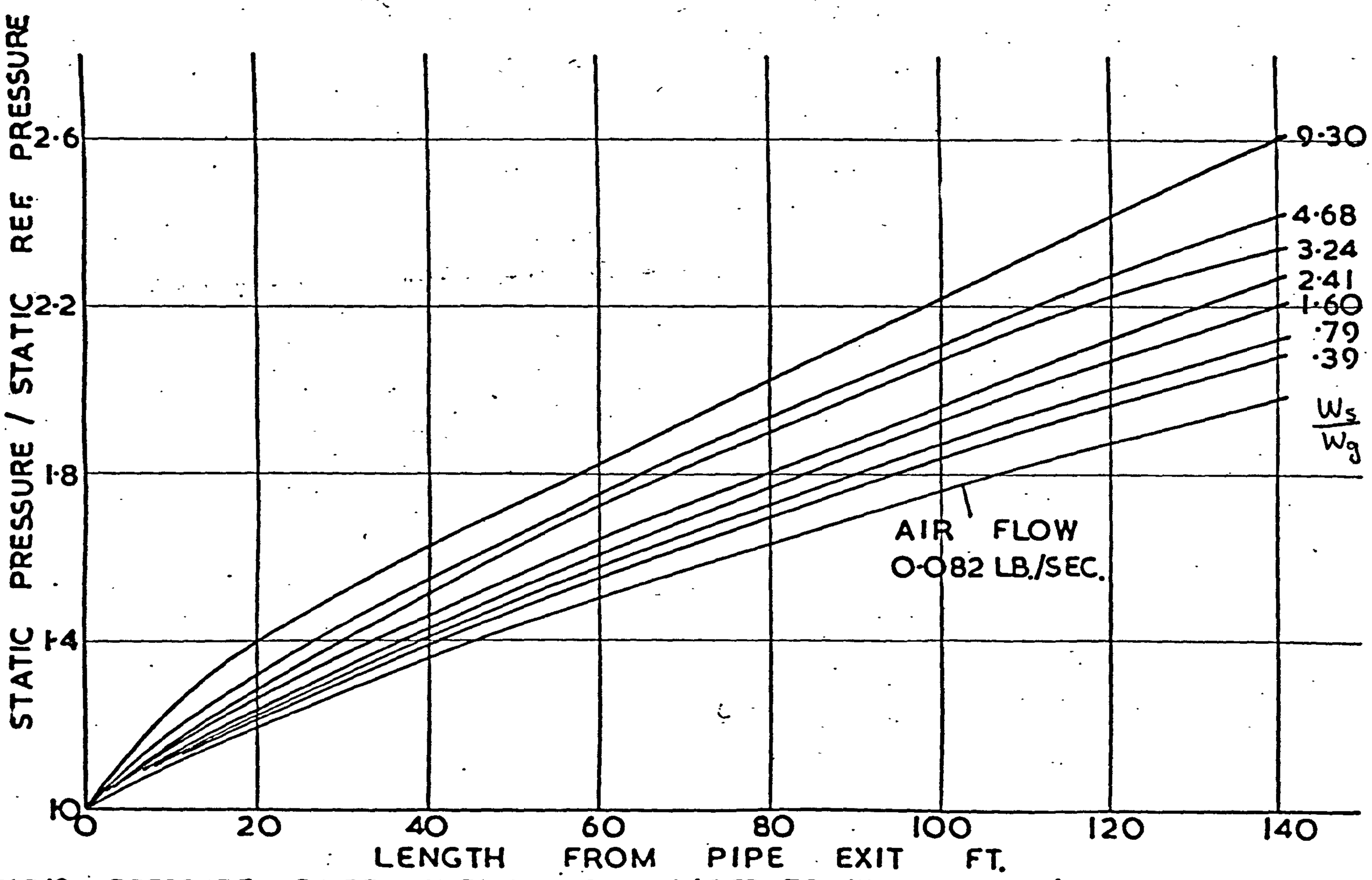

FIG 19 PRESSURE DROP CURVES NORMALISED TO W_g=0·082 LB/SEC.– AIR-SOLIDS FLOW

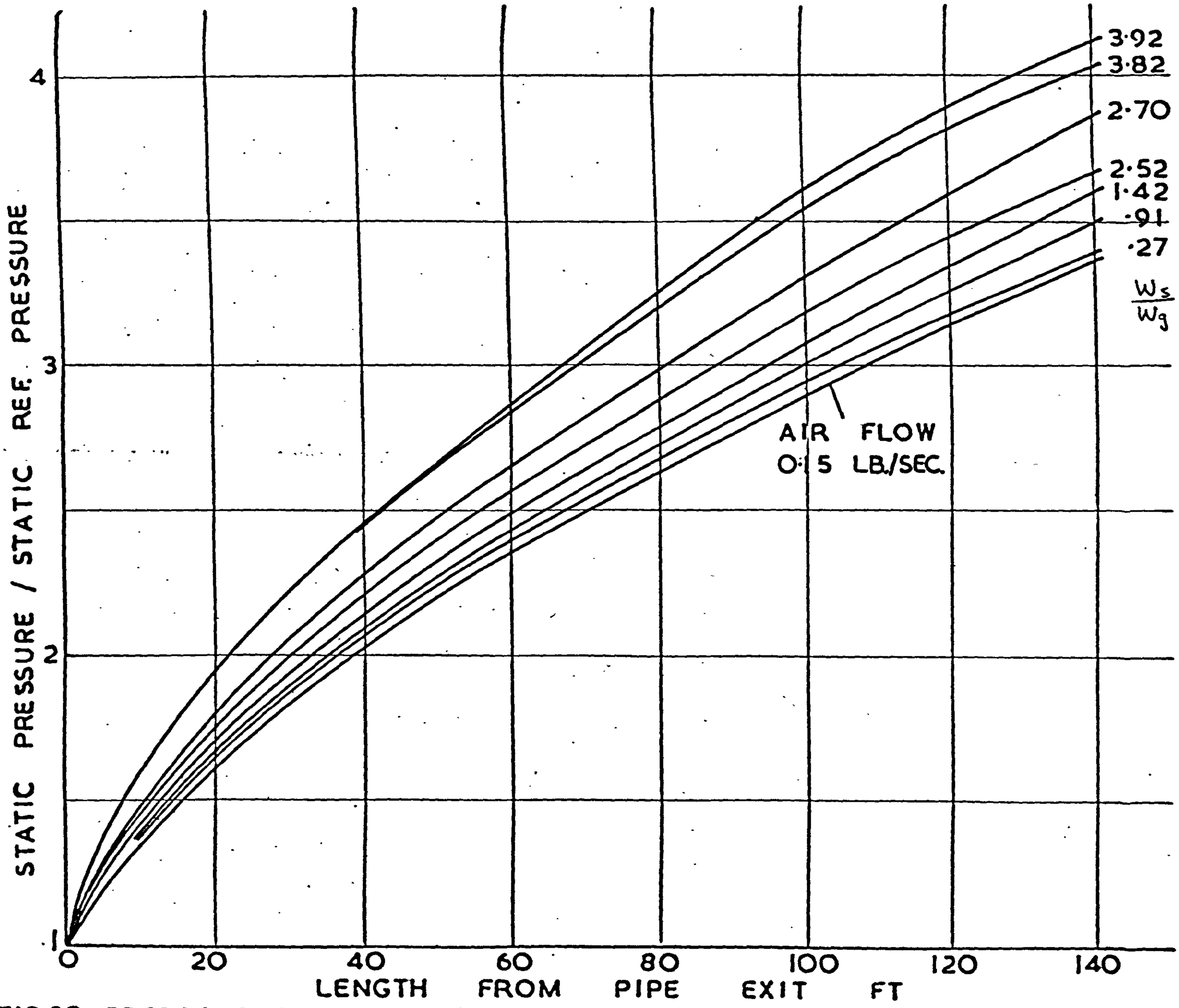

FIG 20 PRESSURE DROP CURVES NORMALISED TO Wg=0·15 LB/SEC.—AIR-SOLIDS FLO

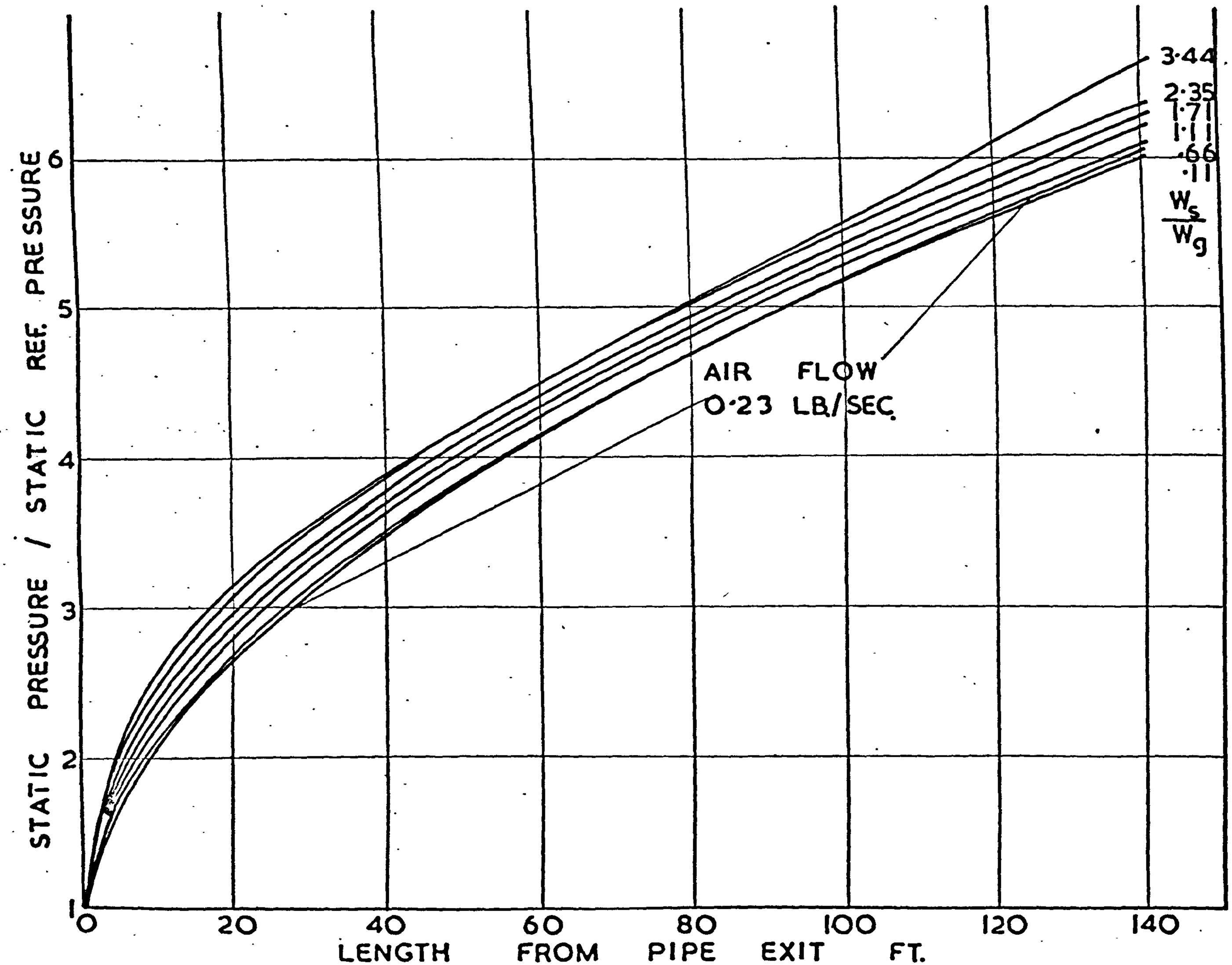

FIG 21 PRESSURE DROP CURVES FOR $W_g \approx 0{\cdot}23$ LB/SEC. — AIR-SOLIDS FLOW

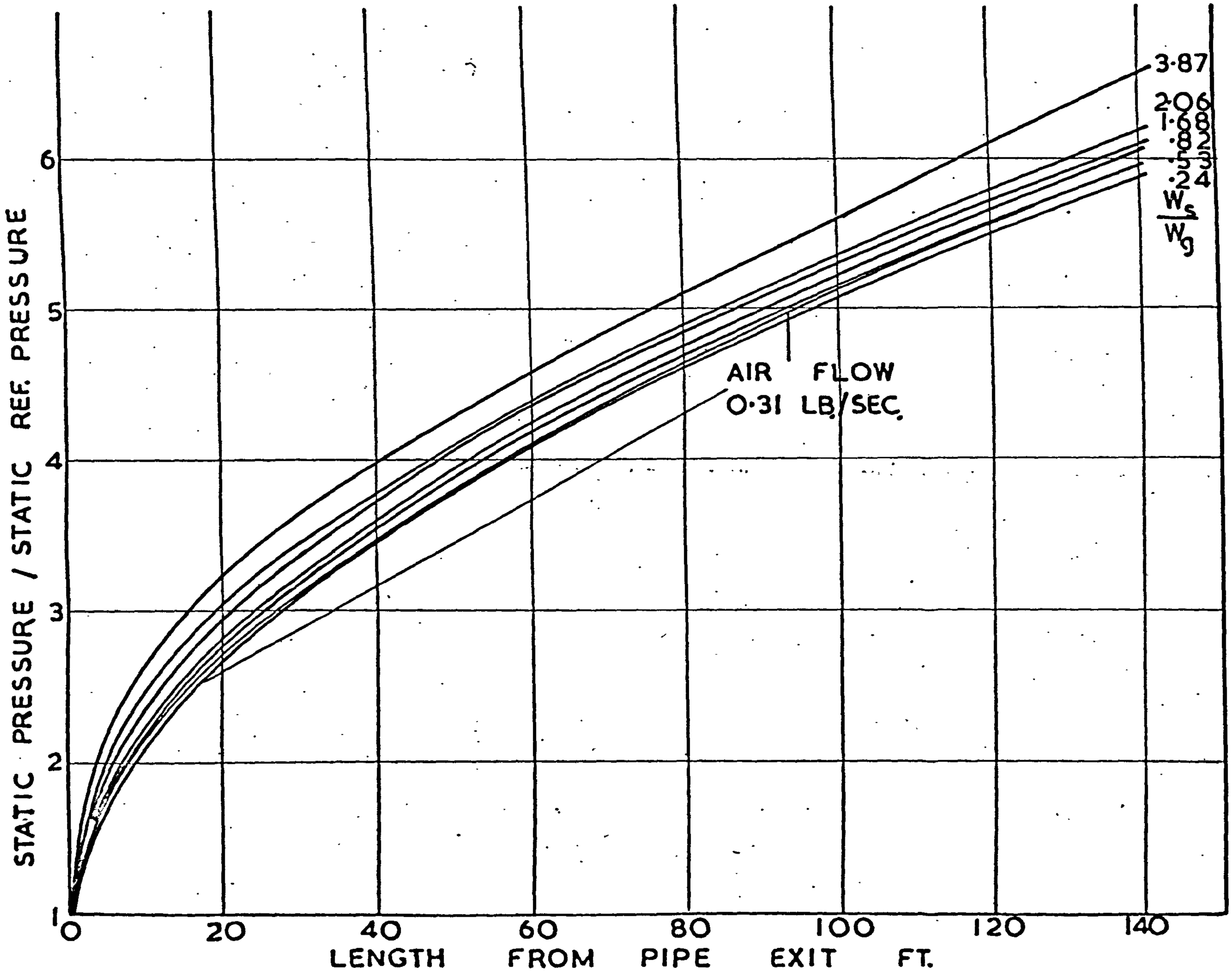

FIG22 PRESSURE DROP CURVES FOR $W_g \approx 0{\cdot}31$ LB/SEC. — AIR-SOLIDS FLOW

A further use has been made of these pressure drop curves in order to obtain some idea of what values of air flow rate and the ratio of solids to air mass loading W_s/W_g constitute an optimum for conveyance along a straight pipe line. The method adopted for obtaining a comparison for the different air flow rates used was to plot the ratio of horse power consumed to solids flow rate in conveying a distance of 141 ft. against the ratio W_s/W_g, Fig. 23. Because, when conveying solids at high speeds in air flow, a diffuser would almost certainly be used to convert as much as possible of the dynamic head available at pipe exit back to pressure head, and hence reduce the total pressure drop, the pressure drop measurement used in deriving the horse power is that occurring from the 141 ft. position to the diffuser exit. The expression for horse power consumed is then:-

$$(p\ (\ell = 141\ \text{ft}) - p(\text{diff. exit})) \times A \times u_g/550.$$

where the air velocity u_g is that at the 141 ft. position and is derived from the continuity of mass flow and gas equation of state expressions.

8.2.2. Cyclone Pressure Drop.

Although no accurate measurements were made of the

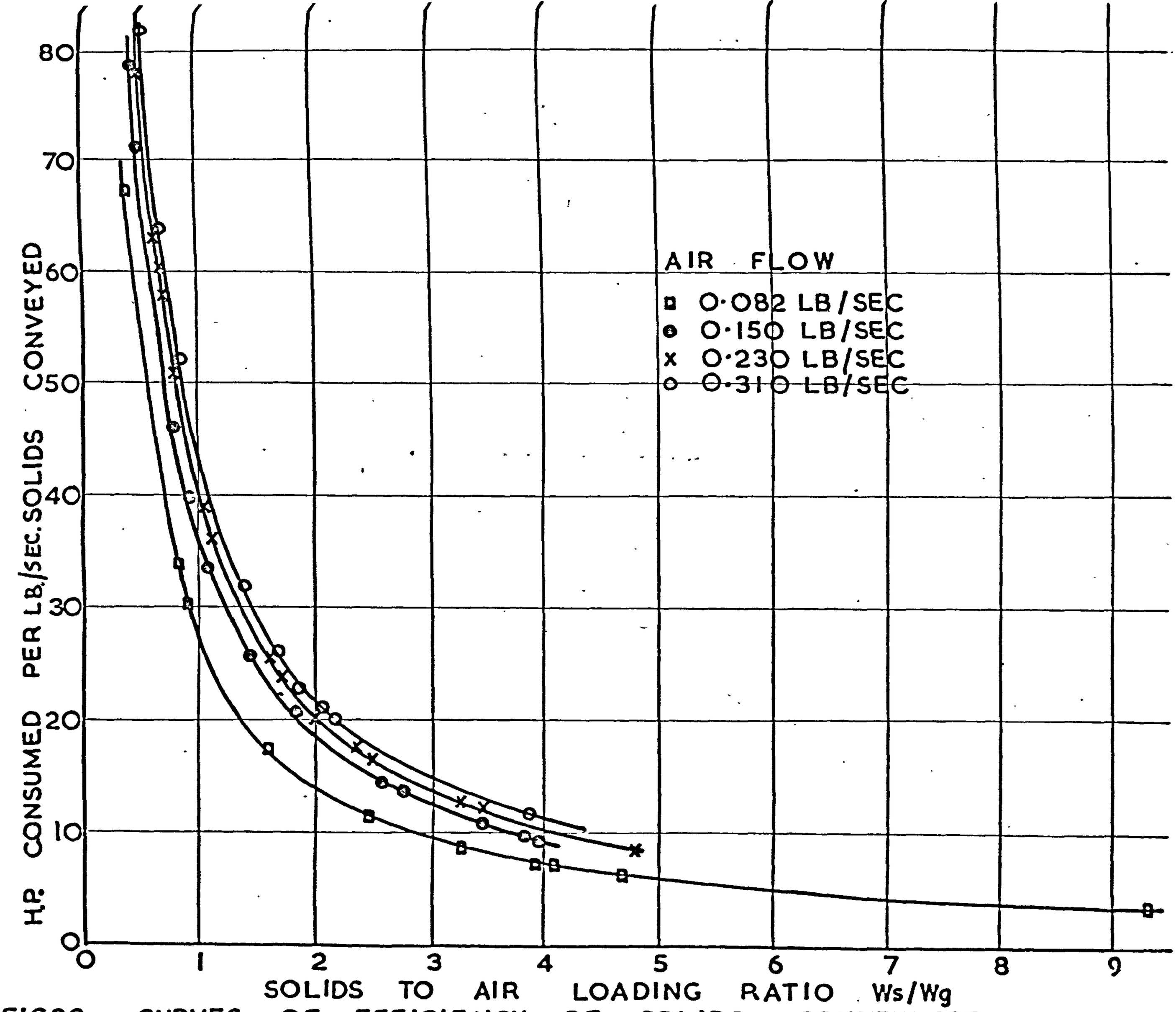

FIG23 CURVES OF EFFICIENCY OF SOLIDS CONVEYANCE

pressure drop between the inlet and exhaust of the cyclone, it is possible from the measurement of pressure at the diffuser exit and the atmospheric pressure measurement to deduce the pressure drop between cyclone inlet and the exit to the air exhaust from the rig. It should be realised that this measurement includes flow through the cyclone, the bag filter, the air flow measurement nozzle and various lengths of piping. It has been observed, however, that this pressure drop does not remain constant with varying solids to air loading ratio. Fig. 24 shows plots of this pressure drop against W_s/W_g for three of the four different air flow rates. Although the experimental readings for these curves show tremendous scatter, which is considered to be entirely due to the lack of accuracy in pressure drop measurement, they do indicate a trend towards decreasing pressure drop as the solids loading is increased, especially at the high air flow rates. Because the flow downstream of the cyclone is almost pure air flow (very few solids particles are carried over into the bag filter) it would seem reasonable to assume that this variation in pressure drop with loading ratio is due entirely to a variation in pressure drop across the cyclone.

8.3. Air Velocity Profile Measurements.

As was previously stated in Section 7.5, the attempt

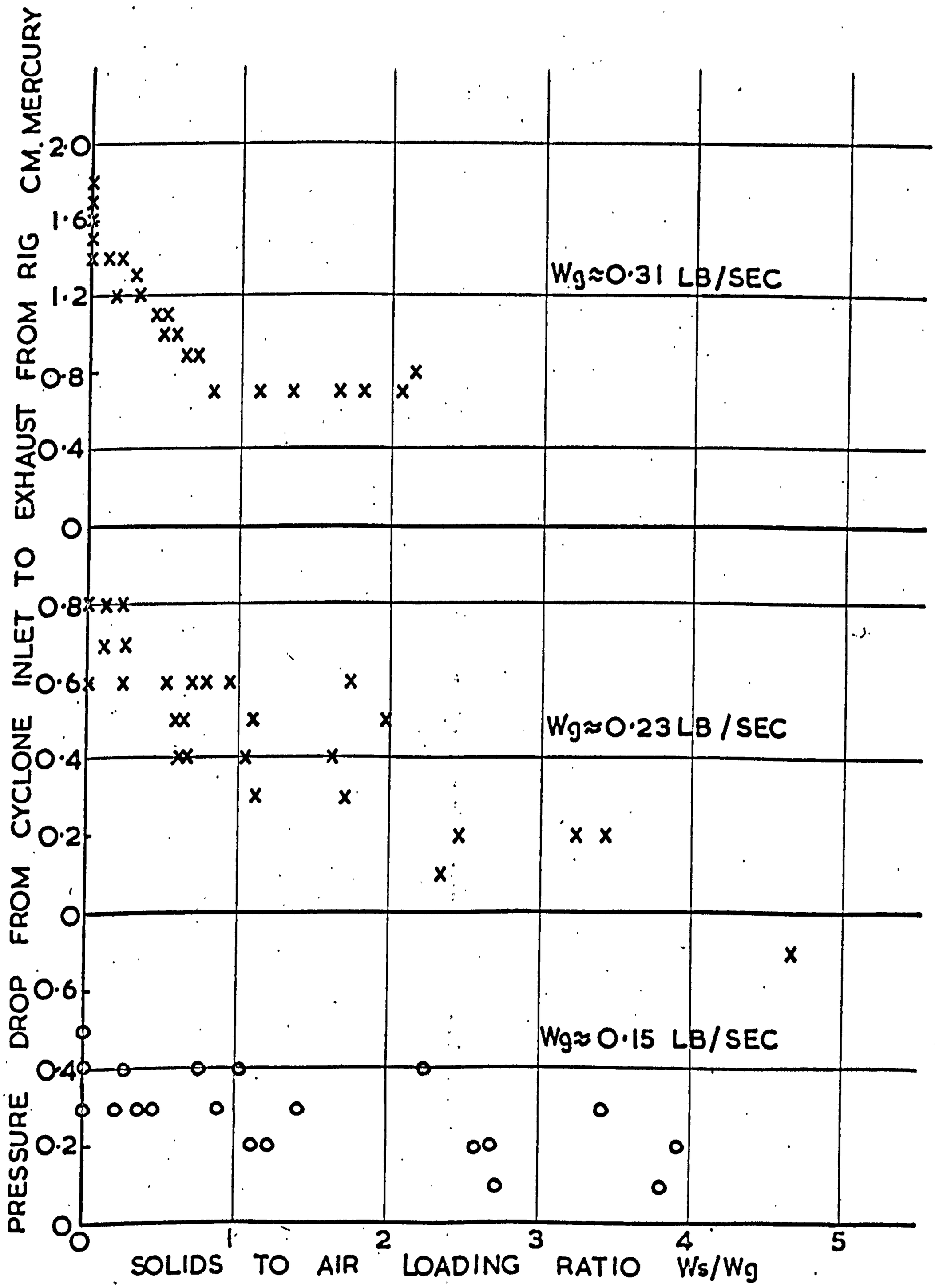

FIG 24 VARIATION OF CYCLONE PRESSURE DROP WITH Ws/Wg

to obtain pitot-tube traverses across a pipe radius have only been partially successful due to blocking of the pitot-tube by the solids particles.

Before considering the traverses made in air-solids flow, the results obtained at various positions along the pipe line and at various air flow rates for traverses in pure air flow will be presented. Because the variables most likely to influence the air velocity profile are pipe Reynolds number and the flow Mach number, the curves are presented with these as the variables and no indication of air flow rate or pipe line position is given. The velocity is made non-dimensional by dividing by the centre-line velocity, and the radius by expressing as the distance from the wall y divided by pipe radius R as this is the usual practice. The curves are drawn on log-log graph paper so that if the velocity profile follows that of a power law, the index of this law may be evaluated. Fig. 25 shows the variation of velocity profile with Mach number and Reynolds number and it can be seen that the plots approximate to straight lines, so the value of n in the index of the power law is also given:

$$\frac{u}{\hat{u}} = \left(\frac{y}{R} \right)^{\frac{1}{n}}$$

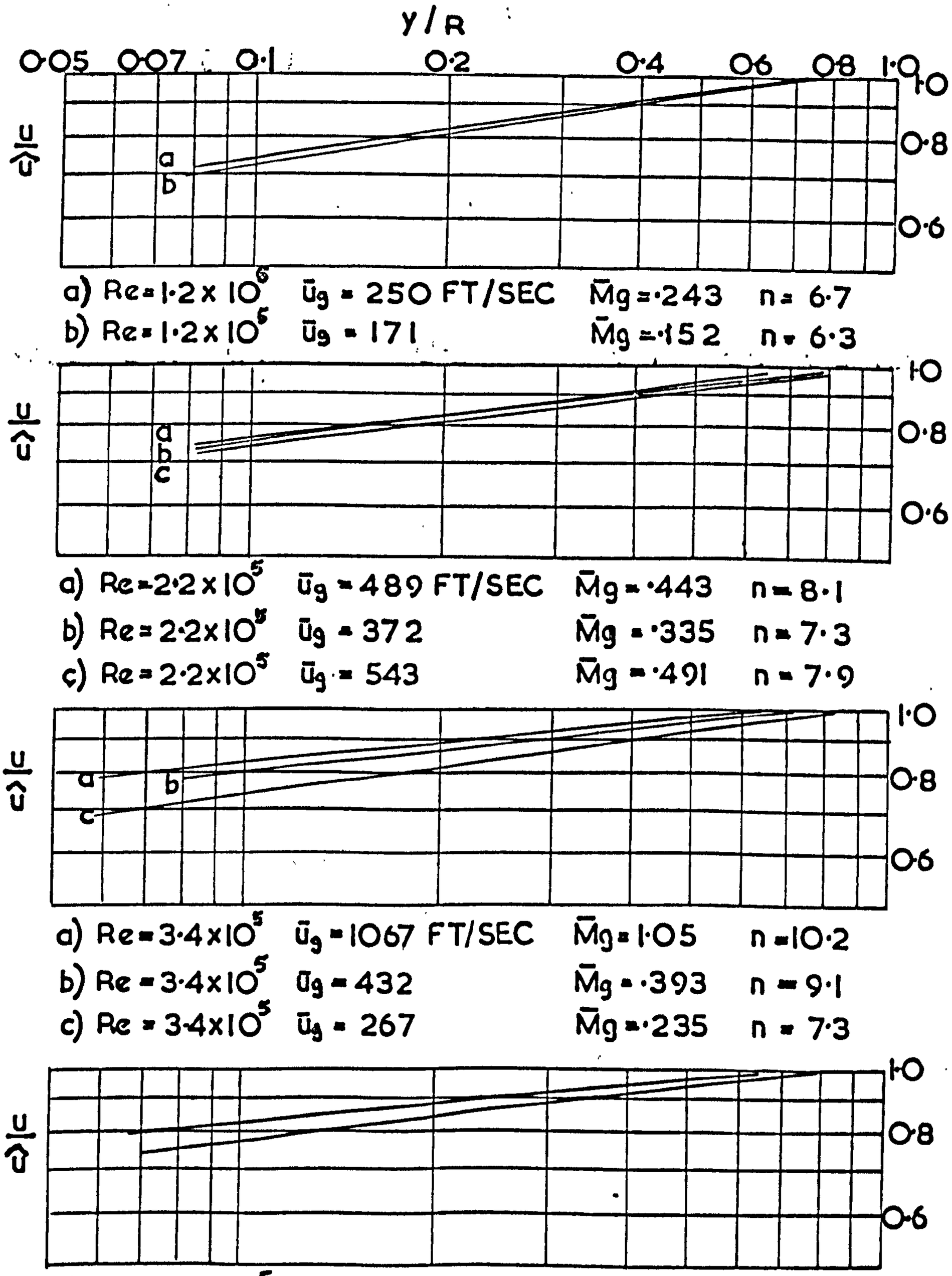

FIG 25 VELOCITY PROFILES FOR AIR FLOW

The method of obtaining $u/\hat{u}$ and the mean Mach number from the pitot traverse are now outlined. From the U-V recorder trace representing the total pressure to static pressure differential across the pipe line, the relevant calibration curve for the pressure transducer and associated galvanometer in the U-V recorder and the absolute static pressure at the pipe line position considered, the total pressure variation across the pipe is determined. The gas Mach number variation is then evaluated from the one-dimensional isentropic flow pressure relationship.

$$\frac{p_o}{p} = \left(1 + \frac{\gamma - 1}{2} M^2\right)^{\frac{\gamma}{\gamma-1}} \qquad \ldots (1)$$

The total temperature to static temperature ratio is given by:

$$\frac{T_o}{T} = 1 + \frac{\gamma - 1}{2} M^2$$

and the air velocity to centre-line velocity by:-

$$\frac{u}{\hat{u}} = \frac{M}{\hat{M}} \sqrt{\frac{T}{T_o} \cdot \frac{T_o}{\hat{T}}} \qquad \ldots (2)$$

As stated in Section 7.5, because of the uncertainties involved, the mass flow predicted from the velocity profile was compared with the measured mass flow rate before the

profile was considered acceptable. By considering the flow through an elemental ring in the pipe cross-section and then integrating this across a pipe radius, after substituting from the gas velocity of sound equation, the gas equation of state and the isentropic temperature relationship it can be shown that the gas mass flow rate is given by:-

$$W_g = 2\pi\sqrt{\frac{\gamma p^2}{RT_o}} \cdot \int_o^R \sqrt{1 + \frac{\gamma - 1}{2} M^2} \cdot Mr \, dr \qquad \ldots (3)$$

The integration was performed by plotting the curve of $\sqrt{1 + \frac{1}{2}(\gamma - 1) M^2} \cdot Mr$ against r and measuring the area under this curve with a planimeter. Then only when the resulting mass flow rate was within 4% of the measured flow rate, was the velocity considered acceptable.

The method of interpreting the readings available from the air-solids flow pitot traverses is not, of course, well defined like that for pure gas flow. The criterion adopted here was to regard the total pressure measured by the pitot-tube as representing the total pressure of the air alone and containing no contribution due to solids velocity. With this assumption it is possible to use the traces from the traverse, along with the static pressure reading to

evaluate the gas Mach number and velocity variations and also to make the comparison between the air mass flow rate predicted from the traverse with that measured, by using equations 1, 2 and 3 above. Fig. 26 shows curves of velocity ratio plotted against dimensionless distance from the wall as obtained from the successful traverses. As stated in Section 7.5, for the majority of the readings the air mass flow rate evaluated from equation 3 was within 5% of the measured flow rate.

There are a number of methods of obtaining a mean value from the varying values of variables across a pipe diameter depending on which variable or function of the flow the equalisation is based. The methods adopted in this project, of deriving the mean Mach number and mean velocity across the pipe diameter are based on the equalisation of the mass flow rate. By comparing the mass flow rate of an "ideal fluid" with uniform velocity profile with that of the actual fluid with its non-uniform profile it can be shown that the mean gas Mach number is given by:

$$\sqrt{1 + \frac{\gamma - 1}{2} \bar{M}^2} \cdot \bar{M} \frac{r^2}{2} = \int_0^R \sqrt{1 + \frac{\gamma - 1}{2} M^2} \cdot M r \, dr$$

whilst the mean velocity is obtained by substituting for the

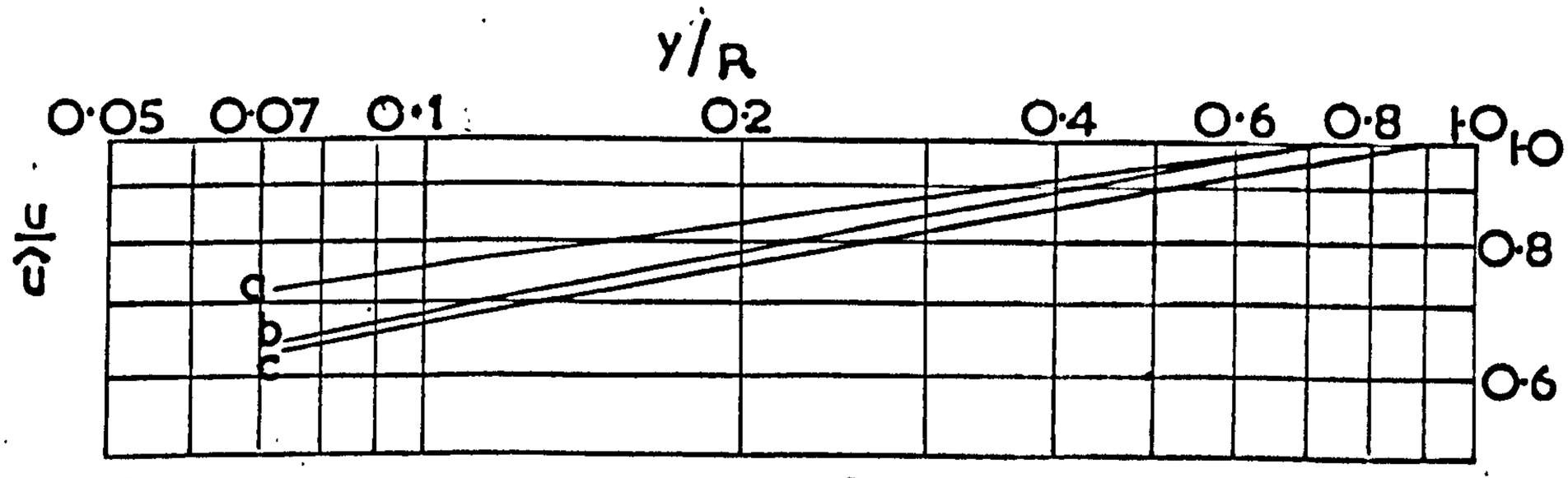

a) Wg=·081 LB/SEC Ws/Wg = 2·1 $\bar{u}_g$ = 200 FT/SEC $\bar{M}_g$=·18 n = 7·0
b) Wg=·084 Ws/Wg = ·14 $\bar{u}_g$ = 223 $\bar{M}_g$=·20 n = 5·6
c) Wg=·084 Ws/Wg=·075 $\bar{u}_g$ = 218 $\bar{M}_g$=·20 n = 5·3

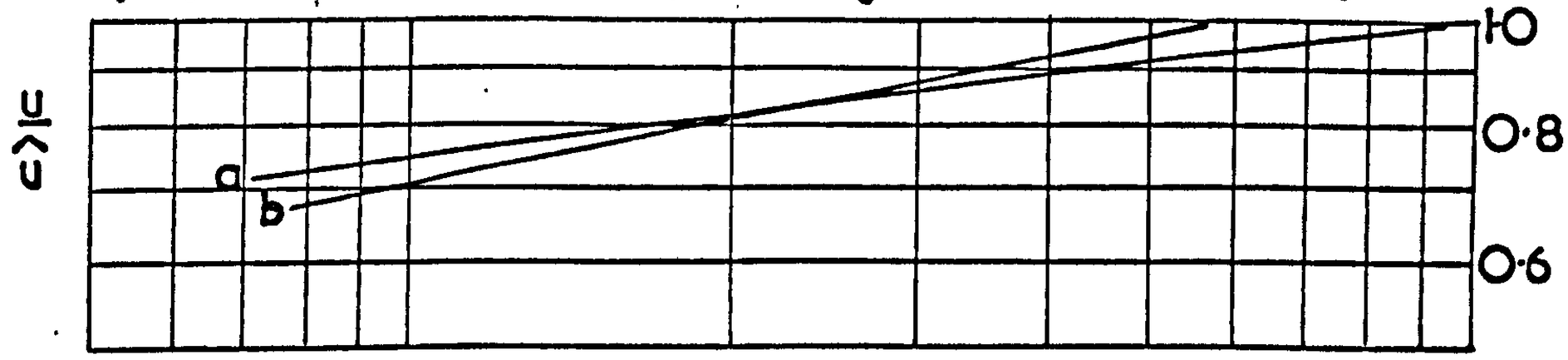

a) Wg=·151LB/SEC Ws/Wg=·28 $\bar{u}_g$ = 488 FT/SEC $\bar{M}_g$=·44 n = 7·9
b) Wg=·151 Ws/Wg=·49 $\bar{u}_g$ = 337 $\bar{M}_g$=·30 n = 5·1

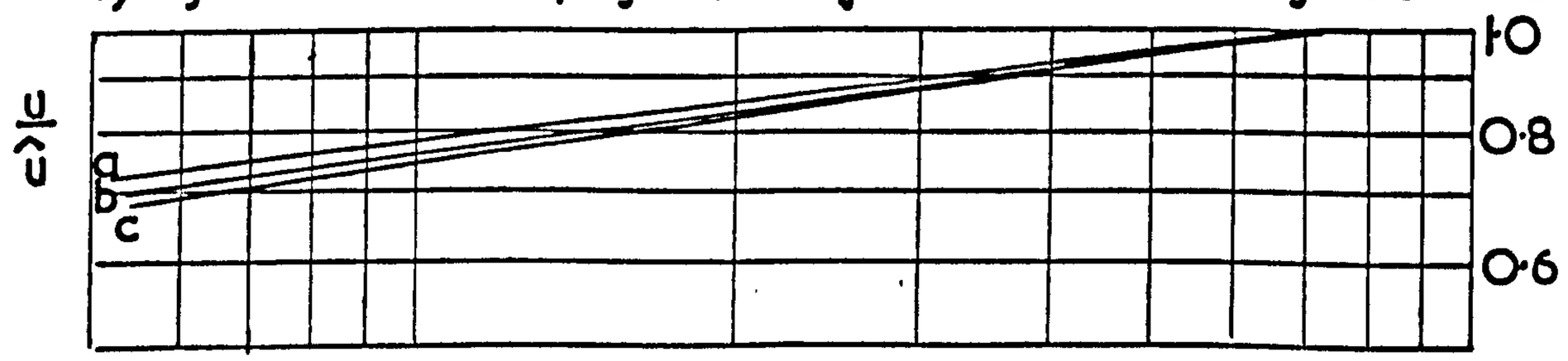

a) Wg=·238LB/SEC Ws/Wg·94 $\bar{u}_g$=240FT./SEC $\bar{M}_g$ = ·21 n=8·0
b) Wg=·236 Ws/Wg=·84 $\bar{u}_g$ = 246 $\bar{M}_g$= ·22 n = 7·7
c) Wg=·231 Ws/Wg=·64 $\bar{u}_g$ = 249 $\bar{M}_g$ = ·22 n = 7·0

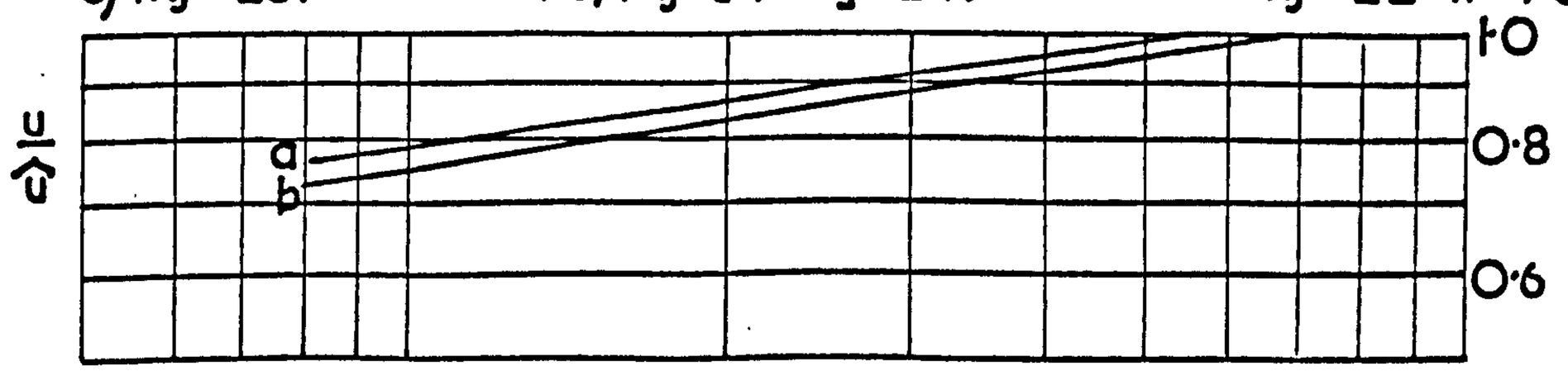

a) Wg = ·311 LB/SEC Ws/Wg = ·17 $\bar{u}_g$ = 406 FT/SEC $\bar{M}_g$ = ·37 n = 6·8
b) Wg = ·310 Ws/Wg = ·11 $\bar{u}_g$ = 412 $\bar{M}_g$ = ·37 n = 6·7

FIG 26 AIR VELOCITY PROFILES FOR AIR-SOLIDS FLOW

mean static temperature from the one-dimensional adiabatic flow equation into the gas velocity of sound and Mach number expressions then

$$\bar{u} = \bar{M}\sqrt{\gamma RT_o/(1 + \frac{\gamma - 1}{2}\bar{M}^2}$$

These expressions are also applied for the evaluation of $\bar{M}_g$ and $\bar{u}_g$ for the air-solids flow. In evaluating $\bar{u}_g$ it is assumed that the value of T_{go} is similar to that at pipe entry. This assumption is not strictly correct as due to the heat transfer from solids to air, the value of T_{go} for the air alone would be expected to be greater than that for the mixture.

8.4. Solids Velocity Measurement.

The technique described in Section 7.6 appears to have been highly successful, and a total of 38 different solids velocity measurements have been obtained. These correspond to the four air flow rates selected, with at least three different solids loading ratios at each air flow, and these have been repeated at each of the three selected stations as described in Section 7.6. The variation of solids velocity with the solids to air loading ratio W_s/W_g is shown in Figs. 27 and 28. Due to the difficulty in controlling the air flow rate, some of the readings are not strictly comparable,

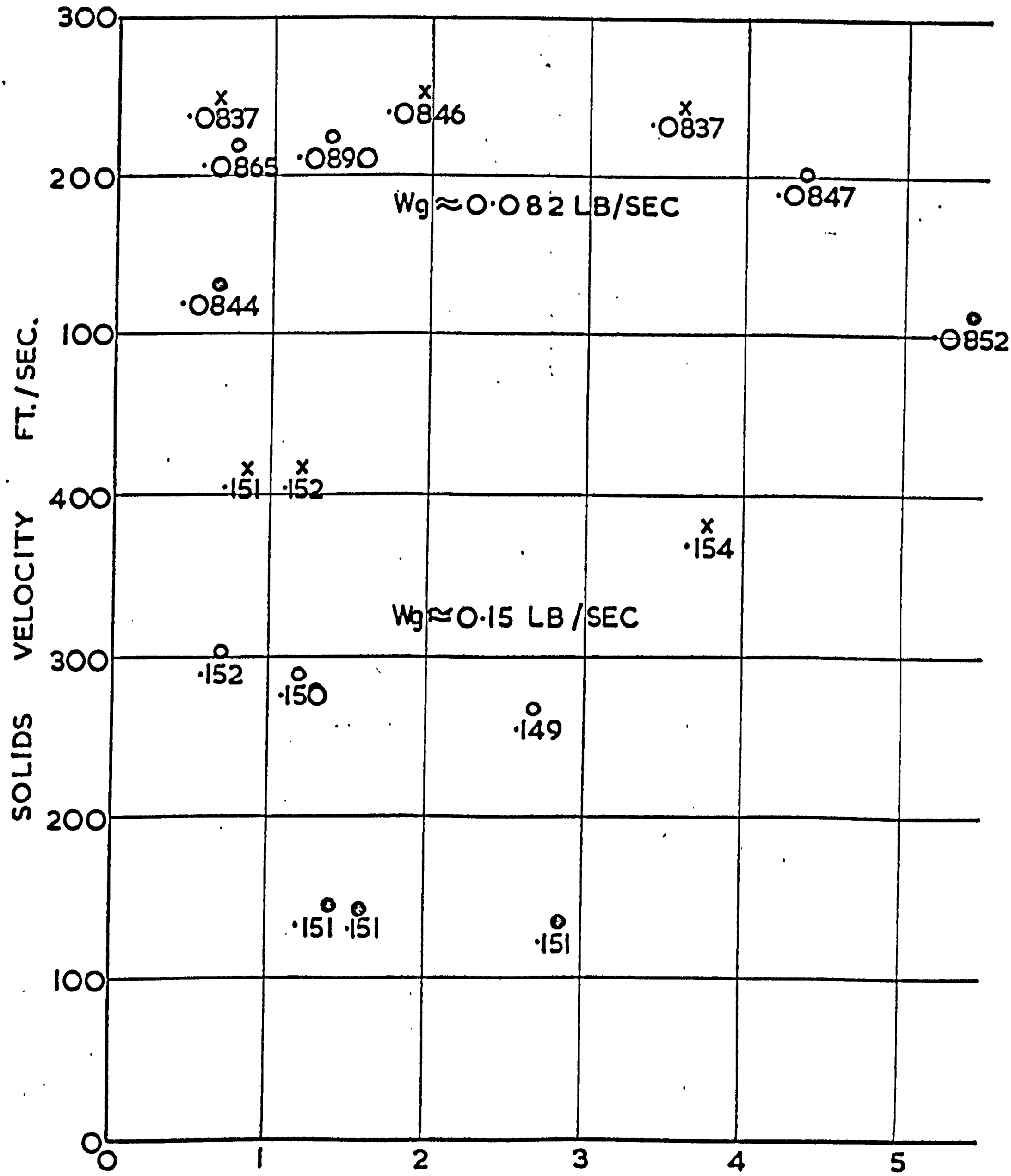

× 7 IN FROM PIPE EXIT
○ 18 FT. 6 IN. " " "
● 130 F.T. " " "

FIG 27 SOLIDS VELOCITIES AT 3 POSITIONS ALONG THE PIPE LINE

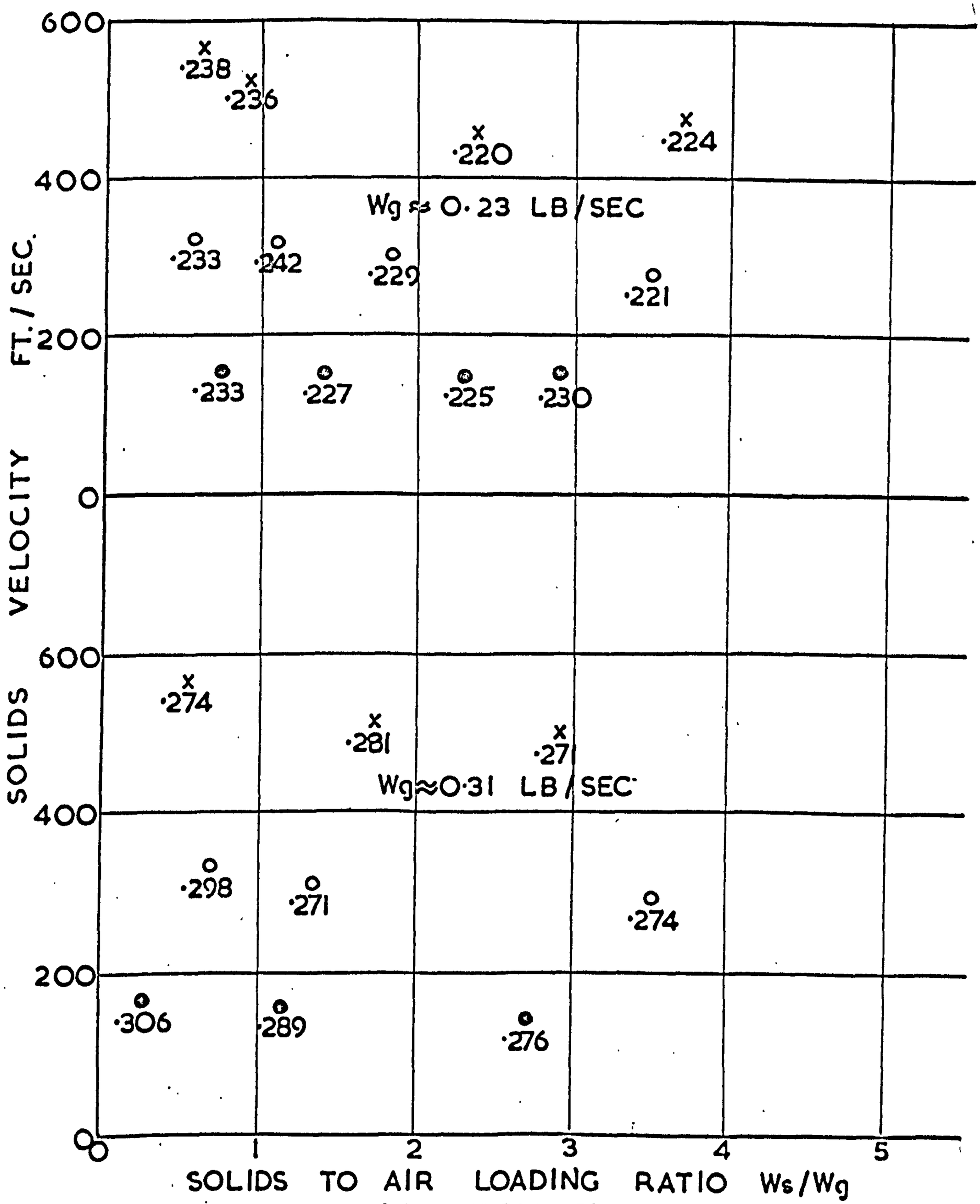

× 7 IN. FROM PIPE EXIT
○ 18 FT. 6 IN. " " "
● 130 FT. " " "

FIG28 SOLIDS VELOCITIES AT 3 POSITIONS ALONG THE PIPE LINE

and an indication of where this is the case is given by the figures representing the air mass flow rates printed beneath the plotted points.

The method of obtaining the solids velocity measurements requires that the velocity is assumed constant over the length of pipe in which the solids particles are photographed. Whilst this is reasonably true for velocities over a 6 in. length of pipe at positions 130 ft. and 18.5 ft. from pipe exit, at the position 0.58 ft. from exit the solids particles would be expected to be subject to a reasonable acceleration. Streak photographs of solids particles accelerating over this 6 in. length should, therefore, result in curved streaks on the photographic negative. This was not observed, however, on any of the films, possibly because sufficient magnification could not be obtained to show it up, but also because the acceleration was never sufficient to cause appreciable streak curvature.

8.5. Electrostatic Measurements.

Investigation of electrostatic effects has mainly taken the form of measurements of the current to earth from the insulated pipe section, as mentioned in Chapters 5 and 7, for various air flow rates and loading ratios and with this section at

different positions along the pipe line. This current to earth would be expected to be proportional to the charge acquired by each solids particle on colliding with the pipe wall, as it traverses this section. The current was found to be a function of the air flow rate, the solids to air loading ratio and the distance of the insulated section from the solids feeding point. By varying the proportion of nylon to brass piping upstream of the insulated section (Section 4.1.2), the current to earth was changed considerably for the same air flow rate and solids to air loading ratio.

The maximum voltage measured has been of the order of 35,000 v. on the 11 ft. long nylon section leading from the top of the damping chamber to the start of the experimental section, and this length includes three 90 degree bends, whilst the maximum measurement of current to earth from this section was of the order of 0.01 m.a. The measurements were obtained by wrapping the section with 20 S.W.G. (0.036 in. diameter) copper wire, with turns at about 1 in. pitch. Higher voltages than that quoted above would probably have been possible if an instrument capable of recording them had been available and with more care over insulation. Even at this order of voltage, however, long axial discharges were

seen to occur inside the tubing, these discharges were sometimes 18 in. long and usually occurred along the pipe to the feeder or to the damping chamber. No discharges were observed in the length of tube wrapped with copper wire.

On the insulated brass section the voltage has been too low to measure with the electrostatic voltmeter, whilst current to earth has generally been much less than that on the nylon section.

8.6. Computer Solutions for Pipe Flow.

An outline of the method of programming a digital computer for solving the basic equations applicable to gas-solids flow through a long pipe has been considered in Section 3.3.6 and it is only necessary here to give details of the data used and to present the solutions. The programmes were written in Algol for the English Electric KDF 9 Computer available at Leeds University.

The properties of the solids particles, the air flow and of the rig which are constant, or which can be given mean values over the range of temperatures and pressures considered in this project are as follows:-

Solids - polystyrene powder.

Specific heat C_s, 0.32 C.H.U./lb°C.

Density ρ_p, 66 lb/cu.ft.

Diameter d_p - the arithmetic mean of sample B (Section 8.1.) was used 0.0112 in.

Air - Specific heat at constant pressure C_p, 0.24 C.H.U./lb°C.

Specific heat at constant volume, C_v, 0.1714 C.H.U./lb°C.

Thermal conductivity k_g, 4.17×10^{-6} C.H.U./sec.ft.°C.

Viscosity μ, 12×10^{-6} lb/ft.sec.

Gas constant R, 96.5 ft.lb/lb°C.

Rig - Pipe bore D, 0.875 in.

General - Heat equivalent J, 1400 ft.lb/C.H.U.

Gravitational constant g, 32.2 ft/sec^2.

As stated in Section 3.3.4, it is necessary to make some assumption regarding attributing values to the friction factor $4C_f$, to obtain the computer solution. Three methods of determining the value of $4C_f$ for each flow have been investigated.

1. The first of these methods was to use the computer to

determine $4C_f$ by assuming that there was no change in velocity over the first step in the integration of the overall momentum equation. This method tended to be rather inaccurate in that although fitting a polynominal curve to the experimental pressure drop results gives a good "fit" as far as absolute values of pressure and length of pipe are concerned, the slope of the curve is not necessarily the same as that obtained by drawing a curve by hand through the experimental points and it is the rate of change of pressure with length that is required.

2. This method was similar to the first, but this time the pressure drop over the first 9 ft. length of pipe after the entry length (i.e. between the first two static pressure tappings) was assumed to occur with no change in velocity. From this pressure drop measurement, the value of the air flow rate, the mean absolute pressure over this length and the mean air temperature (which was in fact assumed to be the stagnation temperature at inlet to the rig) the value of $4C_f$ is given by the Fanning equation, which can be put in the following form:-

$$4C_f = \frac{\Delta p}{\Delta \ell} \cdot \frac{2Dp}{RT_g} \left(\frac{A}{W_g}\right)^2$$

3. Because this second method of determining $4C_f$ was considered to be giving rather too high a value to be applicable to the whole flow, the basic equations were also solved using a third method. In this case the value used was that given for pure air flow in a smooth bore pipe at the pipe flow Reynolds number, given by $Re = W_g.D/A.\mu$. As the Reynolds number range was above that over which the Blasius equation applies, the values of $4C_f$ were obtained from the skin friction factor against Reynolds number curves given by Moody (1944).

From the pressure drop curves given in Figs. 19-22, thirteen different flows were selected, from which computer solutions were to be obtained. These correspond to low, medium and high solids loadings at each of the nominal air flow rates of 0.082, 0.15 and 0.31 lb/sec., whilst four solids flow rates were selected from the results for the nominal air flow rate of 0.23 lb/sec. These solids loadings were selected as being those closest to the loadings used in obtaining the solids velocity measurements given in Section 8.4 and Figs. 27 and 28, so that comparisons could be made. The stagnation temperature used in the computer solution was that given by the mean of the temperature measured in the small air

receiver and that in the bag filter housing (Fig. 6). In all the experimental results plotted the difference between these two readings was less than $4^{o}C$.

Because the slope of the pressure drop curve changes rapidly as the pipe exit is approached, as can be seen in Figs. 19 - 22, in fitting an equation to the experimental pressure drop results, for use in the computer programme, the following method was used. The ratio of static pressure to the static reference pressure P was expressed as:

$$P = 1 + P_o - e^z$$

where P_o is the pressure ratio at pipe entrance and z is the polynomial equation.

$$z = b_o + b_1 L + b_2 L^2 + \ldots\ldots\ldots + b_n L^n = \sum_{o}^{n} b_n L^n$$

then $\frac{dz}{dL} = b_1 + 2b_2 L + \ldots\ldots\ldots + nb_n L^{n-1} = \sum_{1}^{n} nb_n L^{n-1}$

and the slope of the curve, which is required for the overall momentum equation is:

$$\frac{dP}{dL} = \frac{dP}{dz} \cdot \frac{dz}{dL} = -e^z \cdot \frac{dz}{dL} = -\exp.\left(\sum_{o}^{n} b_n L^n\right) \times \sum_{1}^{n} nb_n L^{n-1}$$

where b_1, b_2 etc. are polynomial coefficients and L is the nondimensional pipe length, which was considered the length of pipe from the first static pressure tapping divided by the

total length of pipe measured from the first pressure tapping.

A check on the accuracy of the results from the computer solution was obtained by constructing finite difference tables, as mentioned in Section 3.3.6, from the air velocity results. The air velocity was selected, as being one of the variables showing most variation over the whole flow. By making z an 8th order polynomial equation and by using integration step lengths of 0.05L up to 0.6L, 0.02L up to 0.9L, 0.01L up to 0.98L and 0.002L up to 1.00L an accuracy in computation was obtained, which was rather better than the general accuracy of the experimental determinations.

Figs. 29-41 show the results of the computer solution plotted as air velocity, solids velocity, air temperature, solids temperature and stagnation temperature against length of pipe from exit. The curves are all drawn for the extremes of skin friction factor given by methods 2 and 3 above. Also plotted are the measured values of solids velocity and air velocity for similar flow conditions. The experimentally measured solids velocities given are those from Section 8.4, whilst the mean air velocities are given in Section 8.3.

Figs. 42, 43, 44 and 45 show the computer solutions

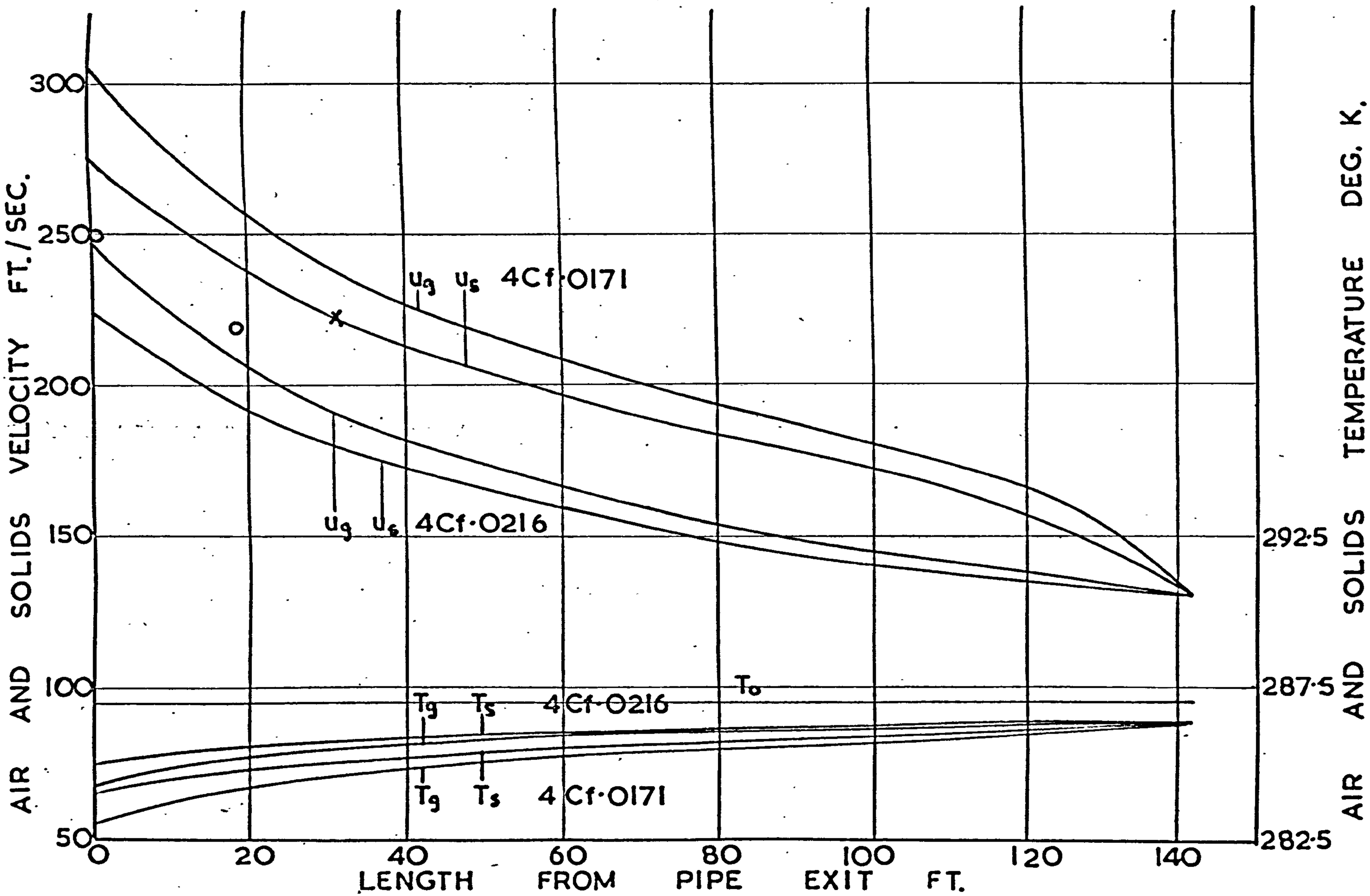

FIG 29 VELOCITY AND TEMPERATURE CURVES FROM THE COMPUTER SOLUTION FOR $W_g = 0{\cdot}083$ AND $W_s/W_g = 0{\cdot}79$

o MEASURED SOLIDS VELOCITY x MEASURED MEAN AIR VELOCITY

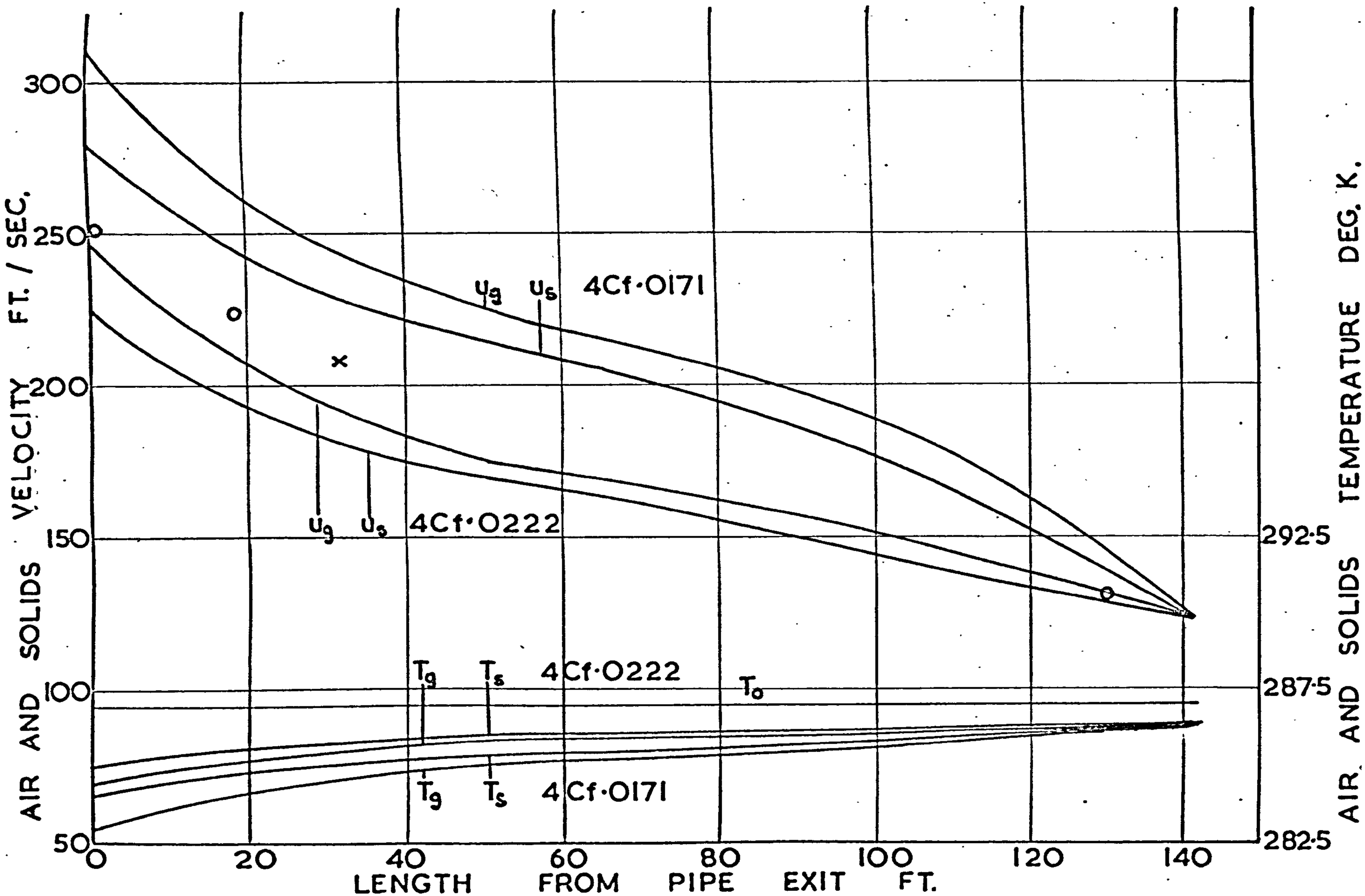

FIG30 VELOCITY AND TEMPERATURE CURVES FROM THE COMPUTER SOLUTION FOR W_g = 0·083 LB./SEC. AND W_s/W_g = 1·60

o MEASURED SOLIDS VELOCITY x MEASURED MEAN AIR VELOCITY

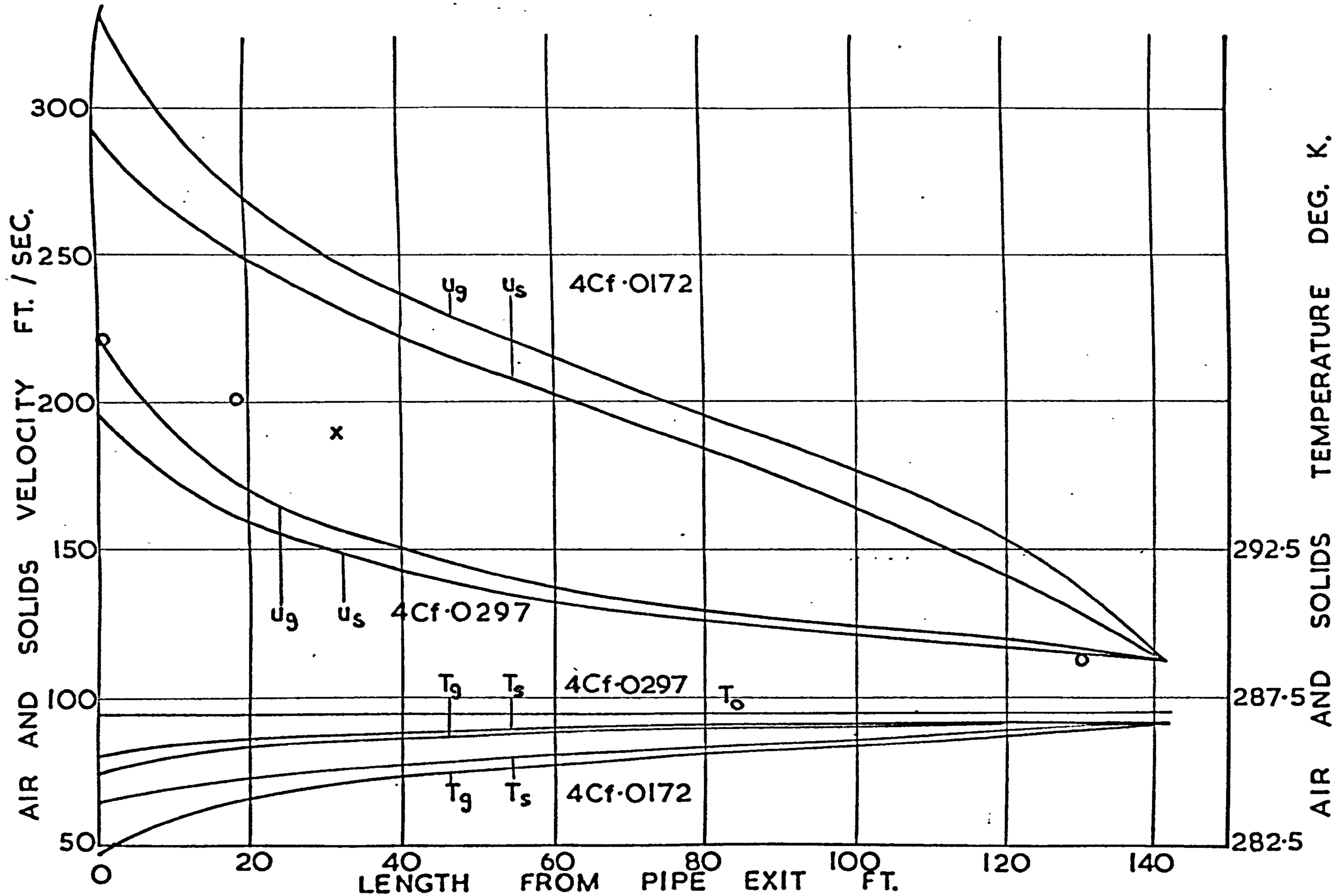

FIG31 VELOCITY AND TEMPERATURE CURVES FROM THE COMPUTER SOLUTION FOR W_g = 0·079 LB./SEC. AND W_s/W_g = 4·68
o MEASURED SOLIDS VELOCITY x MEASURED MEAN AIR VELOCITY

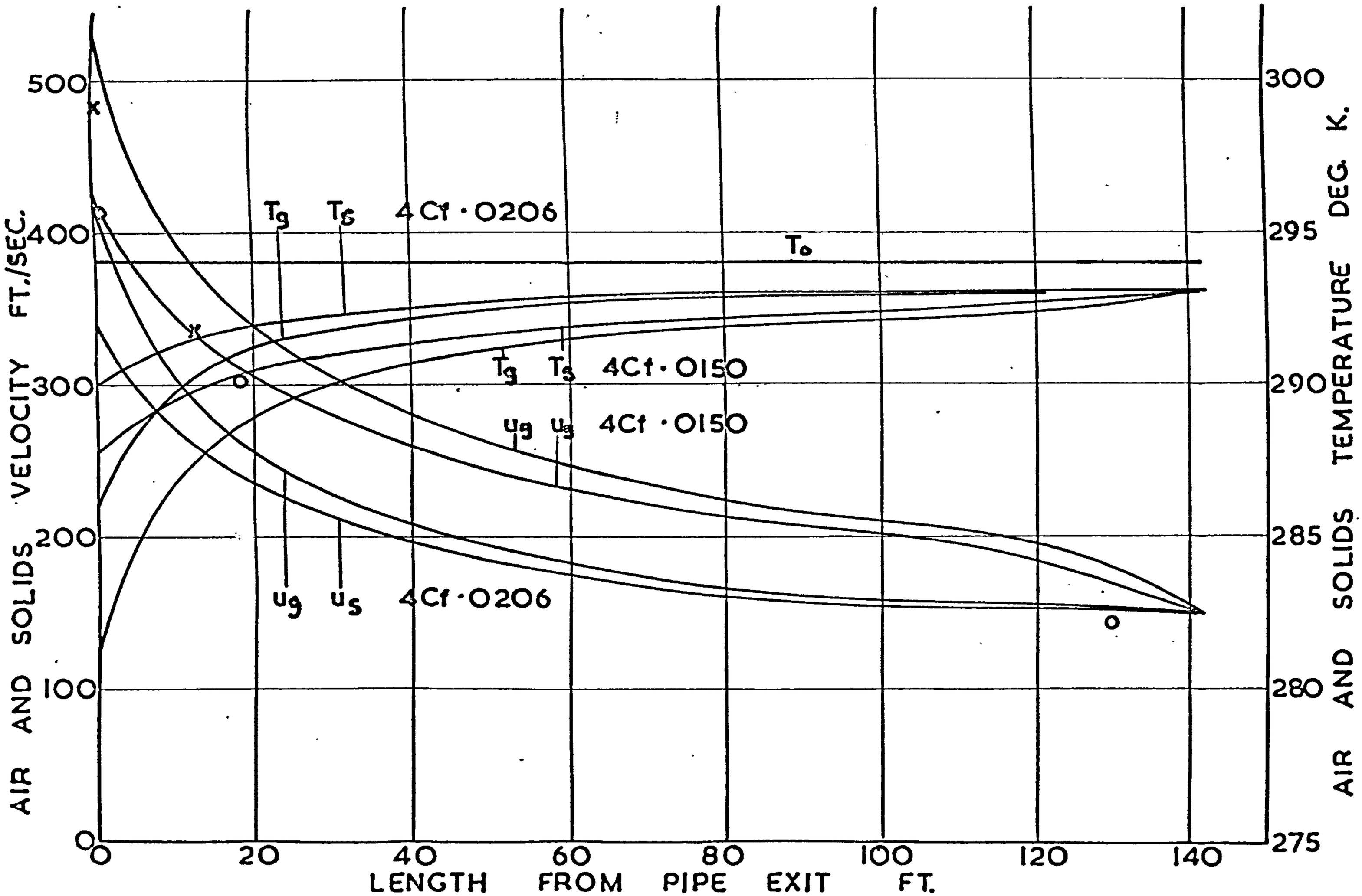

FIG 32 VELOCITY AND TEMPERATURE CURVES FROM THE COMPUTER SOLUTION FOR Wg=0·153 LB/SEC AND Ws/Wg=0·91
o MEASURED SOLIDS VELOCITY x MEASURED MEAN AIR VELOCITY

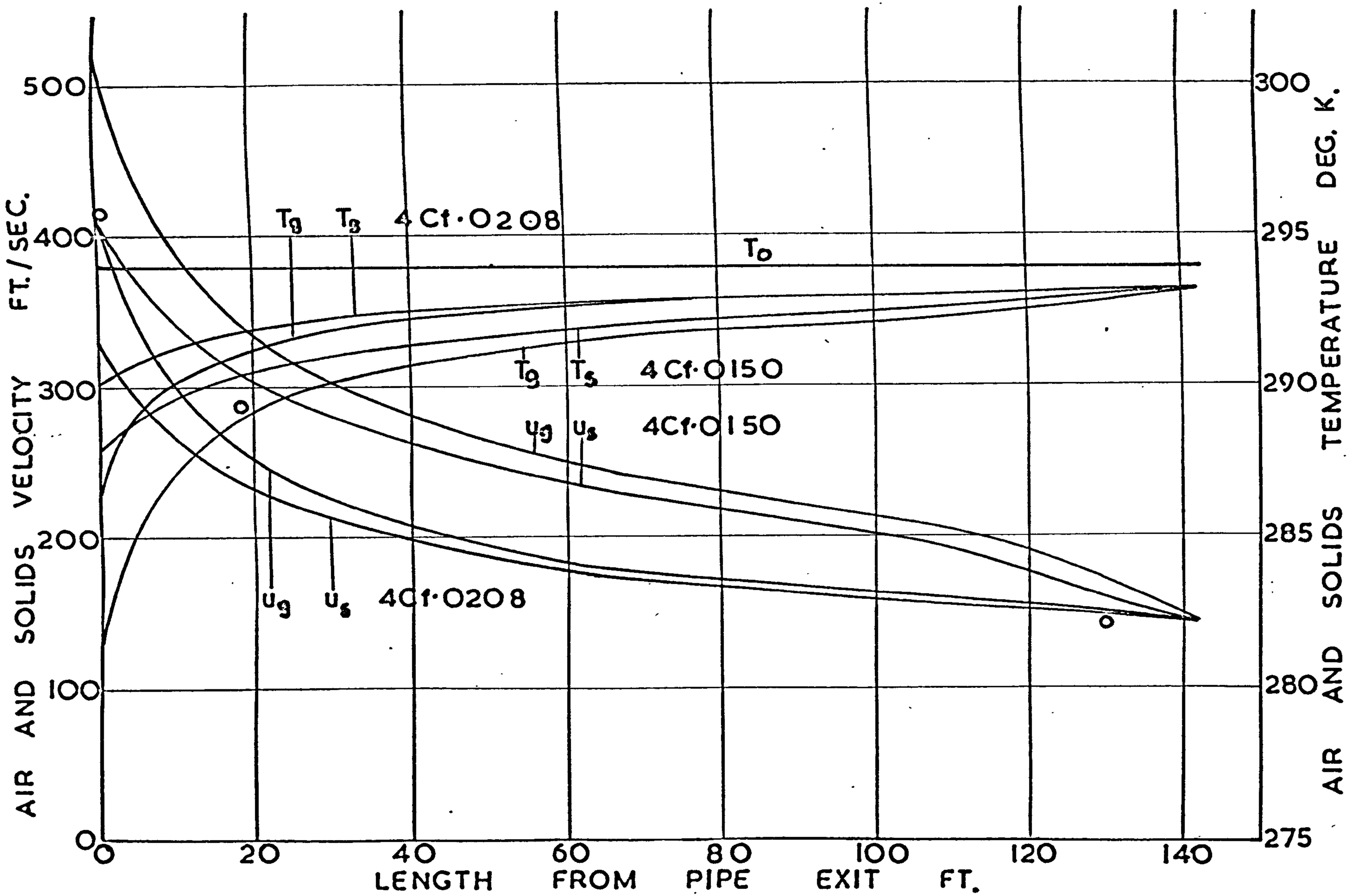

FIG 33 VELOCITY AND TEMPERATURE CURVES FROM THE COMPUTER SOLUTION FOR W_g=0·153 LB./SEC. AND W_s/W_g = 1·42
o MEASURED SOLIDS VELOCITY

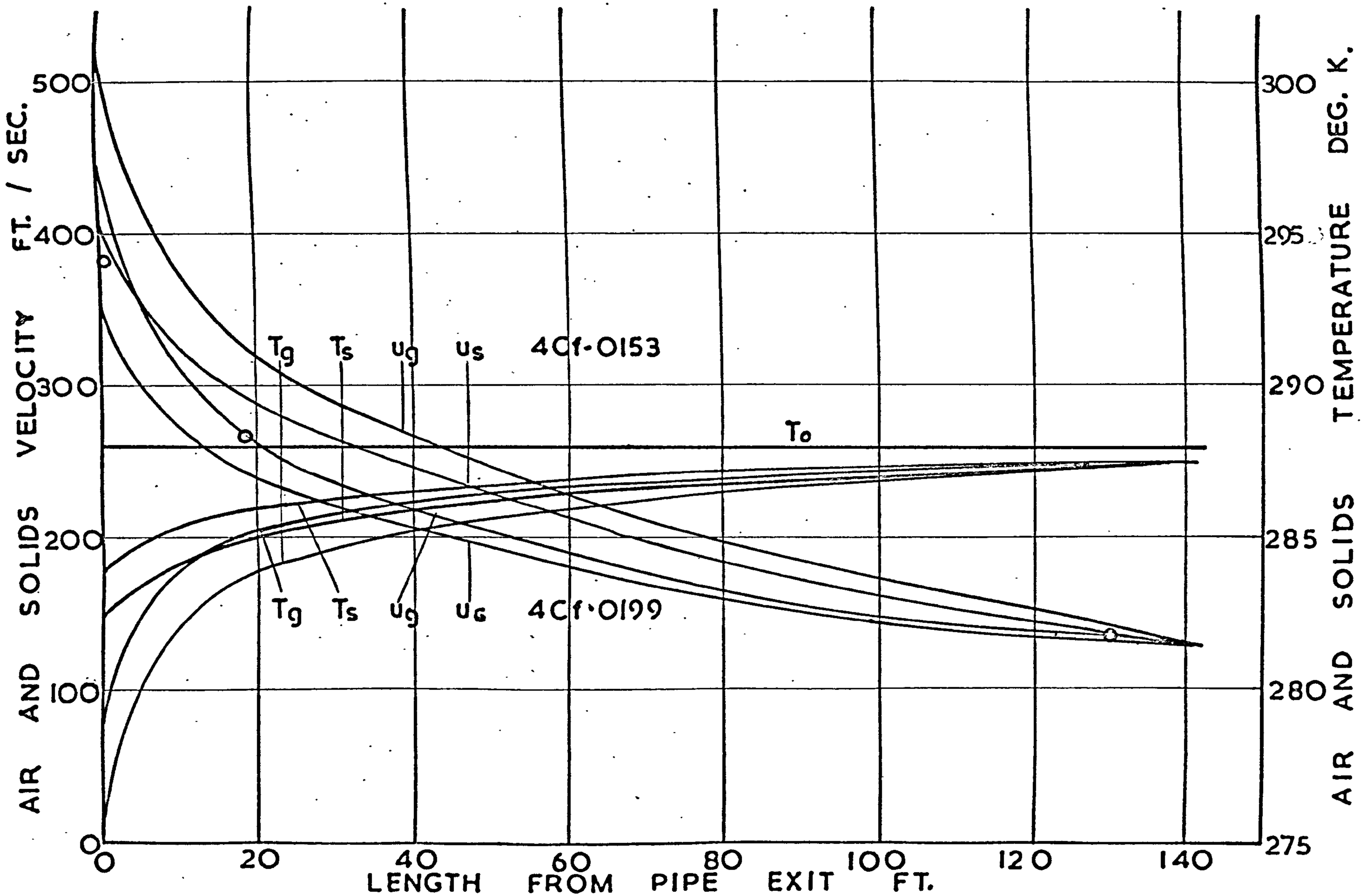

FIG 34 VELOCITY AND TEMPERATURE CURVES FROM THE COMPUTER SOLUTION FOR $W_g = 0{\cdot}147$ LB./SEC. AND $W_s / W_g = 3{\cdot}82$

o MEASURED SOLIDS VELOCITY

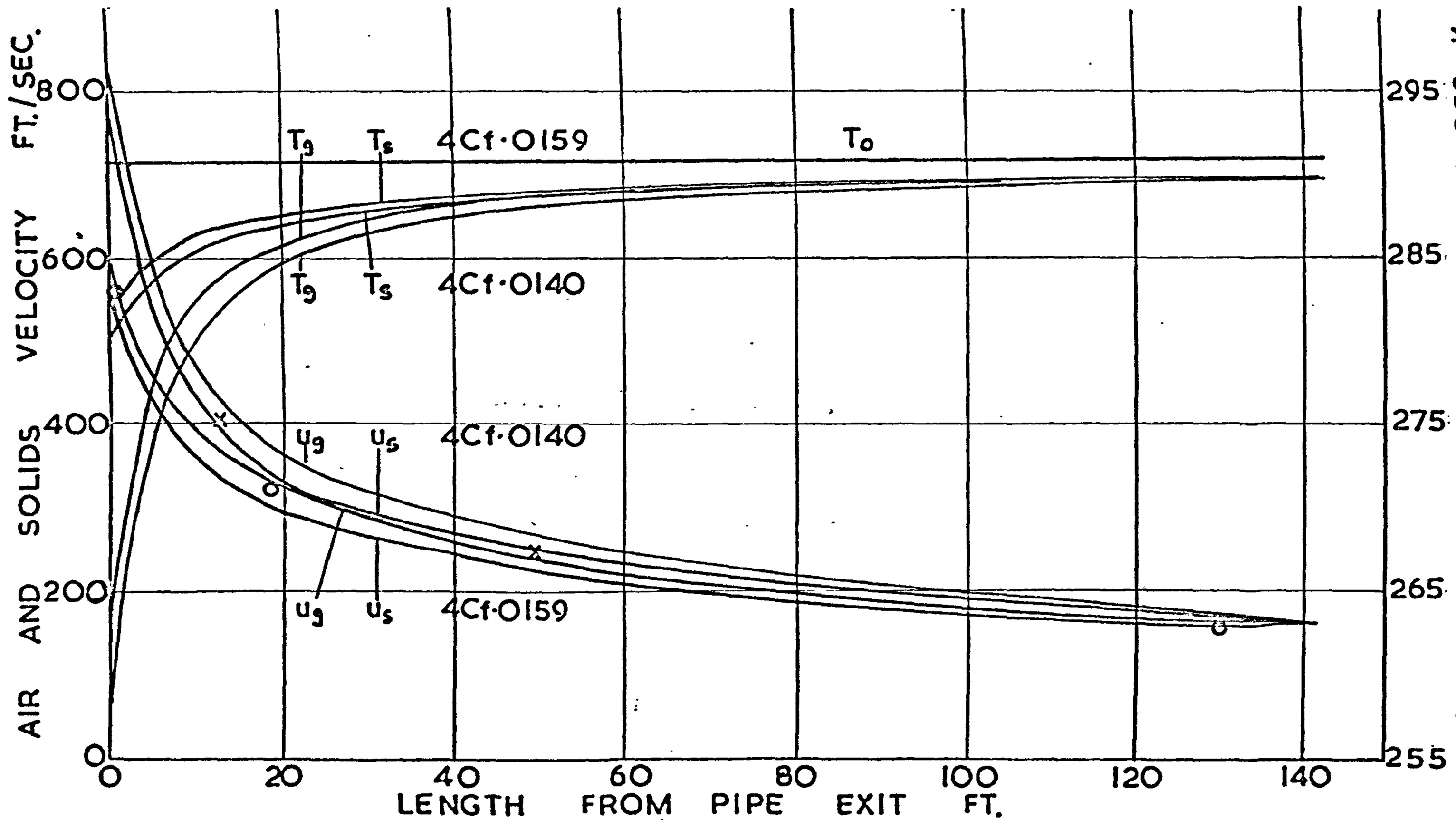

FIG 35 VELOCITY AND TEMPERATURE CURVES FROM THE COMPUTER SOLUTION FOR $W_g = 0{\cdot}230$ LB/SEC AND $W_s/W_g = 0{\cdot}66$

o MEASURED SOLIDS VELOCITY x MEASURED MEAN AIR VELOCITY

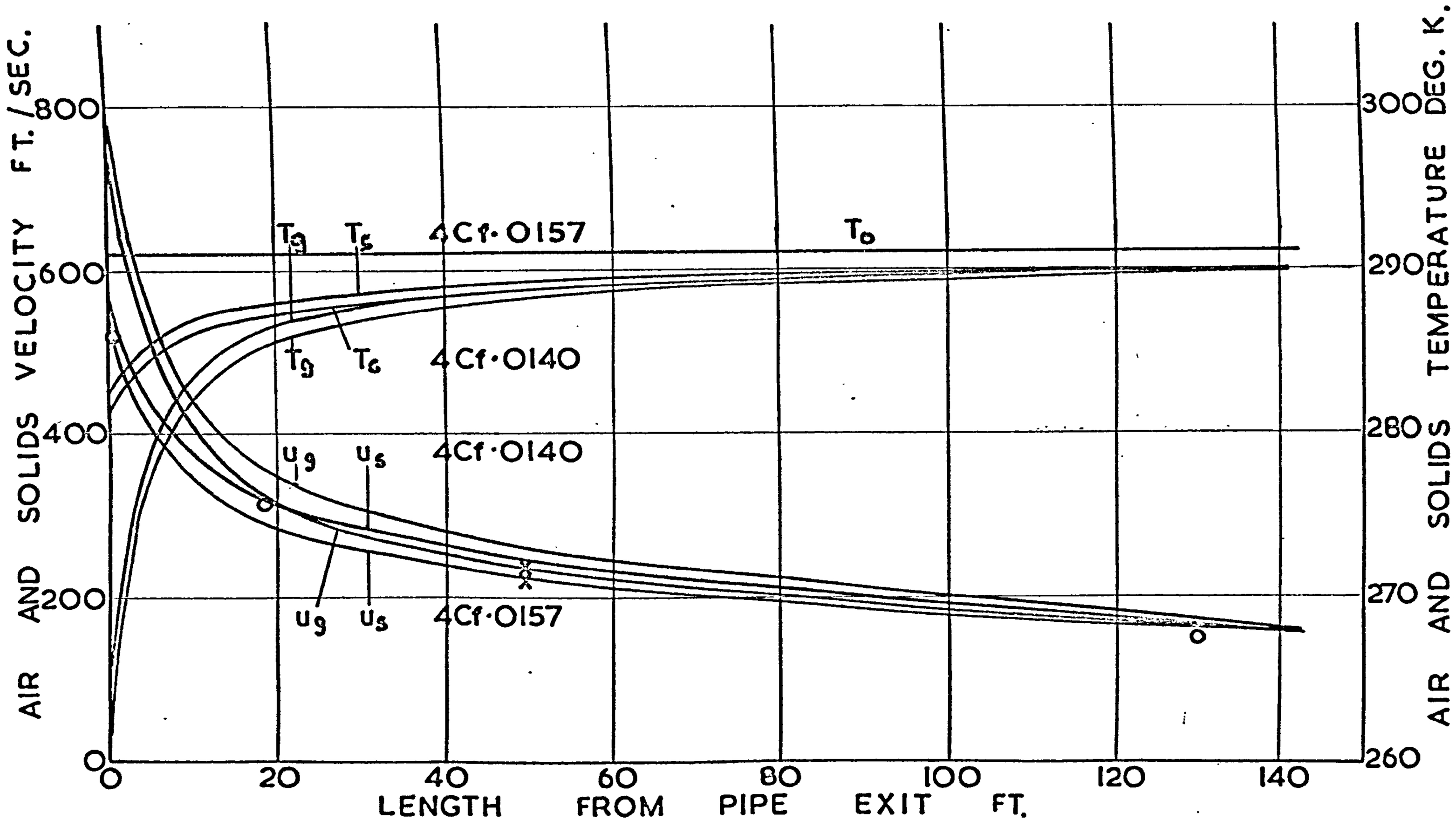

FIG36 VELOCITY AND TEMPERATURE CURVES FROM THE COMPUTER SOLUTION FOR W_g = 0·229 LB./SEC. AND W_s/W_g=1·11

o MEASURED SOLIDS VELOCITY x MEASURED MEAN AIR VELOCITY

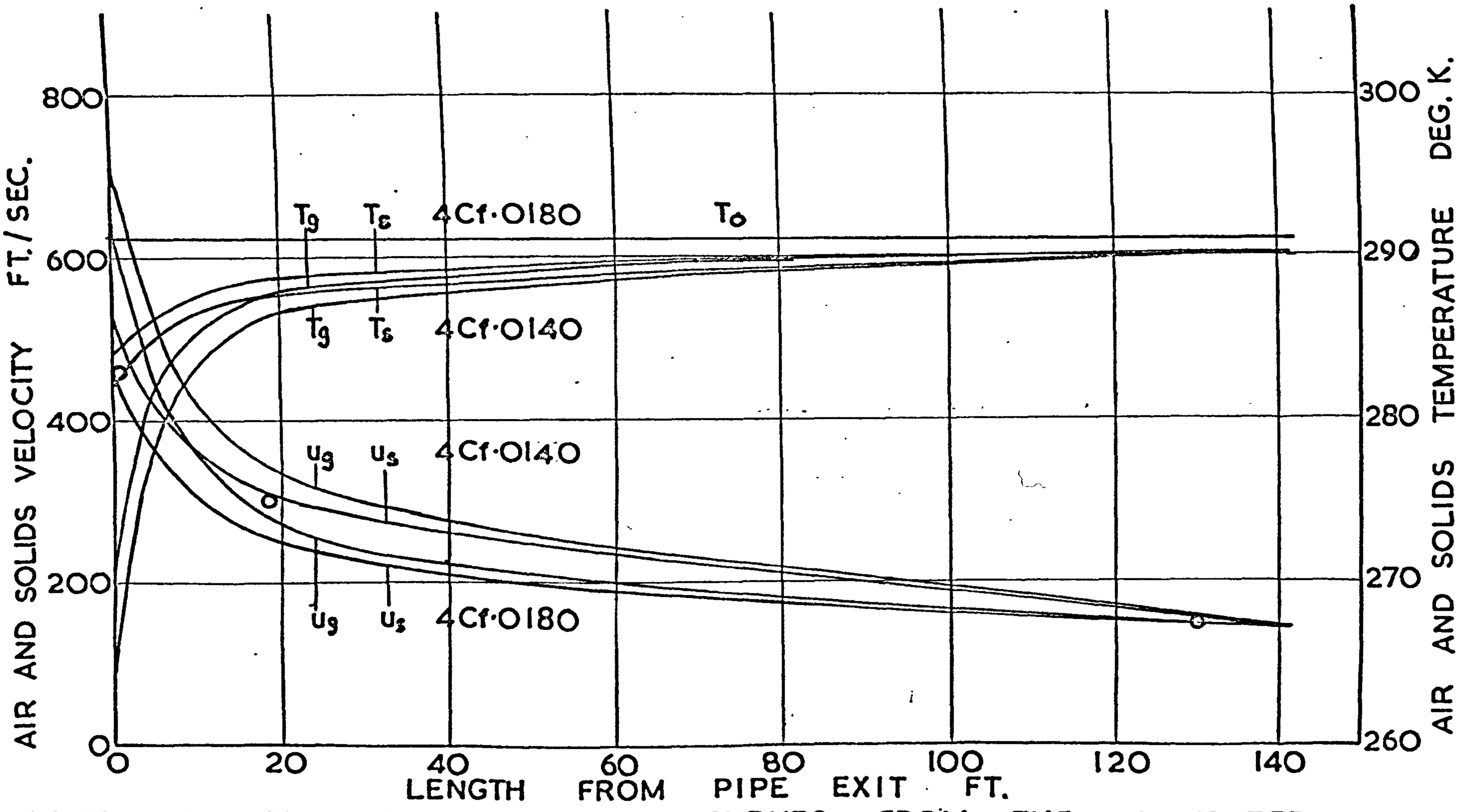

FIG 37 VELOCITY AND TEMPERATURE CURVES FROM THE COMPUTER SOLUTION FOR $W_g = 0{\cdot}229$ LB/SEC. AND $W_s/W_g = 2{\cdot}35$

o MEASURED SOLIDS VELOCITY

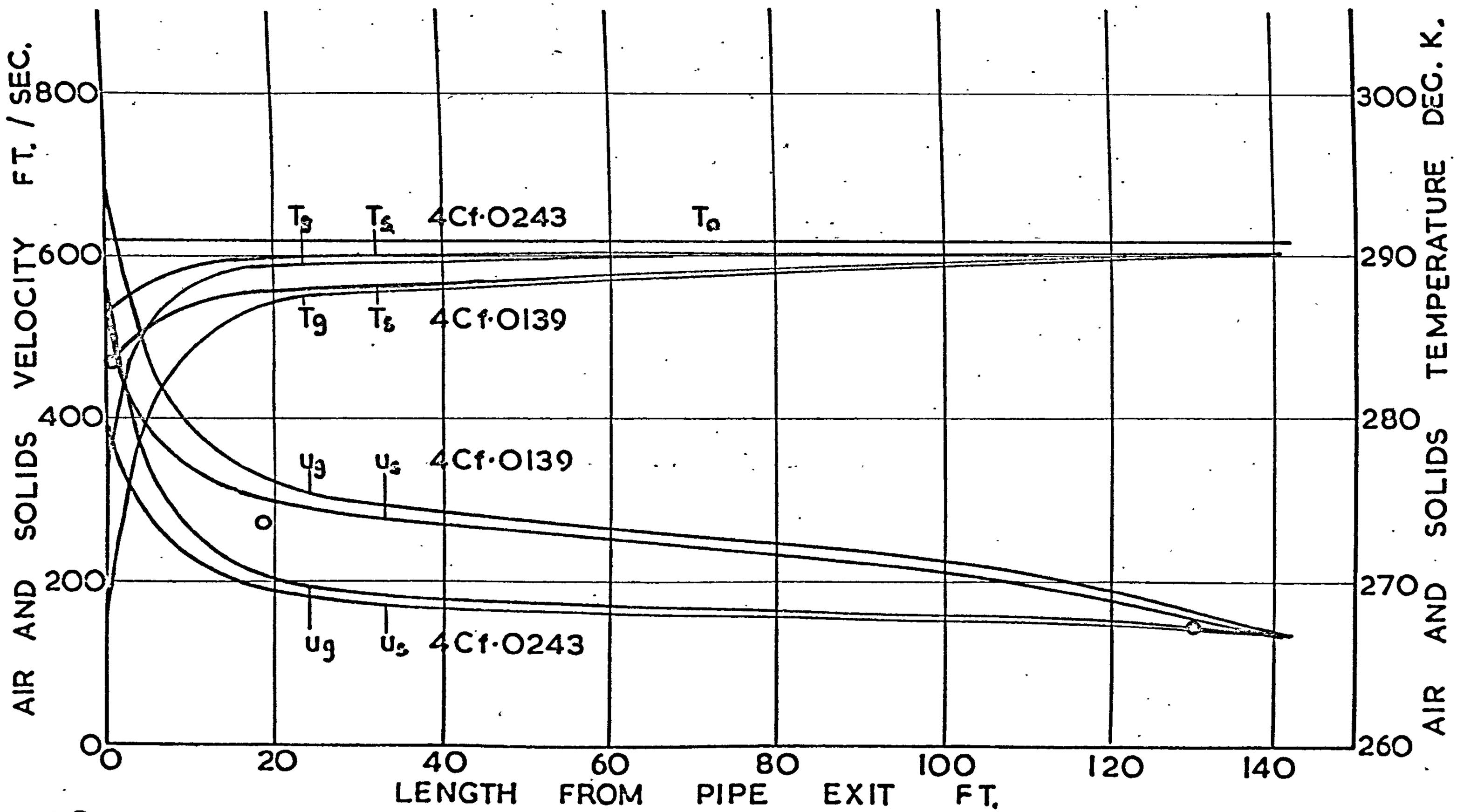

FIG 38 VELOCITY AND TEMPERATURE CURVES FROM THE COMPUTER SOLUTION FOR $W_g = 0{\cdot}239$ LB./SEC. AND $W_s/W_g = 3{\cdot}44$

o MEASURED SOLIDS VELOCITY

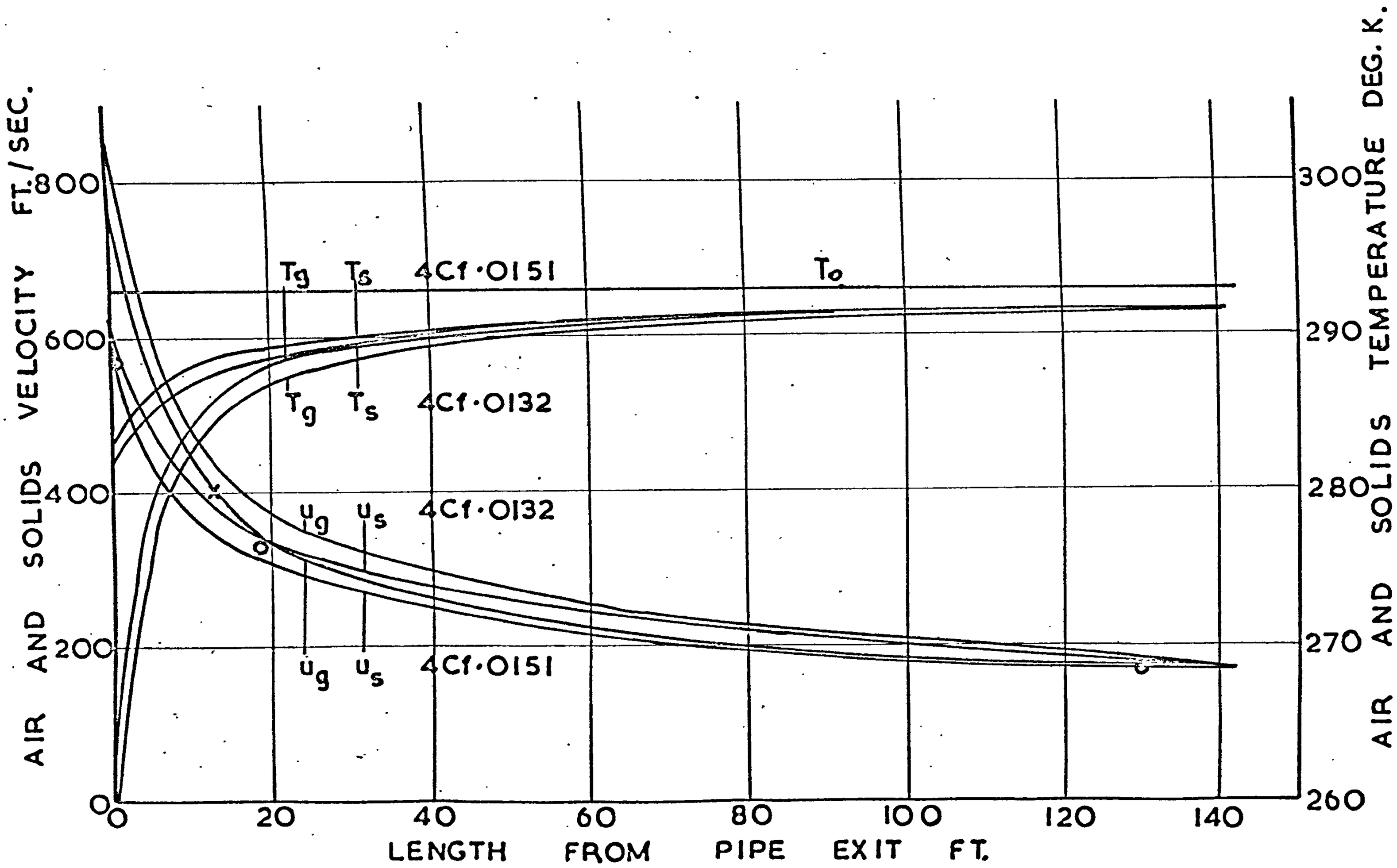

FIG 39 VELOCITY AND TEMPERATURE CURVES FROM THE COMPUTER SOLUTION FOR $W_g = 0{\cdot}315$ LB / SEC AND $W_s / W_g = 0{\cdot}53$

o MEASURED SOLIDS VELOCITY x MEASURED MEAN AIR VELOCITY

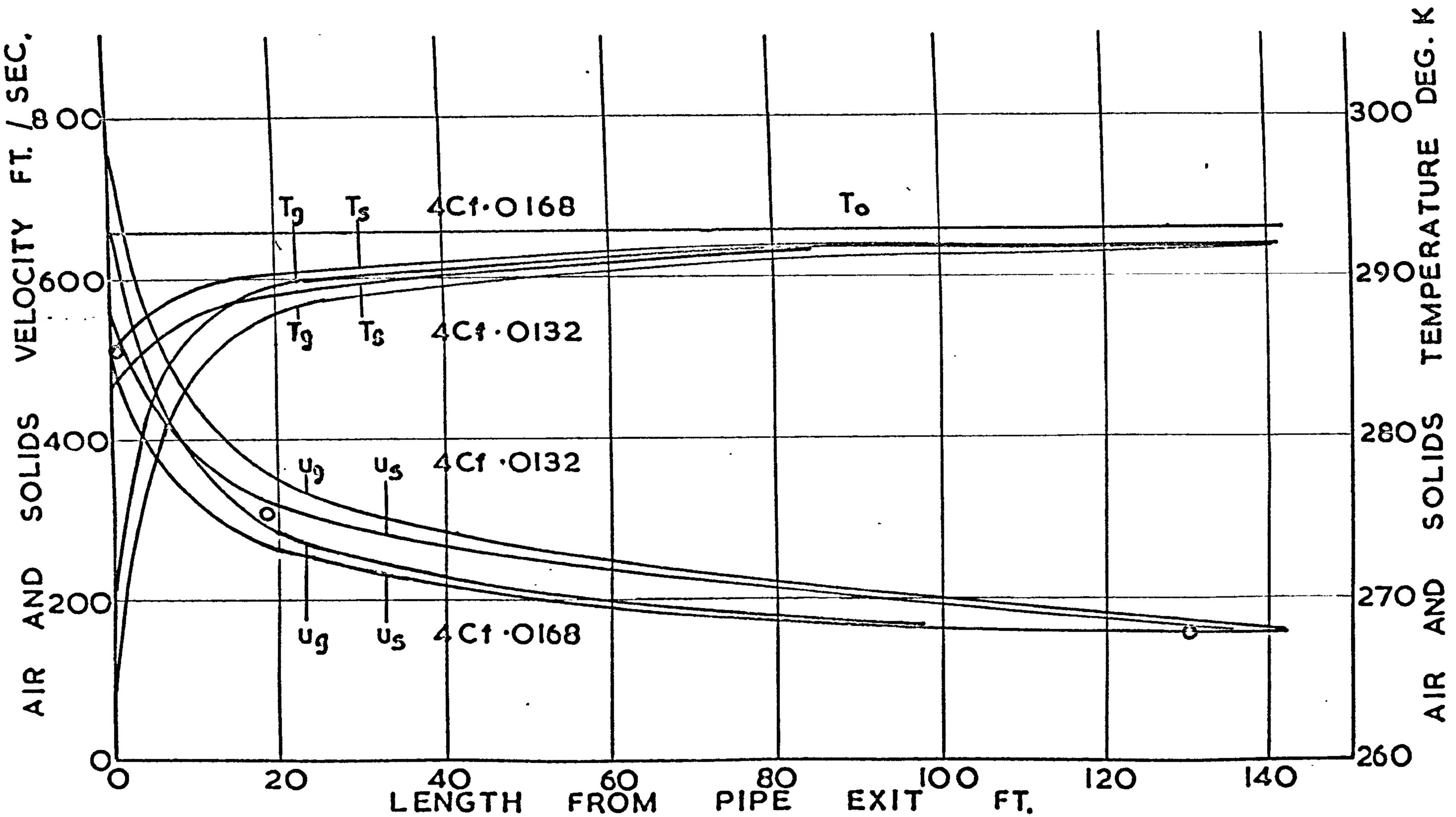

FIG 40 VELOCITY AND TEMPERATURE CURVES FROM THE COMPUTER SOLUTION FOR $W_g = 0{\cdot}306$ LB / SEC AND $W_s / W_g = 1{\cdot}68$

o MEASURED SOLIDS VELOCITY

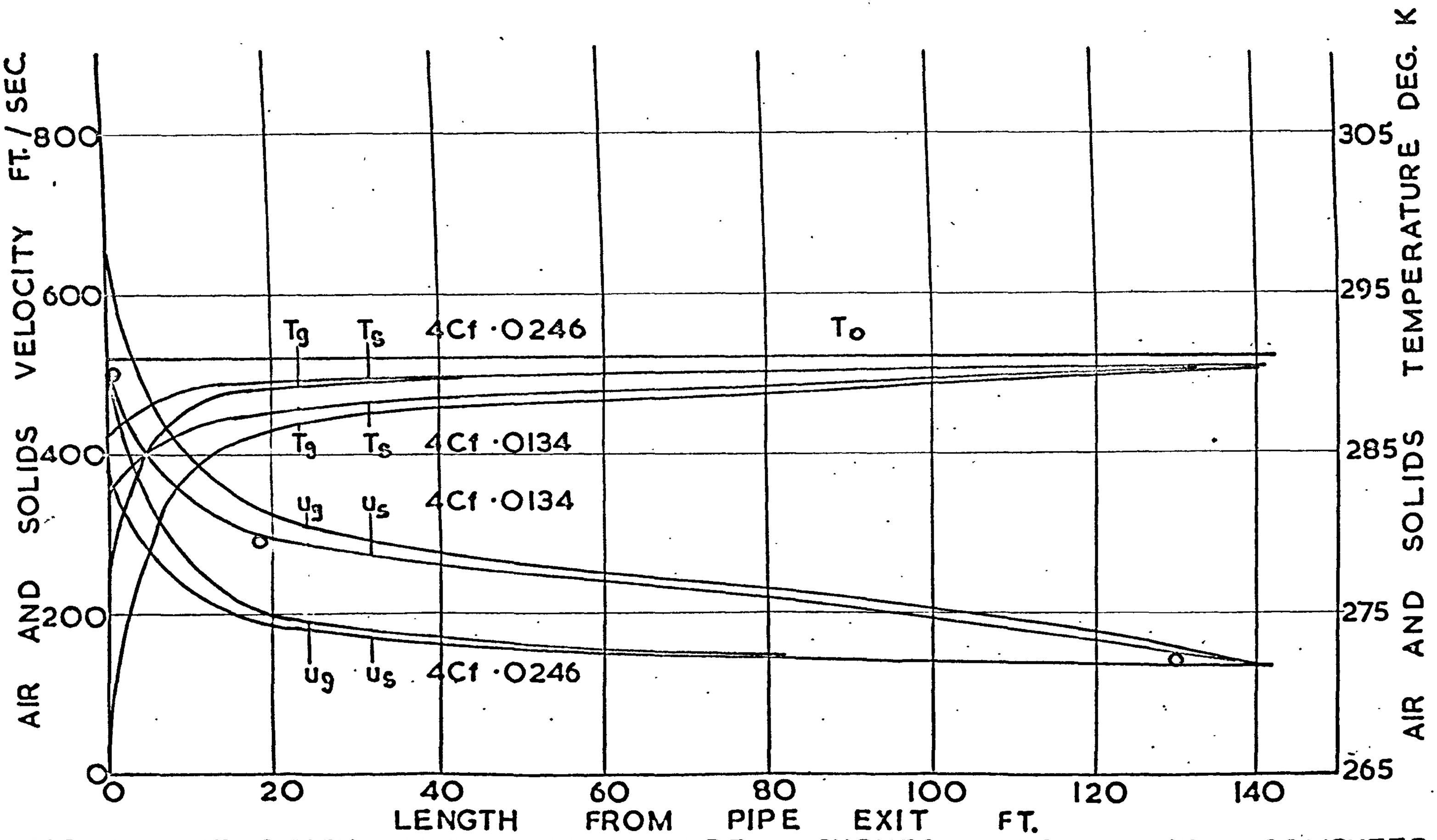

FIG 41 VELOCITY AND TEMPERATURE CURVES FROM THE COMPUTER SOLUTION FOR $W_g = 0{\cdot}284$ LB./SEC. AND $W_s/W_g = 3{\cdot}87$

o MEASURED SOLIDS VELOCITY

obtained from the pressure drop curves for pure air flow at flow rates of 0.082, 0.150, 0.232 and 0.296 lb/sec. These solutions were obtained by assuming the air to be conveying a very small amount of solids (0.00001 lb/sec) so that the same computer programme as for the air-solids flow could be used. In the case of the two high air flow rates, sensible solutions could only be obtained by using rather low values of the skin friction factor. In the case of W_g = 0.296 lb/sec. a $4C_f$ value of 0.0128 had to be used in order to obtain a solution, and this is rather lower than the 0.0133 value given by the friction factor - Reynolds number curve for a smooth pipe or the value of 0.0136 given by evaluating $4C_f$ over the first 9 ft. length of pipe assuming no velocity change. For W_g = 0.232 lb/sec. it was necessary to use $4C_f$ = 0.014, which is the value given by the friction factor - Reynolds number curve instead of the value 0.0145 given by evaluating $4C_f$ over the first 9 ft. length of pipe. In the cases of W_g = 0.150 and 0.082 lb/sec., the values given by evaluation over the first 9 ft. length of pipe were used, namely $4C_f$ = 0.016 and 0.017 respectively, and these compare with the values of 0.0152 and 0.0171 given by the skin friction factor - Reynolds number curve.

In Figs. 46 - 58, the non-dimensional quantities Mm, n, k and j, as defined in Section 3.3.6 and Appendix 1, have been

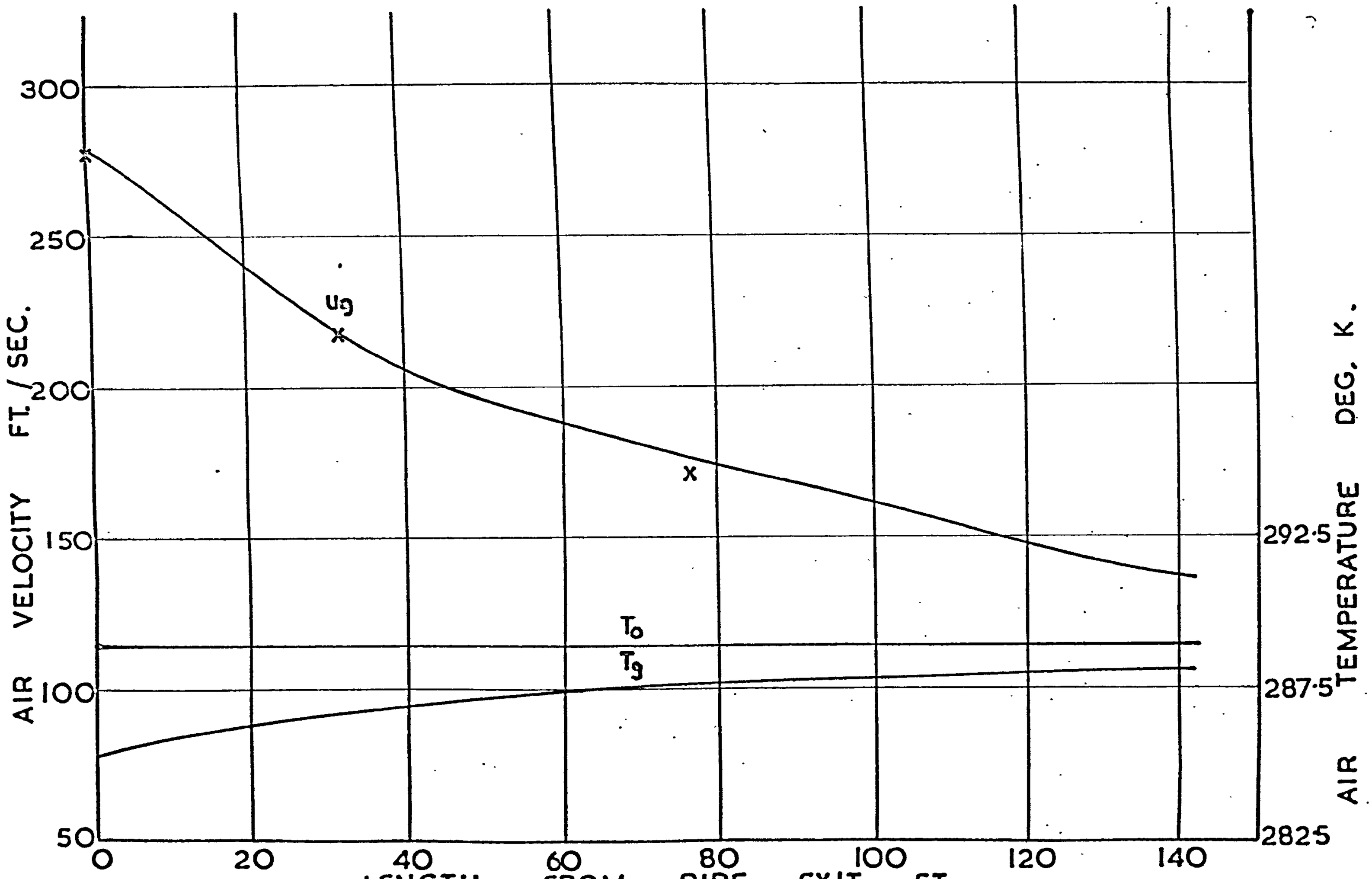

FIG 42 VELOCITY AND TEMPERATURE CURVES FROM THE COMPUTER SOLUTION FOR AIR FLOW WITH W_g = 0·002 LB./SEC. & $4C_f$ = 0·017

x MEASURED MEAN AIR VELOCITY

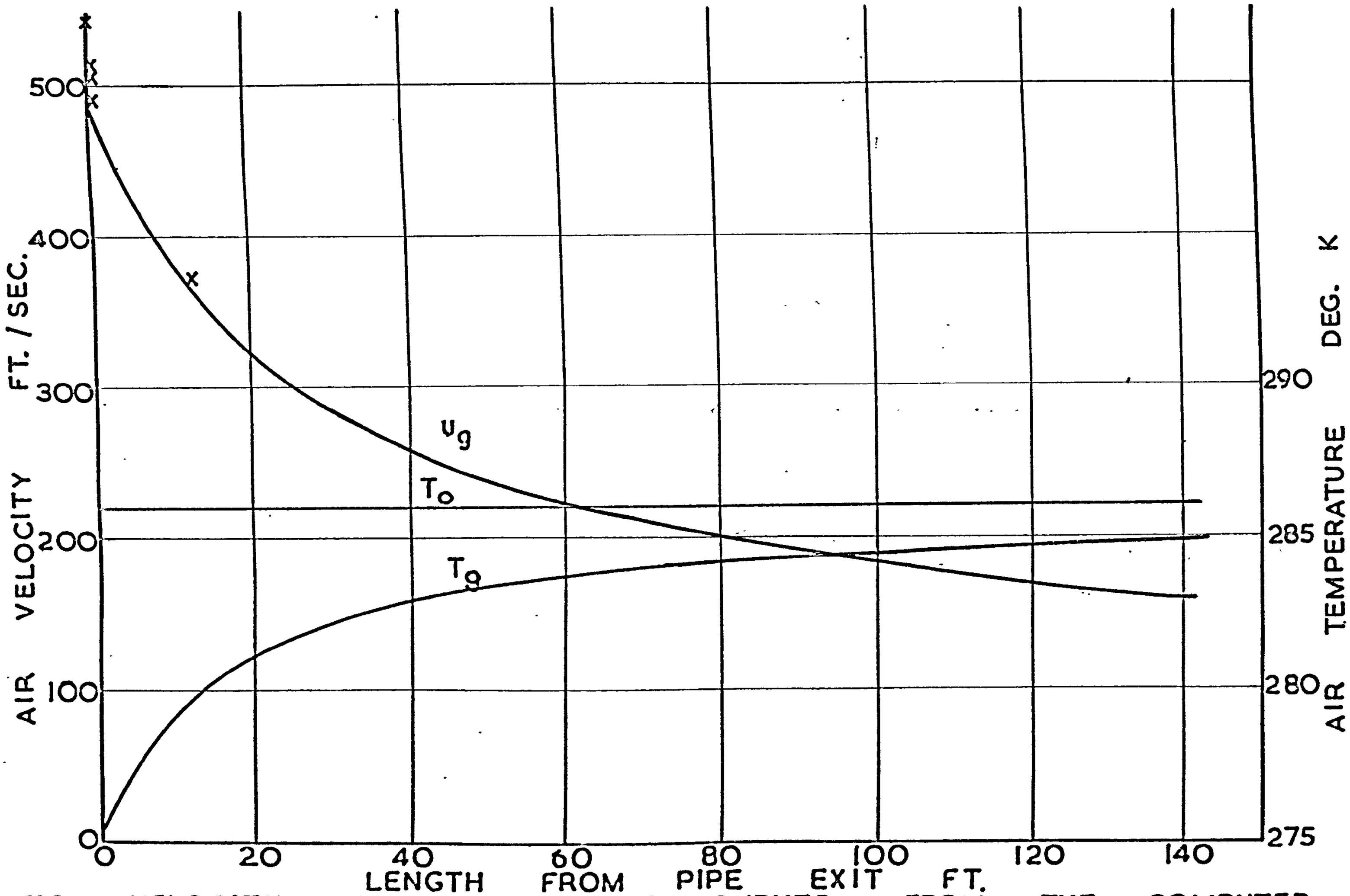

FIG43 VELOCITY AND TEMPERATURE CURVES FROM THE COMPUTER SOLUTION FOR AIR FLOW WITH $W_g = 0{\cdot}150$ LB/SEC. & $4C_f = 0{\cdot}016$
x MEASURED MEAN AIR VELOCITY

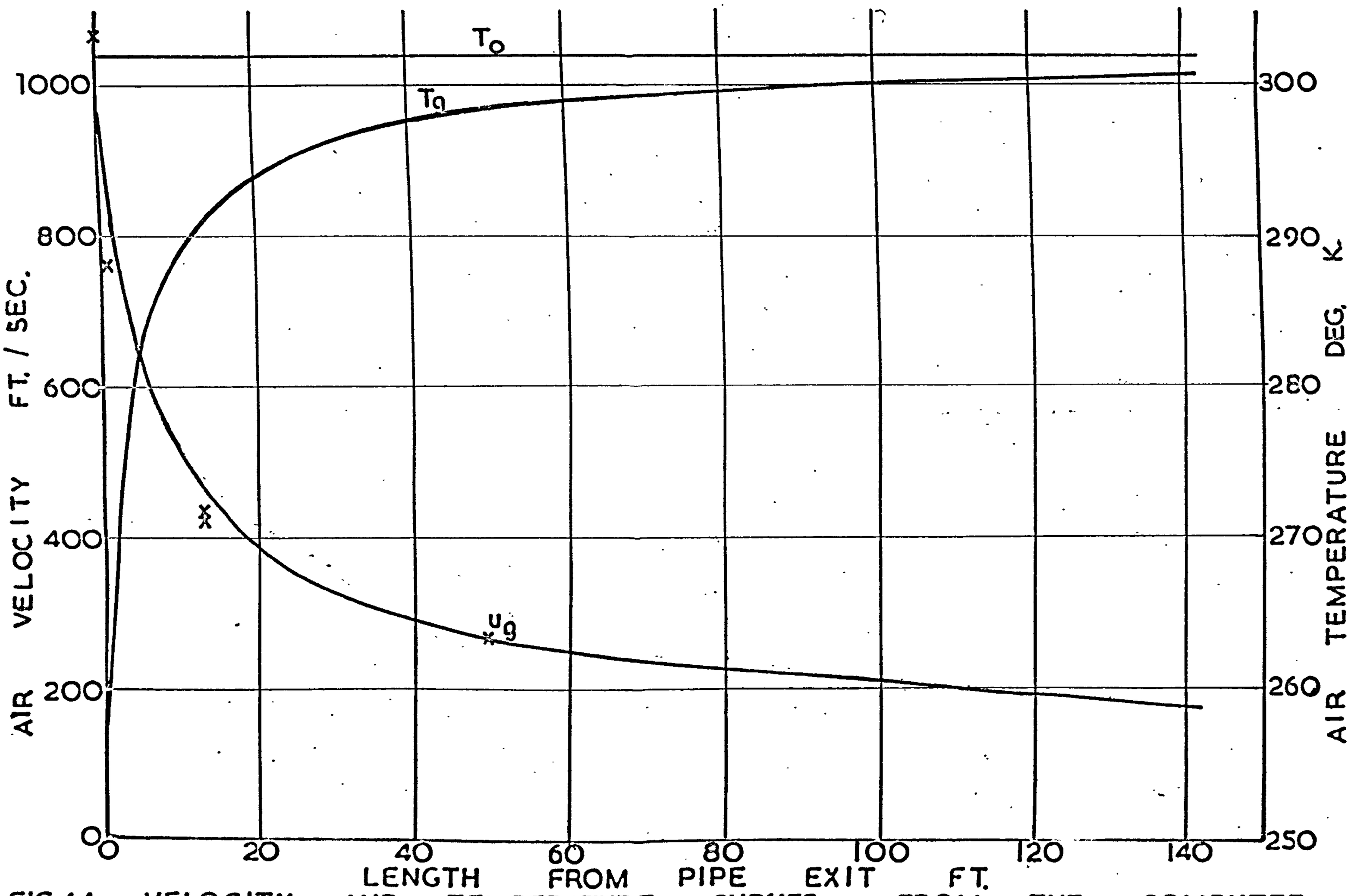

FIG 44 VELOCITY AND TEMPERATURE CURVES FROM THE COMPUTER SOLUTION FOR AIR FLOW WITH $W_g = 0{\cdot}232$ LB/SEC. & $4C_f = 0{\cdot}014$

x MEASURED MEAN AIR VELOCITY

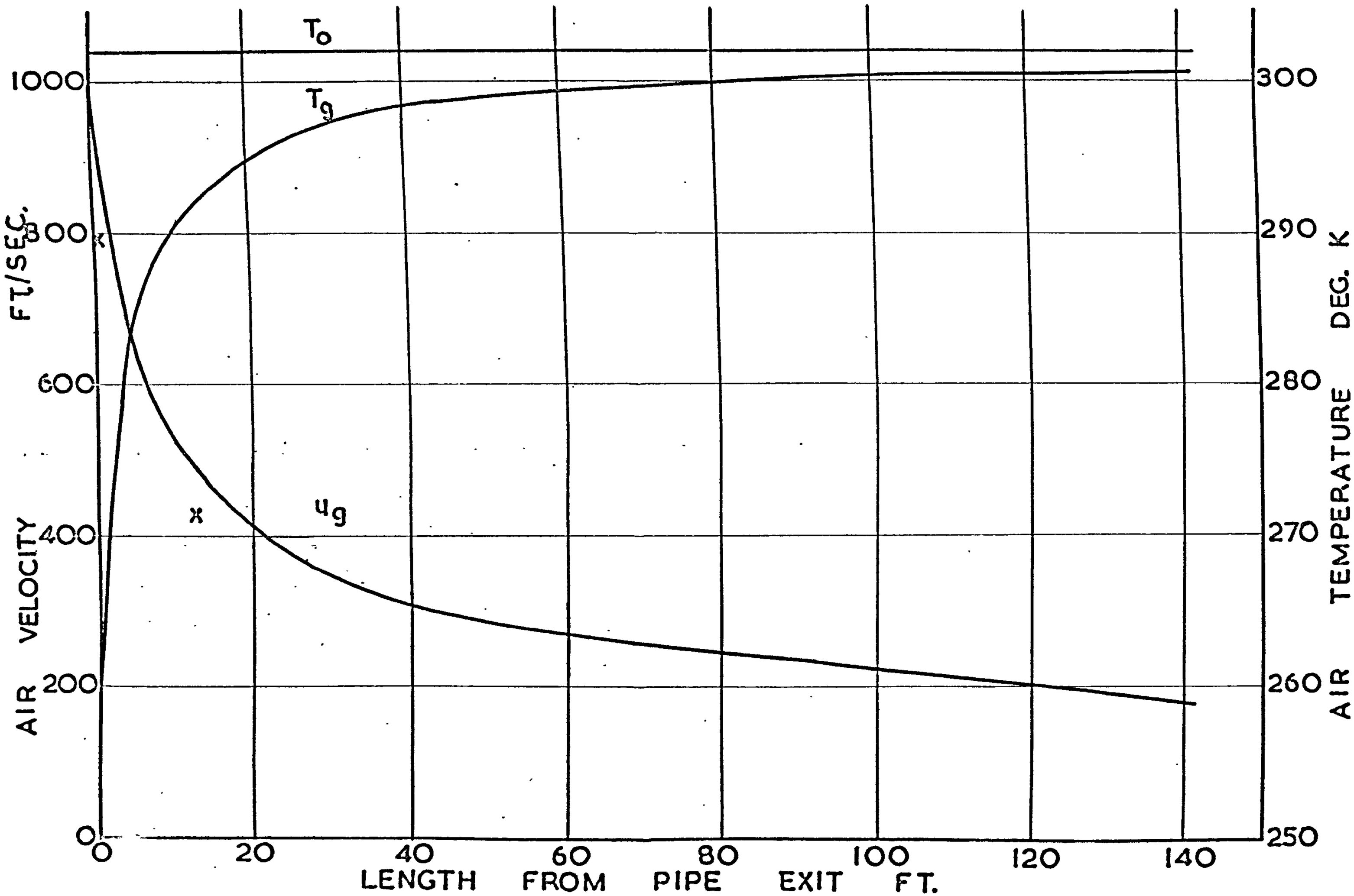

FIG 45 VELOCITY AND TEMPERATURE CURVES FROM THE COMPUTER SOLUTION FOR AIR FLOW WITH $W_g = 0{\cdot}296$ LB./SEC. & $4C_f = 0{\cdot}0128$
x MEASURED MEAN AIR VELOCITY

plotted. These were evaluated from the air and solids velocity and temperature results available from the computer programme. They were plotted in order to determine whether the mixture Mach number approaches unity at pipe exit, and also to investigate the value of the compressible flow index n throughout the flow. As with the plots of velocities and temperatures the curves of Mm, n, k and j are given for the two extremes of friction factor.

Curves of gas Mach number against L are plotted in Fig. 59. These were obtained from the velocity and temperature results for pure air flow, available from the computer solution. Experimentally determined mean Mach numbers from Section 8.3 are also given on these curves to facilitate comparisons.

In all the curves obtained from the computer solution there was a certain amount of scatter in the plots in the regions of low Mach number. This was particularly so for the values of j and k, so that in Figs. 46-58 the curves are only drawn where this scatter was not severe. The scatter was caused by the size of the step in the numerical integration. It is also apparent from some of these curves that the values of j and k at the upstream end of the pipe are somewhat less than unity.

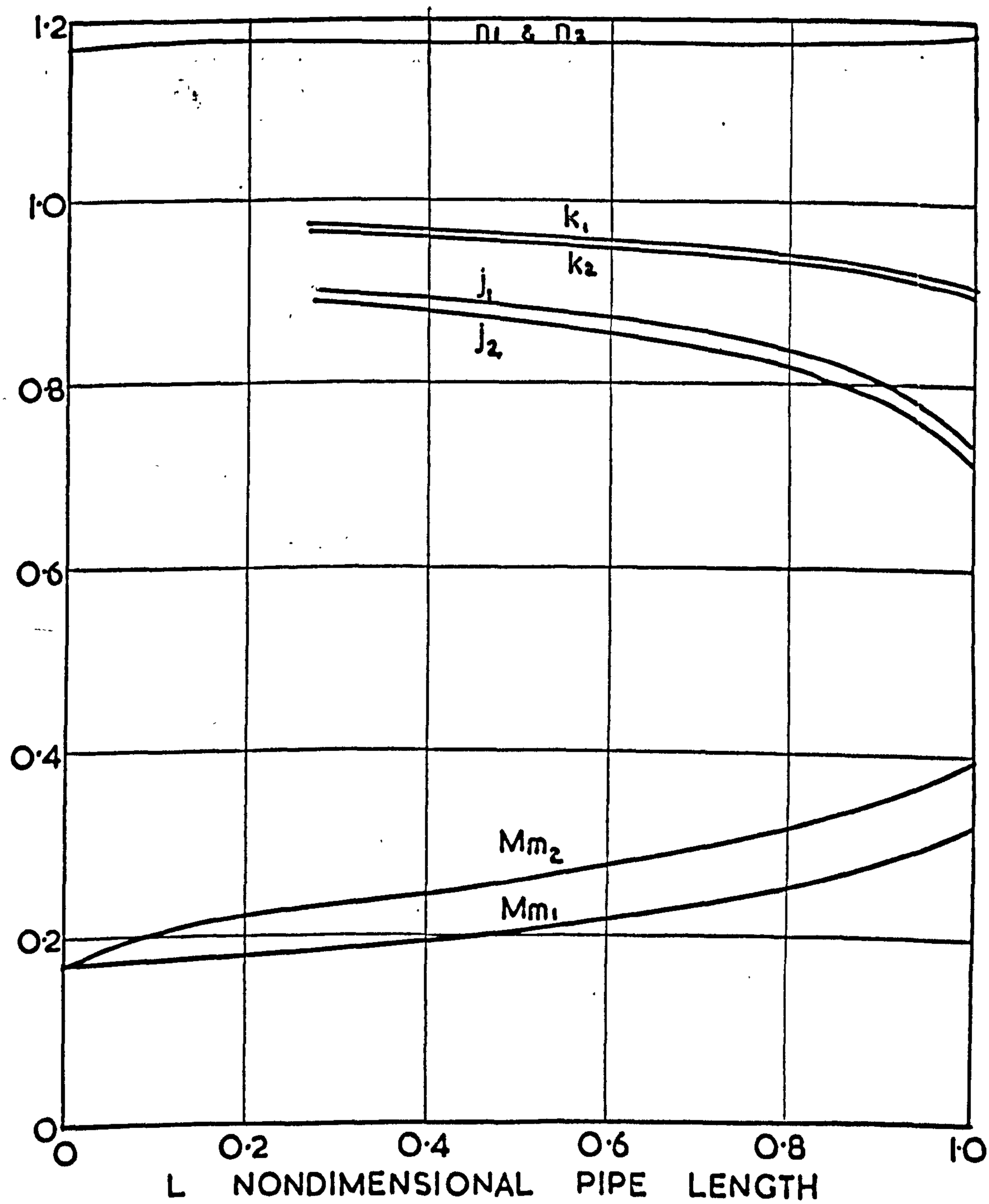

FIG 46 CURVES OF n, k, j & Mm FROM THE COMPUTER SOLUTION FOR Wg 0·083LB/SEC AND Ws/Wg 0·79
SUFFICES (1) 4Cf = 0·0216 (2) 4Cf = 0·0171

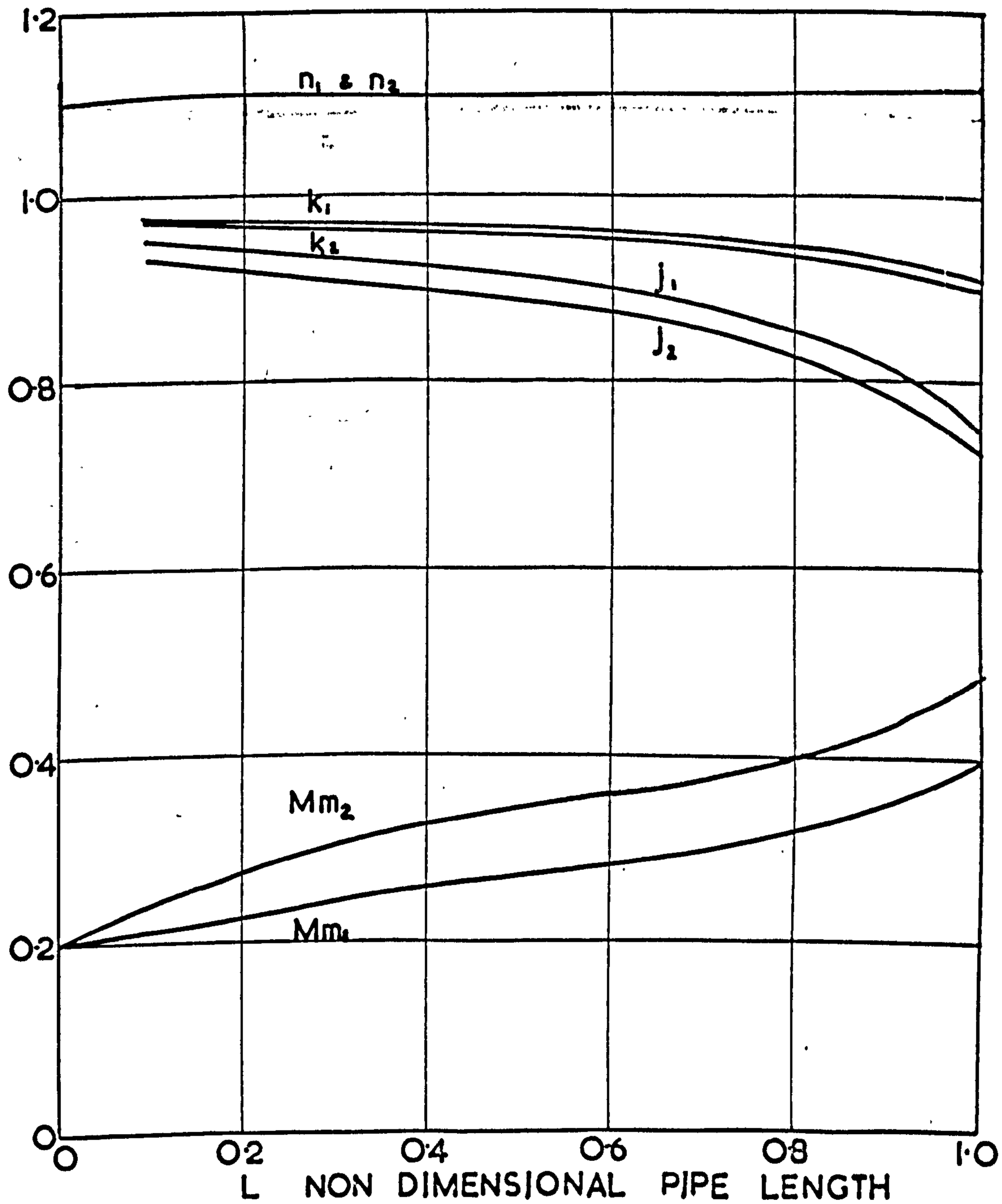

FIG47 CURVES OF n, k, j & Mm FROM THE COMPUTER SOLUTION FOR W_g = 0·083 LB/SEC AND W_s/W_g = 1·60
SUFFICES (1) 4Cf = 0·0222 (2) 4Cf = 0·0171

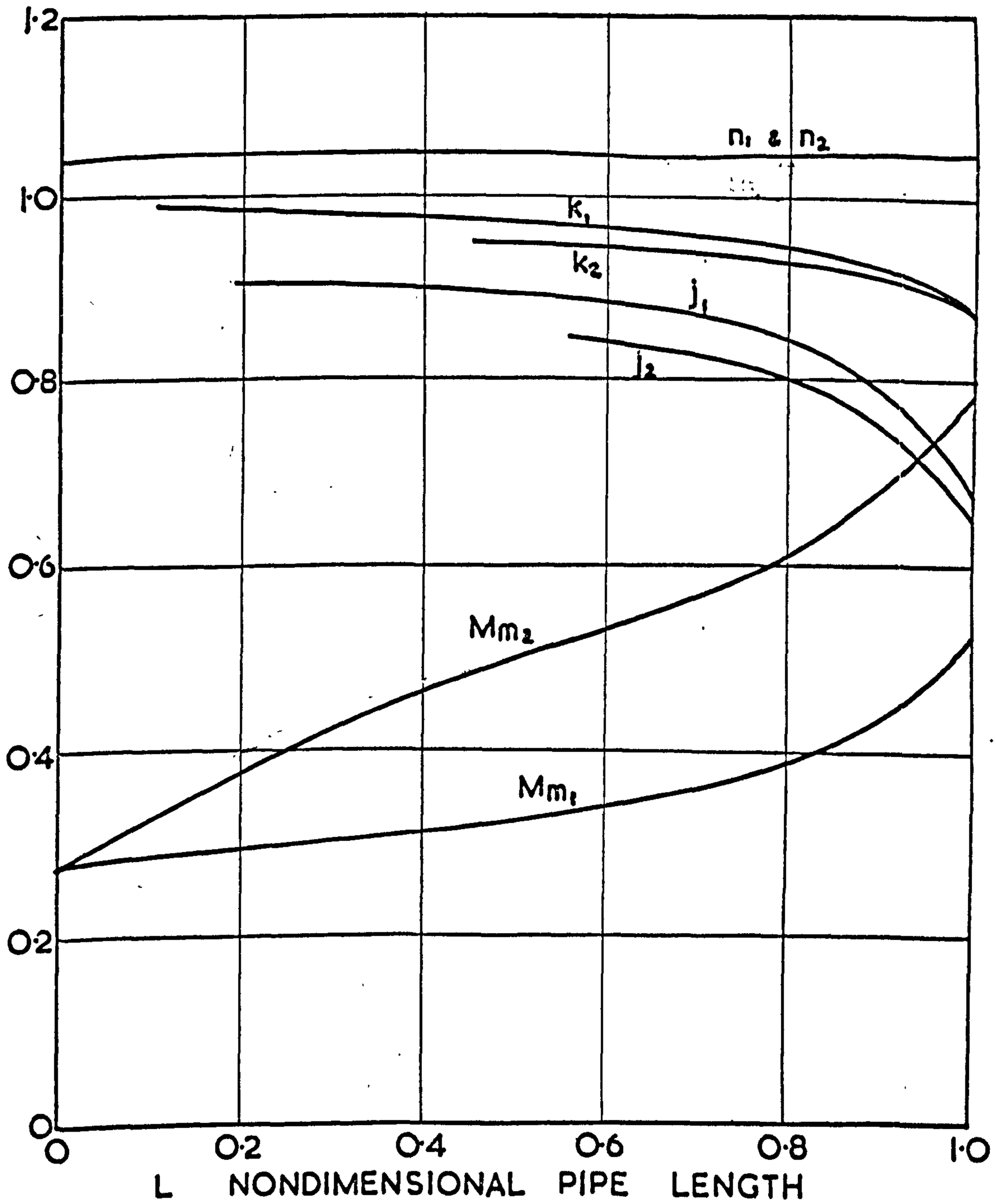

FIG48 CURVES OF n, k, j & Mm FROM THE COMPUTER SOLUTION FOR $W_g = 0{\cdot}079$ LB/SEC AND $W_s/W_g = 4{\cdot}68$
SUFFICES (1) $4C_f = 0{\cdot}0297$ (2) $4C_f = 0{\cdot}0172$

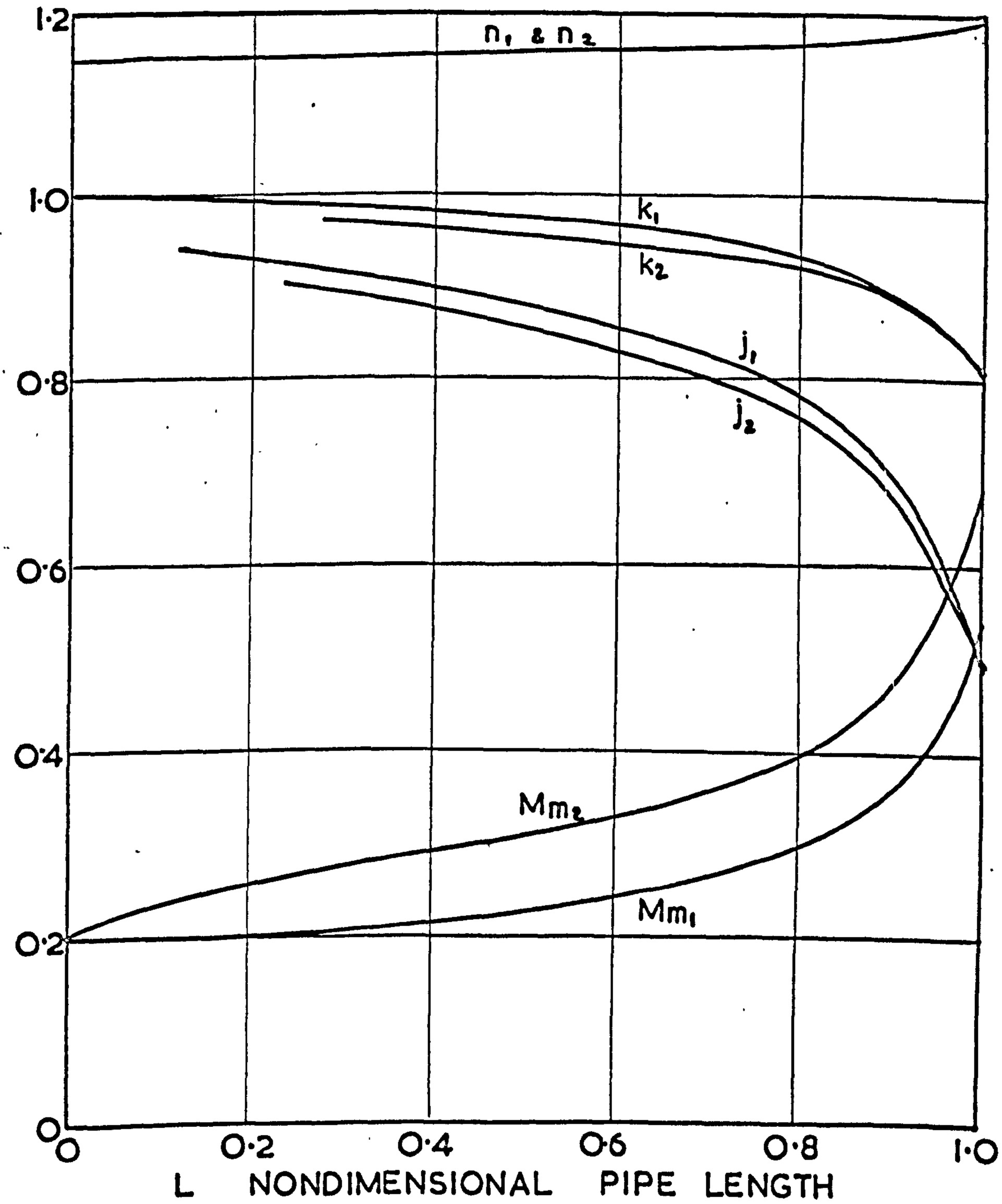

FIG 49 CURVES OF $n_1 k_1 j$ & Mm FROM THE COMPUTER SOLUTION FOR $W_g = 0{\cdot}153$ LB/SEC AND $W_s/W_g = 0{\cdot}91$ SUFFICES (1) $4C_f = 0{\cdot}0206$ (2) $4C_f = 0{\cdot}0150$

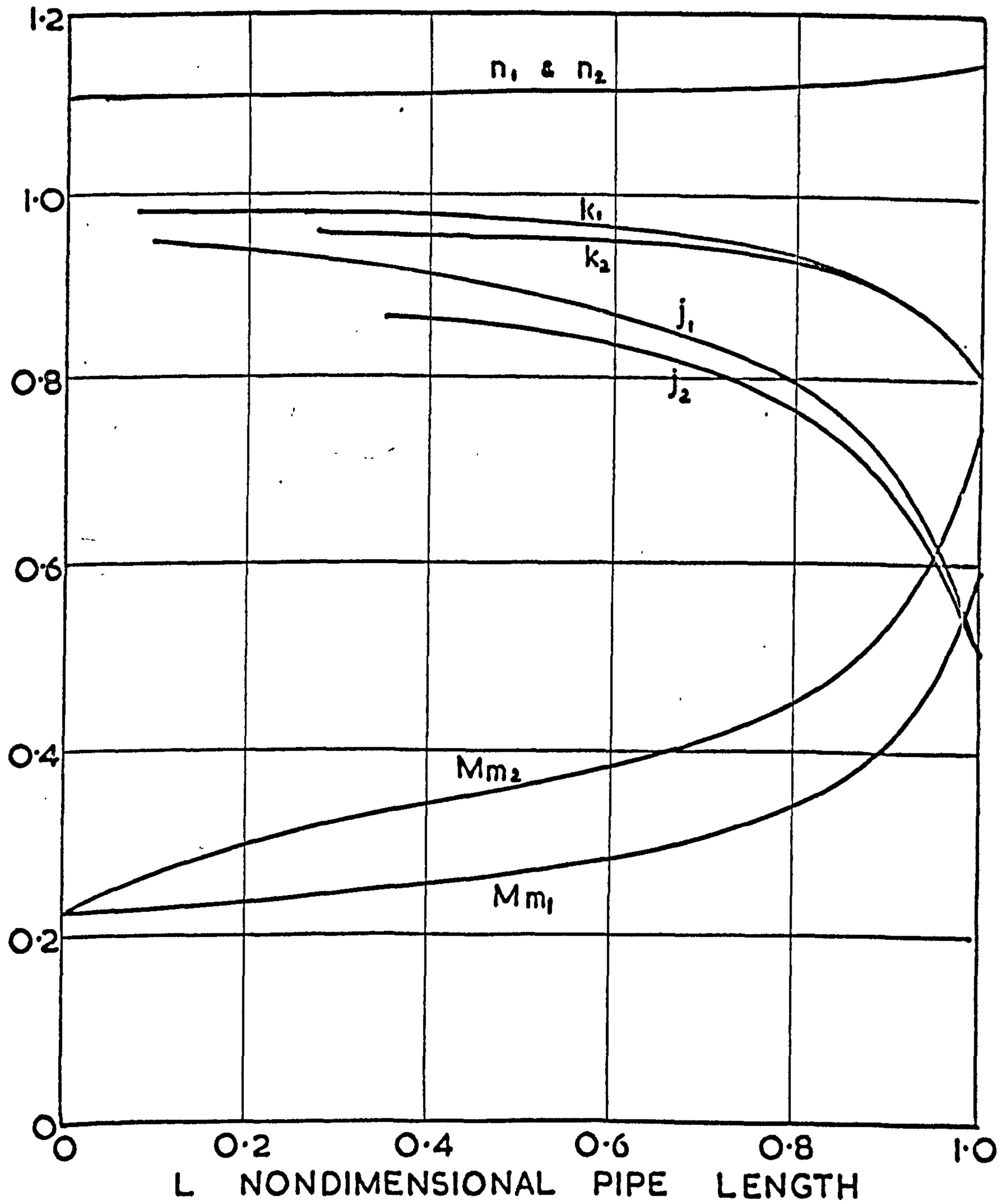

FIG 50 CURVES OF n, k, j & Mm FROM THE COMPUTER SOLUTION FOR $W_g = 0{\cdot}153$ LB SEC AND $W_s/W_g = 1{\cdot}42$ SUFFICES (1) $4C_f = 0{\cdot}0208$ (2) $4C_f = 0{\cdot}0150$

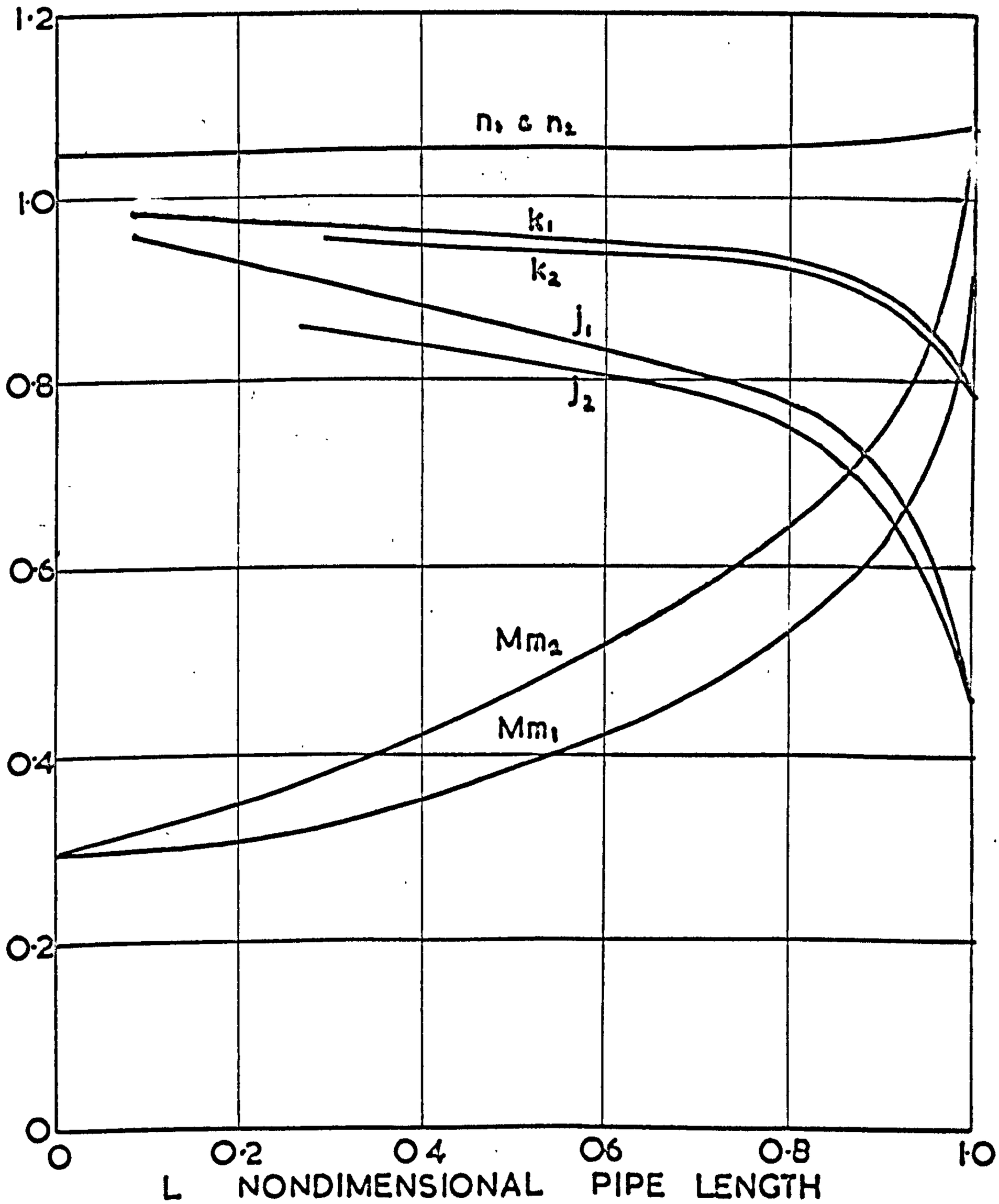

FIG 51 CURVES OF n, k, j & Mm FROM THE COMPUTER SOLUTION FOR Wg = 0·147 LB/SEC AND Ws/Wg = 3·82
SUFFICES (1) 4Cf = 0·0199 (2) 4Cf = 0·0153

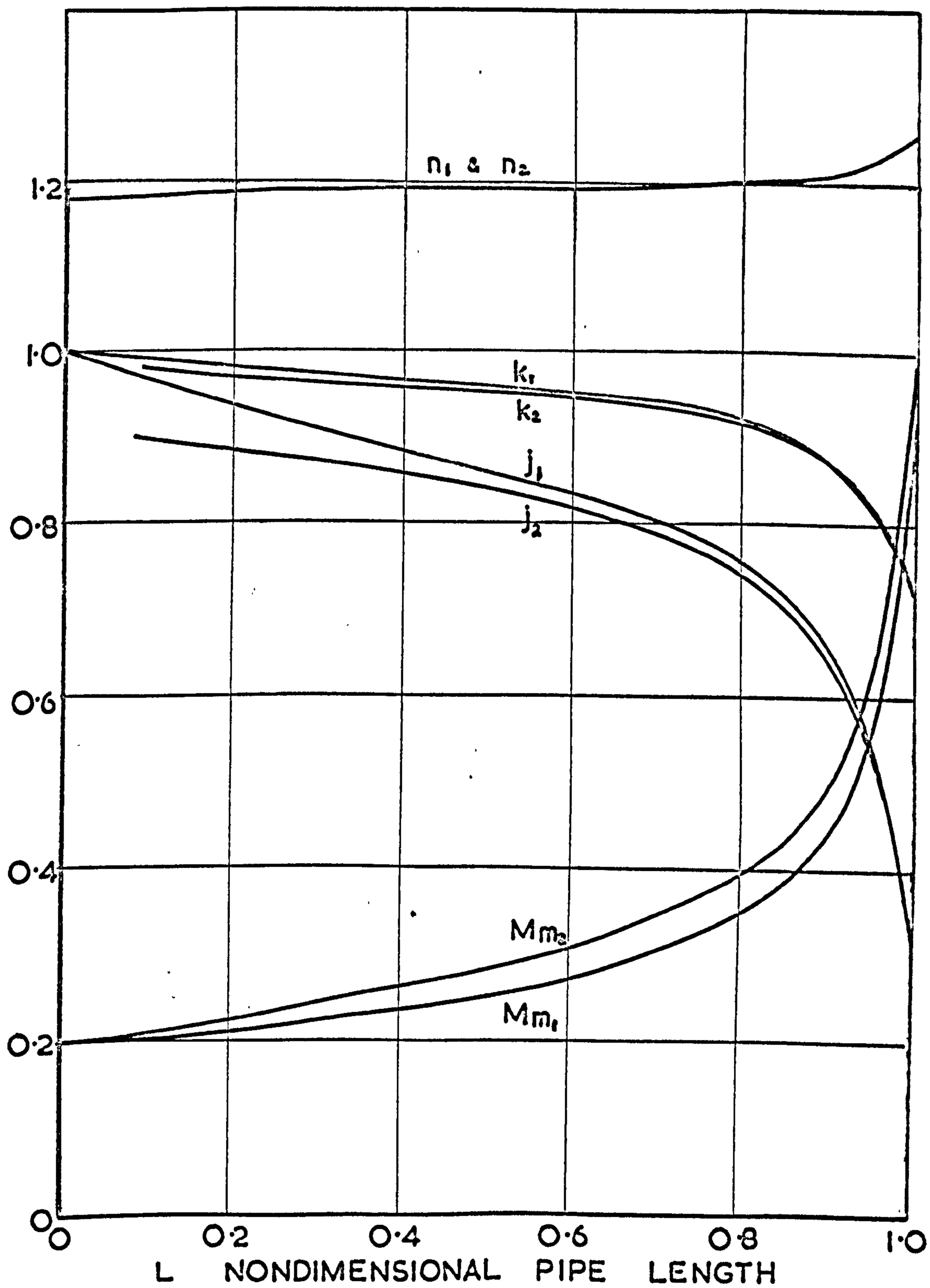

FIG 52 CURVES OF n, k, j & Mm FROM THE COMPUTER SOLUTION FOR Wg=0·230LB/SEC AND Ws/Wg=0·66 SUFFICES (1) 4Cf=0·0159 (2) 4Cf=0·0140

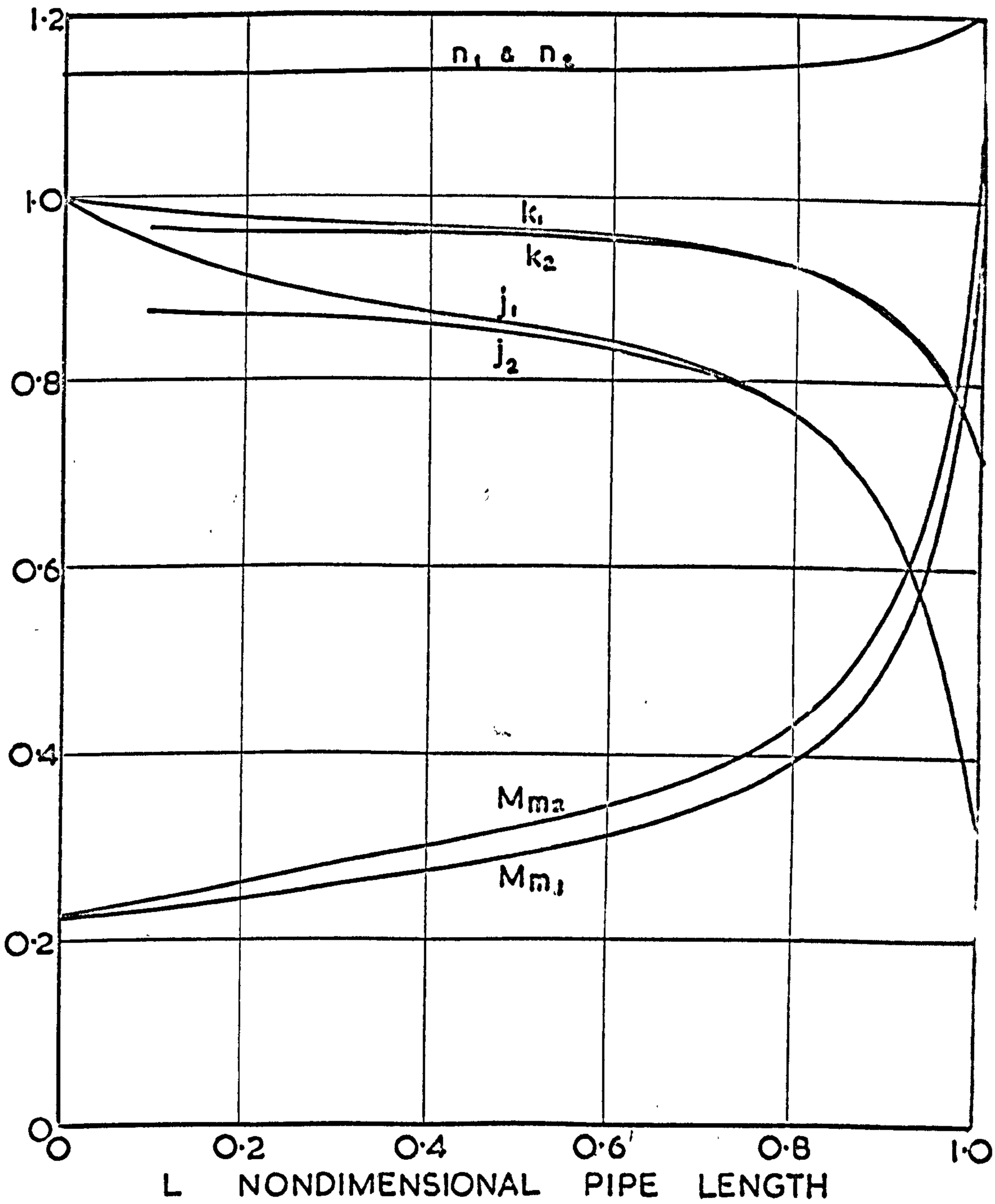

FIG 53 CURVES OF n, k, j & Mm FROM THE COMPUTER SOLUTION FOR W_g=0·229LB/SEC AND W_s/W_g=1·11
SUFFICES (1) 4Cf=0·0157 (2) 4Cf=0·0140

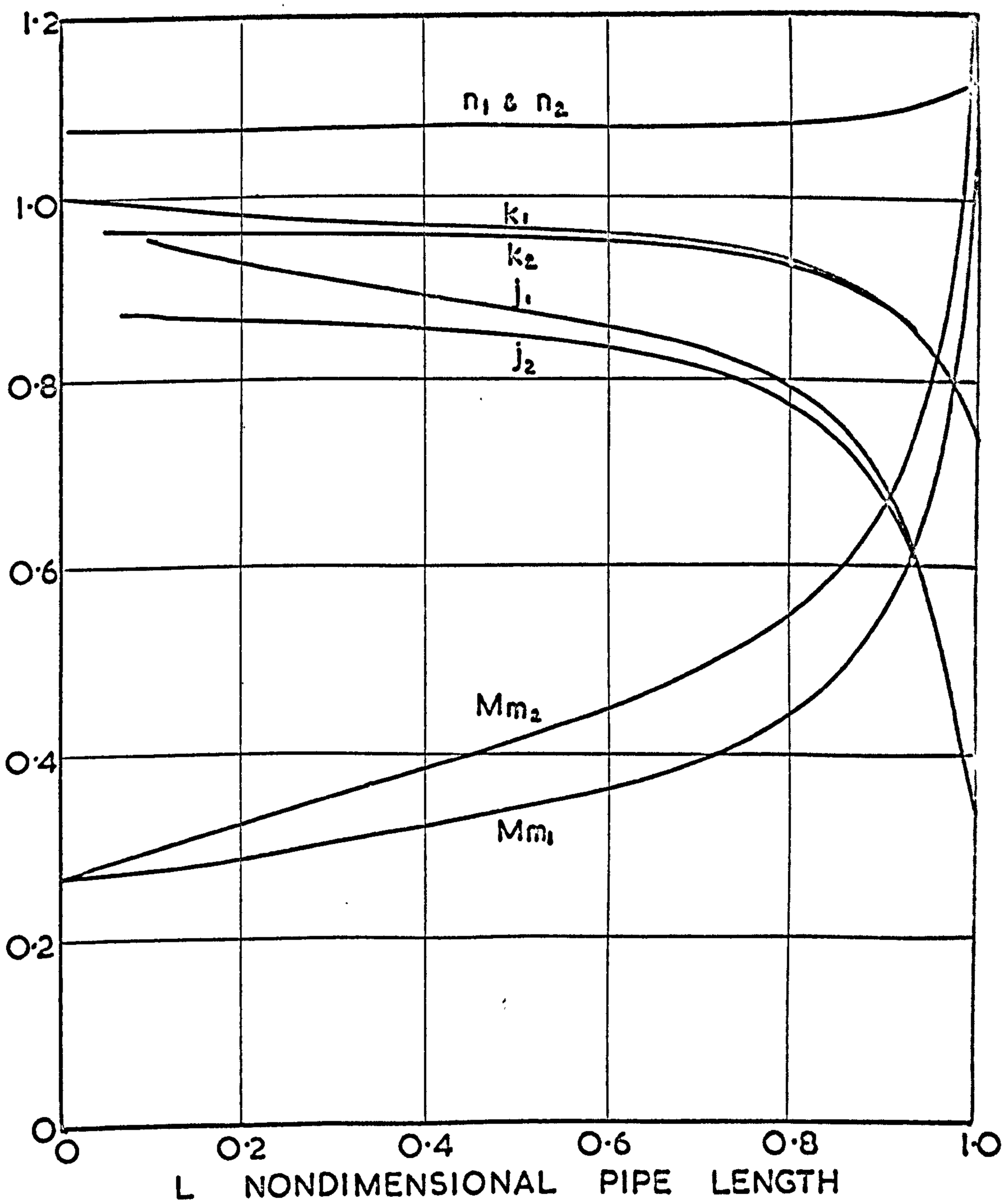

FIG 54 CURVES OF n, k, j & Mm FROM THE COMPUTER SOLUTION FOR W_g=0·229 LB/SEC AND W_s/W_g=2·35
SUFFICES (1) $4C_f$=0·018 (2) $4C_f$=0·0140

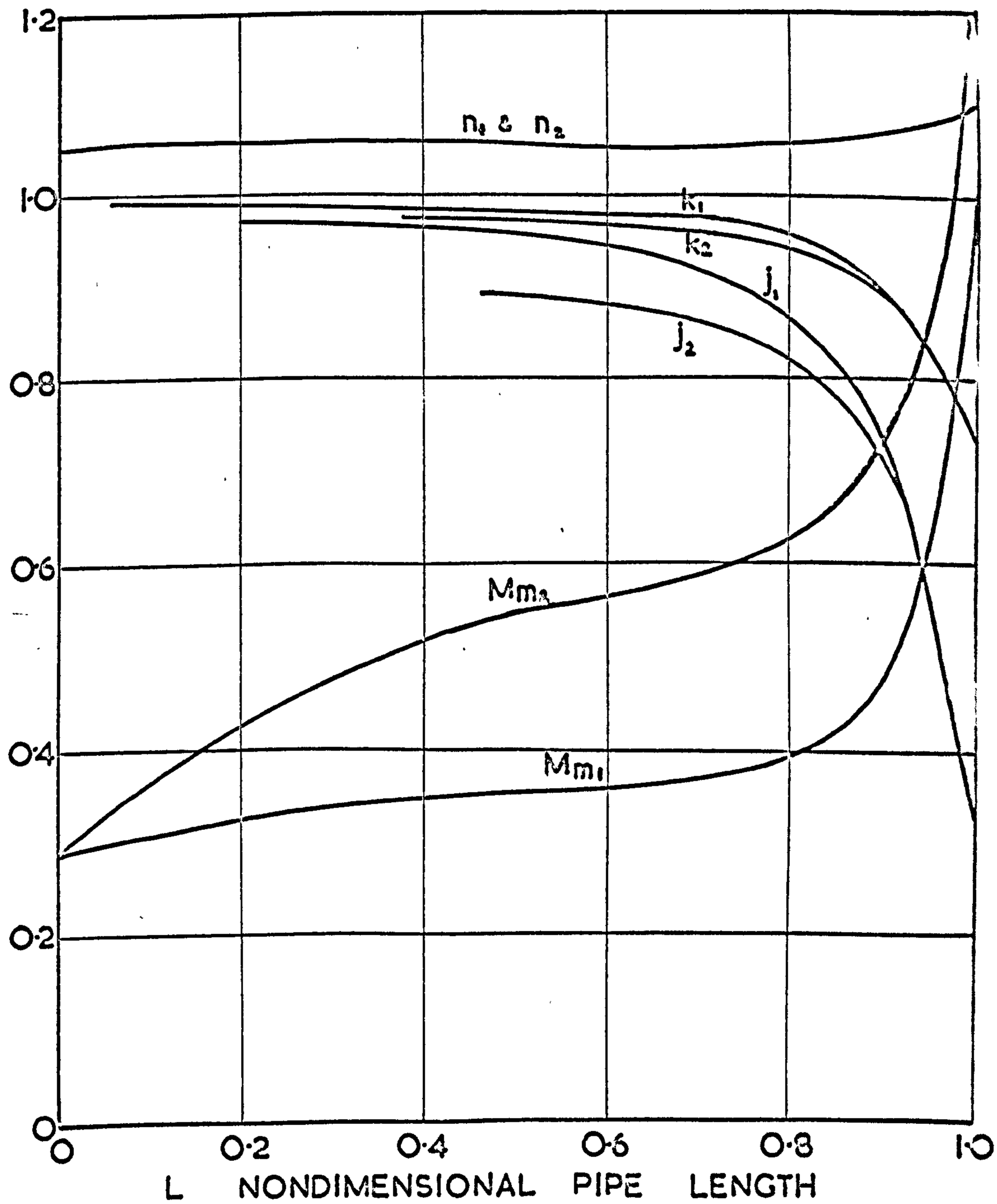

FIG 55 CURVES OF n, k, j & Mm FROM THE COMPUTER SOLUTION FOR Wg=0·239LB/SEC AND Ws/Wg=3·44 SUFFICES (1) 4Cf = 0·0243 (2) 4Cf = 0·0139

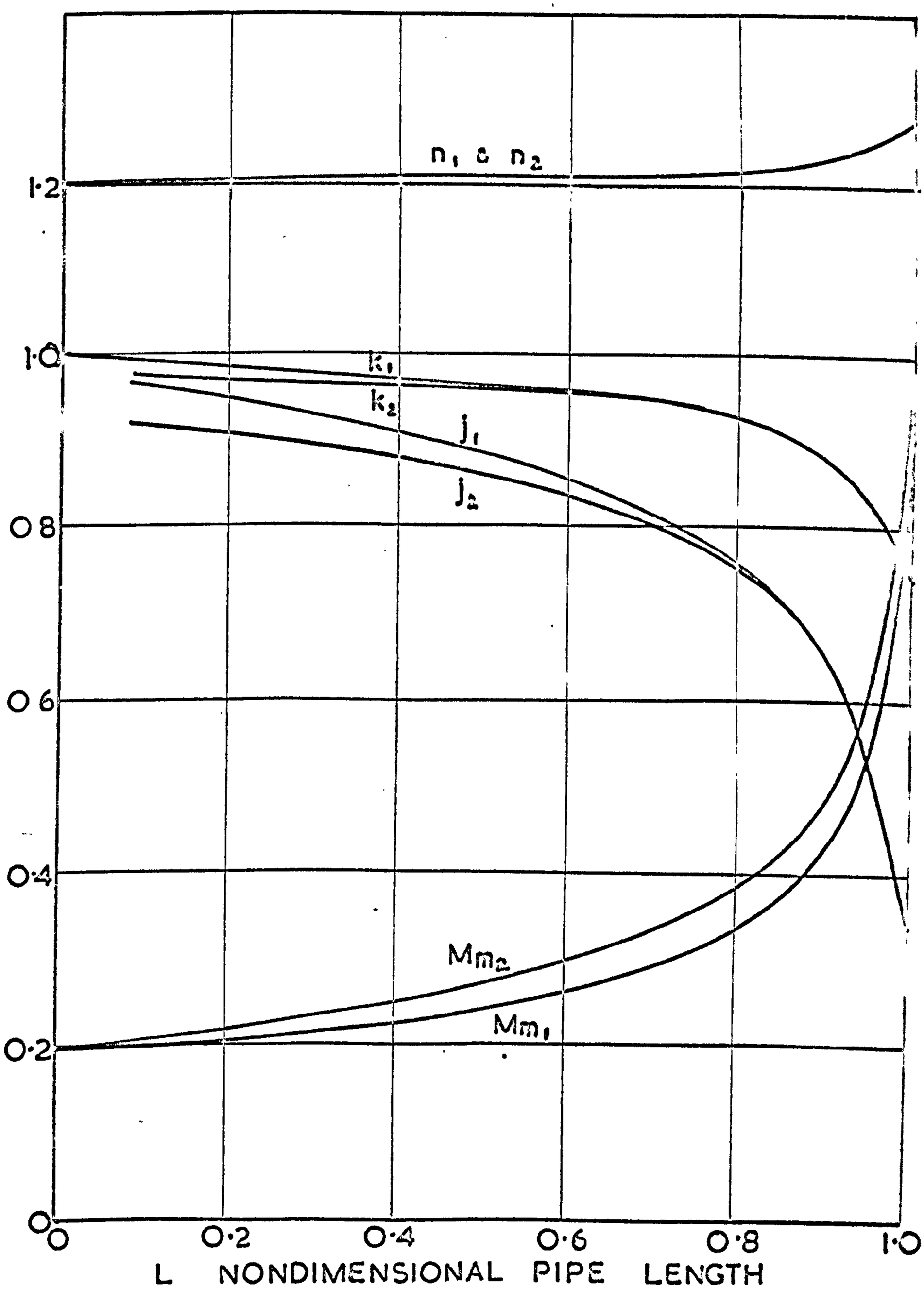

FIG 56 CURVES OF n, k, j & Mm FROM THE COMPUTER SOLUTION FOR W_g=0·315LB/SEC AND W_s/W_g=0·53
SUFFICES (1) 4Cf = 0·0151 (2) 4Cf = 0·0132

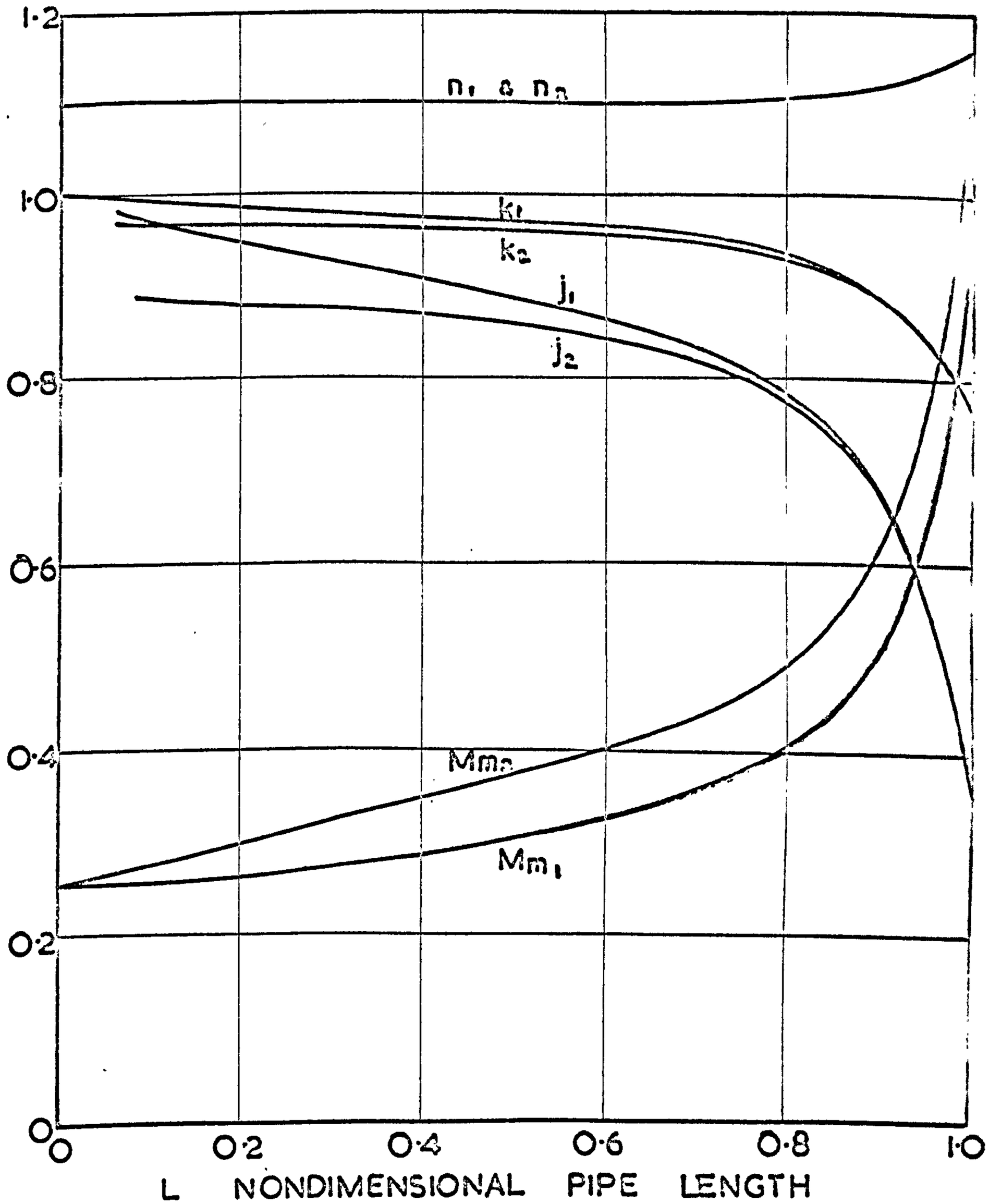

FIG57 CURVES OF n, k, j & Mm FROM THE COMPUTER SOLUTION FOR W_g=0·306 LB/SEC AND W_s/W_g=1·68 SUFFICES (1) 4Cf=0·0168 (2) 4Cf=0·0132

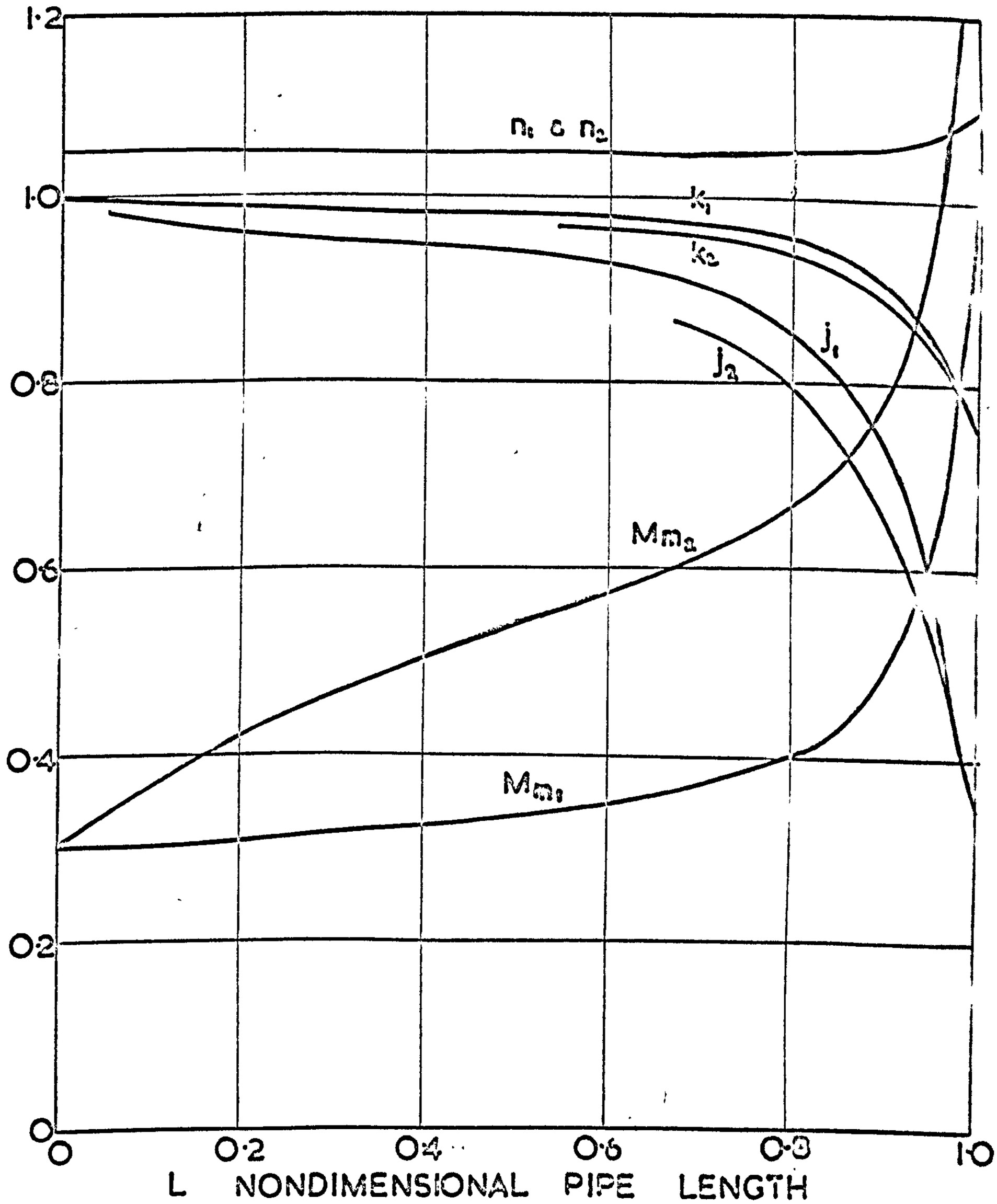

FIG 58 CURVES OF n, k, j & Mm FROM THE COMPUTER SOLUTION FOR W_g=0·284 LB/SEC AND W_s/W_g=3·87 SUFFICES (1) 4Cf=0·0246 (2) 4Cf=0·0134

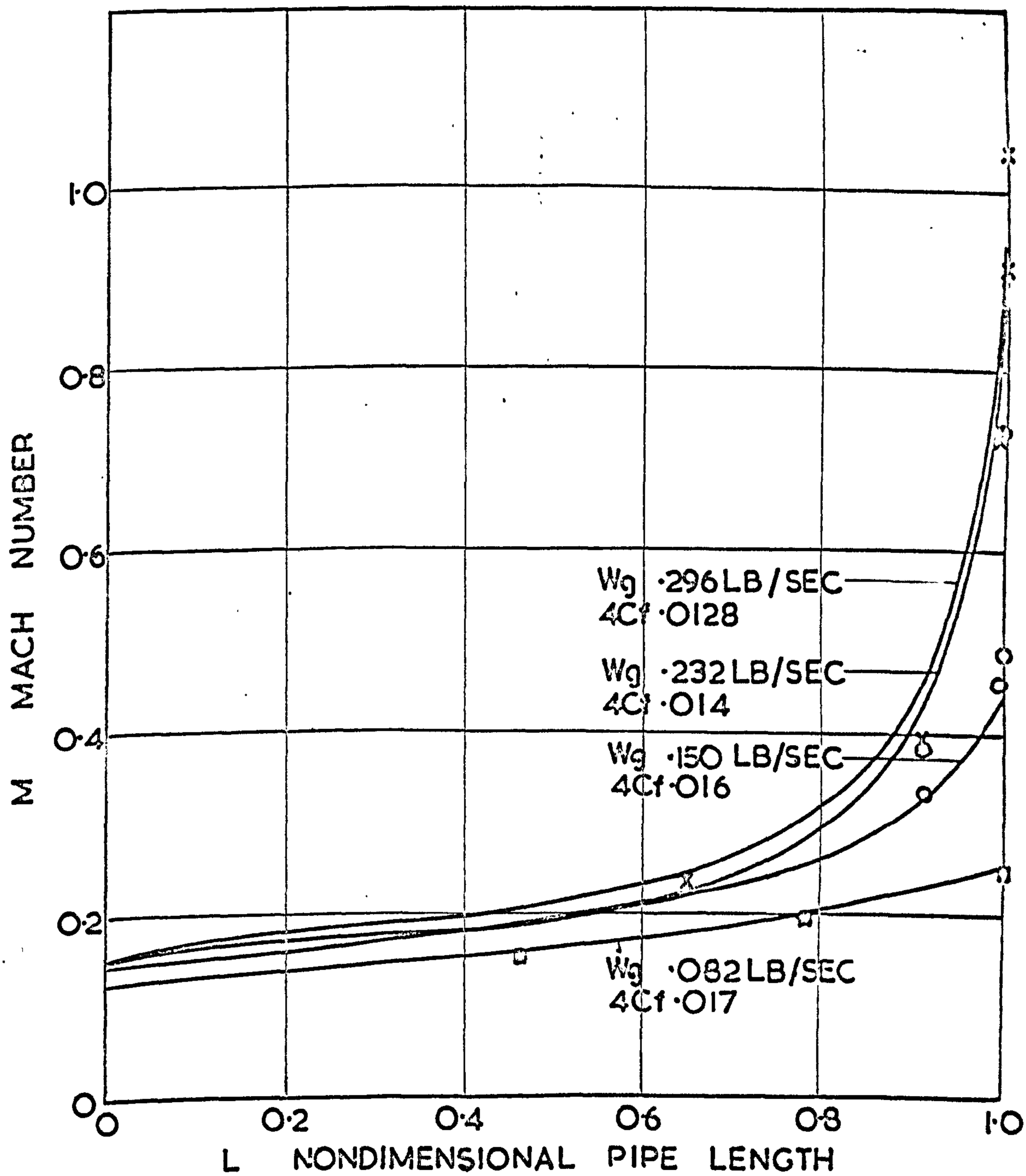

FIG 59 CURVES OF AIR MACH NO. FROM THE COMPUTER SOLUTION AND EXPERIMENTALLY DERIVED MEAN MACH NOS. ▫ Wg≈0·082 LB/SEC o Wg≈0·15 LB/SEC x Wg≈0·23 LB/SEC o Wg≈0·31 LB/SEC

In Section 3.3.5, a "hand" solution of the basic equations was outlined, this was in fact performed for one of the sets of conditions, before the computer programme was written. Since the results from this solution were very similar to those from the computer, though there was more scatter due to the crudeness of the method, no plots are given.

CHAPTER 9.

DISCUSSION.

In this chapter a discussion is given of the experimental techniques used, the experimantal results obtained by both direct measurement and from the computer solution of the basic equations, and an analysis of these results in the light of the theoretical approach put forward in Chapter 3. Where possible, comparison will be made with the results of other workers as outlined in the Literature Review Chapter 2. It will be convenient to continue the presentation under sub-headings corresponding to the points under discussion.

9.1. Pipe Line Pressure Drop.

The experimentally and theoretically determined pressure drop curves in Figs. 17 and 18 indicate that even for pure air flow in the pipe line rig the uncertainties in the determination of the variables are such that in only one case, i.e. for an air flow of 0.15 lb/sec. is good agreement obtained between the experimentally determined pressure drop curve and the theoretical curve using a $4C_f$ value obtained from the first 9 ft. portion of the experimental curve, and one dimensional

adiabatic compressible flow theory. For the other flow rates the lack of agreement is probably due to one or all of the following:-

(a) An incorrect estimation of friction factor.

(b) In the cases of flow rates of 0.232 and 0.296 lb/sec. the incorrect positioning of the pipe exit. The method of non-dimensionalising with reference to the pipe exit suffers from the disadvantage that because the pressure gradient in an axial direction is so steep at pipe exit for compressible gas flow, any small inaccuracy in positioning pipe exit can lead to a significant error in p_e and hence in p/p_e.

(c) The incorrect assessment of pipe exit Mach number; this also probably largely applies to the high air flow rates and is really dependant on (b) above as the derivation of exit Mach number requires a value of pipe exit static pressure.

A value of $4C_f$ of 0.018 instead of the value 0.017 obtained over the first 9 ft. length of flow would give good agreement in the case of an air flow rate of 0.082 lb/sec. For the high air flow rates, substitution of pipe exit conditions

into the equation to determine exit Mach number as quoted in Section 8.2.1. indicates that for both air flow rates the exit mean Mach number is in fact 1.012; this, if correct, only partially accounts for the lack of agreement between measured pressure drop curve and that obtained theoretically.

Because of the difficulty in evaluating an exit mixture Mach number and the values of k and j, it is difficult to make comparisons between pressure drop curves evaluated from constant fractional lag theory and the measured pressure drop curves for air-solids flow. An attempt has been made, however, to compare the measured pressure drop curves with those obtained by substituting mean values of k, j, n and $4C_f$ from the computer solution into the constant fractional lag equations. This was only performed for flows where the exit mixture Mach number was assumed to be unity. The indications are that much larger lags than those given in the computer solution, or much larger values of the friction factor are required to obtain any agreement. Because in all the references to gas-solids pipe flow with experimental results seen by the Author of this Thesis, the flow was assumed incompressible, and the relationship between pressure and pipe length for a given set of flow conditions was hence linear, it has not been possible to give any comparison between the pressure drop curves

and those predicted by the empirical expressions of other workers.

9.2. Efficiency of Solids Conveyance.

From the curves of horse power consumed per unit solids flow rate against the solids to air loading ratio in Fig. 23, it is immediately apparent that below a loading ratio of about 3, conveying at any air flow rate is inefficient, whilst it would also appear that some efficiency is sacrificed by going to higher air flow rates. A further indication, especially from the curve W_g = 0.082 lb/sec., is that increasing the loading ratio above 5 results in only a small increase in efficiency, whilst physical limitations, such as erosion of the pipe (especially at bends) and vibration of the pipe line might become unduly severe in an actual plant.

9.3. Comparison of Friction Factors with those of Other Workers.

It is of some interest to compare the values of friction factor $4C_f$ for air-solids flow evaluated over the initial 9 ft. section of the pipe with the values predicted by other workers for similar flow conditions, though not necessarily using polystyrene particles as solids material. In Fig. 60 are shown curves of $4C_f$ against W_s/W_g evaluated for the four

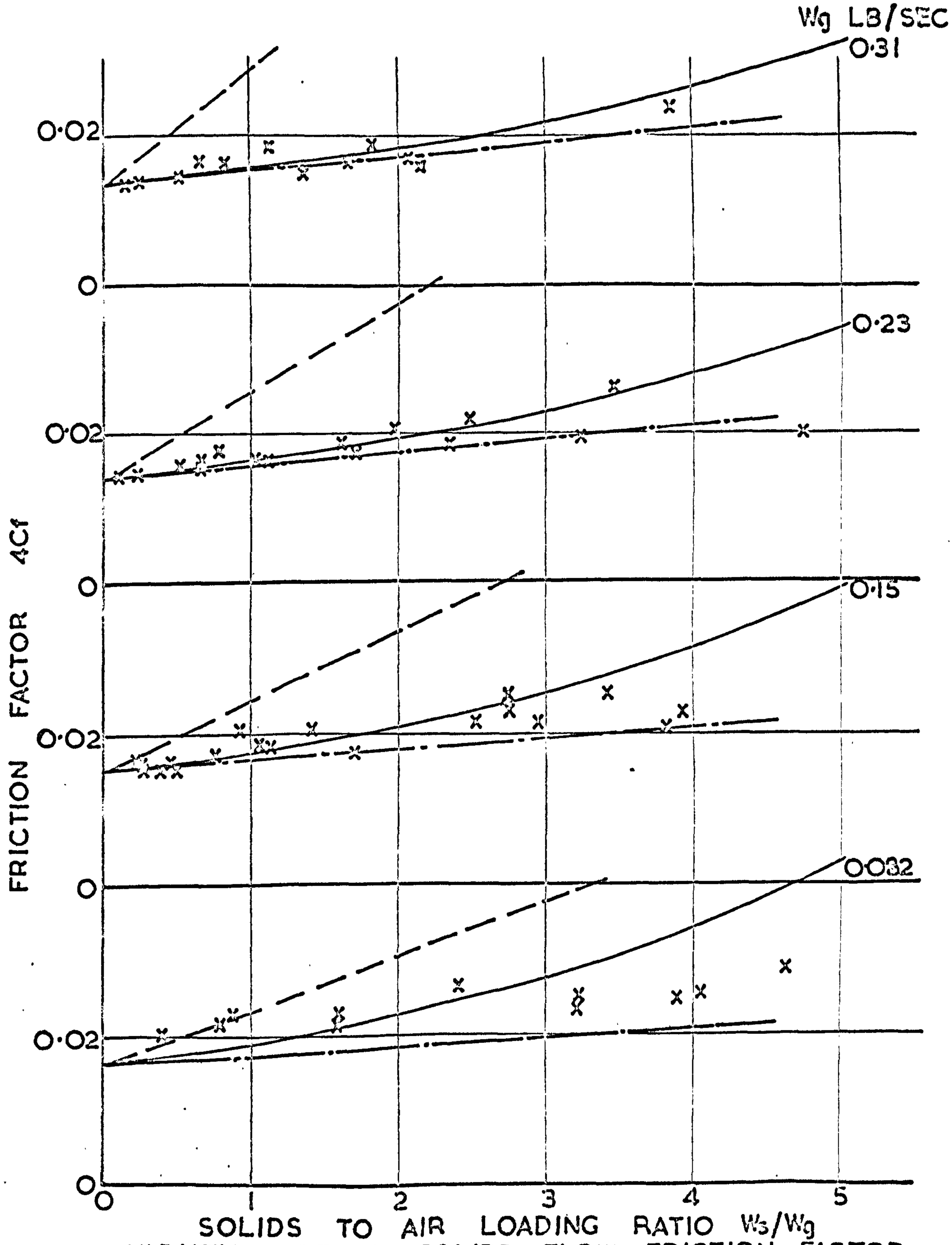

FIG 60 VARIATION OF AIR-SOLIDS FLOW FRICTION FACTOR WITH LOADING RATIO AND AIR FLOW

x DERIVED VALUES —UEMATSU'S EXPRESSION

— — HINKLE'S EXPRESSION —·— RICHARDSON & McLEMAN'S EXPR.

different air flow rates from the expression put forward by Uematsu, Hinkle and also an equivalent friction factor derived from the expression of Richardson & McLeman (Section 2.1.1.). The curves of Hinkle's and Richardson & McLeman's expressions were evaluated using their expressions for solids velocity to obtain u_s, and in the case of Hinkle's expression, the particle drag coefficient from the standard drag curve at the relevant particle Reynold's number. The plotted values are those obtained from a large number of the pipe flow experiments, and it is apparent that there is appreciable scatter in these values. It is felt that this mainly results from inaccuracies involved in obtaining the slope of the pressure drop curve, where a slight inaccuracy in pressure drop reading can result in a significant change in the value of $dp/d\ell$. Apart from the results at the air flow rate of 0.082 lb/sec., the expression of Richardson and McLeman appears to give the best agreement with the plotted points. This is rather to be expected as their experiments were performed in a 114 ft. long 1 in. bore brass pipe, whilst the experiments of Hinkle were performed in 2 and 3 in. glass pipes. In his paper, Uematsu does not specify his pipe diameter.

9.4. Cyclone Pressure Drop.

The plots in Fig. 24 show fairly conclusively that an

increase in solids loading leads to a decrease in cyclone pressure drop. A similar effect has been noticed previously by other workers, and Briggs (1946) put forward the following equation:

$$1 - \frac{\Delta p}{\Delta p_o} = 0.013\ c$$

for the flow of a polydisperse dust of mean particle diameter 16 microns and specific gravity 2.8, in air flow through a cyclone 22 cm. diameter. Where Δp is the cyclone pressure drop associated with dust concentration c (gm. per cu.m.) and Δp_o is the pressure drop for clean air. Other workers have observed that this effect increases with increased particle size.

Because the pressure drop values in Fig. 24 include a contribution due to flow through the other components of the separation system besides the cyclone, no attempt is made to derive an expression similar to the above.

9.5. Air Velocity Profiles.

The air velocity profiles for pure air flow in Fig. 25 are in general agreement with those obtained for pipe flow by other workers. Knudsen and Katz (1958) show values of n the power law index, in the range $n = 6$ for $Re = 4 \times 10^3$ to

$n = 10$ at $Re = 3.24 \times 10^6$. No indication from previous work, however, is given of the variation with Mach number. The curves in Fig. 25 indicate that the value of n as well as increasing with increasing Reynold's number, also tends to increase with increasing Mach number. The significance of this would appear to be that increasing Mach number results in a flatter velocity profile with a large velocity gradient in the laminar sublayer region leading to increased skin friction factors. This is not, in fact, borne out by other workers, who indicate that the skin friction factor remains constant (Keenan and Naumann) or decreases slightly with increasing Mach number up to Mach one.

Straight lines have been drawn in Fig. 26 from the air velocity measurements in air-solids flow, though the plots did not approximate to straight line graphs quite so well as the pure air flow plots did. However, where straight lines can be reasonably drawn, the resulting value of n in the power law index shows the following tendencies:-

(a) For constant air mass flow rate and air Mach number, n tends to increase with increasing solids to air loading ratio.

(b) For constant air mass flow rate and reasonably constant

loading ratio, the plots indicate that, as for air flow, the value of n tends to increase with increasing air Mach number.

Due to difficulty in obtaining these plots, and the subsequent lack of accuracy, these are only tentative observations.

Peskin and Dwyer state that for their experiments in a square section duct of 3 in. wall, the addition of solids to the air flow, producing W_s/W_g ratios of about 3 to 1, had no effect on the air velocity profiles. This is fairly well substantiated by the plot for $W_s/W_g = 2.1$ at $W_g = 0.081$ lb/sec. in Fig. 26. The other plots at $W_g = 0.081$ lb/sec., however, indicate that at low ratios of W_s/W_g, the air velocity profile is no longer similar to that for pure air flow, and if curves were drawn with linear axes, the profiles would be seen to be considerably less steep than those for pure air flow. This would then indicate that the actual skin friction drag is considerably less for low loading ratios of air solids flow than it is for pure air flow. Although the pipe line pressure drop profile is not generally less than that for pure air flow, because of the drag force between particles and air and also because of the particle to particle and particle to wall inter-

action, it might conceivably be possible to obtain pressure drops for low W_s/W_g ratio gas-solids flows which were less than those for pure gas flow. This is, in fact, what is thought to be the case for the two low loading ratios at W_s = 0.23 and 0.31 lb/sec. in Figs. 21 and 22. For these flows, pressure drop curves were obtained which were lower than those for pure air flow, indicating that the reduction in pressure drop from air to wall skin friction due to a less steep velocity profile, was greater than the pressure drop arising from particle to air frictional drag and particle to particle and particle to wall interaction. This is also substantiated by a comparison of the air velocity profiles for low W_s/W_g ratios with the velocity profiles at low Mach numbers for pure air flow from Figs. 25 and 26.

In Section 2.1.3. of the Literature Review, a classification of gas-solids flows by Peskin and Dwyer is quoted. It would appear, therefore, that at low solids loading ratios, the flow of 0.012 in. diameter polystyrene particles in air can be classified in their Region 1, where the presence of the solids particles can cause increased viscous damping in the boundary layer, with the result that the laminar sublayer extends further away from the pipe wall, with a subsequent decrease in wall

shear stress compared with that for pure gas flow. Generally, however, the flow of these particles in air would be in their Region 2, where the mean velocity profile is not changed significantly by the presence of the solids particles.

It was always the case that the evaluated air mass flow rate from the pitot traverse was less than that measured by the air flow measurement nozzle, and was appreciably less at the high loading ratios. At first sight, this would indicate that the total head measured by the pitot tube contained no appreciable contribution due to the kinetic energy of the solids. It should be realised, however, that as soon as solids were introduced into the air flow, the pitot tube started to block, with the result that the pitot tube system response time increased, probably giving a total pressure profile slightly lower than the true curve. From equation 2 in Appendix 6 it can be seen that a restriction in pitot tube bore reducing the diameter to 1/3 of the original could increase the response time from 0.005 sec. to 0.4 sec. As the only traverses obtained at a really high loading ratio $W_s/W_g = 2.1$ were obtained manually, such that the response time expression would not apply, it is considered that the response time in the other traverses was not sufficiently impaired to give appreciably erroneous results.

A further mitigating factor is that the traverses were always started from the pipe wall, so that the blockage would not be expected to become significant until the traverse was out of the high pressure gradient region, and away from this region a larger response time can be tolerated.

9.6. Solids Velocity.

The only limitation to the method of solids velocity measurement appears to be the lack of a means of determining how far into the field of view the streak photographs of the solids particles relate. Comparison of the results with those predicted by the computer programme give no indication of this, because of the uncertainties in specifying a friction factor. Because the values of solids velocity were in each case obtained from the mean of a large number of streaks, it is probable that the values represent a mean. This mean value, however, may not necessarily be the mean velocity of all the particles across a pipe diameter, as the depth of view would be expected to vary with solids loading.

In a paper on velocity and concentration distributions in incompressible gas-solids pipe flow though with W_s/W_g ratios less than 0.15, Soo (1962) states that the solids velocity can be expressed in the form of a power law, analogous to the power laws for

pure gas flow, of the form:

$$U_s = (\hat{U}_s - U_{sw})(y/R)^{\frac{1}{n}} + U_{sw}$$

where $\hat{U}_s$ and U_{sw} are the solids velocities on the pipe centre-line and at the wall respectively. He states that for his conditions the value of n is not very much greater than unity, and this would indicate a considerably less steep profile than that for the gas flow. The measurements made in this project do not substantiate such a solids velocity profile as none of the steak photographs showed streaks corresponding to very much lower solids velocities than the mean, as is inferred by Soo's expression.

The plots of solids velocity against loading ratio in Figs. 27 and 28 generally tend to indicate that for similar air flow rates, the velocity of the solids decreases with increasing loading ratios. The expressions of Hinkle, and Richardson & McLeman given in Section 2.1.2. and Fig. 1 indicate, on the other hand, that the solids velocity is not influenced by the solids loading.

A further point of disagreement between the results from this project and the expressions for solids velocity given by Hinkle and Richardson & McLeman is that their prediction of

$v_g - v_s$ is greater than that measured in this project where the results are comparable. In this respect, however, for the size of particle and velocities being considered, the expression of Richardson & McLeman gives velocity differences somewhat closer than those predicted by Hinkle's expression. If, in fact, the free falling velocity of 5.3 ft/sec. quoted by Richardson & McLeman as being the free falling velocity for this size of polystyrene particle is used in their expression rather than the value given by the Stokes flow equation, their resulting value of $v_g - v_s$ is probably only slightly greater than the values indicated in Figs. 29 - 41.

9.7. Computer Solution of the Basic Equations.

The most striking observation from the computer solution of the basic equations is the tremendous differences in results obtained with variation in friction factor, $4C_f$. The results in Figs. 29 - 41 are plotted for what are considered to be the two extremes of friction factor, and obviously better agreement would be obtained if a value somewhere between these two extremes were chosen. The real issue here is that unlike pure gas flow in a pipe where the friction factor remains reasonably constant, it would appear to be no longer permissible to assume $4C_f$ constant in compressible gas-solids pipe flow. The value of the factor

should vary from that evaluated assuming no change in velocity over a short section in the low velocity region of flow, to a value approaching the value of $4C_f$ for pure gas flow in the regions of high velocity. Examination of Figs. 29 - 41 shows that it would probably not be correct to take the value of $4C_f$ for gas flow in the high velocity regions for all cases, though for the flows at 0.23 and 0.31 lb/sec. this might be quite reasonable. For the lower air flow rates it would be necessary to use values of $4C_f$ in the high velocity regions somewhat higher than those given for pure gas flow.

The reason for the apparent non-constancy of the friction factor throughout compressible gas-solids flow is almost certainly due to the variation in solids dispersed density throughout the flow. Although the mass ratio of solids to gas increases as the velocities increase, due to the variation in the velocity fractional lag k, with the result that the ratio of solids dispersed density to gas density also increases, the absolute value of the solids dispersed density is decreasing rapidly, such that a given volume of pipe in the high velocity region contains considerably fewer solids particles than the same volume in a low velocity region. The result of this would be expected to be a much lower contribution to the friction factor from solids particle to particle and particle to wall interaction.

Hence the reduction in friction factor.

In the foregoing discussion of the effect of friction factor on the resultant velocities and temperatures in gas-solids flow, no account was taken of the part played by the assumptions made regarding solids particle drag coefficient and Nusselt number. These obviously have considerable influence on the resulting solids velocity and temperature, but probably only a lesser effect on air velocity and temperature, provided the expressions used for C_D and Nu are not too inaccurate. As these expressions, or similar expressions, have been used by previous workers, there is no reason to assume this to be the case. Also in Figs. 29 - 41 for the few cases where solids velocities and mean air velocities have been evaluated at similar positions in the flow, the resulting value of k is of the order predicted by the computer solution.

In this discussion on the results obtained for velocities and temperatures from the computer solution, it should be pointed out that the air temperatures and densities obtained do not necessarily satisfy the gas equation of state when considered in conjunction with the pressure from the relevant pressure drop curve. In most cases there is considerable discrepancy between the density evaluated from the computer programme and that

evaluated by considering the temperature from the computer programme and the relevant pressure. This is because apart from being used to evaluate the initial conditions for the solution of the equations, the gas equation of state is a redundant equation in the computer solution as a result of specifying the pressure drop curve. If, however, the correct value of friction factor were used, it would probably be found that agreement would be obtained between values of the gas density evaluated from the computer solution and from the gas equation of state, and this equation could then be used as a check on the evaluated results.

In applying the mixture Mach number equation obtained for constant fractional lag theory to the results obtained from the computer solution, some care is required since this equation is only strictly applicable for constant values of k and j. In the case of the index n, this would be expected to apply to any point in the flow for which the values of k and j are known. However, now j is rather better defined as $dT_s = jdT_g$, and this becomes equal to the definition for constant fractional lag where the stagnation temperature remains constant throughout the flow.

Regarding the value of k, because in the passage of a small discontinuity at any position in the flow there is no means of determining the change in k through the discontinuity, the effect of a varying k value on the mixture velocity of sound expression is unpredictable. It will be assumed, however, that the variation in k obtained in this project is not sufficient to cause the constant fractional lag mixture velocity of sound expression to be unduly incorrect. In spite of these limitations, it is still considered significant that the evaluated mixture Mach numbers at pipe exit should lie close to unity, and would probably be closer still if it were possible to introduce the correct values of a variable friction factor into the computer solution.

9.8. Pipe Exit Mach Number for Air Flow.

From the results of the pipe flow pressure drop measurements for pure air flow in Fig. 18, the pitot tube traverse at pipe exit for choked flow (Fig. 25), and the Mach number curves in Fig. 59, it is of some interest to consider the value of

the pipe exit mean Mach number. The indications from the pressure drop curves and the pitot tube traverse at pipe exit are that the exit mean Mach number is unity. This implies, because there must be a Mach number variation across the pipe, that the Mach number on the centre-line of the pipe is greater than unity. The computer solution, which made use of the same pressure drop curves, however, indicates a mean Mach number less than unity for both "runs" with "choked" flow. Also classical gas dynamics theory states that a Mach number greater than unity can only result by accelerating the flow through a convergent-divergent system.

A possible explanation of the above discrepancy is that when a pipe terminates in a relatively shallow angled diffuser (as in this rig) the pipe exit position is not, in fact, constant and possibly varies from flow to flow. It was only possible to estimate the pipe exit position with flow rates less than that necessary for the onset of "choked" flow. This was because the pressure drop traverse obtained from static pressure tappings over the pipe exit region shows a continual decrease from pipe exit into the diffuser for choked flow, until a shock wave occurs. At flow below the "choked"

condition, however, the pressure drop traverse of the pipe exit section reaches a minimum value, and this was assumed to to occur at pipe exit.

If the pipe exit position is not constant, the readings obtained in Fig. 18 could be greater than those actually occurring, with the result that a pressure drop curve evaluated from compressible flow tables with a mean exit Mach number less than unity would give agreement. In the case of the pitot tube traverse, it is probable that the presence of the pitot tube could cause a disturbance in the flow, such that the pipe exit position is pushed upstream and the pitot tube was actually in a region of supersonic flow.

As no reference has been found to elucidate this point, and as the results from this project could be contradictory, it is not possible to give an indication of the mean Mach number at the pipe exit for "choked" pure gas flow.

9.9. Electrostatic Measurements.

From the electrostatic measurements taken, it may be fairly confidently stated that the electrostatic forces involved in conveying polystyrene solids particles in air flow through a brass pipe are of a much lower order than the aerodynamic forces.

This, however, may not necessarily be the case for flow through plastic tubing, as has been indicated by the measurements from the short lengths of nylon tubing in this rig. For this flow, it may, in fact, be necessary to include an electrostatic force term in the overall momentum equation.

As indicated in Section 8.5, some measurements of current to earth from the electrically isolated brass pipe section in the pipe line have been obtained. Although there are many factors influencing this current to earth, sufficient reproducibility has been obtained to indicate that readings similar to these might be used, with suitable calibration, to indicate the solids content of a gas-solids flow.

CHAPTER 10.

CONCLUSIONS.

The theoretical approach to the project has resulted in the idealised concepts of Equilibrium Flow, which has previously been considered by other workers; Constant Fractional Lag Flow, a concept suggested by Kliegel (1962), although in this project it has been applied rather differently to obtain more usable and general equations by not attempting to solve the solids particle momentum and heat transfer equations; and the more realistic Computer Solution of the basic equations. The equilibrium flow theory would only be expected to apply to flows in which the solids particle size is very small, the solids loading ratios are low and the rate of change of velocity is gradual.

The constant fractional lag theory gives poor agreement between predicted pressure drops and the measured pressure drops for pipe flow, when mean values of k and j are used. It provides, however, the mixture Mach number expression, which gives every indication of being a reliable gas-solids compressible flow dimensionless parameter, equivalent to that of the gas Mach number. This project has shown there are indications to

suggest that if the variation of k and j in the flow is small, then the mixture Mach number, as derived for constant fractional lag flow, is applicable to non-constant fractional lag flow as considered in the computer solution. In particular the computer solution has indicated that the flow of gas-solids mixtures through pipes cannot occur when the mixture Mach number at the pipe exit is greater than unity. This is similar to the "choked" flow condition for pure gas flows.

From the computer solution of the basic equations, as far as compressible gas-solids flows through pipes are concerned, the parameter requiring most investigation appears to be the friction factor. This is a factor incorporating the gas flow skin friction factor, plus an additional term to account for the presence of the solids particles. Unlike pure gas flows up to Mach one, or incompressible gas-solids flows, this factor does not appear to remain constant as the Mach number is varied. There is, in fact, reason to believe that in high speed flows the value of this factor approaches that of the skin friction factor for pure gas flow, whilst in low speed flows its value is somewhat greater than this.

The expression used for the solids particle drag coefficient, an equation "fitted" to the Standard Drag Curve, appears to have given reasonable results. In the case of the solids particle Nusselt number, because no static temperature measurements have been obtained, the accuracy of the expression used cannot be commented upon, but it is suspected that heat transfer effects are not of primary importance in this type of flow.

On the experimental side, rigs have been successfully established for the investigation of air-solids flows at speeds extending into the supersonic region. Although both pipe flow and rectangular duct flow rigs have been established, for the investigation of one dimensional and two dimensional flow respectively, it has only been possible, in this project, to obtain measurements with one type of solids material from the pipe flow rig.

The main emphasis, regarding experimental measurements, has been placed on obtaining air and solids flow rate measurements, and air and solids velocity measurements over the pipe-line. Great difficulty has been encountered in obtaining total pressure traverses, in air-solids flow, using pitot-tubes made from hypodermic tubing due to blocking of the mouth of the pitot-tube with solids particles and this was especially severe at high Mach

numbers. In fact, traverses have only been obtained at air Mach numbers less than 0.45. From the traverses obtained, however, it seems likely that, except at low loading ratios, the air velocity profiles for air-solids flow are generally similar to those for pure air flow at the same air mass flow rate and Mach number. As a result of this, it would appear reasonable to assume, for incompressible flow, that the pressure drop along the pipe can be represented by a Fanning type equation, in which the friction coefficient comprises that for the gas plus a factor to take into account the presence of the solids. In the case of low solids loading ratios, there are indications that the air velocity profile for air-solids flow is not so steep in the laminar sublayer region as the profile for pure air flow. Because of this it is possible to obtain gas-solids flows where the overall pressure drop for the gas-solids flow is less than that for a pure gas flow at the same gas mass flow rate.

A photographic technique, using a high speed cine-camera, has been established for obtaining a mean solids velocity measurement from observation glasses in the pipe-line wall. These measurements have tended to indicate a rather flat solids velocity profile. From measurements made in regions of the flow where comparison with the empirical expressions of other

workers are possible, there are indications that the expressions for incompressible gas-solids flow of Hinkle, and Richardson & McLeman predict gas to solids velocity differences which are greater than those measured in this project. In this respect, however, the expression of Richardson and McLeman gives rather better agreement for the particle sizes considered than does that of Hinkle.

From pressure drop measurements in regions of the flow which would be assumed to be incompressible, evaluated friction factors have been compared with those given by the expressions of Uematsu, Hinkle and Richardson & McLeman. The best agreement has been obtained with Richardson and McLeman's expression, though Uematsu's expression gave fair agreement. The agreement with Hinkle's expression was rather poor.

There appear to be no advantages to be gained by using high-speed gas-solids flow for pneumatic conveying of granular materials. The experimental results from conveying polystyrene solids particles through the pipe-line have, however, shown that there is a sharp rise in the horse power consumed per pound of solids delivered if solids to air loading ratios less than between three and five are used.

Finally it should be mentioned that this project is being continued in this Department with the emphasis on the following:-

(a) The investigation of electrostatic effects by observing air-solids flow through nylon piping.

(b) The investigation, both theoretically and experimentally, of supersonic air-solids flows with the subsequent formation of normal shock waves.

(c) The effect of theoretically considering polydisperse powders as the solids constituent.

(d) Measurements with solids powders other than the polystyrene used in this project.

APPENDIX 1.

A Theory for the Compressible, Equilibrium and Constant Fractional Lag Flow of Gas-Solids Mixtures.

Consider a flow in which the solid particles have velocity and temperature lags with respect to the gas such that:-

$$u_s = ku_g \qquad (1)$$

$$\text{and } T_s - Tg_o = j(Tg - Tg_o) \qquad (2)$$

(i) Adiabatic Change Applied to Gas-Solids Mixtures.

Because of the velocity and temperature lags in gas-solids flow the adiabatic energy equation must be considered as the energy flux per unit time remaining constant throughout the flow

$$W_g(u_g du_g + C_v dT_g + d(\frac{p}{\rho_g})) + W_s(u_s du_s + C_s dT_s + \frac{dp}{\rho_p}) = 0 \qquad (3)$$

Then, by differentiating (1) and (2) $du_s = kdu_g$, $dT_s = jdT_g$, putting $x = W_s/W_g$, and $C_s/C_v = \beta$, and since $C_p/C_v = \gamma$, $C_p - C_v = R$ then $C_v = R/\gamma - 1$ and $p = \rho_g RTg$

$$(1 + xk^2)u_g du_g + (\frac{1 + xj\beta}{\gamma - 1})\, d(\frac{p}{\rho_g}) + d(\frac{p}{\rho_g}) + x\frac{dp}{\rho_p} = 0 \qquad (4)$$

Consider unit mass of gas with mass m of solids in elemental pipe length, $\delta\ell$,

$$\text{mass of gas } 1 = W_g\frac{\delta\ell}{u_g}, \text{ mass of solids } m = W_s\frac{\delta\ell}{u_s}$$

then $\frac{m}{l} = \frac{W_s}{W_g} \cdot \frac{u_g}{u_s} = \frac{x}{k}$ (5)

Let $y = \frac{V_s}{V_g} = \frac{m}{\rho_p} \cdot \rho_g = \frac{\rho_g}{\rho_p} \cdot \frac{x}{k}$ (6)

ρ_p is the actual particle density.

Substituting for x/ρ_p in (4)

$$(1 + xk^2)u_g du_g + \left(\frac{1 + xj\beta}{\gamma - 1} + 1 \right) d\left(\frac{p}{\rho_g}\right) + \frac{kydp}{\rho_g} = 0 \qquad (7)$$

The one-dimensional momentum equation for frictionless flow may be written as:

$$\rho_g u_g \frac{A}{1 + y} \cdot du_g + \rho_p u_s y \frac{A}{1 + y} \cdot du_s + A\, dp = 0 \qquad (8)$$

where the solids are considered as an incompressible flow of volume y relative to the gas, i.e. total volume = 1 + y, gas flow area = A/(1 + y) and solids flow area = Ay/(1 + y).

Then by substituting from (1) and (6) in (8)

$$u_g\, du_g = - \frac{(1 + y)\, dp}{(1 + xk)\rho_g}$$

Substituting this in (7)

$$\left(\frac{1 + xj\beta}{\gamma - 1} + 1\right) d\left(\frac{p}{\rho_g}\right) - \left(\frac{(1 + y)(1 + xk^2)}{(1 + xk)} - ky\right) \frac{dp}{\rho_g} = 0 \qquad (9)$$

or $\frac{\rho_g dp - p d\rho_g}{\rho_g^2} \left(\frac{1 + xj\beta}{\gamma - 1} + 1 \right) - \left(\frac{(1 + y)(1 + xk^2)}{1 + xk} - ky \right) \frac{dp}{\rho_g} = 0$

then $\left(1 + \frac{1 + xj\beta}{\gamma - 1} - \frac{(1 + y)(1 + xk^2)}{(1 + xk)} + ky\right)\frac{dp}{p} - \left(1 + \frac{1 + xj\beta}{\gamma - 1}\right)\frac{d\rho_g}{\rho_g} = 0$

therefore $\frac{p}{\rho_g^{\,n}}$ = a constant (10)

$$\text{where } N = \frac{1 + \frac{1 + xj\beta}{\gamma - 1}}{1 + \frac{1 + xj\beta}{\gamma - 1} - \frac{(1 + y)(1 + xk^2)}{(1 + xk)} + ky} \qquad (11)$$

For Equilibrium Flow $k = j = 1$ then $n = \frac{\gamma + x\beta}{1 + x\beta}$ (12)

<u>Note</u>. Because y is a variable, the index n is normally only constant in flows where the solids volume is small in comparison to the gas volume. For the case of k = 1 however, the value of n remains constant when solids volume is included.

(ii) <u>Velocity of Sound for Gas-Solids Mixtures.</u>

Let there be introduced a discontinuity in gas pressure and velocity propagating at velocity u_g. In a short interval the solids particles may be assumed to attain a new equilibrium condition such that:-

$$u_s + \delta u_s = k(u_g + \delta u_g), \text{ or } \delta u_s = k\delta u_g$$

$$T_s - Tg_o + \delta T_s = j(Tg - Tg_o) + j\delta T_g \text{ or } \delta T_s = j\delta T_g$$

Consider the particles to form an incompressible flow superimposed on the compressible gas flow

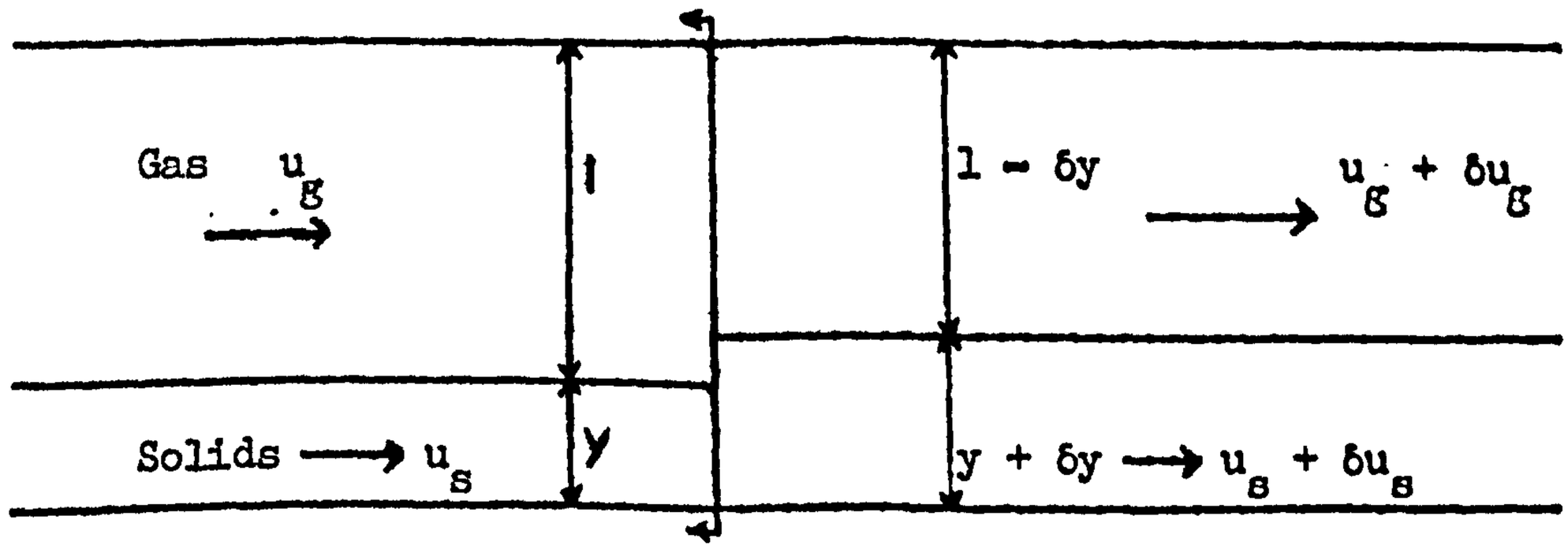

Solids Continuity.

$$u_s \rho_p y = (u_s + \delta u_s)\rho_p(y + \delta y)$$

or $0 = y\delta u_s + u_s \delta y$ neglecting higher order terms

therefore $\delta y = -y \dfrac{\delta u_s}{u_s}$ (13)

Gas Continuity.

$$u_g \rho_g = (u_g + \delta u_g)(\rho_g + \delta \rho_g)(1 - \delta y)$$

but from (13) $1 - \delta y = 1 + y \dfrac{\delta u_s}{u_s}$ and since $\delta u_s = k\delta u_g$

$$0 = u_g \delta \rho_g + \rho_g \delta u_g + \rho_g u_g \, y \frac{\delta u_g}{u_g}$$

or $0 = u_g \delta \rho_g + \rho_g (1 + y)\delta u_g$ (14)

Momentum Equation

$$- \delta p(1 + y) = \rho_g u_g \delta u_g + \rho_p u_s y \delta u_s$$

using (6) $\rho_p = \dfrac{\rho_g}{y} \cdot \dfrac{x}{k}$ and (14) $\rho_g \delta u_g = - \dfrac{u_g \delta \rho_g}{1 + y}$

then $\delta p(1 + y) = \dfrac{u_g^2 \delta \rho_g}{1 + y} \left(1 + \dfrac{xk^2}{k} \right)$

therefore $a_m^2 = u_g^2 = \dfrac{(1 + y)^2}{(1 + xk)} \cdot \dfrac{\delta p}{\delta \rho_g}$ (15)

i.e. the velocity of propagation of a small discontinuity, or the "velocity of sound", is given by equation (15). c.f. the velocity of sound in pure gas $a_g = \sqrt{\dfrac{\delta p}{\delta \rho_g}}$

From (10) $\dfrac{\delta p}{\delta \rho_g} = N \dfrac{p}{\rho_g}$ or $N R T_g$

then $a_m = (1 + y)\sqrt{\frac{N\ R\ Tg}{(1 + xk)}}$ (16)

When $V_g \gg V_s$, $y \longrightarrow 0$ and $a_m = \sqrt{\frac{n\ R\ Tg}{(1 + xk)}}$ (17)

For Equilibrium Flow $a_e = \sqrt{\frac{n\ R\ Tg}{1 + x}}$, (18)

and n is given by equation (12)

(iii) <u>Equations Relating Flow Variables to Stagnation Conditions.</u>

By substituting $p = \rho_g RT_g$ in the Energy equation (7) and integrating

$$(1 + xk^2)\frac{u_g^2}{2} + (1 + \frac{1 + xj\beta}{\gamma - 1})\ RTg + \frac{kyp}{\rho_g} = \text{a constant} \quad (19)$$

Let $p \longrightarrow p_o$, $T_g \longrightarrow Tg_o$ and assume k and j remain constant as u_g and $u_s \longrightarrow 0$, also let n represent the compressible flow index for $y \longrightarrow 0$ - and N for $y \neq 0$

$$\text{then } n = \frac{(\gamma + xj\beta)(1 + xk)}{(\gamma + xj\beta)(1 + xk) - (\gamma - 1)(1 + xk^2)}$$

$$n - 1 = \frac{(\gamma - 1)(1 + xk^2)}{(1 + xk)(\gamma + xj\beta) - (\gamma - 1)(1 + xk^2)}$$

$$\text{and } \frac{n}{n - 1} = \frac{(\gamma + xj\beta)(1 + xk)}{(\gamma - 1)(1 + xk^2)} \quad (20)$$

$$\text{and } N = \frac{\gamma + xj\beta}{(\gamma + xj\beta) - (\gamma - 1)(1 + y)(\frac{1 + xk^2}{1 + xk}) + ky(\gamma - 1)} \quad (21)$$

The energy equation then becomes:-

$$(1 + xk^2)\frac{u_g^2}{2} + \left(\frac{1 + xk^2}{1 + xk} \cdot \frac{n}{n - 1} + ky\right)RT_g = \left(\frac{1 + xk^2}{1 + xk} \cdot \frac{n}{n - 1} + ky_o\right)RT_{g_o} \tag{22}$$

from (16) $a_m^2 = (1 + y)^2 N.RT_g/(1 + xk)$ then

$$\frac{(1 + xk^2)u_g^2(1 + y)^2 N}{2(1 + xk)a_m^2} + \frac{(1 + xk^2)}{(1 + xk)} \cdot \frac{n}{n - 1} + ky = \left(\frac{1 + xk^2}{1 + xk} \cdot \frac{n}{n - 1} + ky_o\right) \times \frac{T_{g_o}}{T_g}$$

therefore $(1 + y)^2 \frac{N M_m^2}{2} = \left(\frac{T_{g_o}}{T_g} - 1\right)\frac{n}{n - 1} + \frac{1 + xk}{1 + xk^2} \cdot k\left(\frac{y_o T_{g_o}}{T_g} - y\right)$

or $(1 + y)^2 \cdot \frac{NM_m^2}{2} = \left(\frac{T_{g_o}}{T_g} - 1\right)\left(\frac{n}{n - 1} + \frac{1 + xk}{1 + xk^2} \cdot k\left(\frac{y_o T_{g_o} - yT_g}{T_{g_o} - T_g}\right)\right)$ (23)

For $V_g \gg V_s$, y and $y_o \longrightarrow 0$ and $N = n$

then $\frac{nM_m^2}{2} = \left(\frac{T_{g_o}}{T_g} - 1\right)\frac{n}{n - 1}$

or $\frac{T_{g_o}}{T_g} = 1 + \frac{(n - 1)}{2} M_m^2$ (24)

and from (10)

$$\frac{p_o}{p} = \left(1 + \frac{(n - 1)}{2} M_m^2\right)^{\frac{n}{n-1}} \tag{25}$$

$$\frac{\rho_{go}}{\rho_g} = \left(1 + \frac{n-1}{2} M_m^2\right)^{\frac{1}{n-1}} \qquad (26)$$

where $M_m = u_g/a_m$ = Mixture Mach Number (27)

It is apparent, therefore, that for flows where the solids to gas volume ratio is small, the above equations are identical with the isentropic flow equations of pure gas flow with similar values of n. Though the velocity of sound equation and hence Mach number are not the same as those for gas flows.

(iv) Combined Flow Equation.

The one-dimensional momentum equation including friction is:

$$\tau_o s + \rho_g u_g \frac{A}{1+y} du_g + \rho_p u_s y \frac{A}{1+y} du_s + A dp = 0 \qquad (28)$$

where $\tau_o s$ is the friction term including solids particle to particle and particle to wall interaction. Then by substituting from (1) and (6) and dividing by $A\rho_g u_g^2(1 + xk)/(1 + y)$

$$\frac{\tau_o s(1+y)}{A\rho_g u_g^2(1+xk)} + \frac{du_g}{u_g} + \frac{dp(1+y)}{\rho_g u_g^2(1+xk)} = 0$$

and by substituting from equation (16) $(1 + xk)\rho_g = (1 + y)^2 Np/a_m^2$ then

$$\frac{\tau_o s}{(1+y)NpM_m^2 A} + \frac{du_g}{u_g} + \frac{dp}{(1+y)NpM_m^2} = 0$$

$$\text{or } \frac{dp}{p} = -N(1 + y)M_m^{\,2}\frac{du_g}{u_g} - \frac{\tau_o{}^s}{A_{\bullet}p} \qquad (29)$$

The gas equation of state may be written as $\frac{dp}{p} = \frac{d\rho_g}{\rho_g} + \frac{dT_g}{T_g}$ (30)

The energy equation (7) may be written as

$$(1 + xk^2)u_g\, du_g + \left(\frac{\gamma + xj\beta}{\gamma - 1}\right)RdT_g + \frac{kxdp}{\rho_g} = 0$$

then dividing throughout by $RT_g(1 + xk^2)/(1 + xk)$ and substituting from (20) and (21) for n/(n-1) and N and from (16) for $RT_g/(1 + xk)$

$$(1 + y)^2 NM_m^{\,2}\frac{du_g}{u_g} + \frac{n}{n - 1}\,\frac{dT_g}{T_g} + \frac{1 + xk}{1 + xk^2}\cdot ky\cdot\frac{dp}{p} = 0$$

$$\text{or } \frac{dT_g}{T_g} = -\frac{n - 1}{n}(1 + y)^2\, NM_m^{\,2}\frac{du_g}{u_g} - \frac{n - 1}{n}\cdot\frac{1 + xk}{1 + xk^2}\cdot ky\cdot\frac{dp}{p} \qquad (31)$$

Solids Continuity with Varying Area.

$$u_s\rho_p\,\frac{y}{1 + y}A = (u_s + \delta u_s)\rho_p\left(\frac{y + \delta y}{1 + y}\right)(A + \delta A)$$

neglecting terms above the first order and dividing by $u_s yA$

$$0 = \frac{\delta u_s}{u_s} + \frac{\delta y}{y} + \frac{\delta A}{A}$$

$$\text{or } \delta y = \left(-\frac{\delta u_g}{u_g} - \frac{\delta A}{A}\right)y \qquad (32)$$

Gas Continuity with Varying Area

$$u_g\rho_g\,\frac{A}{1 + y} = (u_g + \delta u_g)(\rho_g + \delta\rho_g)(A + \delta A)\left(\frac{1 - \delta y}{1 + y}\right)$$

but from (32) $1 - \delta y = 1 + y \frac{\delta u_g}{u_g} + y \frac{\delta A}{A}$

therefore $0 = \frac{\delta \rho_g}{\rho_g} + \frac{\delta u_g}{u_g} + \frac{\delta A}{A} + y \frac{\delta u_g}{u_g} + y \frac{\delta A}{A}$

or $\frac{\delta \rho_g}{\rho_g} = - (1 + y) \frac{\delta u_g}{u_g} - (1 + y) \frac{\delta A}{A}$.

and in the limit $\frac{d\rho_g}{\rho_g} = - (1 + y) \frac{du_g}{u_g} - (1 + y) \frac{dA}{A}$ (33)

From equations (30) and (33)

$$\frac{dp}{p} = \frac{dT_g}{T_g} - (1 + y) \frac{du_g}{u_g} - (1 + y) \frac{dA}{A}$$

then substituting from (31) into this equation

$$\frac{dp}{p} = \left(\frac{n - 1}{n}\right)(1 + y)^2 NM_m^2 \frac{du_g}{u_g} - \frac{n - 1}{n} \cdot \frac{1 + xk}{1 + xk^2} \cdot ky \frac{dp}{p} - (1 + y)$$

$$\times \frac{du_g}{u_g} - (1 + y) \frac{dA}{A}$$

Substituting for dp/p from (29)

$$\left(1 + \frac{n - 1}{n} \cdot \frac{1 + xk}{1 + xk^2} \cdot ky\right)\left(-(1 + y)NM_m^2 \cdot \frac{du_g}{u_g} - \frac{\tau_o s}{Ap}\right) =$$

$$- \frac{n - 1}{n} (1 + y)^2 \cdot NM_m^2 \frac{du_g}{u_g} - (1 + y) \frac{du_g}{u_g} - (1 + y) \frac{dA}{A}$$

or

$$\left(-(1 + y)NM_m^2 - (1 + y)\frac{n - 1}{n} \cdot \frac{1 + xk}{1 + xk^2} \cdot ky \cdot NM_m^2 + (1 + y)^2\right.$$

$$\left. \times \frac{n - 1}{n} \cdot NM_m^2 + (1 + y)\right)\frac{du_g}{u_g} =$$

$$= -(1+y)\frac{dA}{A} + \left(1 + \frac{n-1}{n}.\frac{1+xk}{1+xk^2}.ky.\right)\frac{\tau_o{}^s}{A.p}$$

this simplifies to

$$\left(1 + \frac{NM_m{}^2}{n}\left(\frac{y(n-1)(1-k)}{1+xk^2} - 1\right)\right)\frac{du_g}{u_g} = -\frac{dA}{A} + \left(1 + \frac{n-1}{n}.\frac{1+xk}{1+xk^2}.ky\right)$$

$$\times \frac{\tau_o{}^s}{(1+y)A.p}$$

From the expressions for N and $\frac{n}{n-1}$ in equations (20) and (21) by substituting from (20) into (21)

$$N = \frac{1}{1 - (1+y).\frac{n-1}{n} + ky.\frac{n-1}{n}.\frac{1+xk}{1+xk^2}} \qquad (34)$$

$$\text{therefore } \frac{N}{n} = \frac{1}{n + \frac{(n-1)}{(1+xk^2)}(-1 - xk^2 - y - yxk^2 + ky + yxk^2)}$$

$$= \frac{1}{n - (n-1)\left(\frac{y(1-k)}{1+xk^2} + 1\right)} \qquad = \frac{1}{1 - \frac{(n-1)y(1-k)}{1+xk^2}}$$

also from (34) $1 + \frac{n-1}{n}.\frac{1+xk}{1+xk^2}.ky = \frac{1}{N} + (1+y)\frac{n-1}{n}$

Then substituting this expression and the expression for N/n into the combined flow equation

$$(1 - M_m{}^2)\frac{du_g}{u_g} + \frac{dA}{A} = \left(\frac{1}{N} + (1+y)\frac{n-1}{n}\right)\frac{\tau_o{}^s}{(1+y)A.p} \qquad (35)$$

Then it is apparent that, as for gas flows, when friction is neglected the critical condition of $M_m = 1$ is attained at a throat.

For $V_g \gg V_s$, $y \longrightarrow 0$ and $N = n$ then:-

$$(1 - M_m^2)\frac{du_g}{u_g} + \frac{dA}{A} = \frac{\tau_o s}{Ap} \qquad (36)$$

and this is similar to the expression for pure gas flow.

For an expansion process n is normally > 1 and $k < 1$ then $N > n$ and the friction term coefficient in equation (35) is less than unity. Physically this reduction in the friction term in equation (35) is due to the gas flow taking place in what is in effect a duct of variable area, as a result of the presence of the incompressible solids; i.e. for a subsonic flow the effect of the friction term is to accelerate the flow, but this leads to an effective increase in gas flow area, which has an opposite (decelerating) effect.

(v) <u>Frictionless Flow Area Ratio.</u>

The overall continuity equation may be written as:

$$\rho_g u_g \frac{A}{1+y} + \rho_p u_s y \frac{A}{1+y} = \rho_g^* u_g^* \frac{A^*}{1+y^*} + \rho_p u_s^* y^* \frac{A^*}{1+y^*}$$

or by substituting from (1) and (6)

$$\rho_g u_g \frac{A}{1+y} + x \rho_g u_g \frac{A}{1+y} = \rho_g^* u_g^* \frac{A^*}{1+y^*} + x \rho_G^* u_G^* \frac{A^*}{1+y^*}$$

where * indicates conditions at a throat. This simplifies to:-

$$\frac{A}{A^*} = \frac{\rho_g^*}{\rho_g} \cdot \frac{u_g^*}{u_g} \cdot \frac{(1+y)}{(1+y^*)} \qquad (37)$$

Writing the energy equation (22) as

$$(1+xk^2)\frac{u_g^2}{2} + \left(\frac{1+xk^2}{1+xk} \cdot \frac{n}{n-1} + ky\right)RT_g = (1+xk^2)\frac{u_g^{*2}}{2} +$$

$$\left(\frac{1+xk^2}{1+xk} \cdot \frac{n}{n-1} + ky^*\right) RT_g^*$$

then by substituting for RT_g from (16)

$$(1+xk^2)\frac{u_g^2}{2} + \left(\frac{1+xk^2}{1+xk} \cdot \frac{n}{n-1} + ky\right)\frac{(1+xk)a_m^2}{(1+y)^2 N} = (1+xk^2)\frac{u_g^{*2}}{2} +$$

$$\left(\frac{1+xk^2}{1+xk} \cdot \frac{n}{n-1} + ky^*\right)\frac{(1+xk)a_m^{*2}}{(1+y^*)^2 N^*}$$

$$\text{or } 1 + \left(\frac{n}{n-1} + \frac{1+xk}{1+xk^2} \cdot ky\right)\frac{2}{(1+y)^2 N M_m^2} = \frac{a_m^{*2}}{u_g^2}\left(1 + \left(\frac{n}{n-1} + \frac{1+xk}{1+xk^2} \cdot ky^*\right)\right.$$

$$\left. \times \frac{2}{(1+y^*)^2 N^*}\right) \qquad (38)$$

From equation (26)

$$\frac{\rho_g^*}{\rho_g} = \frac{\rho_{go}}{\rho_g} \cdot \frac{\rho_g^*}{\rho_{go}} = \left(\frac{Tg_o}{T_g} \cdot \frac{T_g^*}{Tg_o}\right)^{\frac{1}{N-1}} = \left(\frac{T_g^*}{T_g}\right)^{\frac{1}{N-1}} \qquad (39)$$

then substituting in (37) for a_m^*/u_g and ρ_g^*/ρ_g from (38) and (39) and putting $\frac{n}{n-1} + \frac{1+xk}{1+xk^2}.ky = \frac{n}{(n-1)N} + (1+y)$ from (34) then

$$\left(\frac{A}{A^*}\right)^2 = \left(\frac{T_g^*}{T_g}\right)^{\frac{2}{N-1}} \cdot \frac{(1+y)^2 + \left(\frac{n}{(n-1)N} + (1+y)\right)\frac{2}{NM_m^2}}{(1+y^*)^2 + \left(\frac{n}{(n-1)N^*} + (1+y^*)\right)\frac{2}{N^*}} \qquad (40)$$

For $V_g \gg V_s$, y and $y^* \to 0$ and $N = N^* = n$ then from (26) + (39)

$$\left(\frac{A}{A^*}\right)^2 = \left(\frac{T_g^*}{T_g}\right)^{\frac{2}{n-1}} \cdot \left(\frac{1 + 2/(n-1)M_m^2}{1 + 2/(n-1)}\right)$$

$$= \left(\frac{T_g^*}{T_g}\right)^{\frac{2}{n-1}} \left(\frac{1 + \frac{1}{2}(n-1)M_m^2}{1 + \frac{1}{2}(n-1)} \cdot \frac{n-1}{(n-1)M_m^2}\right)$$

substituting from (24)

$$\left(\frac{A}{A^*}\right)^2 = \left(\frac{T_g^*}{T_g}\right)^{\frac{n+1}{n-1}} \cdot \frac{1}{M_m^2} \qquad (41)$$

and this is similar to the expression for pure gas flow.

(vi) <u>Ultimate Velocity Ratio.</u>

Writing the energy equation (22) as

$$(1 + xk^2)\frac{u_g^2}{2} + \left(\frac{1+xk^2}{1+xk}.\frac{n}{n-1} + ky\right)RT_g = \left(\frac{1+xk^2}{1+xk}.\frac{n}{n-1} + ky_o\right)$$

$$\times RTg_o = (1 + xk^2)\frac{c^2}{2}$$

where c = the ultimate velocity i.e. when $T_g = 0$, then dividing by $\frac{1 + xk^2}{1 + xk}$ and substituting $\frac{n}{n - 1} + \frac{1 + xk}{1 + xk^2}.ky = \frac{n}{N(n - 1)} + (1+y)$ from (34)

$$\frac{c^2}{2} = \left(\frac{n}{N_o(n - 1)} + (1 + y)\right) \frac{RTg_o}{(1 + xk)}$$

$$\text{then } \left(\frac{u_g}{c}\right)^2 = \frac{M_m^2 a_m^2}{c^2} = \frac{M_m^2(1 + y)^2 NR\, T_g\, (1 + xk)}{(1 + xk)\, 2RTg_o\left(\frac{n}{N_o(n - 1)} + (1 + y)\right)}$$

$$= \frac{M_m^2 N(1 + y)^2}{2\left(\frac{n}{N_o(n - 1)} + (1 + y)\right)} \cdot \frac{T_g}{Tg_o} \qquad (42)$$

For y and $y_o \longrightarrow 0$ $N = N_o = n$ then

$$\left(\frac{u_g}{c}\right)^2 = \frac{M_m^2}{2}(n - 1).\frac{T_g}{Tg_o} \qquad (43)$$

i.e. similar to the expression for pure gas flow.

(vii) <u>Gas-Solids Flow in a Constant Area Duct with Friction.</u>

As for pure gas flow, it is possible to express the velocity, density and pressure ratios in terms of the temperature ratio derived for overall adiabatic flow. Expressions will be derived for the case V_s not negligible whenever this is possible.

Temperature Ratio for $V_g \gg V_s$

from (24) $\frac{Tg_o}{T_g} = 1 + \frac{n - 1}{2} M_m^2$, then $\frac{Tg_o}{T_g^*} = \frac{n + 1}{2}$

and $$\frac{T_g}{T_g^*} = \frac{n + 1}{2 + (n - 1)M_m^2} \tag{44}$$

Velocity Ratio

From (16) and (27) $u_g = a_m M_m = M_m(1 + y)\sqrt{\frac{NRT_g}{1 + xk}}$

then $$\frac{u_g}{u_g^*} = M_m \cdot \frac{1 + y}{1 + y^*}\sqrt{\frac{NT_g}{N^*T_g^*}} \tag{45}$$

and for $V_g \gg V_s$, $$\frac{u_g}{u_g^*} = M_m\sqrt{\frac{n + 1}{2 + (n - 1)M_m^2}} \tag{46}$$

Density Ratio

from (37) for a constant area duct and from (45)

$$\frac{\rho_g}{\rho_g^*} = \frac{1 + y}{1 + y^*} \cdot \frac{u_g^*}{u_g} = \frac{1}{M_m}\sqrt{\frac{N^*T_g^*}{NT_g}} \tag{47}$$

and for $V_g \gg V_s$, $$\frac{\rho_g}{\rho_g^*} = \sqrt{\frac{2 + (n - 1)M_m^2}{(n + 1)M_m^2}} \tag{48}$$

Static Pressure Ratio

From the gas equation of state $\frac{p}{p^*} = \frac{\rho_g}{\rho_g^*} \cdot \frac{T_g}{T_g^*}$

and substituting (47) $$\frac{p}{p^*} = \frac{1}{M_m} \cdot \sqrt{\frac{N^*T_g}{NT_g^*}} \tag{49}$$

then for $V_g \gg V_s$, $$\frac{p}{p^*} = \frac{1}{M_m}\sqrt{\frac{n + 1}{2 + (n - 1)M_m^2}} \tag{50}$$

Stagnation Pressure Ratio for $V_g \gg V_s$

From (10) $\frac{p_o}{p} = \left(\frac{Tg_o}{T_g}\right)^{\frac{n}{n-1}}$ and $\frac{p_o^*}{p^*} = \left(\frac{Tg_o}{T_g^*}\right)^{\frac{n}{n-1}}$ as Tg_o is constant

then $\frac{p_o}{p_o^*} = \frac{p}{p^*} \cdot \left(\frac{T_g^*}{T_g}\right)^{\frac{n}{n-1}}$

substituting for p/p^* from (49) $\frac{p_o}{p_o^*} = \frac{1}{M_m} \cdot \sqrt{\frac{N^*}{N}} \cdot \left(\frac{T_g^*}{T_g}\right)^{\frac{n+1}{2(n-1)}}$ (51)

and for $V_g \gg V_s$ $\frac{p_o}{p_o^*} = \frac{1}{M_m} \left(\frac{2 + (n-1)M_m^2}{(n+1)}\right)^{\frac{n+1}{2(n-1)}}$ (52)

Length of Duct - Friction Factor Equation

Writing the momentum equation (29) for the case $V_g \gg V_s$

$$\frac{dp}{p} + nM_m^2 \frac{du_g}{u_g} + \frac{\tau_o . s}{A . p} = 0$$

If the shear stress is expressed in terms of a friction factor

i.e. $\tau_o s = C_f . \frac{1}{2}\rho_g u_g^2 . \pi D . \delta \ell$

and from (17) $p = \frac{(1 + xk)a_m^2 \rho_g}{n}$

substituting these in the above equation for the case $A = \frac{\pi}{4}D^2$ and dividing by nM_m^2

$$\frac{1}{nM_m^2}\frac{dp}{p} + \frac{du_g}{u_g} = -\frac{4C_f}{2D} \cdot \frac{\delta \ell}{(1 + xk)}$$

differentiating equations (50) and (46) gives

$$\frac{1}{nM_m^2}\frac{dp}{p} = \frac{d}{dM_m}\left(\frac{1}{2nM_m^2} + \frac{n-1}{4n}\log\left(\frac{1+\frac{n-1}{2}M_m^2}{M_m^2}\right)\right) dM_m$$

$$\text{and } \frac{du_g}{u_g} = \frac{d}{dM_m}\left(-\tfrac{1}{2}\log\left(\frac{1+\frac{n-1}{2}M_m^2}{M_m^2}\right)\right) dM_m$$

Then substituting these in the above and integrating from conditions at M_m, ℓ to critical sonic conditions $M_m = 1$ at $\ell = \ell^*$

$$\left(\frac{1}{2nM_m^2} + \frac{n-1}{4n}\log\left(\frac{1+\frac{n-1}{2}M_m^2}{M_m^2}\right) - \tfrac{1}{2}\log\left(\frac{1+\frac{n-1}{2}M_m^2}{M_m^2}\right)\right)_{M_m}^{1} =$$

$$-\frac{4C_f}{2D}\cdot\frac{(\ell^* - \ell)}{(1+xk)}$$

reversing limits

$$-\left(\frac{1}{nM_m^2} + \frac{n+1}{2n}\log\left(\frac{M_m^2}{1+\frac{n-1}{2}M_m^2}\right)\right)_{1}^{M_m} = -\frac{4C_f}{D}\frac{(\ell^* - \ell)}{(1+xk)}$$

$$\text{or } \frac{4C_f}{D}\frac{(\ell^* - \ell)}{(1+xk)} = \frac{1}{n}\cdot\frac{1-M_m^2}{M_m^2} + \frac{n+1}{2n}\log\left(\frac{\frac{n+1}{2}M_m^2}{1+\frac{n-1}{2}M_m^2}\right) \qquad (53)$$

Apart from the term $(1 + xk)$ on the left hand side of the equation, this expression is similar to that for pure gas flow. The expressions (44), (46), (48), (50) and (52) are all similar to those for pure gas flow.

(viii) Normal Shock Relations.

If it is assumed that constant fractional lag of velocity

and temperature apply across the shock in a constant area duct and if suffices (1) and (2) refer to conditions on either side of the shock the equations of state, continuity, momentum and energy can be written, for the case $V_g \gg V_s$, as:

Equation of State $\dfrac{p_1}{\rho_{g1}\,T_{g1}} = \dfrac{p_2}{\rho_{g2}T_{g2}}$ (54)

Continuity $\rho_{g1}u_{g1} = \rho_{g2}u_{g2}$ and $\rho_{s1}u_{s1} = \rho_{s2}u_{s2}$ (55)

Momentum - for frictionless flow and with $y = 0$, (28) can be integrated, as $\rho_g u_g$ is constant, to give:-

$$(1 + xk)\rho_{g1}u_{g1}^{\,2} + p_1 = (1 + xk)\rho_{g2}u_{g2}^{\,2} + p_2 \qquad (56)$$

Energy - for $V_g \gg V_s$ equation (22) can be written as:-

$$(1 + xk^2)\frac{u_{g1}^{\,2}}{2} + \frac{1 + xk^2}{1 + xk} \cdot \frac{n}{n - 1} \cdot \frac{p_1}{\rho_{g1}} = (1 + xk^2)\frac{u_{g2}^{\,2}}{2} + \frac{1 + xk^2}{1 + xk} \cdot \frac{n}{n - 1} \cdot \frac{p_2}{\rho_{g2}} \qquad (57)$$

or $\dfrac{n}{(n - 1)(1 + xk)}\left(\dfrac{p_1}{\rho_{g1}} - \dfrac{p_2}{\rho_{g2}}\right) = \frac{1}{2}(u_{g2} - u_{g1})(u_{g2} + u_{g1})$

From (55) and (56) $(1 + xk)\rho_{g1}u_{g1}(u_{g2} - u_{g1}) = p_1 - p_2$

then $\dfrac{n}{n - 1}\left(\dfrac{p_1}{\rho_{g1}} - \dfrac{p_2}{\rho_{g2}}\right) = \frac{1}{2}(p_1 - p_2)\left(\dfrac{1}{\rho_{g2}} + \dfrac{1}{\rho_{g1}}\right)$ (58)

This equation is then similar to the Rangine-Hugoniot expression for pure gas flow and the pressure, Mach number, density, temperature and velocity ratios across the shock are derived as for gas flow (Reference Houghton and Brock).

Pressure Ratio Across Shock

$$\frac{p_2}{p_1} = \frac{2n}{n+1} M_{m1}^2 - \frac{n-1}{n+1} \tag{59}$$

Mach Number $$M_{m2}^2 = \frac{(n-1)M_{m1}^2 + 2}{2nM_{m1}^2 - (n-1)} \tag{60}$$

Density Ratio across Shock

$$\frac{\rho_{g2}}{\rho_{g1}} = \frac{(n+1)M_{m1}^2}{2 + (n-1)M_{m1}^2} \tag{61}$$

Temperature Ratio across Shock

$$\frac{T_{g2}}{T_{g1}} = \left(\frac{2nM_{m1}^2 - (n-1)}{n+1}\right)\left(\frac{2 + (n-1)M_{m1}^2}{(n+1)M_{m1}^2}\right) \tag{62}$$

Velocity Ratio across Shock

$$\frac{u_{g2}}{u_{g1}} = \frac{2 + (n-1)M_{m1}^2}{(n+1)M_{m1}^2} \tag{63}$$

(ix) <u>Prandtl-Meyer Expansion</u>.

If there is constant fractional lag between the gas and

the solids as a Mach Wave propagates through the mixture the angle of this Mach Wave to the direction of flow (μ) should be given by an expression similar to that for gas dynamics, i.e. $\mu = \sin^{-1} 1/M_m$. Then it follows that the change in direction of the flow will also be given by a similar expression

$$dv = \frac{du_g \cos \mu}{u_g \sin \mu} = (M_m^{\ 2} - 1)^{\frac{1}{2}} \frac{du_g}{u_g} \qquad (64)$$

where u_g is the velocity of the gas before the Mach Wave.

Substituting from (17) into the Energy Equation (22) for $V_g \gg V_s$:-

$$(1 + xk^2) \frac{u_g^{\ 2}}{2} + \frac{(1 + xk^2)}{(n - 1)} a_m^{\ 2} = \text{a constant}$$

then $(1 + xk^2) \frac{u_g^{\ 2}}{2} + \frac{(1 + xk^2)}{n - 1} a_m^{\ 2} = \frac{(1 + xk^2)}{n - 1} a_{mo}^{\ 2} = (1 + xk^2)\frac{c^2}{2}$

or $M_m^{\ 2} = \frac{2}{n - 1} \cdot \frac{u_c^{\ 2}}{1 - u_c^{\ 2}}$, where $u_c = \frac{u_g}{c}$

Substituting this into (64) and integrating gives:-

$$\int dv = \int \left(\frac{\frac{n+1}{n-1} \cdot u_c^{\ 2} - 1}{1 - u_c^{\ 2}} \right)^{\frac{1}{2}} \cdot \frac{du_c}{u_c}$$

This is similar to the expression for gas dynamics (Reference F. Cheers) so that the expression for the Prandtl-Meyer angle (i.e. the angle through which a stream, initially sonic, is turned to attain Mach number M) is also similar.

$$v = \left(\frac{n+1}{n-1}\right)^{\frac{1}{2}} \tan^{-1}\left(\frac{(n-1)(M_m^{\,2}-1)}{n+1}\right)^{\frac{1}{2}} - \tan^{-1}(M_m^{\,2}-1)^{\frac{1}{2}} \qquad (65)$$

The absolute change in angle of the Mach Waves between the beginning and end of expansion is similarly given by:-

$$\theta = \left(\frac{n+1}{n-1}\right)^{\frac{1}{2}} \tan^{-1}\left(\frac{(n-1)(M_m^{\,2}-1)}{n+1}\right)^{\frac{1}{2}} \qquad (66)$$

APPENDIX 2.

Aerodynamic Mean Effective Diameter.

Assuming a powder conforms to the normal distribution for particle size with standard deviation σ

then $y = \frac{1}{\sqrt{2\pi}} \cdot e^{-\frac{t^2}{2}}$ where $t = \frac{d - d_m}{\sigma}$

the mean diameter dm being the arithmetic mean of the diameter of all the particles. Then that fraction of the whole which has a particle diameter corresponding to any particular value of t is y dt. Assuming that the aerodynamic drag on a particle is proportional to d^2 (which implies that all the particles are moving at the same velocity and have the same drag coefficient) then the drag on a fraction of the particles

$$\alpha \frac{1}{\sqrt{2\pi}} \cdot e^{-\frac{t^2}{2}} \, dt.d^2$$

$$\text{or} \quad \alpha \frac{(\sigma t + d_m)^2}{\sqrt{2\pi}} \cdot e^{-\frac{t^2}{2}} \, dt$$

and the drag on all the particles $\alpha \frac{1}{\sqrt{2\pi}} \int_{-\infty}^{+\infty} (\sigma t + d_m)^2 . e^{-\frac{t^2}{2}} \, dt$

If all the particles are replaced by the same number of uniform rigid particles of aerodynamic mean effective

diameter d_{ma}, the total drag $\alpha\ d_{ma}^2$

Therefore $\sqrt{2\pi}\ d_{ma}^2 = \int_{-\infty}^{+\infty} (\sigma t + d_m)^2 e^{-\frac{t^2}{2}} dt$

$$= \sigma^2 \int_{-\infty}^{+\infty} t^2 e^{-\frac{t^2}{2}} + 2\sigma d_m \int_{-\infty}^{+\infty} t e^{-\frac{t^2}{2}} dt + d_m^2 \int_{-\infty}^{+\infty} e^{-\frac{t^2}{2}} dt$$

$$= \sigma^2 \left(\int_{-\infty}^{+\infty} e^{-\frac{t^2}{2}} dt - t.e^{-\frac{t^2}{2}} \right) - 2\sigma d_m . e^{-\frac{t^2}{2}}$$

$$+ d_m^2 \int_{-\infty}^{+\infty} e^{-\frac{t^2}{2}} dt$$

$$= ((\sigma^2 + d_m^2) \int e^{-\frac{t^2}{2}} dt - \sigma(\sigma t + 2d_m) e^{-\frac{t^2}{2}})_{-\infty}^{+\infty}$$

$$= (\sigma^2 + d_m^2) \sqrt{2\pi}$$

Therefore $d_{ma}^2 = \sigma^2 + d_m^2$

For $\sigma = 0$, so that all the particles are the same size then

$$d_{ma} = d_m$$

Explanation of the Integrations.

The area under the Normal Probability Curve is unity.

Therefore $\frac{1}{\sqrt{2\pi}} \int_{-\infty}^{+\infty} e^{-\frac{t^2}{2}} dt = 1$

Integration of $t.e^{-\frac{t^2}{2}}$

put $z = e^{-\frac{t^2}{2}}$ then $\log z = -\frac{t^2}{2}$

and $\frac{1}{z} = -t\frac{dt}{dz}$

therefore $\frac{dz}{dt} = -tz = -t\,e^{-\frac{t^2}{2}}$

therefore $\int t\,e^{-\frac{t^2}{2}}\,dt = -z = -e^{-\frac{t^2}{2}}$

Integration of $t^2.e^{-\frac{t^2}{2}}$

using substitution z as above $\frac{d}{dt}.\frac{dz}{dt} = -t\frac{dz}{dt} - z$

Therefore $\frac{d^2z}{dt^2} = -(z + t\frac{dz}{dt})$

$$= -(e^{-\frac{t^2}{2}} - t^2\,e^{-\frac{t^2}{2}})$$

$$= (t^2 - 1)\,e^{-\frac{t^2}{2}}$$

Therefore $\int (t^2 - 1)\,e^{-\frac{t^2}{2}}\,dt = \frac{dz}{dt} = -t\,e^{-\frac{t^2}{2}}$

or $\int t^2.e^{-\frac{t^2}{2}}\,dt = \int e^{-\frac{t^2}{2}}\,dt - t\,e^{-\frac{t^2}{2}}$

APPENDIX 3.

Cyclone Design.

The cyclone is essentially a settling chamber in which gravitational acceleration is replaced by centrifugal acceleration. The most efficient cyclones are usually those with small diameter, long bodies and fairly small outlet diameters. As the pressure in a cyclone is often less than atmospheric, it is also important that the solids collector at the base of the cyclone should be an air-tight fit.

Although normally much greater efficiency and the capture of smaller particle sizes is obtained by using a bank of small diameter cyclones, say 3 in. diameter, it was felt that for this project this might not be the case. The reason was that the solids particles will almost certainly be entering the cyclone at speeds greater than the air velocity, due to the high velocity of the solids at the rig pipe or duct exit and their relatively high inertia. This could then lead to the particles bouncing off the walls of the cyclone with the possible result that a large number of particles could be carried away in the air leaving the cyclone, if the cyclone were of very small diameter.

The cyclone proportions selected are those recommended in the Chemical Engineers Handbook - editor J.H. Perry, and the length of the cyclone was arrived at by taking into account the headroom available in the area where the cyclone was to be housed. The diameter was also checked to give an estimate of the smallest size of particle likely to be caught by the cyclone, and it was ensured that this size was very much less than any size likely to be used in this project.

Davis (1952-53) gives the following expression to predict the minimum size of particle to be captured:-

$$d\ min = 2\sqrt{\frac{9\ \mu\ R_2}{8\ (\rho_p - \rho_g) V_o \frac{H}{R_2}} \left(1 - \left(\frac{R_1}{R_2}\right)^4\right)}$$

where R_2 = cyclone body radius.

R_1 = cyclone exit radius.

H = length of cylindrical portion of cyclone.

V_o = entry velocity.

d min = minimum particle diameter.

Other terms are defined by the notation on page 242.

Fuchs (1964) gives the expression:

$$d\ min = 2.74\sqrt{\frac{\mu\ R_2}{\pi\ V_o\ \rho_p S}}$$

where S = number of revolutions made by a particle in the cyclone, and this is in the range 1-3.

Both the above expressions assume Stokes drag law and that the flow in the cyclone approximates to a free vortex.

Substituting the selected cyclone parameters into the above equations, i.e. R_1 = 2.5 in., R_2 = 5 in., H = 20 in. and assuming S = 3 for a tall cyclone, gives the following:-

Davis d min = 4.4×10^{-4} in. or 11.1 microns.

Fuchs d min = 3.8×10^{-4} in. or 9.7 microns.

The above size particles are well below any particle size likely to be used in this project.

APPENDIX 4.

Air Flow Measurement Nozzle Design.

The equation given in B.S. 1042 : 1943 for the calculation of the diameter of a nozzle installed in a pipe line, when the flow rate is known is:

$$C\ z\ m\ E = \frac{W_g}{359.1 \times D^2 \times \sqrt{h \times \rho_g}}$$

where m = the area ratio nozzle to pipe a/A.

d = nozzle throat diameter (in.)

D = pipe diameter (in.)

ρ_g = density of fluid at position of high pressure tapping (lb./cu.ft.)

$E = 1/\sqrt{1 - m^2}$ = velocity of approach factor.

W_g = fluid mass flow rate (lb/hr.)

z is a multiplier, the combination of 3 correction factors for Reynolds number, pipe size and fluid compressibility.

C is the discharge coefficient of the nozzle.

h = pressure drop across the nozzle (in water).

The lowest air flow rate to be used in the rig was estimated to be about 0.08 lb/sec. For this flow, it was assumed that sufficient accuracy would be obtained if this flow

rate gave a 0.4 in. of water pressure drop across the nozzle, as this is easily measureable on an inclined manometer.

In order to solve the above equation and obtain a value for the nozzle diameter d, it was first assumed that z = 1 and C = 0.96. With this assumption the above equation can be put in the form:

$$\frac{a^2 \times D^4}{A^2 - a^2} = \frac{W_g^{\,2}}{C^2 \times h \times \rho_g \times 359.1^2}$$

then by putting D = 3.606 in. (the diameter of the exhaust pipe)

and ρ_g = 0.076 lb/cu.ft.

the values d = 2.125 in., and m = 0.349 are obtained.

Using this value of m, the correction factors and discharge coefficient can now be determined accurately from the data sheets in B.S. 1042. From Data sheet 5 for m = 0.349, then C = 0.964. The correction factors for the Reynolds number associated with each flow rate and for the pipe diameter are also given by this Data sheet. The correction factor for compressibility effects is given by Data sheet 11.

The above equation then becomes:-

$$W_g = 359.1 \times 0.964 \times 1.066 \times 13 \times 0.349 \times z \times \sqrt{h \times \rho_g}$$

$$= 1675\ z\sqrt{h\ \rho_g}$$

and the values of z and ρ_g are obtained from the experimental measurements and Data Sheets 5 and 11.

The nozzle was machined in brass to the tolerances stated in Data sheet 1, and piezometer rings with the dimensions suggested in this data sheet were mounted in front of and behind the nozzle to give the static pressure readings.

APPENDIX 5.

Rectangular Duct Flow Rig Design.

The criterion in the design of the rectangular duct flow rig was that the nozzle in the rig should be capable of accelerating the flow to a mixture Mach number greater than unity, and that the subsequent flow should pass through a normal shock wave. Although the constant fractional lag theory has great limitations, its use greatly simplifies the calculations for the design of the nozzle profile of this rig. If also the constants k and j are made sufficiently small, which is almost certainly the case for rapidly accelerating flows, the resulting design would probably be capable of the above flow pattern. It will also be ensured that the nozzle will accelerate a pure air flow to at least Mach one.

In designing the duct to the constant fractional lag theory, the following assumptions are made:

(a) That the flow through the convergent-divergent nozzle is such as to achieve $M_m = 1$ at the nozzle throat, and that the subsequent flow to nozzle exit is supersonic. The supersonic condition is defined as that of a flow with a mixture Mach number greater than unity.

(b) That a normal shock wave occurs at a position close to nozzle exit.

(c) That the flow between the normal shock wave and duct exit is subsonic.

(d) That the flow at the duct exit is such as to give a mixture Mach number of unity.

(e) That the diffuser giving entry to the cyclone converts a proportion of the kinetic energy of the flow at the duct exit to pressure head. It can be readily shown that, assuming the constant fractional lag criteria, the following expression is obtained for the isentropic efficiency of a diffuser. This efficiency is defined as the ratio of kinetic energy which would have been transformed without losses to produce the observed pressure recovery, to that actually transformed.

$$\frac{p_e}{p_i} = \left(\frac{(n-1)Mm_i^2}{2} \cdot \eta + 1 \right)^{\frac{n}{n-1}}$$

where suffices i and e refer to diffuser inlet and exit conditions.

The pressure available just upstream of the nozzle

is expected to be of the order of 150 p.s.i., and if the pressure recovery through the normal shock wave and the diffuser approaches that given by the calculations, this would be ample to obtain a fairly high Mach number at nozzle exit. Due to the uncertainties in the design, however, the nozzle was designed to achieve a mixture Mach number at exit close to two, and this should leave ample pressure drop available if the actual pressure drop through the rig turns out to be greater than that allowed for in the design.

As stated previously, the method of designing the nozzle is identical with that of the Mach Wavelet Method for pure gas flow, but with a very much smaller specific heat ratio. This method is fully described in the book by F. Cheers. The basis of the method is to consider the wall of the divergent part of the nozzle as a finite number of straight sections such that for supersonic flow past it a fan of expansion waves stands at the intersection of each straight section. This fan of waves is then replaced by a single wave at an angle midway between the first and last waves of each fan. The flow field is then divided by the waves into a number of cells in each of which conditions are assumed to be uniform. A streamline from a centred fan was used to give the initial expansion, in terms of the first few straight sections of wall,

and this was drawn for two degree increments of the Prandtl-Meyer angle. The starting position on this fan is not very important as there is no need to work to a fixed scale, since on completion the whole nozzle can be scaled down to the desired size. In this case, the selected starting point was where the first up-going wave meets the wall. Then working back from this point and also inserting the waves from the wall corners, positions the centre-line of the nozzle. It is then just a case of proceeding with this process along the diffusing section to obtain the final wall shape. The constant fractional lag conditions for which the nozzle is designed are $n = 1.075$ and an exit Mach number of 2.1, and this gives an area ratio, exit to throat, of 2.39 to 1. The value of n was arrived at by considering a solids to air loading ratio of 3.36 to 1, with polystyrene powder of specific heat ratio $C_s/C_v = 1.87$, and with the fractional lags $k = 0.5$ and $j = 0.4$. These values were selected as being fair estimates of mean values of k and j over the flow conditions applying.

The flow was then considered to almost immediately pass through a normal shock wave, such that the relationship between Mach numbers on the upstream and downstream side of the shock is given by:

$$Mm_3^2 = \frac{(n-1)Mm_2^2 + 2}{2n\,Mm_2^2 - (n-1)}$$

where suffices 1, 2, 3, 4 and 5 and t refer to conditions at nozzle entry and exit, just downstream of the shock, at duct exit and diffuser exit and nozzle throat respectively.

The subsequent subsonic flow was then assumed to accelerate to Mm = 1 at the duct exit, with the length of duct necessary to achieve this flow given by:

$$\frac{4C_f\,(\ell^* - \ell)}{De\,(1 + xk)} = \frac{1}{n}\cdot\frac{1 - Mm_3^2}{Mm_3^2} + \frac{n+1}{2n}\log\left(\frac{\frac{n+1}{2}Mm_3^2}{1 + \frac{n-1}{2}Mm_3^2}\right)$$

where De is the equivalent diameter of the duct, which must be estimated at this stage, and $4C_f$ is a skin friction factor for gas-solids flow, which in this case was obtained from Uematsu's expression and using an estimated Reynold's number.

The pressure drops were then obtained from the following expressions:

(1) For flow through the nozzle, the relationship between static and stagnation pressure for frictionless flow is:-

$$\frac{p_1}{p_2} = \left(1 + \frac{n-1}{2} Mm_2^{\,2}\right)^{\frac{n}{n-1}}$$

where the gas-solids upstream of the nozzle were assumed to be at stagnation conditions.

(2) For flow through a normal shock wave

$$\frac{p_3}{p_2} = \frac{2n}{n+1} \cdot Mm_2^{\,2} - \frac{n-1}{n+1}$$

(3) For flow from downstream of the shock to the duct exit.

$$\frac{p_3}{p_4} = \frac{1}{Mm_3} \left(\frac{n+1}{2 + (n-1)\, Mm_3^{\,2}} \right)^{\frac{1}{2}}$$

(4) For flow through the exit diffuser

$$\frac{p_5}{p_4} = \left(\frac{n-1}{2} Mm_4^{\,2}\, \eta + 1 \right)^{\frac{n}{n-1}}$$

By putting $n=1.075$ in the above, assuming that the pressure at the exit of the diffuser is 15 p.s.i. and that the diffuser efficiency is 25%, a low figure being assumed because of the probably poor recovery of kinetic energy of the solids, then with $M_t = 1.0$, $M_2 = 2.1$, $M_3 = 0.5$ and $M_4 = 1.0$ the pressures are $p_1 = 9.1\, p_2$, $p_2 = p_3/4.53$, $p_3 = 2.028\, p_4$ and $p_4 = p_5/1.14$ and for $p_5 = 15$ p.s.i. $p_1 = 53.6$ p.s.i. With

$4C_f = 0.02$ the length of duct from nozzle exit to duct exit becomes 11 ft.

Assuming the stagnation pressure for conditions just upstream of the nozzle to be p_1, it is possible to obtain the area of the throat of the nozzle in terms of the gas mass flow rate from the following equation:-

$$A = \frac{W_g}{p_o}\sqrt{\frac{RTg_o}{n} \cdot \frac{\left(1 + \frac{n-1}{2} Mm^2\right)^{\frac{n+1}{n-1}}}{Mm^2} \cdot (1 + xk)}$$

This is obtained by substituting into the continuity equation from the mixture Mach number and velocity of sound equations and the static to stagnation pressure and temperature equations for frictionless flow.

Then for Mm = 1 at the throat and $p_o = p_1$

$$A = \frac{W_g}{p_1}\sqrt{\frac{RTg_o}{n} \cdot \left(\frac{1+n}{2}\right)^{\frac{n+1}{n-1}} \cdot (1 + xk)}$$

Using the above values of x, k, p_o and n, and putting $Tg_o = 293^oK$ gives $A = 1.45 \cdot W_g$ in^2.

Then since $W_g = 0.236$ lb/sec. represents an air flow rate

easily attainable in the duct flow rig the area of the nozzle throat was made 0.342 sq. in., resulting in a throat section of 0.4 x 0.855 in. and a duct section of 0.4 x 2.03 in. to give an aspect ratio of 5 to 1 in the duct.

A length of straight duct of 11 ft, after the nozzle, is considered large by supersonic puro gas flow standards, (it represents almost 200 diameters). Provision was therefore made so that lengths of duct after the nozzle of 5 or 11 ft. could be achieved. Because in the experiments to be performed on this rig the flow through normal shock waves is of major importance, the length of ducting after the nozzle is not critical.

Applying a similar procedure to the above to the flow of air in the rig indicates that for a length of duct from nozzle exit to duct exit less than about 3.9 ft., supersonic flow could be achieved with a return to subsonic flow through a normal shock wave at nozzle diffuser exit, and the subsequent return to M = 1 at the duct exit, for a minimum overall pressure ratio of 2.8. Because, however, the minimum length of duct referred to above has been made 5 ft. and the profile of the nozzle diffuser is not designed for air flow, this will probably mean that the shock wave will occur in the nozzle diffuser and the maximum Mach number will not be very much greater than unity.

At this stage, the internal dimensions of the duct and the nozzle profile have been calculated, and the design of the sections making up this rig are now considered. As shown previously, the minimum overall pressure drop possible for supersonic flow is about 3.6; but as the maximum available pressure is anticipated to be about 150 p.s.i., all the rig sections apart from the diffuser leading into the cyclone are designed to withstand this pressure. As explained in Section 4.2.1, three 6 ft. long sections were decided upon to comprise the total experimental section, two of these having transparent walls, so that the flow both upstream and downstream of the nozzle could be investigated, or if necessary, an 11 ft. length of transparent walled section could be placed downstream of the nozzle. The third section is metal walled and serves as an entry length.

In designing the upper and lower beams of the transparent walled sections, it was assumed that these could be treated as uniformly loaded pin-jointed members, as this gives the most pessimistic case. The transparent walls are considered as uniformly loaded plates with simple supports 2 in. apart. As explained in Section 6.5, although the initial design was based on the pressure only acting on the Tufnol spacer mounted

in the upper and lower beams due to the sealing problem, in the final design it was assumed that the pressure acted on the whole 1.7 in. width of these beams. With these assumptions, the following maximum stresses were arrived at for the duct being subjected to a test pressure of 300 p.s.i. (i.e. twice the maximum working pressure), the material of each component also being included.

Upper and lower beams	18,500 p.s.i.	Aluminium alloy HE 30 swp.
Transparent walls	2,500 p.s.i.	Polished Perspex.
Support struts	19,700 p.s.i.	Aluminium alloy HE 30 swp.
Dowel pins	28,000 p.s.i.	Silver steel.
Bolts retaining transparent walls	1000 lb/bolt at 2 in. pitch	H.T.S.

Most of the remaining parts of the rig are also constructed from the H.E. 30 s.w.p. material. The entry length has side walls $\frac{1}{4}$ in. thick with upper and lower sides 3/8 in. thick, whilst the small diffuser is made from 3/16 in. thick plate. Both these items are of welded construction.

APPENDIX 6.

Methods of Estimating Manometer Response Times.

In the book "Experimental Fluid Mechanics", Bradshaw suggests the following expression for the time constant of a system where the volume of the manometer is much greater than the volume of the connecting leads.

$$\tau = \left(\frac{A}{2\rho_e \cdot g} + \frac{V}{p_2} \right) \frac{128\mu l}{\pi d^4} \qquad (1)$$

where μ is the viscosity of gas in the connecting lead.

l and d are the length and diameter of connecting lead.

A and V are the cross-sectional area and the initial enclosed volume of fluid in the manometer.

ρ_e is the density of the manometric fluid.

p_2 is the initial pressure at the manometer.

This expression was obtained by equating the mass flow rate through the connecting lead to the rate of increase of mass of gas in the manometer.

For the case where the gas is flowing through a small bore tube into a reservoir of constant volume (V), the above expression becomes:-

$$\Upsilon = \frac{128\,\mu\, l}{\pi d^4} \cdot \frac{V}{p_2} \qquad (2)$$

If, on the other hand, the volume of the connecting leads is greater than the volume of gas in the manometer, and the diameter of the connecting leads is not too small, then it would seem reasonable to regard the volume in the connecting leads and the manometer as a reservoir of constant volume. The system response time would then be given by equating the mass flow rate through the static tapping hole in the pipe wall to the rate of increase of mass of gas in the connecting leads and manometer.

$$C_d . a\sqrt{2g\,\rho_g\,(p_1 - p_2)} = \frac{d}{dt} \cdot \rho_g V = V\,\frac{d\rho_g}{dt}$$

where C_d is the discharge coefficient of the tapping hole.

a the area of this hole.

p_1 and p_2 are the pipe line and manometer pressures.

V is the volume of connecting leads and manometer,

then if $V\,\frac{d\rho_g}{dt}$ is expressed as $\frac{\rho_g V}{p_2}\,\frac{dp_2}{dt}$ the equation can be integrated to give:

$$\Upsilon = \frac{V}{C_d . a\sqrt{2gRT}} \cdot \frac{1}{2}\left(\frac{\pi}{2} - \sin^{-1}\frac{2p_2 - p_1}{p_1}\right) \qquad (3)$$

For this project, the U-tube limbs and the bulb of the inclined manometer have the same order of magnitude volume as the

long connecting lead volume. Because of this, it is considered that the response time for the measurement of static pressure from the 0.04 in. diameter tappings in the pipe wall via long lengths of 0.11 in. bore tubing to U-tubes of 0.3 in. bore, might be estimated from a combination of equations (1) and (3). A pessimistic estimate is probably given by summing the times from the two equations. For the measurement of the air flow rate nozzle pressure differential using long lengths of similar tubing, because of the relatively large area of the inclined manometer bulb and the slight pressure differentials being considered, only equation (1) will be applied. For the measurement of total pressure using a pitot tube and pressure transducer, equation (2) is considered to apply.

For the static pressure measurement, the worst case is given for 150 ft. long leads, a 4 ft. air column in the U-tube and assuming the discharge coefficient for the tapping hole is 0.6, with pressures close to atmospheric.

From equation (1) - for mercury as manometric liquid τ = 0.6 sec.

- for water as manometric liquid τ = 2.4 sec.
- for liquid of specific gravity 0.785 as manometric liquid, but with leads 120 ft. long, τ = 2.2 sec.

From equation (2) - for $(p_1 - p_2) = 1$ p.s.i. at atmospheric pressure $\tau = 1.0$ sec. In the case of pressure differentials using the inclined tube manometer, where the diameter of the bulb is 1.4 in. and the height of the air column 1 in., equation (1) gives $\tau = 28.8$ sec.

For the total pressure measurement, the volume on the total pressure side of the transducer diaphragm was measured as 0.02 cu. in., and the bore and length of the smallest pitot tubes from which any readings were useable was 0.022 in. and 6 in. Substituting these values in equation (2) for the case $p_2 = 12$ p.s.i., which was considered the minimum, gives $\tau = 0.005$ secs.

LIST OF SYMBOLS.

A	Pipe or duct cross-section area.
a	Local gas acoustic velocity.
a_e	Local equilibrium flow acoustic velocity.
a_g	Local gas acoustic velocity.
a_m	Local constant fractional lag acoustic velocity.
a_p	Projected area of a solids particle.
a_s	Surface area of a solids particle.
C_D	Gas-solid particle drag coefficient.
C_f	Total gas-solids friction factor or skin friction factor for gas flow.
Cp	Specific heat of gas at constant pressure.
C_s	Specific heat of solids particles.
Cv	Specific heat of gas at constant volume.
c	Ultimate velocity.
D	Pipe diameter.
d_p	Particle diameter.
d_m or $\bar{d}$	Mean particle diameter.
dma	Aerodynamic effective particle diameter.
F	Frictional force term in momentum equation.
h	Gas-solids heat transfer coefficient.
j	Gas-solids temperature fractional lag (see Equation 2, Appendix 1)
J	Heat equivalent.
k	Gas-solids velocity fractional lag (see Equation 1 Appendix 1)
kg	Gas thermal conductivity.

L	Non dimensional pipe length = ℓ/λ or pipe length in Ch. 2.
ℓ	Pipe length.
M	Gas Mach number.
Mm	Mixture Mach number (see Equation 27 Appendix 1).
m_p	Mass of a single solids particle.
m	Mass of solids in unit mass of gas.
N	Constant fractional lag compressible flow index for the case solids volume not negligible.
Nu	Gas-solid particle Nusselt number.
n	Constant fractional lag compressible flow index (see Equation 11 Appendix 1) or index in gas velocity power law.
n_p	Number of particles of size d_p.
P	Pipe-line reference static pressure (absolute).
Pr	Prandtl number.
p	Pressure (absolute).
R	Gas constant in equation of state or pipe radius.
Re	Pipe or duct Reynolds number.
Re_p	Solids particle Reynolds number.
r	Radial distance from pipe centre-line.
s	Peripheral area of pipe or duct.
T	Temperature (absolute).
u	Velocity.
V	Volume.
W	Mass flow rate (lb/sec).
x	Ratio of solids to gas mass flow rates = W_s/W_g

y	Ratio of solids volume to gas volume = V_s/V_g or distance from pipe wall.
z	Polynomial equation.
β	Ratio C_s/C_v.
γ	Ratio of gas specific heats C_p/C_v.
η	Diffuser efficiency (see Appendix 5).
λ	Total pipe length from upstream datum to reference position.
μ	Gas viscosity.
ρ	Density.
σ	Standard deviation (see Appendix 2)
τ_o	Surface friction force per unit area of pipe.

<u>Suffices.</u>

e	Pipe exit of equilibrium flow condition.
g	Gas.
m	Mixture of gas and solids.
o	Stagnation or total conditions.
p	Solid particle.
s	Solids dispersed.
t	Conditions at a throat.
*	Conditions when M or Mm = 1

REFERENCES.

Bradshaw P. Experimental Fluid Mechanics, Pergamon Press, 1964.

Briggs W. Transactions of the American Institution of Chemical Engineers 42, 511 (1946).

Brown B. Detonation and Two Phase Flow (Editors S.S. Penner and F.A. Williams) Academic Press 1962.

Carlson D.J. A.R.S. Journal 32, 1107 (1962)

Cheers F. Elements of Compressible Flow. John Wiley & Sons 1963.

Coulson J.M. & Richardson J.F. Chemical Engineering Volumes 1 and 2. Pergamon Press 1962.

Culgan J.M. Ph.D. Thesis, Georgia Institute of Technology, 1952.

Davis C.N. Separation of Airbourne Dust and Particles. Institution of Mechanical Engineers Proceedings B Volume 1 B p. 185 (1952-53)

Fisher J. Pneumatic Conveying of Granular Plastics. Chemical Engineering Progress Volume 58. No.1 (Jan. 1962).

Fuchs N.A. The Mechanics of Aerosols (Edited by C.N. Davis) Pergamon Press 1964.

Fulmer R.D. & Wirtz D.P. Measurement of Individual Particle Velocities in a Simulated Rocket Exhaust. A.I.A.A. Journal Volume 3 No. 8 (Aug. 1965).

Garrett T. Heat Transfer Characteristics of Dilute-Phase Solids-Air Suspensions in Turbulent Pipe Flow. Ph.D. Thesis, Emmanuel College, Cambridge.

Goldstein S. Modern Developments in Fluid Dynamics Volume 1. 1938. p. 252.

Hariu O. & Molstad M.C. Industrial Engineering Chemistry 14 1148 (1949)

Hinkle M. Ph.D. Thesis, Georgia Institute of Technology (1953).

Hoglund R.F. Recent Advances in Gas-Particle Nozzle Flows. A.R.S. Journal, May 1962.

Houghton E.L. & Brock A.E. Tables for the Compressible Flow of Dry Air - Edward Arnold (1961).

Kay J.M. An Introduction to Fluid Mechanics and Heat Transfer. Cambridge University Press (1963).

Keenan J.H. & Naumann E.P. Measurement of Friction in a Pipe for Subsonic and Supersonic Flow of Air. Journal of Applied Mechanics, June 1946.

Kliegel J.R. Gas-Particle Nozzle Flows. The Combustion Institute 9th Symposium on Combustion. p.811. New York 1963. Academic Press.

Knudsen J.G. & Katz D.L. Fluid Dynamics and Heat Transfer. McGraw-Hill Book Co. (1958).

Kriebel A.R. Analysis of Normal Shock Waves in Particle Laden Gas. A.S.M.E. Journal of Basic Engineering (Dec. 1964).

Kuethe A.M. Some Features of Boundary Layers and Transition to Turbulent Flow - Journal of Aeronautical Sciences Volume 23. (1956).

Kunz K.S. Numerical Analysis p. 40, McGraw-Hill Book Co. (1957)

Mehta N.C. Effect of Solids Flow Rate and Particle Diameter on Pressure Drop in Pneumatic Transport Systems. Ph.D. Thesis 1955. Purdue University.

Mills B. & Cole B.N. Compressible Gas Flow in Commercial Pipes. The Institution of Mechanical Engineers (Dec. 1956)

Milne W.E. Numerical Solution of Differential Equations p. 72. John Wiley and Sons (1953).

Mitlin A. A Study of Pneumatic Conveying with Special Reference to Solid Velocity and Pressure Drop during Transport. Ph.D. Thesis 1954. University of London.

Moody L.F. Friction Factors for Pipe Flow. Transactions A.S.M.E. Volume 66. No. 8. p. 671. (November 1944)

Noble B. Numerical Methods 1. p.9. Oliver and Boyd 1964.

Oseen. See Fuchs N.A. The Mechanics of Aerosols.

Perry J.H. (Editor) Chemical Engineers Handbook. p.20-69. McGraw-Hill Book Co. 1963.

Peskin R.L. & Dwyer H.A. A Study of the Mechanics of Turbulent Gas-Solid Shear Flows. Winter Annual General Meeting of the American Society of Mechanical Engineers (Nov. 1965).

Pneumatic Handling of Powdered Materials (Including Fluidisation) E.E.U.A. Handbook No. 15, 1963. Constable & Co.

Richardson J.F. & McLeman M. Pneumatic Conveying Part 2. Solids Velocities and Pressure Gradients in a One-Inch Horizontal Pipe. Transactions of the Institution of Chemical Engineers. Vol. 38. 1960.

Rogers G.F.C. & Mayhew Y.R. Engineering Thermodynamics - Work and Heat Transfer. Longmans Green and Co.

Rudinger G. & Chang A. Analysis of Nonsteady Two-Phase Flow. The Physics of Fluids. Volume 7. No. 11. (Nov. 1964)

Rudinger G. Some Effects of Finite Particle Volume on the Dynamics of Gas-Particle Mixtures A.I.A.A. Journal Volume 3. No. 7 (July 1965).

Serafini J.S. Impingement of Water Droplets on Wedges and Double-Wedge Airfoils at Supersonic Speeds. N.A.C.A. Report 1159. 1954.

Soo S.L. Statistical Properties of Momentum Transfer in Two-Phase Flow. Chemical Engineering Science Volume 5. No. 2. April, 1956.

Soo S.L. Gas Dynamic Processes Involving Suspended Solids. American Institution of Chemical Engineers. Volume 7. No. 3. (Sept. 1961).

Soo S.L. Fully Developed Turbulent Pipe Flow of a Gas-Solid Suspension. Industrial and Engineering Chemistry Fundamentals. Volume 1. No. 1. (February 1962).

Soo S.L., Trezek G.J., Dimick R.C. & Hohnstreiter G.F. Concentration and Mass Flow Distributions in a Gas-Solids Suspension. Industrial and Engineering Chemistry Fundamentals. Volume 3. No. 2 (May, 1964).

Torobin L.B. & Gauvin W.H. Fundamental Aspects of Solids-Gas Flow Parts 1 - 6. The Canadian Journal of Chemical Engineering. August 1959 - June, 1961.

Uematsu T. Pneumatic Conveyance of Granular Solids Through a Pipe. Hydraulics and Fluid Mechanics. Proceedings of First Australasian Conference (1964).

Urick R.J. & Ament W.S. The Propagation of Sound in Composite Media. The Journal of the Acoustical Society of America. p. 115. Volume 21 Nos. 1 - 6 (1949).

Zenz F.A. & Othmer D.F. Fluidisation and Fluid Particle Systems. Reinhold Publishing Corporation 1960.

British Standards.

B.S. 885: 1963. Brass Tubes for General Purposes.

B.S. 1042: 1943. Code for Flow Measurement.

B.S. 1500. Fusion welded Pressure Vessels for Use in the Chemical Petroleum and Allied Industries. Part 1. 1958. Carbon and low Alloy Steels.

B.S. 1796: 1952. Methods for the Use of British Standards fine-mesh test sieves.

B.S. 3601: 1962. Steel pipes and tubes for Pressure Purposes.

COMPUTER PROGRAMME

```
→ESTABLISH EBMHBGS05AP3;
GAS SOLIDS PIPE FLOW;          O/P L,8→

begin library A0,A6,A12;
integer n,m;

  open(20);   open(70);
repeat:n:=read(20);
  if n=0 then goto finish;
  m:=read(20);
  write text(70,[[p]]);

  begin integer i,j,sa,sb,sc;
  real ka,kb,kc,kd,ke,kf,kg,kh,kp,N,P,f,D,w,d,r,t,
     K,c,R,dL,W,A,C,To,J,g,M,T,q,k,s,Re,Cd,Z,jt,nt,am,Mm;
  array a[1:n,0:n], b,db[1:n], sum[0:n+n], L,p,z[1:m], y,F[1:3];

  real procedure poly(a,x,n);
  value x,n;
  integer n;
  real x;
  array a;
  begin integer i;
     real sum;
     sum:=a[n];
     for i:=n-1 step -1 until 1 do sum:=sum×x+a[i];
     poly:=sum;
  end of poly;

  procedure solve(x,a,n);
  value a,n;
  integer n;
  array a,x;
  begin integer i,r,c;
     real z;
     for i:=n-1 step -1 until 1 do
         for r:=1 step 1 until i do
         begin z:=a[r,i+1]/a[i+1,i+1];
               for c:=0 step 1 until i do
                   a[r,c]:=a[r,c]-a[i+1,c]×z;
         end;
     for r:=1 step 1 until n do
     begin z:=a[r,0];
           for i:=r-1 step -1 until 1 do z:=z-x[i]×a[r,i];
           x[r]:=z/a[r,r];
     end;
  end of solve;
```

```
procedure fLy(L,y,F);
value L;
real L;
array F,y;
begin real ku,kv,kx,u,v,kj;
   u:=y[1];
   v:=y[2];
   k:=v/u;
   ku:=abs(u-v);
   kv:=1.0+kxkd;
   kx:=1.0+kxkxkd;
   T:=To+kex(To-y[3])-kxxuxu/kf;
   jt:=(To-y[3])/(To-T);
   kj:=1.4+1.4xkexjt;
   nt:=kj/(kj-0.4xkx/kv);
 am:=sqrt(ntxRxT/kv);
        Mm:=y[1]/am;
        q:=kh/u;
             Re:=kgxqxku;
   Cd:=if Re>800.0 then 0.438 else
            (Re↑0.6666666667x3.79+24.0)/Re;
   F[1]:=(exp(poly(b,L,n))xpoly(db,L,n-1)xP/(qxu)-kaxu)/kv;
   F[2]:=kbxCdxqxkuxku/v;
   F[3]:=(sqrt(Re)x0.53+2.0)xkcx(T-y[3])/v;
end of fLy;

procedure print;
begin fLy(s,y,F);
   write(70,sa,s);
   write(70,sb,y[1]);
   write(70,sb,y[2]);
   write(70,sb,y[3]);
   write(70,sb,T);
   ~~write(70,sb,Tb);~~
      write(70,sc,q);
   write(70,sc,k);
   write(70,sc,jt);
        write(70,sc,nt);
        write(70,sb,am);
        write(70,sc,Mm);
        newline(70,1);
end of print;
```

```
procedure int step(x,y,n,h,f,fxy);
value n,h;
real x,h;
array y,f;
integer n;
procedure fxy;
begin array v,w[1:n], a[1:5];
   integer i,j;
   real xe;
   a[1]:=a[2]:=a[5]:=h/2.0;
   a[3]:=a[4]:=h;
   xe:=x;
   for i:=1 step 1 until n do v[i]:=w[i]:=y[i];
   for j:=1 step 1 until 4 do
   begin fxy(xe,w,f);
         xe:=x+a[j];
         for i:=1 step 1 until n do
         begin w[i]:=v[i]+a[j]×f[i];
               y[i]:=y[i]+a[j+1]×f[i]/3.0;
         end;
   end;
   x:=xe;
end of int step;
         z[1]:=0.0;→

L[1]:=read(20);    p[1]:=read(20);
kp:=1.0+p[1];
for j:=2 step 1 until m do
begin L[j]:=read(20);
   p[j]:=read(20);
   z[j]:=ln(kp-p[j]);
end of reading curve;

for j:=0 step 1 until n+n do sum[j]:=0.0;
for j:=1 step 1 until  n  do a[j,0]:=0.0;
sum[0]:=m;
for i:=1 step 1 until m do
begin ka:=L[i];
   kb:=1.0;
   for j:=1 step 1 until n+n do
   begin kb:=kb×ka;
         sum[j]:=sum[j]+kb;
   end;
   kb:=z[i];
   for j:=1 step 1 until n do
   begin a[j,0]:=a[j,0]+kb;
         kb:=kb×ka;
   end;
end;
```

```
for i:=1 step 1 until n do
  for j:=1 step 1 until n do a[i,j]:=sum[i+j-2];

sa:=format([s-nd.dddd]);
sb:=format([s-nddd.dd]);
sc:=format([ss-d.ddddp+ndc]);
solve(b,a,n);
for j:=1 step 1 until n-1 do db[j]:=b[j+1]×j;

write(70,format([nds]),n-1);
write text(70,[TH*ORDER*POLYNOMIAL[3c6s]L[8s]P[5s]ERROR[5s]DP/DL[c]]);
for j:=1 step 1 until m do
begin write(70,sa,L[j]);
   write(70,sa,p[j]);
   Z:=exp(poly(b,L[j],n));
   write(70,sa,p[j]-kp+Z);
   write(70,sc,-Z×poly(db,L[j],n-1));
end;

N:=read(20);    P:=read(20);    f:=read(20);
D:=read(20);    w:=read(20);    d:=read(20);
r:=read(20);    K:=read(20);    c:=read(20);
R:=read(20);    W:=read(20);    A:=read(20);
C:=read(20);   To:=read(20);    J:=read(20);
g:=read(20);    M:=read(20);

ka:=0.5×N/D;
kb:=N/(d×r);
kc:=6.0×K×kb/(c×d);
kb:=0.75×kb;
kd:=w/W;
ke:=kd×c/C;
kf:=2.0×J×g×C;
kg:=d/M;
kh:=W/A;

y[1]:=kh×To×R/(P×(kp-exp(b[1])));
ka:=ka×f;
y[2]:=0.999×y[1];
y[3]:=To-(1.0+0.998001×kd)×y[1]↑2/((1.0+ke)×kf);
s:=0.0;

write text(70,[[3c]FLOW*OF*AIR****]);
write(70,sa,W);
write text(70,[***LBS/SEC[c]FRICTION*COEFFT.]);
write(70,sa,f);
write text(70,[[c]SOLIDS*LOADING**]);
write(70,sa,kd);
write text(70,[[3c6s]L[7s]U[8s]V[8s]S[8s]T[9s]Z[8s]Q[9s]K[9s]J[9s]N[
              A[9s]M[c]]);
sc:=format([s-nd.ddddd]);
print;
```

```
    for j:=1 step 1 until 4 do
    begin dL:=read(20);
      t:=read(20);
    B:intstep(s,y,3,dL,F,fLy);
      print;
      if s<t then goto B;
    end;

  end of block 1;
  goto repeat;

inish:close(70);
  close(20);
end→
→
```

SYMBOLS FOR COMPUTER PROGRAMME

A - Pipe cross-section area
am - a_m
C - Cp
c - Cs
Cd - Cd
D - Pipe diameter
d - Solids particle diameter
f - 4Cf
g - Gravitational constant
i and j - integers - subscripts in arrays
J - Heat equivalent
jt - j temperature lag
K - Gas thermal conductivity
k - v/u - velocity lag
ka - Length along pipe or 0.5 x N/D
kb - Length along pipe or N x r/d
M - Gas viscosity
Mm - Mm
m - Number of pressure increments
N - Pipe reference length
n - Order of polynomial + 1
nt - n
P - Reference pressure
q - Gas density
R - Gas constant
Re - Solids particle to gas Reynolds number
r - Solids particle density ρp
s - Distance along pipe (non-dimensional)
sa, sb, sc - formats
T - Gas temperature
To - Stagnation temperature
t - Distance along pipe at which step length is changed
W - Gas flow rate Wg
w - Solids flow rate Ws
Z - exp. (poly (b, L(j), n))
dL - Step length (non-dimensional)

Arrays

L(1:m) - Distand along pipe (non-dimensional)
p(1:m) - Corresponding pressure (non-dimensional)
z(1:m) - ln (kp - p(j))
y(1) - u gas velocity
y(2) - v solids velocity
y(3) - Ts solids temperature
F(1) - differential du/dL
F(2) - differential dv/dL
F(3) - differential dTs/dL

p(j) - kp + Z - Error in fitting curve
$\frac{dp}{dL}$ - -Z x poly (db, L(j), n - 1)

a(1) to (5), v(i), w(i), y(i), x - Terms in Runge-Kutta solution of differential equations.